Evaporation partitioning of forest stands

The role of forest structure

Jimenez Rodriguez, C.D.

DOI
10.4233/uuid:046a7cc0-1d66-4c7a-b294-feea556d7246

Publication date
2020

Document Version
Final published version

Citation (APA)
Jimenez Rodriguez, C. D. (2020). *Evaporation partitioning of forest stands: The role of forest structure*. [Dissertation (TU Delft), Delft University of Technology]. https://doi.org/10.4233/uuid:046a7cc0-1d66-4c7a-b294-feea556d7246

EVAPORATION PARTITIONING OF FOREST STANDS

THE ROLE OF FOREST STRUCTURE

César Dionisio Jiménez-Rodríguez

Evaporation partitioning of forest stands

The role of forest structure

Evaporation partitioning of forest stands

The role of forest structure

Dissertation

for the purpose of obtaining the degree of doctor
at Delft University of Technology
by the authority of the Rector Magnificus prof.dr.ir. T.H.J.J. van der Hagen
chair of the Board for Doctorates
to be defended publicly on
Thursday 27 August 2020 at 10:00 o'clock

by

César Dionisio Jiménez Rodríguez

Master of Science and Engineering in Hydrology and Water Resources,
IHE-Delft, the Netherlands
and
Bachelor of Science in Forest Engineering,
Tecnológico de Costa Rica
born in San José, Costa Rica.

This dissertation has been approved by the promotors.

Composition of the doctoral committee:

Rector Magnificus,	chairperson
Prof.dr.ir. H.H.G. Savenije	Delft University of Technology, promotor
Dr.ir. A.M.J. Coenders-Gerrits	Delft University of Technology, copromotor
Independent members:	
Prof.dr.ir. S.C. Steele-Dunne	Delft University of Technology
Prof.dr. T. Roeckmann	University of Utrecht
Prof.dr.ir. A.B.K. van Griensven	Vrije University Brussels, Belgium
Dr. I. van Meerveld	University of Zurich, Switzerland
Prof.dr.ir. N.C. van de Giesen	Delft University of Technology, reserve member
Other members:	
Dr. T.A. Bogaard	Delft University of Technology

Keywords: evaporation, ecosystems, water stable isotopes, canopy

Printed by: Ipskamp Printing

Front & Back: Designed by M.Sc. Adriana del Pilar González–Angarita and Manuel González–Angarita.

ISBN 978-94-6366-300-7

An electronic version of this dissertation is available at
http://repository.tudelft.nl/.

To my wife, for all your unconditional support.

Contents

Summary

Forest evaporation (E) is considered the main source of water vapor at a continental scale. Its quantification has been carried out in many ecosystems worldwide, applying the classical partitioning method to differentiate among sources of water vapor. This partitioning differentiates between transpiration (E_t), soil evaporation (E_s), water intercepted by plant and ground surfaces (E_i), and open water evaporation (E_w) in flooded forests and mangroves. The partitioning of evaporation has been carried out by applying different methodologies such as eddy–covariance, conventional micro–meteorological measurements, stable water isotopes, and the combination of some of these methodologies. However, the classical partitioning approach can have large uncertainties in specific forest ecosystems as a consequence of the canopy structure. Instead, including canopy structure into the evaporation partitioning allowed us to better understand this flux. Forest canopy structure is difficult to assess and is determined by latitude, altitude, water availability, and growing stage of the forest. However, using the canopy layering (overstory, understory, ground layer and forest floor layer) we can assess the contribution from the structural point of view.

Forest succession is one factor affecting the classical partitioning in Tropical Deciduous Broadleaf Forest. Using cumulative daily collectors in three different stages of Tropical Dry Forest in Costa Rica, we were able to depict how the increment in forest complexity affects the interception of precipitation. Also, the Plant Area Index was the only structural parameter significantly correlated with the estimates of both, interception and effective precipitation. The capacity of the other parameters (e.g., tree densities, tree heights, number of species) was not enough to describe the effect of a growing forest on the interception of precipitation.

Tropical forests with less water stress during the dry season allocate more biomass to their canopies. This increases the forest complexity in terms of the number of species, canopy height, and plant types. Tropical Evergreen Broadleaf forests have a more complex canopy structure than the Deciduous ones. The tropical wet forest in Costa Rica has a canopy of 45 m height and a large number of plant species including trees, lianas, palms and bushes that provide a completely different canopy structure than mono–specific forests. Here, we were able to define three canopy layers according to canopy height (overstory, lower and upper understory) and monitor the evaporation process during one dry season. Applying conventional micro–meteorological measurements we were able to determine that the lower and upper understory layers contributed 9 % and 15 % of the evaporation, respectively. Meanwhile, the use of water stable isotopes did not allow us to

determine the contribution of transpiration using the keeling plot method. However, the signatures of the stable water isotopes allowed us to determine that the source of water used by the plants depends on its type (liana, tree, palm or bush). Also, we quantified the evaporation during precipitation events as one third of the amount measured during dry sunny days. The proportion did not change during rain events per canopy layer. This water vapor was produced by the "splash droplet evaporation" process, that together with the energy convection and low air temperature produced the visible vapor plumes. We were able to identify the conditions during which the visible vapor plumes can be spotted. These conditions are the presence of precipitation, air convection, and a lifting condensation level at the top of the canopy with values lower than 100 m.

Plants growing in arid environments developed strategies that help them to cope with the scarcity of water. Usually, these plants grow lumped in patches and the introduction of tree species to fight desertification changed the landscape introducing a forest–like land cover. In a Temperate Shurbland in China, we evaluated the effect of Willow trees (*Salix matsudana*) and Willow bushes (*Salix psammophila*) on the soil water after summer. Using stable water isotopes we identified the redistribution of groundwater beneath the plants through the hydraulic lift process.

Mono–specific forest ecosystems such as the Temperate Evergreen Needleleaf Forest may modify the micro–meteorological conditions beneath their canopies. In Speulderbos, we monitor the evaporation process through eddy–covariance and stable water isotope techniques in a Douglas–Fir (*Pseudotsuga menziesii*) stand. Also, the evaporation process in the forest floor layer was analyzed in detail under laboratory conditions. Different forest floor layers evaporates up to 1.5 mm d^{-1}, differing from field conditions, where the evaporation from these layers do not exceed the 0.2 mm d^{-1}. This evaporation, represents only the 5.5 % of the total measured during the monitoring period. However, there is no evidence that the forest floor evaporation move upwards to contribute to the total evaporation measured above the overstory. This was confirmed by the eddy–covariance footprint and stable water isotopes signatures of the air measured continuously on the forest. Finally, the partitioning of evaporation based on canopy structure is suitable for complex ecosystems with a large number of species and a multilayered canopy. This leaves the classical partitioning for more homogeneous ecosystems where it can be carried out with a smaller monitoring investment.

Samenvatting

Verdamping door bossen wordt beschouwd als de hoofdbron van waterdamp op continentschaal. Deze verdamping is wereldwijd gekwantificeerd in vele ecosystemen, en opgesplitst in verschillende bronnen door middel van de klassieke partitiemethode. Hiermee kan onderscheid gemaakt worden tussen transpiratie, bodemverdamping, interceptieverdamping, en openwaterverdamping in overstroomde bossen en mangroves. Verdamping is met verschillende methodes gepartitioneerd, zoals eddy-correlatie, conventionele micrometeorologische metingen, stabiele waterisotopen, en de combinatie van deze technieken. Echter, de klassieke partitie methode kan een grote onzekerheid hebben in bepaalde bos ecosystemen, vanwege de structuur van de vegetatie. Door rekening te houden met de vegetatiestructuur kunnen wij deze verdampingsflux beter begrijpen. De vegetatiestructuur is moeilijk om te beoordelen, en wordt bepaald door de hoogtegraad, breedtegraad, waterbeschikbaarheid, en groeistadium van het bos. Met behulp van de vegetatiegelaagdheid (hoogste etage, lagere ondergroei, hogere ondergroei, en bodemlaag) kunnen we de contributie vanuit een structuur oogpunt vaststellen.

Successie is een van de factoren die de klassieke partitiemethode in tropische bladverliezende loofbossen beïnvloed. Met cumulatieve dagelijkse regenmeters in drie verschillende stadia van een tropisch droog bos in Costa Rica konden wij voorspellen hoe een verhoging van boscomplexiteit de regenvalinterceptie beïnvloedde. De plantoppervlakte–index was de enige structuurparameter die significant correleerde met schattingen van zowel interceptie als regenval. De andere parameters (bijvoorbeeld boomdichtheid, boomhoogte, aantal soorten) waren van te weinig invloed om het effect van een groeiend bos op interceptie te beschrijven.

Tropische bossen die minder waterstress ervaren tijdens het droogteseizoen wijzen meer biomassa aan hun kroonlaag toe. Dit zorgt voor een verhoging in boscomplexiteit qua aantal soorten, hoogte van de kroonlaag, en soorten planten. Tropische groenblijvende loofbossen hebben een complexere structuur dan de bladverliezende bossen. In tegenstelling tot de bladverliezende droge bossen in Costa Rica, heeft het tropisch regenwoud een complexe structuur, met een kroonhoogte van 45 m, en een grote hoeveelheid plantensoorten, zoals bomen, lianen, palmen en struiken. In dit bos konden we drie lagen definiëren aan de hand van de kroonhoogte (hoogste etage, lagere en hogere ondergroei) en hebben we het verdampingsproces tijdens één droog seizoen gemeten. Met conventionele micrometeorologische metingen konden we bepalen dat de contributie aan de totale verdamping van de lagere en hogere ondergroei respectievelijk 9 % en 15 % was. Met metingen van stabiele waterisotopen en de "keeling plot" methode konden

we daarentegen niet de contributie van transpiratie bepalen. Echter, de kenmerken van de stabiele waterisotopen maakte het mogelijk om vast te stellen dat de waterbron per type plant (liaan, boom, palm of struik) verschilt. Daarnaast kwantificeerden we de verdamping tijdens neerslag als een derde van de hoeveelheid gemeten op droge zonnige dagen. De verhoudingen van de verdampingscontributie van de verschillende lagen veranderde niet gedurende neerslag. Tijdens regenval werd waterdamp geproduceerd door het "splash droplet evaporation" proces, wat in combinatie met convectie en een lage luchttemperatuur zichtbare waterdamppluimen produceerde. We konden de condities bepalen waarin de pluimen zichtbaar waren. Deze condities zijn regenval, convectie, en een optillingscondensatieniveau op 43 m hoogte van minder dan 100 m.

Planten die in een droge omgeving groeien hebben strategieën ontwikkeld om met waterschaarste om te gaan. Vaak groeien deze planten in kluitjes bij elkaar, en het gebruik van boomsoorten om verwoestijning tegen te gaan veranderde het landschap door de introductie van een bos-achtige bodembedekking. In een gematigd scrubland in China evalueerden we het effect van krulwilgen (*Salix matsudana*) en wilgenstruiken (*Salix psammophila*) op het bodemvocht na de zomer. Met stabiele waterisotopen identificeerde we de herverdeling van grondwater onder de planten door middel van het 'hydraulic lift' proces. Monospecifieke bos ecosystemen zoals gematigde naaldwouden veranderen de micrometeorologische omstandigheden onder hun bladerdak. In het Speulderbos bestudeerden we het verdampingsproces in een Douglasspar (*Pseudotsuga menziesii*) opstand met behulp van eddy-correlatie en stabiele waterisotopen. Het verdampingsproces in de bodemlaag analyseerden we in detail onder lab condities. Verschillende bodemlagen verdampten tot wel 1.5 mm d^{-1}, in tegenstelling tot de veldomstandigheden waar de verdamping van de bodemlagen niet groter was dan 0.2 mm d^{-1}. Deze verdamping vertegenwoordigd maar 5.5 % van de totaal gemeten verdamping tijdens de meetperiode. Echter was het niet mogelijk om de contributie van verdamping van de bodemlaag te verbinden aan de evaluatie van de kroonlaag. Dit werd bevestigd door de eddy–correlatie voetafdruk en de kenmerken van de stabiele waterisotopen van de lucht. Het partitioneren van verdamping op basis van bosstructuur is geschikt voor complexe ecosystemen met een grote hoeveelheid soorten en een meerlaags bladerdak. Dit laat de klassieke partitiemethode over voor homogenere ecosystemen waar het uitgevoerd kan worden met een kleinere meetopstelling.

1

Introduction

The forest covers the landscape
and the raindrops wash its leaves,
as the trees have to breathe
the water can move and leave.

Parts of this chapter are based on:

Calvo-Alvarado, J., **Jiménez-Rodríguez, C.**, Calvo-Obando, A., Marcos do Espírito-Santo, M., and Gonçalves-Silva, T. (2018). *Interception of Rainfall in Successional Tropical Dry Forests in Brazil and Costa Rica.* Geosciences, 8(12), 486.

Jiménez–Rodríguez, C.D., Coenders–Gerrits, M., Uhlenbrook, S. and Wenninger, J. (2019). *What Do Plants Leave after Summer on the Ground?-The Effect of Afforested Plants in Arid Environments.* Water. 11(12), 2559.

Jiménez-Rodríguez, C.D., Coenders-Gerrits, M., Wenninger, J., Gonzalez-Angarita, A., and Savenije, H. (2020). *Contribution of understory evaporation in a tropical wet forest during the dry season.* Hydrol. Earth Syst. Sci., 24, 2179–2206

Jiménez–Rodríguez, C.D., Coenders–Gerrits, M., Schilperoort, B., Gonzalez-Angarita, A.P. and Savenije, H. (2020). *Vapor plumes in a tropical wet forest: spotting the invisible evaporation.*Hydrol. Earth Syst. Sci. Discuss. in review.

1

1.1. Evaporation of forest ecosystems

Water vapor in the atmosphere is maintained by ocean and land evaporation (Webster, 1994; Wild et al., 2015). This flux is the second largest of the hydrological cycle, exceeded only by precipitation (Coenders-Gerrits et al., 2014; Miralles et al., 2011a; Wallace, 1995; Wang et al., 2014). The water vapor originated from continental environments is recycled in the atmosphere at different time and spatial scales, giving origin to the 40 % of the worldwide precipitation (van der Ent et al., 2010). These inland environments have been affected in the last 30 years by strong changes on the land cover. The tropics had experienced a net reduction on the tree and shrub vegetation, meanwhile the other regions replaced bare soil covers for agricultural lands and tree cover (Song et al., 2018). Despite these changes of land cover and the larger accumulation of ground biomass in mature forests in the temperate regions respect to the tropics (Liu et al., 2014), tropics are able to export more than 1000 mm yr^{-1} as water vapor while temperate latitudes transports ~500 mm yr^{-1} (Miralles et al., 2011a,b; Kumagai et al., 2016).

Evaporation is determined by factors such as soil water availability, plant physiology, atmospheric conditions and tree size or age (Calder, 1998; de Simón et al., 2017). The access to different water pools such as soil water (Carminati et al., 2010) or groundwater (Lamontagne et al., 2005; Miller et al., 2010), influences the growing rates of forest stands and consequently the evaporation from the ecosystem (Tamkevičiūtė et al., 2018). Environments with low water availability force the vegetation to be more efficient using this resource (Poorter et al., 2017; Troch et al., 2009). While environments with water surplus such as the Amazon forest are limited by other factors such as solar radiation (Ahlstrom et al., 2017). Also, the ecosystem complexity in terms of species richness (Forrester, 2015) or presence of specific plants such as lianas (Chen et al., 2015b) can alter the evaporation at stand level through the increment of leaf area index (LAI) (Rodríguez-Ronderos et al., 2016).

The evaporation (E) of any ecosystem (see Equation 1.1) is a mixture of the water vapor originated from water bodies (E_w), water intercepted on plant and ground surfaces (E_i), soil water (E_s) and plant transpiration (E_t) (Abtew and Melesse, 2013; Roberts, 1999; Savenije, 2004; Shuttleworth, 1993; Sun et al., 2016).

$$E = E_w + E_i + E_s + E_t \tag{1.1}$$

Partitioning of evaporation into these components had been applied to multiple ecosystems such as wetlands (Zhang et al., 2017), croplands (Roupsard et al., 2006; Xiao et al., 2016; Zhao et al., 2015) and forests (Allen et al., 2017; Kang et al., 2018; Whitehead et al., 1994; Wilson et al., 2000; Sulman et al., 2016). Most of these evaluations focused on the differentiation of E_t from E, where large variations were observed due to variations on the $\frac{E_t}{E}$ of vegetation covers (Wang et al., 2014). However, the role played by the structure of different forested ecosystems on the partitioning of evaporation had not been deeply analyzed yet.

Evaporation partitioning of forest ecosystems is important in order to determine its contribution to the forest hydrological cycle (Blyth and Harding, 2011; Scott et al., 2003). Evaporation contributions from different canopy components depend on the canopy layers differentiation. However, this differentiation will depend on the forest type (Leiterer et al., 2015; Tang et al., 2019), forest age (Kalacska et al., 2004) and species composition (Asner et al., 2015).

1.2. How to approach evaporation partitioning?

The precise estimation of evaporation is critical for improving hydrological models and water management decisions (Guo et al., 2017). Savenije (2004) remarks the importance to differentiate between the different evaporation processes, due to its importance for the way we should model evaporation. This flux is driven by meteorological variables such as temperature (T), vapor pressure deficit (VPD), solar radiation (R), and wind speed (u) (Raghunath, 2006). However, these variables differ depending on latitude, ecosystem type and structure. Several approaches have been applied to partition evaporation in agricultural and natural ecosystems (Lauenroth and Bradford, 2006; Lawrence et al., 2007b; Raz-Yaseef et al., 2010; Sauer et al., 2007; Tobón Marin et al., 2000). Evaporation partitioning can be performed through modelling, direct measurements and the combination of both approaches (Kool et al., 2014). Method's selection depends on the research question, forest type and climate.

The eddy covariance method is used as a standard method to measure land fluxes as vapour, carbon and energy exchange (Aubinet et al., 2012; Liu et al., 2011). However, the estimations do not allow the complete understanding of the evaporation processes beneath the forest canopy. This method does not allow the energy balance closure with reduced wind velocities (lower than 0.6 $m\,s^{-1}$), being relevant for evaporation estimates (Franssen et al., 2010). Euser et al. (2014) propose a new method to estimate evaporation based on the Bowen-Ratio method (Bowen, 1926; Liu and Foken, 2001) and the Distributed Temperature Sensing (DTS) system (Ukil et al., 2012). The evaluation of this system in an agricultural land provided some insights of the technique, while its application in more complex land covers as forest ecosystems started to be tested (Schilperoort et al., 2018). Canopy energy storage is a significant component of the surface energy budget (Haverd et al., 2007) and its quantification at forest level will improve the energy balance in complex ecosystems (Coenders-Gerrits et al., 2020; Lindroth et al., 2010); allowing a better estimation of the ground heat flux to estimate the evaporation through the Bowen-Ratio method.

The accurate quantification of evaporation fluxes requires the rainfall interception partitioning into canopy, stem, and litter interception (Carlyle-Moses and Gash, 2011; Crockford and Richardson, 2000; Gerrits et al., 2007, 2010; Gerrits and

Savenije, 2011; Gupta and Usharani, 2009; Schaap and Bouten, 1997; Staelens et al., 2008; Tobón Marin et al., 2000; feng Zhang et al., 2015), while the transpiration is an important parameter that is influenced by layering vegetation, physiology, and seasonality (Granier, 1987; Kunert et al., 2012; Tyree, 2003).

Nowadays, a wide range of tools to follow water from its source is available. Some techniques as dyes (Hu et al., 2013; Lichner et al., 2011; Salvador et al., 2011), electric conductivity (Cirpka et al., 2007; Vogt et al., 2010), ion concentrations (Capell et al., 2011; Speed et al., 2010), and isotope signatures of different elements (Feng et al., 2013b; Lu, 2014; Rice and Hornberger, 1998; Speed et al., 2010; Visser et al., 2013; West et al., 2006a) have been used to trace the water paths. Nevertheless, the water stable isotopes (^{2}H and ^{18}O) provide a reliable signature to identify and differentiate among water sources, storage, and paths (Dawson et al., 2002; West et al., 2006a). Additionally, the signatures of these isotopes make it possible to link the water source with specific seasons and times (Feng et al., 2013a; Gat, 2005; Gourcy et al., 2005; Jouzel et al., 2013; Rozanski, 2005; Visser et al., 2013).

Using stable water isotopes to study the behaviour of water and analyse water fluxes has become more common over the last decade, with a number of recent studies that have examined water fluxes in forests and other natural ecosystems (De Wispelaere et al., 2017; Wang et al., 2017). The isotopic composition of precipitation is the main key to relating surface, ground- or soil water to its original source, including information about spatial and temporal distributions. The isotopic composition of throughfall in a forest is subject to change through processes of evaporation, mixing or interaction with other sources, thus allowing to gather information about the evaporation process and fluxes within a system (Hsueh et al., 2016).

Both stable isotopes ^{2}H and ^{18}O are considered ideal tracers in hydrology because of their natural occurrence and signature variation linked to the isotope ratio dependency on temperature (West et al., 2006b). Water phase change drives physical isotope fractionation, as well as diffusion and mixing but at lower proportions (Gat et al., 2000; Rothfuss et al., 2010). Evaporation from soil and wet surfaces depends on the amount of water vapor transferred towards the atmosphere, and will undergo physical fractionation (Soulsby et al., 2017; Sprenger et al., 2017a; Van Bavel and Hillel, 1976). Whilst the fractionation caused during photosynthesis is an example of the chemical fractionation, determining the isotope signature of the water transpired by plants (Butt et al., 2010; Cernusak et al., 2016; Farquhar et al., 2007). Physical and chemical fractionation of water stable isotopes characterizes the kinetic fractionation process, which is unidirectional and mass dependent (Young et al., 2002).

The introduction of stable water isotopes in hydrology allowed the refinement of evaporation partitioning (Miralles et al., 2011a; Wang et al., 2014). Thus comple-

menting the hydrometric data and providing information about the source of water vapor as a descriptor of the evaporation process (Blyth and Harding, 2011; Dubbert et al., 2017; Silvertown et al., 2015). Stable isotope signatures (^{18}O and ^{2}H) of different soil water reservoirs may differ due to isotope fractionation, as well as mixing and diffusion processes (Barnes and Turner, 1998; Hsueh et al., 2016; Sprenger et al., 2016). These processes happen throughout the soil profile with differences in magnitude. Soil evaporation drives the isotopic fractionation of soil water at the superficial soil layers (Dawson and Simonin, 2011; Sutanto et al., 2012). The soil evaporation rate is affected by the presence of different vegetation types or ground layer types (Magliano et al., 2017; Sprenger et al., 2017a; Raz-Yaseef et al., 2010). This will change the spatial distribution of isotope signatures with augmented differences because of the enriched isotope signature of throughfall water reaching the forest floor (Allen et al., 2016; Dawson and Simonin, 2011).

Plant water uptake has been considered as a non-fractionation process (Ehleringer and Dawson, 1992; Guo et al., 2016) except for plant species growing in saline or xeric environments (Ellsworth and Williams, 2007). However, recent evidence has shown that tree species such as *Pinus sylvestris* L., *Quercus subpyrenaica* Villar, *Persea americana* Mill., *Fagus sylvatica* L. and *Populus euphratica* Oliv. are able to fractionate the isotope signatures of xylem water (Barbeta et al., 2019; Martín-Gómez et al., 2016; Vargas et al., 2017; Zhao et al., 2016). This arise the question if trees do modify the isotope signature of xylem water, as a response to their plasticity to seasonal changes despite their similar root distribution (Schwendenmann et al., 2015). Different vegetation types determine partly the plant root system (Groff and Kaplan, 1988) and with it, the capacity to access specific soil water reservoirs. The transpired water has heavier isotope signatures than xylem water as a consequence of the photosynthesis process (Dubbert et al., 2014; Yakir and Sternberg, 2000), differing from the water source used by the plant. This provides a tool to trace or compare the different sources of water vapor in the air.

Currently, the evaluation of the isotope signatures of water vapor can be performed with three different methods. Firstly, the Craig-Gordon model (CG–model) (Craig and Gordon, 1965) was developed to determine the water vapor signature of evaporation originated from open waters (Horita et al., 2008) and has also been applied in transpiration and soil evaporation studies (Dubbert et al., 2013; Ferrio et al., 2009; Williams et al., 2004). The CG–model includes the equilibrium effect (as a consequence of the change from liquid to vapor) as well as the kinetic effect (due to the diffusion of heavy and light isotopes of water vapor in the air) (Roden and Ehleringer, 1999). The model is based on the differentiation of three interface layers between the liquid water and atmosphere. The liquid boundary layer is dominated by the equilibrium fractionation process, followed by a layer dominated by the molecular diffusivity and the last layer is characterized by the turbulent mixing (Craig and Gordon, 1965; Gat, 2008; Horita et al., 2008; Roden and Ehleringer, 1999). The high sensitivity of ^{18}O to temperature makes some assumptions of this model unreliable for the application in soil evaporation or plant transpiration

processes (Dubbert et al., 2013). Leading to important differences in ^{2}H and ^{18}O signatures between the modelled and measured signatures (Horita et al., 2008). The second method uses uses cold traps to condensate and freeze the air water vapor in a canister immersed in liquid nitrogen or dry ice (He and Smith, 1999; Kool et al., 2014; Sheppard, 1958; Wen et al., 2016). This process has a high risk of fractionation due to phase changes, leading to heavier isotope signatures if the collection efficiency is not perfect (Griffis, 2013). Finally, recent developments and improvements in measurement techniques such as mass spectrometers and laser-based spectroscopy allow to measure air water vapor directly in the field (Braden-Behrens et al., 2019; Gaj et al., 2016; Iannone et al., 2010; Steen-Larsen et al., 2013, 2014, 2015; Sun et al., 2014; Volkmann et al., 2016; Wang et al., 2013; Wei et al., 2015; Zhang et al., 2010).

1.3. A knowledge gap beneath the canopy

Global hydrological models require reliable measurements of evaporation and its partitioning to estimate the global patterns and flux drivers (Lawrence et al., 2007b). The inclusion of forest heterogeneity within the simulations of evaporation will enhance the model reliability (Ukkola et al., 2016). This heterogeneity can be assessed through forest attributes such as canopy layers, forest age or plants diversity. These attributes are linked to different parameters (e.g., soil properties, leaf area index or stomatal conductance) that influence the seasonal-scale processes that link soil moisture and evaporation (Ukkola et al., 2016) or throughfall and deep percolation (Klos et al., 2014).

Global forest heterogeneity is described by the presence of broadleaved or coniferous vegetation with evergreen or deciduous trees, forest stands with a mixture of them, savannas and shrublands (Tang et al., 2019). However, this classification requires the inclusion of canopy structure to refine the parameterization of forest heterogeneity (Leiterer et al., 2015). Forest canopy is defined as all the branches, leaves and twigs located between the forest floor and the canopy interface with the atmosphere (Figure 1.1). It can be divided as follows (Nadkarni et al., 2004; Parker, 1995):

- Overstory (ov): includes all the upper trees fully illuminated from above.
- Understory (u): contains the woody plants on the lowest shady layers. This layer can be segmented in two or more layers according with forest height and species composition.
- Ground layer (g): is formed by tree seedlings and herbaceous vegetation such as ferns or bushes.
- Forest floor (ff): is made up of the uppermost layer of soil that includes organic debris (litter) and various vegetation growing attached to it as mosses.

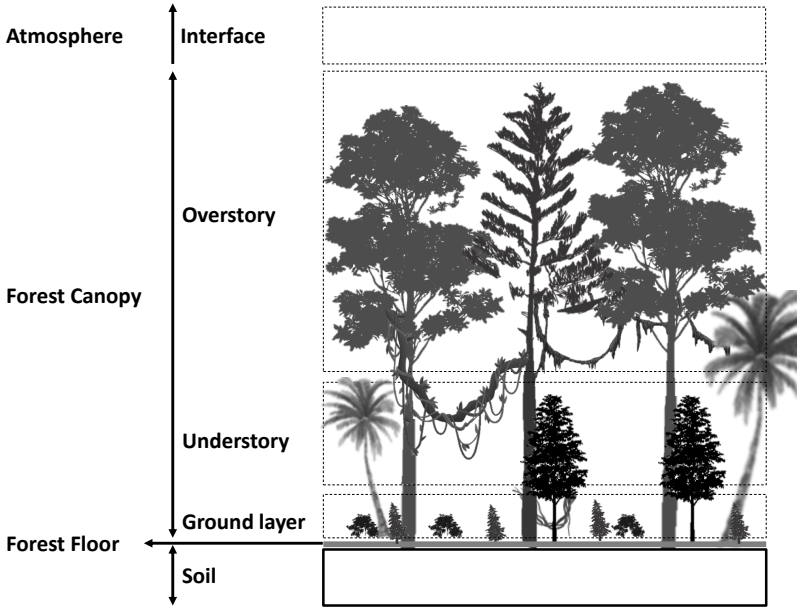

Figure 1.1: Vertical forest structure according to the classification by Parker (1995). Understory layer can be segmented into upper, middle and lower understory depending in forest height and plant species. Note: individual plant images adapted from the source (IMGBIN, 2020).

Specific interactions within the forest environment underline the importance of canopy layers on the water paths. As an example, an understory layer beneath Scots pine (*Pinus sylvestris* L.) trees in xeric environments reduces the soil water content as a consequence of their interception capacity (Giuggiola et al., 2018). This effect can be increased by the presence of a forest floor, which plays an important hydrological role as it contributes to the water and energy exchange of forest ecosystems (Heijmans et al., 2004; Sato et al., 2004). This layer define the air movement rates between the soil water and the air above the forest floor (Raz-Yaseef et al., 2010; Magliano et al., 2017). However, most of the evaporation studies focused on the quantification of the whole ecosystem (Silva et al., 2017; Soubie et al., 2016; Sun et al., 2016). Meanwhile studies focusing on the different forest layers is limited. Some studies placed the contribution of understory layers in temperate and boreal ecosystems ranging from 8% to 50%. This wide range depends on species composition, canopy closeness, leaf dynamics, and micro-meteorological conditions (Blanken et al., 1997; Iida et al., 2009; Jung et al., 2013; Kasurinen et al., 2014; Unsworth et al., 2004). However, the quantification of understory evaporation in other environments (e.g., tropical forest, temperate mixed forest) is still missing.

1

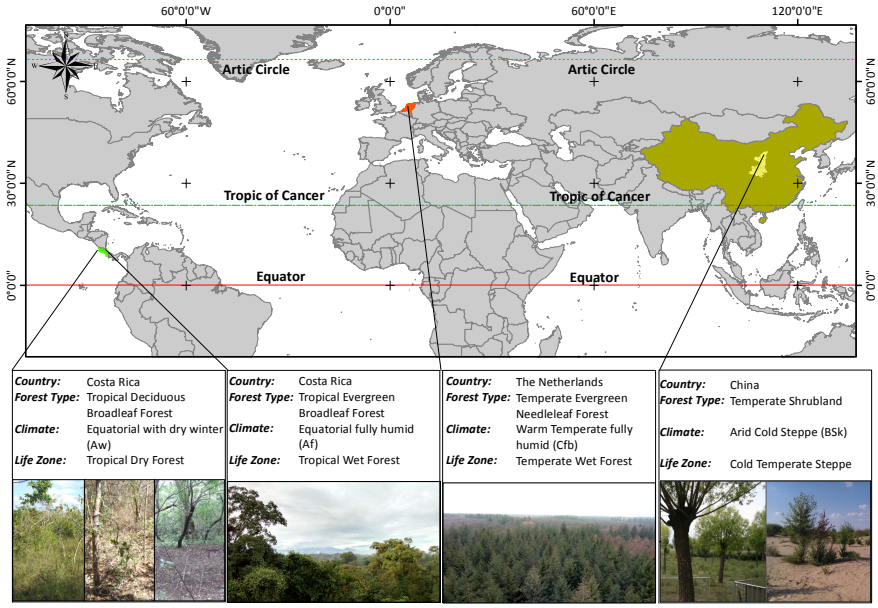

Figure 1.2: Location of the experimental sites selected for this thesis.

1.4. What is this thesis about?

This thesis aims to determine the role played by the forest structure during evaporation, considering the canopy layering and environmental conditions. The canopy layering includes the differentiation among overstory (ov), understory (u), ground (g) and forest floor (ff) layers (Equation 1.2). Each canopy layer can be also partitioned according to Equation 1.1, allowing the development of a twofold partitioning method when it is required (Equation 1.3).

$$E = E_{\mathrm{ov}} + E_{\mathrm{u}} + E_{\mathrm{g}} + E_{\mathrm{ff}} \tag{1.2}$$

$$E = \left(E_{\mathrm{i-ov}} + E_{\mathrm{t-ov}}\right) + \left(E_{\mathrm{i-u}} + E_{\mathrm{t-u}}\right) + \left(E_{\mathrm{i-g}} + E_{\mathrm{t-g}}\right) + \left(E_{\mathrm{i-ff}} + E_{\mathrm{s-ff}}\right) \tag{1.3}$$

Some of these layers can be present depending on the forest type and latitude, whilst environmental conditions define specific limitations to the forest growth. These limitations can modify the role played by the forest structure. In order to determine this, four study sites were selected: one in The Netherlands, two in Costa Rica, and one in China (Figure 1.2). On these sites, specific research questions were addressed according with the forest type and environmental conditions:

-*How does a growing forest affect the evaporation by intercepting precipitation?* Chapter 2 analyses the precipitation partitioning within a Tropical Deciduous Broadleaf

Forest in Costa Rica (N: 10°26′0″ – W: 83°59′0″). This analysis is based on hydrometric data and evaluates the effect of an increasing forest complexity on the determination of forest interception. Forest complexity is addressed through the selection of three different forest stands characterizing the successional stages of tropical dry forests: early, intermediate and late. The evaluation of forest interception was performed in nine forest plots measuring gross precipitation, throughfall and stemflow.

-*What is the relative contribution of different canopy layers in a complex ecosystem?*
Chapters 3 and 4 analyze the evaporation process during the dry season within a Tropical Evergreen Broadleaf Forest in Costa Rica (N: 10°26′0″ – W: 83°59′0″). Chapter 3 quantifies the evaporation of different canopy layers within a highly complex ecosystem. It incorporates the signature of water stable isotopes to explain the difficulties to differentiate between layers and water sources. Chapter 4 describes the formation of visible vapor plumes as the result of evaporation processes happening during rain events. This evaporation is linked with the evaporation by intercepted water in wet surfaces.

-*How do different canopy types affect soil evaporation?*
Chapter 5 explains how the presence of Willow trees and Willow bushes reduce the effect of soil evaporation after summer in arid environments in China. Here, the presence of natural and planted covers increased the soil moisture respect to bare soil conditions. Also, how the presence of soil water with stable water isotope signatures close to groundwater reflect the hydraulic lift process carried out by both plant species.

-*How does the presence of a dense overstory affect the understory and forest floor evaporation?*
Chapters 6, 7 and 8 analyze the evaporation process within a Temperate Evergreen Needle Forest in The Netherlands (N: 52°15′4″ – E: 5°41′24″). Chapter 6 explores the influence of the forest floor layer on the evaporation process. This chapter explains how the thin layer composed by mosses and litter affects the soil evaporation and the isotopic signature of soil water. Chapter 7 compares the main methods used to sample water vapor in the air for stable isotope analysis. The evaluation includes cryogenic bath, three types of sampling bags and a laser spectrometer as benchmark. Chapter 8 investigates the evaporation process at stand level applying continuous measurements of stable water isotopes along the forest canopy. It combines hydrometric measurements with stable isotope data to provide a comprehensive analysis of the evaporation. Finally, Chapter 9 compiles the main conclusions of all the chapters providing a description of how forest structure affects evaporation.

2

A thirsty growing forest

Tropical seasonality and structural complexity

The seasonal showers on the horizon arise
moving forward like a wall of dark,
wetting everything along their path
turning the brown into a green alive.

Parts of this chapter are based on:

Calvo-Alvarado, J., **Jiménez-Rodríguez, C.**, Calvo-Obando, A., Marcos do Espírito-Santo, M., and Gonçalves-Silva, T. (2018). *Interception of Rainfall in Successional Tropical Dry Forests in Brazil and Costa Rica.* Geosciences, 8(12), 486.

2.1. Introduction

According to the Holdridge life zone system (Holdridge, 1967), Tropical Dry Forests (TDF) have a bio-temperature greater than 17 °C, an annual precipitation between 500–2000 mm yr^{-1} and a dry season that lasts 4-6 months. Last forest cover assessments concluded that the total potential extent of TDF in the Americas was 1 520 659 km^2, but there was only 519 597 km^2 (34 %) in 2010. Sadly, only 4.5 % (23 417 km^2) of the total TDF currently in the Americas is under protection by conservation areas. Remnants of TDF that are not protected are now highly fragmented across the continent and are under high anthropogenic pressure. As a result, most TDF cannot longer be considered pristine old-growth forests, but rather as a mosaic of successional stages. On the positive side, during recent decades, several studies have shown that TDF are recovering in some areas through natural restoration (Calvo-Alvarado et al., 2013; Portillo-Quintero and Sánchez-Azofeifa, 2010).

TDF landscapes are densely populated, because agriculture development is favored by the good climate and soil conditions for cropping; therefore, there is a high dependency on the availability of surface or underground water resources. Recent analysis indicated that > 44 % of the cities of the Neotropics are located within dry ecoregions and > 66 % of reservoirs and dams in the neotropics are located within these dry ecoregions (Portillo-Quintero et al., 2015). Consequently, it is necessary to avoid greater negative effects from soil erosion, pollution, and sedimentation of rivers, streams, and reservoirs. It is important to understand that conservation of TDF maintains and enhances ecosystem services by increasing the landscape's resilience to hydrological impacts from climate change. Hence, more research is needed on the hydrological dynamics of TDF landscapes and their interaction with land use and climate change scenarios to generate suitable strategies to reduce a myriad of detrimental consequences.

Forest ecosystems have a direct influence on the spatial and temporal distribution of precipitation because of their canopy structure (Guswa, 2012). This layer is highly heterogeneous due to the angle, size, and location of twigs, branches, leaves, species composition, tree density, and heights (Pypker et al., 2011). Thus, interception of precipitation in forest ecosystems plays an important role by capturing water on plant surfaces, increasing evaporation, and delaying the response of streams to rainfall events. Tropical forests have a high capacity to reduce significantly the effective or net precipitation that reaches the soil, and this could modify infiltration (Bruijnzeel, 2004; Cavelier and Vargas, 2002).

In the meantime, the effects of forest age or successional forest stages on interception of precipitation have only been studied widely in forest plantations, temperate forests, and a few tropical rain forests (Cavelier and Vargas, 2002; Crockford and Richardson, 2000). The interception capacity of TDF successional stages has not been studied with the same effort, except in Costa Rica, Panama, and Brazil (Jiménez-Rodríguez and Calvo-Alvarado, 2013; Oliveira-Freitas et al., 2016; Zimmermann et al., 2013). Evaluation of precipitation interception is indispensable

to determine the effective precipitation reaching the soil, which provides a better hydrological application to determine the water fluxes. However, structural elements of the forest as canopy density, tree species and characteristics change with forest age; modifying the canopy (Pypker et al., 2011). As a consequence, it is expected to experience changes in the interception of precipitation capacity of successional stages of TDF. Considering the registered changes of seasonality's patterns in tropical dry regions (Feng et al., 2013b), it is necessary to understand the role of interception in dry forests. This chapter aims to evaluate and to compare the interception fluxes of three successional stages of TDF in Costa Rica. Thus describing how the forest structural parameters affect the estimates of precipitation interception of the three successional stages of TDF.

2.2. Methods

2.2.1. Study Site: a Tropical Deciduous Broadleaf Forest

Santa Rosa National Park (N: 10°50′28″ – W: 83°37′10″) is located in the Área de Conservación Guanacaste on a Cretaceous geological formation at the North-West Pacific coast of Costa Rica (Figure 2.1). Leiva et al. (2009) described a wide variety of soil types, where the study site soils are classified as Entisols, Vertisols, and Mollisols under the USDA soil classification System (Staff, 2014). Also, these soils have an Ustic soil water regime. The selected locations are characterized by the presence of a volcanic tuff layer beneath 50 cm depth, creating an impermeable soil layer during the wet season (Leiva et al., 2009). This protected area has a mean annual temperature of 26.6 °C, a mean annual precipitation of 1678.0 mm yr^{-1} (period from 1979 to 2009), and a potential evaporation of 1551.4 mm yr^{-1}. The dry period of five months extends from December to April each year, while the monthly water availability during wet season exceeds the 100 mm $month^{-1}$.

The ecosystem is classified as a Tropical Dry Forest (Holdridge, 1967) and the land cover as Tropical Deciduous Broadleaf Forest (Tang et al., 2019). Santa Rosa National Park is characterized by a heterogeneous landscape dominated by a matrix of secondary forests in three successional stages (Kalacska et al., 2004). Early stage is dominated by deciduous tree species, with a high abundance of shrubs, small trees, grasses, and bare soil. Intermediate stage is composed by lianas, deciduous trees, and presence of shadow tolerant species. Late stage is dominated by evergreen and deciduous species at the canopy and shadow tolerant species at the understory. Nine permanent plots of 1000 m^2 (50 m x 20 m) were distributed in the three successional stages of TDF described by Kalacska et al. (2004) for Santa Rosa National Park. Meteorological data was recorded by a permanent station located at 301 m asl within the national park. This station is located at a maximum distance of 5 km from the plots.

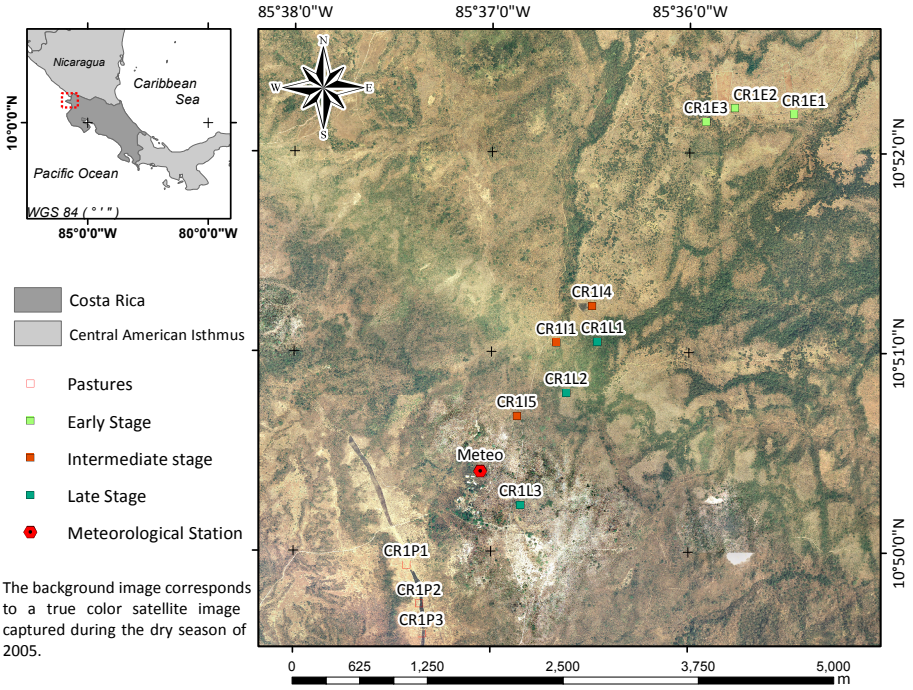

Figure 2.1: Location of the permanent plots of Tropical Dry Forest selected within Santa Rosa National Park. The pastures describe the initial condition that gave origin to the successional stages of TDF (early, intermediate and late) according to Kalacska et al. (2004).

2.2.2. Experimental Design: Interception Trial

Due to logistic limitations, the study evaluated only one rainy season and three plots per stage in each site between August and October 2013. The sampling protocol described by Jiménez-Rodríguez and Calvo-Alvarado (2013) was followed. All samples were collected before 8:00 am after every rainy day to prevent evaporation from the gauges and the stemflow containers in the following order: early, intermediate, and late successional stages. Each plot was equipped with one rain gauge at 1.5 m above the ground that was placed in a nearby open area to measure gross precipitation (P_{Gr}). Due to the absence of large canopy gaps, most of the plots required to place a funnel at least 2 m above the canopy and connected to a hose towards a 5 L container which was placed at ground level for daily measurements. Due to the reduced time available for measuring the nine plots in each site, 20 funnel type gauges were placed to sample throughfall (P_{TF}) in each plot. A revolving sampling technique was implemented to reduce the standard error of the estimation caused by the high variability in the horizontal distribution of the tree crowns (Lloyd and F., 1988). Hence, the throughfall gauges were distributed on the forest floor at 2.5 m from each other along the central axis of the plot. After measuring five events, the sampling line was moved 5 m to either side of the central axis, and

then it was moved 10 m, 15 m, and 20 m away from the central axis for subsequent sampling to cover the entire plot area. Once one rotation was completed, the trial was reset again from the central axis. The volume of water collected by each rain gauge (P_{Gr} and P_{TF}) was converted into mm d^{-1} with respect to the funnel collection area.

Stemflow (P_{SF}) was measured by selecting four trees per plot that corresponded to the 20, 40, 60, and 80 percentiles of the distribution of plot tree diameters for a total sample of 12 trees per successional stage. For each selected tree, the projected crown area was estimated with the average tree crown diameter using the longest and shorter diameters of the crown. The trees were chosen with no regard to species (Table 2.1), but rather to the required diameter class, straightness of the stem, and with uniform distribution of branches. The stemflow was collected through a spiral collar attached to the trunks with nails and sealed with silicone paste. Each spiral collar conducted the stemflow to a polyethylene container of 50–200 L depending on the tree size and placed at the foot of the tree. The collected volume of water in L per tree was converted into mm d^{-1} with respect to tree crown area. Stemflow was projected to an area of 1.0 m^2 by calculating the average stemflow (mm) of all evaluated trees and multiplying it by the mean number of trees per square meter per plot (Gerrits et al., 2009).

2.2.3. Data Analysis: Forest Structure and Water Fluxes

Forest composition was evaluated using the number of tree species in each plot (ρ_{sp}, species 0.1 ha^{-1}). Forest structure was evaluated through the tree basal area (A_{trees}, m^2 0.1 ha^{-1}), mean tree height (z_{tree}, m), tree density (ρ_{trees}, trees 0.1 ha^{-1}), Holdridge Complexity Index ($\mathrm{H_{CI}}$), and the plant area index (PAI). PAI was measured during the rainy season using hemispherical photographs analyzed with the software Gap Light Analyzer (Frazer et al., 1999) and $\mathrm{H_{CI}}$ (Holdridge, 1967) is determined with equation 1. Net precipitation (P_{Net}) was defined as the water that

Table 2.1: List of the tree species selected for stemflow measurements per successional stage in Santa Rosa National Park.

Early	Intermediate	Late
Cochlospermum vitifolium	*Astronium graveolens*	*Chrysophyllum brenesii*
Genipa americana	*Ateleia hebert–smithii*	*Exostema mexicanum*
Gliricidia sepium	*Bursera simarouba*	*Guettarda macrosperma*
Luehea candida	*Cochlospermum vitifolium*	*Lysiloma divaricatum*
Machaerium biovulatum	*Cordia panamensis*	*Sapranthus palanga*
Quercus oleoides	*Lonchocarpus minimiflorus*	*Semialarium mexicanum*
Rehdera trinervis	*Spondias mombin*	
	Trophis racemosa	

reached the forest floor, and it corresponded to the sum of throughfall and stemflow per plot. Intercepted precipitation (P_{Int}) was estimated with Equation 2.2 and corresponds to the the difference between gross rainfall (P_{Gr}) and net precipitation (P_{Net}).

$$\mathrm{H_{CI}} = \frac{z_{\mathrm{tree}} A_{\mathrm{tree}} \rho_{\mathrm{tree}} \rho_{\mathrm{sp}}}{1000} \tag{2.1}$$

$$P_{\mathrm{Int}} = P_{\mathrm{Gr}} - (P_{\mathrm{TF}} + P_{\mathrm{SF}}) \tag{2.2}$$

The relationship among gross rainfall and the other fluxes was evaluated through linear regression models. Linear regression models applied to each successional stage were defined by $y = \alpha + \beta P_{\mathrm{Gr}} \pm \epsilon_{\mathrm{i}}$ (Klamerus-Iwan et al., 2020), where α is the interception with the y axis, β is the slope of the equation that represents the proportion of water retained by the canopy, and ϵ_{i} is the error associated with the estimate. Both the regression coefficient and the intercept were tested to determine if they were statistically different from zero ($p < 0.05$ and $p < 0.10$). For those regressions that produced non-significant intercepts, no attempt to remove them from the model was made aiming to maintain all equations equal.

Finally, a Pearson correlation matrix was obtained to study the relationship of net rainfall with forest structural parameters by pooling all data from the nine plots of all stages. Statistical significance was fixed at $p < 0.05$ and $p < 0.01$. Each significant correlation was examined graphically by plotting the two correlated variables to determine the validity of the relationship. If the trend revealed that the significance of the correlation was from the influence of outliers, then it was discarded.

2.3. Results

Precipitation at Santa Rosa National Park during the hydrological year 2013–2014 was 1118 mm $\mathrm{yr^{-1}}$. Daily temperature fluctuated between 22.4 °C and 27.4 °C, with a mean annual temperature of 25.1 °C. The relative humidity increased from a minimum of 51.4 % in March to a maximum of 98.4 % in the rainy season. During the sampling period, SRNP recorded 372.7 mm of rain in the early successional stage, 385.2 mm in the intermediate stage, and 327.8 mm in the late stage, with a maximum daily rainfall of 83.5 mm $\mathrm{d^{-1}}$. Forest structure differs strongly among and within successional stages (Table 2.2). Forest height, tree species and plant area index increase accordingly with forest age following the trend: Early < Intermediate < Late. Holdridge Complexity Index and tree basal area increases after the early stage, remaining similar in the intermediate and late stages. Tree density is larger in the Intermediate stage than Early and Late stages, mainly due to one plot in particular: CR1I4.

Table 2.2: Summary of the main structural parameters measured in different forest stages of tropical dry forest in Costa Rica.

Stage	Plot	z_{tree}	ρ_{trees}	ρ_{sp}	A_{trees}	H_{CI}	PAI
Early	CR1E1	9.0	21	5	0.3	0.3	2.8
	CR1E2	9.8	72	13	0.4	3.7	1.5
	CR1E3	10.8	32	11	1.1	4.4	4.3
	Average	9.9	41.7	9.7	0.6	2.7	2.9
Intermediate	CR1I1	20.3	46	22	4.1	84.2	7.1
	CR1I4	16.0	199	17	2.3	125.6	4.3
	CR1I5	13.3	38	14	1.1	7.8	5.5
	Average	16.5	94.3	17.7	2.5	72.5	5.6
Late	CR1L1	23.0	74	23	2.7	105.7	6.3
	CR1L2	19.5	63	19	2.4	56.0	6.6
	CR1L3	24.7	49	16	3.1	60.0	5.2
	Average	22.4	62	19.3	2.7	73.9	6.0

Note: z_{tree} is the average tree height, ρ_{trees} is the tree density, ρ_{sp} is the number of tree species, A_{trees} is the tree basal area, H_{CI} is the Holdridge complexity index, and PAI is the plant area index.

Throughfall and stemflow fluxes increased with gross precipitation in all stages (Figure 2.2). Throughfall increases linearly with correlation coefficients higher than 0.96 in all the stages excepting the late stage, which shows an R^2 value of 0.88 due its scattered distribution (Table 2.3). Stemflow increases with the gross precipitation with a wide variability (Figure 2.2) having low determination coefficients. Effective precipitation is influenced by the forest stage considering both, effective precipitation and interception.

As expected, forest interception was higher when rainfall events were small, decreasing with the increment of rainfall event size. This as a consequence of a decline in the interception capacity as the foliage and bark became saturated during the rainfall event. It is important to note that the dispersion of points for throughfall and stemflow have a nearly linear trend in all stages at both sites. However, the dispersion of the points increased as it progressed from the early to the late stages. This dispersion reflected the high variability in forest structure among the plots, particularly in the late stage. Stemflow was lowest in the early stage (0.2 %) and highest in the intermediate and late stages (0.3 %). These results were expected due to the dominance of larger trees in the advanced stages that had higher collecting capacity due to more developed crowns, branches, and trunks. According to Table 2.4 and Figure 2.4, net precipitation resulted in a significant correlation only for PAI ($r = -0.755$, $p < 0.05$). This , proving that more complex TDF structures in Costa Rica can retain more water than simpler forest stands.

The coefficients of determination (R^2) of throughfall were > 0.94 in all stages, using the gross daily precipitation as the independent variable (Table 2.3). These

Table 2.3: Summary of the linear regression analyses of forest interception water fluxes in relation to P_{Gr} in three successional stages of tropical dry forest in Costa Rica.

Water Flux	**Forest Stage**	**n**	**R^2**	**SE**	**Regression Coefficients**	
				ϵ	α	β
Throughfall	Early	89	0.992	1.564	-0.285	0.899 ***
	Intermediate	89	0.980	2.264	-0.670**	0.776 ***
	Late	78	0.940	3.229	0.938 *	0.567 ***
Stemflow	Early	89	0.888	0.022	-0.012 ***	0.003 ***
	Intermediate	89	0.559	0.052	0.005	0.002 ***
	Late	78	0.565	0.064	-0.002	0.003 ***
Effective Precipitation	Early	89	0.992	1.565	-0.298	0.902 ***
	Intermediate	89	0.980	2.257	-0.665 *	0.779 ***
	Late	78	0.939	3.267	0.936 *	0.570 ***
Interception	Early	89	0.656	1.565	0.298	0.098 ***
	Intermediate	89	0.817	2.257	0.665 *	0.221 ***
	Late	78	0.900	3.267	-0.936 *	0.430 ***

Note: $y = \alpha + \beta P_{Gr} + \epsilon$, n = sample size, * is statistically significant ($p < 0.10$), ** is statistically significant ($p < 0.05$), *** is statistically significant ($p < 0.001$), SE= standard error.

Table 2.4: Pearson correlation matrix among interception of precipitation and structural variables within TDFs in Costa Rica.

	z_{tree}	ρ_{trees}	ρ_{sp}	A_{trees}	$\mathbf{H}_{CI}$	**PAI**	P_{Int}
z_{tree}	1.000						
ρ_{trees}	0.137	1.000					
ρ_{sp}	0.808**	0.321	1.000				
A_{trees}	0.886**	0.199	0.835**	1.000			
$\mathbf{H}_{CI}$	0.888**	-0.021	0.851**	0.841**	1.000		
PAI	0.767*	-0.055	0.766*	0.820**	0.783*	1.000	
P_{Int}	0.463	0.085	0.559	0.456	0.423	0.755*	1.000

Note: z_{tree} is the average tree height, ρ_{trees} is the tree density, ρ_{sp} is the number of tree species, A_{trees} is the tree basal area, H_{CI} is the Holdridge complexity index, and PAI is the plant area index. The p-values are significant at $p < 0.05$(*) and $p < 0.01$ (**).

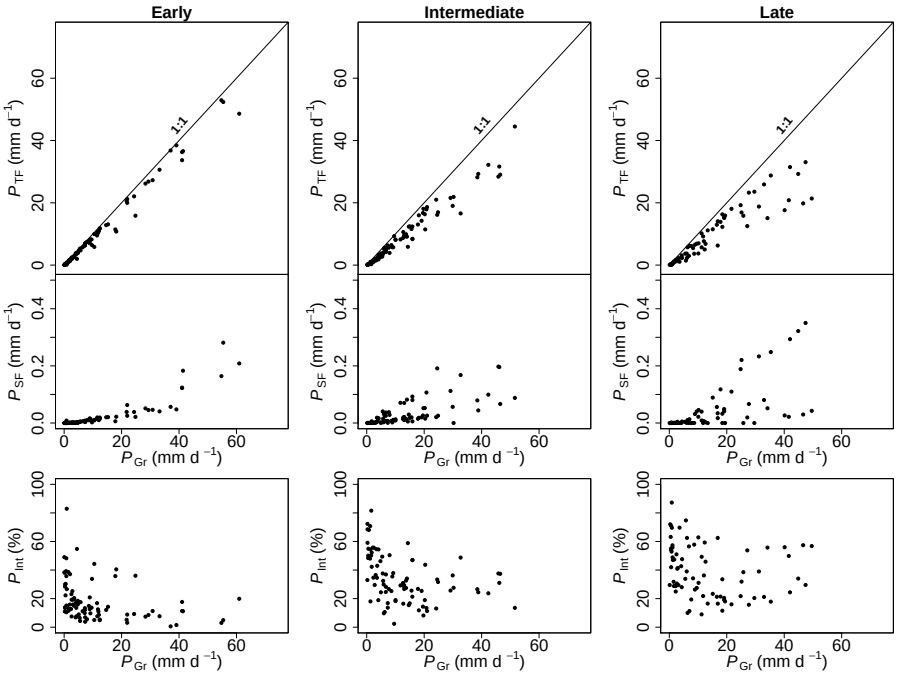

Figure 2.2: Daily fluxes of throughfall and stemflow with respect to gross precipitation among successional stages of Tropical Dry Forest in Costa Rica.

good linear regression adjustments were the result of the sampling technique and the selected sample size for this study. Because throughfall represented the highest proportion of net precipitation, the coefficients of determination for equations for net precipitation had also almost identical values of R^2 and levels of statistical significance compared with the equations for throughfall. Coefficients of determination (R^2) for stemflow were > 0.50 in all stages. Hence, in comparison to equations for throughfall, results for stemflow had lower linear regression adjustments (R^2) because of the small sample size and higher dispersion of data (Figure 2.2). The lower R^2 for the late stage was due to the high variability in structural characteristics among the late stage plots.

In general terms, most of the intercepts (α) in all equations were not significantly different from zero with $p < 0.05$ and $p < 0.10$. Regardless of these results and as stated in the methodology, the models were not forced through the origin, so that all equations were equal and allowed a fair comparison of the slopes (β) among stages and between sites. In all equations, the slopes (β) were statistically significant at $p < 0.05$, hence, these equations provided a tool to estimate the water fluxes in successional TDF of Costa Rica.

There are few studies in the literature that analyze the precipitation partitioning

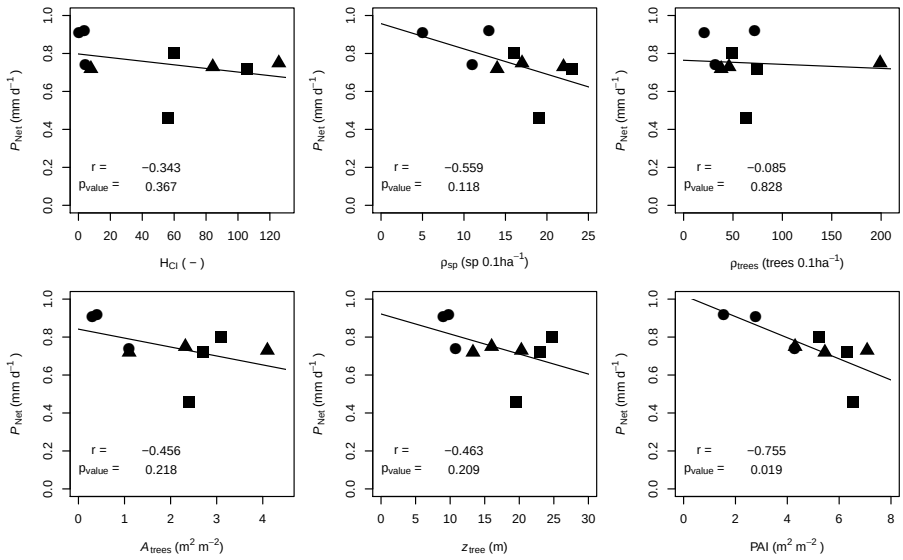

Figure 2.3: Distribution of net precipitation respect to forest structural parameters of the three successional stages (early stage: circles, intermediate stage: triangles, and late stage: squares). Tendency solid lines include the nine plots. The p-values (p) of Pearson coefficients (r) are significant at $p < 0.05$ (*) and $p < 0.01$ (**).

in TDF, and it is even more difficult to find information that considers the effect of successional stages. Oliveira-Freitas et al. (2016) found that throughfall rates in early stages of 79.3 % and in intermediate stages of 72.6 %, and Lorenzon et al. (2013) reported 84.39 % and 73.04 % for TDF in Brazil in early and intermediate successional stages. Oliveira-Freitas et al. (2016) found stemflow rates of 0.44 % and 1.52 % for the early and intermediate stages, whereas Lorenzon et al. (2013) found 0.68 % and 1.8 %, respectively. According to a review by Cavelier and Vargas (2002), stemflow rates ranged from 0.3 % to 1.8 % in 15 studies conducted in Brazil and Colombia in dry to moist tropical forests (1500 mm yr^{-1} to 3140 mm yr^{-1}). Hence, the estimates for stemflow were within the reported range of estimates in the literature. It is important to point out that according to literature review, the slopes (β) of the equations for net precipitation with gross precipitation are the best estimation of the rainfall interception of the forest stages that were analyzed (Carlyle-Moses and Gash, 2011).

2.4. Discussion

Forest canopies have a direct influence on the spatial and temporal distribution of precipitation, as a consequence of the canopy structure (Bulcock and Jewitt, 2012; Gerrits et al., 2007; Guswa, 2012; Livesley et al., 2014; Schumacher and Christiansen, 2015). TDFs are characterized by the presence of a dense canopy

and understory compose by branches and twigs (Janzen, 1988; Murphy and Lugo, 1986). Meanwhile the age of secondary forests in Latin America influences the diversity differences among successional stages of TDF (Mora et al., 2015) as well as biomass recovery due to forest resilience (Poorter et al., 2015, 2016). Intermediate stages of TDF are highly diverse and rich in tree species due to their transitional condition between the young and old forest stages (Hilje et al., 2015). This transitional condition allows them to have larger growth rates than the late stages of TDF (Carvajal-Vanegas and Calvo-Alvarado, 2013). These conditions depict a set of structural variables that drive multiple hydrological parameters needed to be sized in TDFs as the interception of precipitation.

Effective precipitation differs among forest stages, showing a specific pattern for most of the plots with an asymptotic behavior after a specific rainfall size. This tendency can be easily observed in the early plots, increasing the variability with the increment of forest structure. The positive correlation between interception and forest structure in terms of plant area index and canopy height is due to the increment in interception area, allowing to hold more water per rainfall event on a daily basis. Throughfall dependency on precipitation size drives the high correlation coefficients showed for most of the plots, excepting the late stage. The high plant area index of this stage affects the variation of effective precipitation.

Traditional rainfall interception studies analyze the variation of rainfall interception as a linear regression, analyzing the slope as the percentage of rainfall interception. This assumption is based on the fact that forest canopy has the capacity to retain rain, and it changes depending directly with the rainfall event duration and intensity (Carlyle-Moses and Gash, 2011). However, when the data analysis is focused just on the percentage of rainfall retained in terms of a fixed percentage, the dynamic effect of the canopy structure is diminished.

Specific stand characteristics as height and tree morphology influence the total interception of precipitation (Bialkowski and Buttle, 2015; Saito et al., 2013; Schumacher and Christiansen, 2015; Spencer and van Meerveld, 2016). The presence of trees with larger bark roughness as *Quercus oleoides*, *Spondias mombin* and *Lysiloma divaricatum* determine the low stemflow rates observed. Tree species with smooth bark as *Redhera trinervis* or *Genipa americana* allow faster stem flow and low interception. Stemflow plays an important role in limited water environments despite the low rates (Carlyle-Moses, 2004), because the water movement towards the soil and tree architecture allows redistribution of water close to the boles and soil water recharge with it (Bialkowski and Buttle, 2015; Spencer and van Meerveld, 2016).

Forest growth of secondary ecosystems is characterized by a quick change in tree species and morphologies, changing the canopy interception capacity during the forest development (Zimmermann et al., 2013). This change is visible in the high correlation between plant area index and precipitation interception on the

evaluated plots despite the omission of stems and boles, it is how the how the plant area index is a good parameter to correlate the interception capacity of forest stands (He et al., 2014). In temperate climates, the interception of precipitation in seasonal forests correlates positively with tree species diversity (Kramer and Holscher, 2009), while the throughfall can be reduced by wind speed (Staelens et al., 2008).

2.5. Conclusions

Growing stages of Tropical Dry Forest (TDF) increased their canopy height (z_{tree}), species density (ρ_{sp}), tree basal area (A_{trees}), plant area index (PAI) and Holdridge complexity index (H_{CI}) according to their successional stage (Early < Intermediate < Late). Tree density (ρ_{trees}) did not follow this trend because the Intermediate stage had a larger tree density than the other two stages as a consequence of the rotation of tree species among stages. Forest canopy represents the first obstacle of precipitation in its way towards the soil. The canopy cover reduces the amount of water reaching the soil and this change relays in the forest structure in terms of forest species, size, and tree densities. Forest complexity of successional stages of TDF increased with age and consequently its capacity to intercept precipitation. Older forest stands intercept more water than the previous secondary stages. Effective precipitation decreases from a maximum in the Early stage ($\beta = 0.90$) to a minimum in the Late stage ($\beta = 0.57$). This diminution in water fluxes towards the forest floor is driven mainly by throughfall of all stages meanwhile, the stemflow represents a small portion of the effective precipitation during the trial ($P_{\text{SF}} < 0.5\%$). The small stemflows are linked to tree characteristics such as bark roughness degree. Finally, plant area index (PAI) is the best forest structural descriptor of interception and effective precipitation for the successional stages of TDF. This because it encompasses all plant surfaces able to intercept water. PAI had significant correlation coefficients ($p<0.05$) respect to interception and effective precipitation, a condition that was not accomplished by other parameters (e.g., Holdridge complexity index).

3

A shadowed steam machine

Contribution of understory evaporation in a tropical wet forest

Like miners underground
understory plants work hard,
with few sunbeams reaching the ground
they push the water as vapor into the sky.

This chapter are based on:

Jiménez-Rodríguez, C.D., Coenders-Gerrits, M., Wenninger, J., Gonzalez-Angarita, A., and Savenije, H. (2020). *Contribution of understory evaporation in a tropical wet forest during the dry season.* Hydrol. Earth Syst. Sci., 24, 2179–2206

3.1. Introduction

Evaporation from tropical forests export more than 1000 mm yr^{-1} of water to the atmosphere (Lion et al., 2017; Loescher et al., 2005; Sun et al., 2016). Partitioning of E is usually focused on the differentiation among E_t, E_s and E_i (Kool et al., 2014; Moore et al., 2018; Xiao et al., 2018). However, the contributions of different sections of the canopy in forest ecosystems are often not considered and are not yet fully understood. The differentiation of E fluxes according to the vertical forest structure had been performed in savanna woodlands and boreal forests (Heijmans et al., 2004; Iida et al., 2009; Scott et al., 2003; Yepez et al., 2003). However, in tropical regions the vegetation is more complex than the aforementioned ecosystems (savanna woodlands and boreal forests) and few data concerning the differentiation between understory and overstory evaporation is available (Aparecido et al., 2016; Loescher et al., 2005; Read, 1968).

In tropical forest ecosystems (TFE) the available radiation along the canopy determines the photosynthesis rates and consequently the E_t flux (Hogan and Kattan, 2002). The high radiation received by the overstory in tropical forests allow the emergent trees to transpire more water (Aparecido et al., 2016). Thus most of the total evaporation is coming from the overstory during the dry season (Kunert et al., 2017). Differences in forest evaporation between wet and dry seasons depend on energy and water availability, respectively. Water availability during the wet season does not limit the forest evaporation which depends mostly on the available energy along the canopy gradient (Hogan and Kattan, 2002; Loescher et al., 2005). Contrary to the wet season, the dry season experiences a strong reduction on the precipitation rates triggering physiological responses on the trees. One of these responses is the increment of litterfall (Peters, 2016; Raich, 2017), which depends on precipitation and wind conditions. This temporal drop of leaves during dry season allows the creation of a thinner canopy layer respect to the canopy in the wet season, which can alter the transpiration of understory species such as *Geonoma cuneata* H. Wendl. ex Spruce or *Piper arieianum* C.DC. which exploit the most shaded microsites (Chazdon, 1986, 1992).

The understory environment of tropical moist forests is highly variable. This layer receives up to 4 % of the radiation received by the overstory, while canopy gaps can receive 4.3 times more radiation (Tymen et al., 2017) and almost three times higher vapor pressure deficit (Fetcher et al., 1985). These conditions can induce larger transpiration rates as consequence of the plant physiological response to rise in air temperature and vapor pressure deficit (Adelman et al., 2008; Hogg and Hurdle, 1997). This determines the small daily contribution of the understory heat fluxes to the net radiation. However, during days with low net radiation this contribution can be significant at ecosystem level (Loescher et al., 2005). Additionally, the soil water reservoir used by understory shrubs and overstory trees differ. Shrub plants are more dependant on soil water, whereas the trees can access deeper water reservoirs (Ghimire et al., 2018). The number of plant species in TFE can exceed 50 species ha^{-1} (Eilu et al., 2004; Naidu and Kumar, 2016) with

densities above 500 trees ha^{-1}(Crowther et al., 2015). Also, the heterogeneous spatial aggregation of tree species in TFE (Volkov et al., 2005) increases the number of variables that influences the E_t flux. This increases the number of E_t sources, making it difficult to differentiate between other evaporation fluxes such as E_s or E_i.

The structural complexity of TFE is defined by environmental variables such as altitude, climate and geomorphology (Holdridge, 1967; Gomez, 1986; Hartshorn, 2002; Guariguata and Ostertag, 2002). The forest canopy can be segmented into four layers according to vegetation height and light requirements. First, the overstory includes all the trees fully illuminated at the top of the canopy. It is followed by the understory which is composed of woody plants located in the shade beneath the overstory. Third, the ground layer includes all seedlings, herbaceous vegetation and small shrubs. Finally, the forest floor includes the uppermost layer of soil (O Horizon) and the litter layer lying on it (Nadkarni et al., 2004; Parker, 1995).

Tropical canopies have a wide number of epiphytes growing on the tree tops along the canopy that influence the effective precipitation, water uptake and E processes (Ah-Peng et al., 2017; Cavelier and Vargas, 2002; Gotsch et al., 2016; Porada et al., 2018; Zotz, 2016). Thus allowing the tall canopies to create a microclimate bellow its shadow (Fitzjarrald and Moore, 1995; Frey et al., 2016; Nakamura et al., 2017). These differences are linked to the energy balance variation along the forest profile, resulting in changes of total evaporation (Ehleringer and Dawson, 1992). Most of the evaporation studies in the tropics focus on yearly patterns (Baldocchi and Ryu, 2011; Calder et al., 1986; da Rocha et al., 2009; Loescher et al., 2005; Schellekens et al., 2000), the wet season (Read, 1968; Wright et al., 2017) or time windows of less than one day to study specific processes such as aerodynamic conductance (Holwerda et al., 2012). But few attempts deeping the knowledge of dry season evaporation has been found (Harper et al., 2014). Tropical forests are highly sensitive to water variability (Tan et al., 2013) and understory light availability (Brenes-Arguedas et al., 2011), which are the main factors defining the distribution of plant species. This because tree seedlings are prompted to use water dripping from the canopy by the condensation of convective fog during the dry season (Liu et al., 2010). Consequently, changes in the canopy conditions can modify the understory composition and with it the future forest evaporation. The aforementioned underlines the need to provide more information about the evaporation process during the dry season in tropical forests, as well as the role played by understory vegetation during forest evaporation. This chapter aims (1) to estimate the total evaporation flux during the dry season in a tropical wet forest, (2) to differentiate the contribution among canopy layers depending on their location with the canopy, (3) to define the contribution of plant transpiration to the dry season evaporation at forest level, and (4) to describe the temporal dynamics of the stable isotope signatures during dry season. To study this, we made use of the energy balance to quantify the fluxes and stable water isotopes to trace the sources of water vapor.

3.2. Methodology

3.2.1. Study Site: Tropical Evergreen Broadleaf Forest

La Selva Biological Station (LSBS) is located on the Caribbean lowlands of Costa Rica (N: 10°26′0″ – W: 83°59′0″) (Figure 3.1). This region has a mean annual precipitation of 4351 mm yr^{-1}, with a monthly precipitation of more than 100 mm $month^{-1}$ (Loescher et al., 2005). A short dry season is present in this region between February and April and it is characterized by a reduction of precipitation without experiencing a water deficit (Sanford Jr. et al., 1994; Lieberman and Lieberman, 1987). The mean annual temperature is 26.3 °C with a mean daily difference of 9.5 °C between the lowest and the highest temperature. The potential evaporation (E_p) accounts for 1585 mm yr^{-1} (Figure 3.2). The research station is covered by a series of old growth and secondary forests, as well as small forest plantations of different species and mixed plots (Figure 3.1).
(Putman et al., 2019)

The monitoring period included the dry season of 2018 for 62 days between 2018-1-25 and 2018-3-26. During this period the meteorological data was collected continuously and the water sampling was done during 3 different periods: 2018-01-30 to 2018-02-09 (sampling period A), 2018-02-19 to 2018-02-26 (sampling period B) and 2018-03-19 to 2018-03-25 (sampling period C). This study was carried out at the Major Research Infrastructure plot (MRI–plot) which has an area of 1 ha of old growth forest located on the middle terrace of the Puerto Viejo river (Sanford Jr. et al., 1994). The MRI–plot is situated in the upper section of a small hill facing South–West towards an affluent of the Puerto Viejo river. The soil is classified as Inceptisol (Andic Humidotropept) under the USDA classification system (Sollins et al., 1994). This plot has 88 species among trees, lianas and palms with more than 10 cm of diameter. Tree density was 371 trees ha^{-1} in 2017 with 60.6 % of the trees within 10–20 cm diameter. The most abundant species are the palm *Welfia regia* H.Wendl. and the tree *Pentaclethra macroloba* (Willd.) Kuntze with 56 trees ha^{-1} and 43 trees ha^{-1}, respectively. Based on data from Tang et al. (2012), the average leaf area index (LAI) in 2005 of the plot was 3.56 m^2 m^{-2} (Figure 3.1). Also, this plot is located within an area of small changes of top canopy height and a neutral change of tree biomass fixation (Dubayah et al., 2010). Canopy structure on the MRI–plot was split into 3 layers. The lower understory (lu) ranges from the ground surface up to 2 m height, it includes the ground surface, the litter layer and small shrubs. The upper understory (uu) goes up to 10 m height covering the crowns of medium palms, tall bushes and small trees. The overstory (ov) is the tallest canopy layer and it includes the crowns of the tallest trees of the plot.

3.2.2. Instrumentation

A meteorological station is located 750 m East from the MRI–plot (Figure 3.1). This station monitors precipitation, air temperature, relative humidity, solar radiation, photosynthetic active radiation, atmospheric pressure, leaf wetness, wind

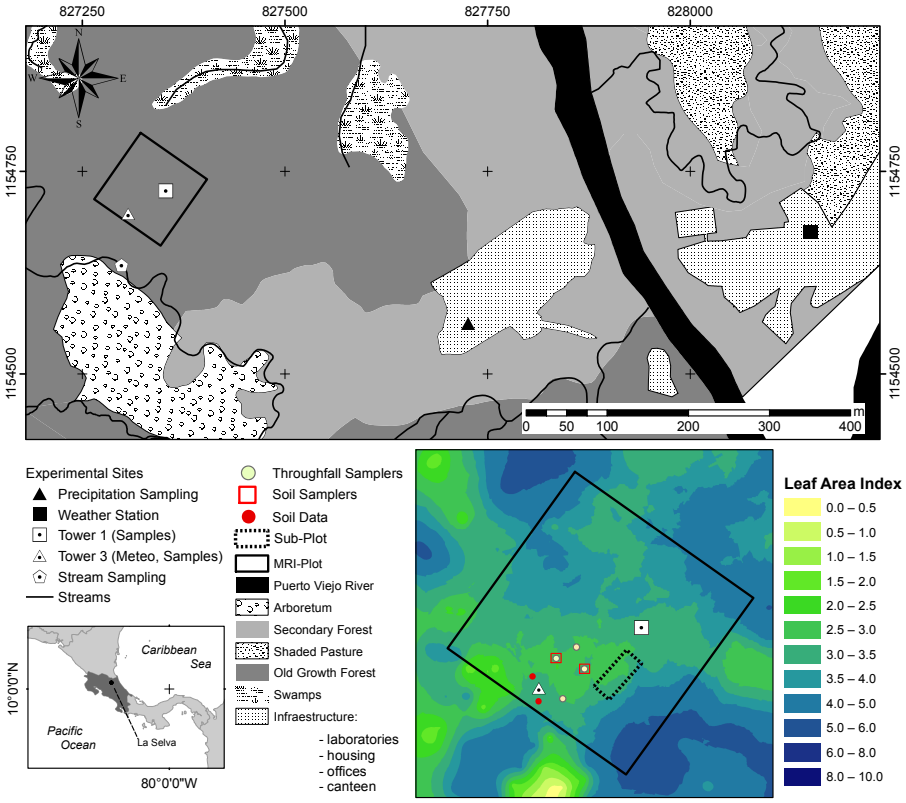

Figure 3.1: Location of sampling points and the Major Research Infrastructure (MRI–plot) plot at La Selva Biological Station in Puerto Viejo de Sarapiquí, Costa Rica. The land cover map shows the location of the MRI–plot in the Old Growth Forest and the bottom left image depicts the leaf area index (LAI) distribution in the plot.

speed and wind direction. All sensors are controlled by a Campbell Scientific© data logger, averaging the data over 15 min time intervals and storing it automatically on an online server at the research station. The MRI–plot has 3 research towers with different heights (Tower 1: 34 m, Tower 2: 25 m (under repair during the experiment) and Tower 3: 43 m). Tower 3 is located within a canopy depression of around 400 m^2, and the other two towers allow the access to the forest canopy at the center of the plot (Figure 3.1). A series of sensors were placed along Tower 3 to monitor different meteorological variables during the study period. Air temperature and relative humidity were installed 1.5 m away from the tower structure at 2 m, 10 m, 37 m and 43 m height; and protected with a radiation shield (ONSET®; RS3-B). Precipitation, solar radiation and photosynthetic active radiation were measured at the highest point of Tower 3. Soil temperature, soil moisture and solar radiation were measured at ground level near the base of the tower. The radiation data was recorded with a Campbell Scientific© data logger (model: CR10x) every 15 min,

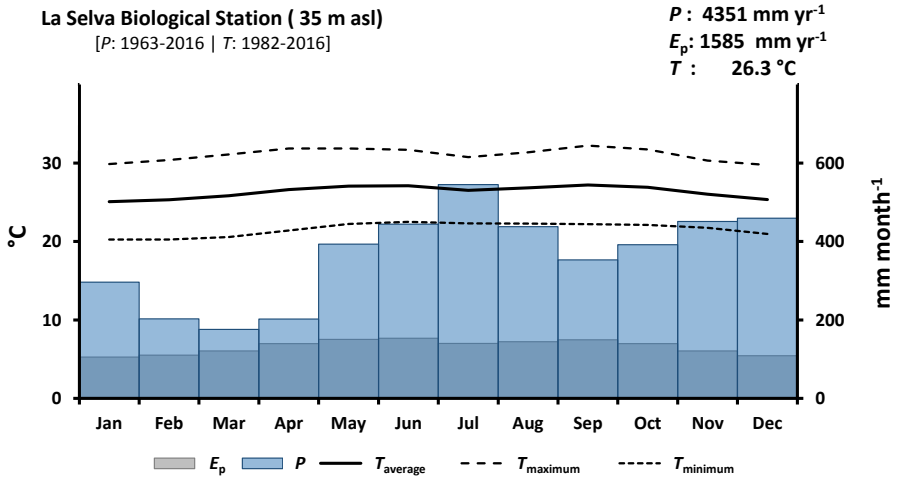

Figure 3.2: Climate diagram of La Selva Biological Station based on records of 54 years of precipitation (P) and 35 years of temperature (T) (Source: https://tropicalstudies.org/). The potential evaporation (E_{p}) was estimated with the temperature data and Thornthwaite equation (Thornthwaite, 1948).

soil temperature was recorded with a HOBO 4-channel data logger (ONSET® part code: U12-008) and the other sensors with a HOBO USB Micro Station (ONSET® part code: H21-USB) every 5 min.

Throughfall measurements were carried out at ground level with 15 rain gauges, 12 of them distributed within a sub plot of 200 m^2 (Figure 3.1) to estimate the bulk throughfall and 3 additional ones placed around Tower 3 to collect daily samples. The measurements were carried out every 24 hr before 7:00 a.m. When isolated rain events happened during the day, the precipitation was measured right after the event. Throughfall was measured in mL with a measuring cylinder of 500 mL with a scale of 0.5 mL. All volumes were translated into mm of water according to the rain gauge surface area. Leaf area index (LAI, $m^2\,m^{-2}$) was determined with hemispherical pictures collected at the raingauge locations within the MRI plot at 50 cm height from the ground. These images were processed with the Gap Light Analyzer (GLA) software (Frazer et al., 1999). All dasometric data of the MRI–plot was provided by the scientific team of LSBS. This data set includes the scientific names of all trees, palms and lianas with more than 10 cm diameter measured at 1.3 m height, as well as the branching heights (m) and tree diameters (cm).

3.2.3. Water Sampling

Different sets of liquid samples were collected at the MRI–plot, in a stream located 50 m downhill the MRI–plot, and at an open area located 400 m South–East from

the MRI–plot (Figure 3.1). Samples of bulk precipitation were collected at the open area on an event basis to determine the isotope variation from individual rainfall events, while overnight precipitation was collected the next day before 6:00 a.m. The samples were collected manually and the reservoir was replaced immediately after the measurement. The additional set of 4 rain gauges collecting bulk throughfall were placed around Tower 3 and sampled on a daily basis or shorter if it was possible. Soil water from the unsaturated zone was collected on a daily basis with soil moisture samplers (Eijkelkamp part number: 19.21.SA) of 10 cm length, with a porous polymer of 0.15μm diameter. Soil water sampling was carried out at 2 locations around Tower 3, extracting the samples from 5 cm and 15 cm depth in each location. The first 0.5 mL of every sampling were discarded to reduce the contamination from previous soil water extractions.

Stream samples were sampled daily during the low flows at the end of the sampling period as a proxy of the groundwater signature. This as a consequence of the absence of boreholes near the MRI-plot. Water vapor samples were collected with a test tube of 30 mL of borosilicate immersed in an isolated container of 500 mL filled with dry ice (-70 °C). The collection was performed at least every three hours depending on the meteorological conditions and dry ice availability during the sampling period. The samples were collected at Tower 3 at 43 m height. Transpired water was collected from the canopy of different plant species surrounding the towers. These samples were collected with polyethylene bags at least every 6 hr and transferred immediately to 1.5 mL borosilicate vials. Xylem water was extracted daily from branches or exposed roots at midday for four types of plants: palms (17 samples from 5 species), trees (21 samples from 11 species), bushes (17 samples from 10 species), and lianas (12 samples from 5 species). Detailed information on the sampled species can be found in the supplemental material. The sampled plants were selected randomly according to the plant type from all the individuals within the MRI-plot. The bark of each sample was removed before the water extraction. The xylem sample was placed within a 50 mL test tube with an insert of 30 mL and a DURAPORE® membrane filter (PES-45/25, 0.45 μm, HV). The water was extracted through centrifugation at 5000 rpm for 30 min, transferring immediately the extracted water to 1.5 mL vials. All liquid samples were stored at 6°C, whilst xylem water was stored at -10 °C to prevent the decomposition of the dissolve organics in the sample and the formation of fungi until the water samples were analyzed.

3.2.4. Energy Fluxes

The latent heat flux ($\rho\lambda E$, W m^{-2}) was determined using the energy balance equation (Equation 3.1) from the ground up to 2 m, 8 m and 43 m (Figure 3.3). This equation is based on the vertical transport of heat, neglecting the advected energy due to the lack of more detailed measurements (e.g., eddy covariance system). However, considering the tower location away from treefall gaps and at a hill top minimizes major effects of understory canopy advection (Loescher et al., 2005). The net radiation (R_{n}, W m^{-2}) was calculated with equation 3.2 applying

an albedo (a) value of 0.12 according to Loescher et al. (2005) for this forest type and incoming short wave radiation ($R_{\downarrow S}$). Incoming ($R_{\downarrow L}$) and outgoing ($R_{\uparrow L}$) long wave radiation (W m^{-2}) were determined for every time step. Ground heat flux (G, W m^{-2}) was calculated with equation 3.3 using the temperature difference (dT) between the soil temperature at 5 cm depth and the superficial soil temperature (T_{s0}). A soil thermal conductivity (k) of 1.58 W m^{-1} °C^{-1} (Pielke, 2013) was used to determine G considering the soil clay content and soil moisture condition of more than 0.40 m^3 m^{-3} during the study period. The sensible heat flux (H, W m^{-2}) was determined using equation 3.4, where T_a is the air temperature (°C) at the different heights, ρ_a is the air density (kg m^{-3}), c_p is the specific heat of the air (1.013× 10^{-3} MJ kg^{-1} °C^{-1}), and r_a (s m^{-1}) is the aerodynamic resistance to heat transfer.

$$\rho\lambda E = R_n - H - G \tag{3.1}$$

$$R_n = (1 - a)R_{\downarrow S} - R_{\uparrow L} + R_{\downarrow L} \tag{3.2}$$

$$G = k\frac{dT}{dz} \tag{3.3}$$

$$H = -\rho_a c_p \frac{T_a - T_{s0}}{r_a} \tag{3.4}$$

3.2.5. Isotopic Analysis

Relative isotope concentration of deuterium (δ^2H) and oxygen–18 (δ^{18}O) with respect to the Vienna Standard Mean Ocean Water (VSMOW) were measured with a Liquid Water Isotope Analyzer (LWIA; model 912-0008) from Los Gatos Research (LGR). We used the software LIMS 10.083 for lasers (Coplen, 2000) during the calibration, correction and determination of stable isotope signatures of the analyzed samples. Stable water isotope signatures of ^{2}H and ^{18}O were expressed in δ values (‰), representing the relative deviation from Vienna Standard Mean Ocean Water (VSMOW) (Craig, 1961). Equation 3.5 determines the line-conditioned excess (lc-excess) based on the Local Meteoric Water Line (LMWL) defined for La Selva Biological Station by Sánchez-Murillo et al. (2013) as $\delta^2H = 14.03 + 8.48\,\delta^{18}O$.

$$\text{lc} - \text{excess} = \delta^2H - 8.48 * \delta^{18}O - 14.03 \tag{3.5}$$

The "Keeling method" (Equation 3.6) was used to determine the contribution of transpiration to the atmospheric water vapor signature of total evaporation (Keeling, 1958; Xiao et al., 2018; Yakir and Sternberg, 2000; Zhang et al., 2010). This method applies the mass balance equation assuming that atmospheric water vapor concentration of the ecosystem (C_{eco}) has the stable isotope signature of δ_{eco} as a result of the mixture of a background atmospheric concentration (C_a) with stable isotope signature of δ_a and water vapor contributed by ecosystem transpiration with an isotope siganture of δ_t. The intercept of this equation represents the net contribution of the ecosystem transpiration.

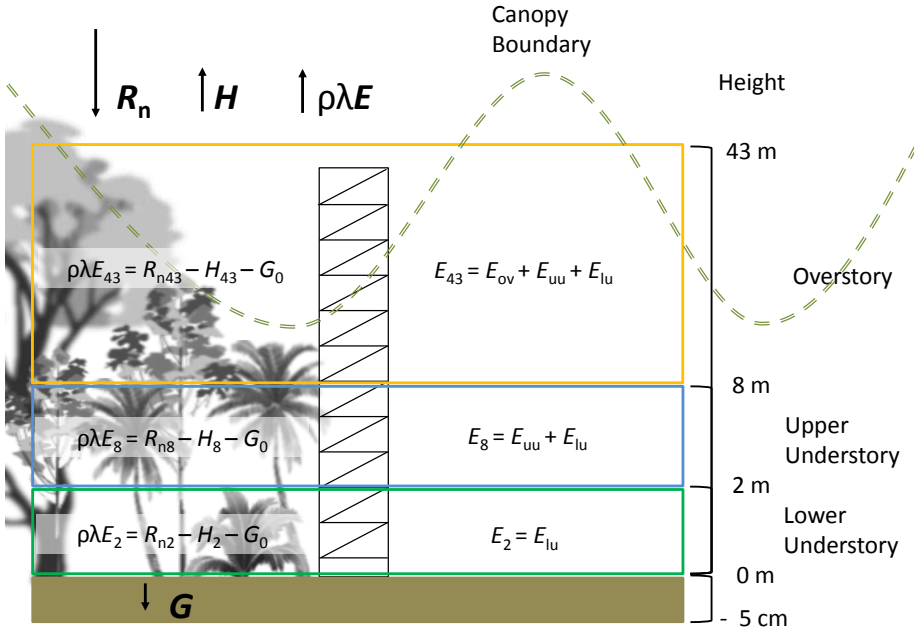

Figure 3.3: Diagram showing the distribution of canopy layers applied for the partitioning of energy and evaporation fluxes. This diagram also shows the components used for the estimation of the energy balance and its relationship with the estimates of evaporation.

$$\delta_{\mathrm{eco}} = C_{\mathrm{a}}(\delta_{\mathrm{a}} - \delta_{\mathrm{t}})(1/C_{\mathrm{eco}}) + \delta_{\mathrm{t}} \tag{3.6}$$

3.2.6. Data Analysis

Data processing and analysis were performed with the software R (R Core Team, 2017). All data collected from the sensors were summarized in 15 minutes time intervals to be comparable with the data from the meteorological station of LSBS. The evaporation contribution of the overstory (ov), upper understory (uu) and lower understory (lu) layers was estimated with equations 3.7–3.9. Also, the vapor pressure deficit (VPD) was calculated in kPa based on the difference between saturation vapor pressure (e_{s}) and actual vapor pressure (e_{a}) calculated based on the air temperature (T_{a}) and dew temperature (T_{dew}) of each height. The lc-excess of the samples was used to determine the presence of statistical differences among sample types and the temporal differences within each sample type. As the samples did not follow a normal distribution, a non-parametric analysis was applied. Presence of differences in lc-excess among and within sample types was determined with a Kruskal–Wallis test and the pairwise comparisons were carried out with a Wilcoxon rank sum test.

$$E_2 = E_{\mathrm{lu}} \tag{3.7}$$

$$E_8 = E_{\mathrm{uu}} + E_{\mathrm{lu}} \tag{3.8}$$

$$E_{43} = E_{\mathrm{ov}} + E_{\mathrm{uu}} + E_{\mathrm{lu}} \tag{3.9}$$

3.3. Results

3.3.1. Meteorological and Canopy Conditions

Canopy openness and LAI at the MRI-plot were 14.4 ± 3.4 % and $2.6 \pm 0.3\,\mathrm{m^2 m^{-2}}$, respectively. During the dry season some trees species experienced a partial loss of leaves (e.g., *P. macroloba*, *Pterocarpus* sp. or *Virola koschnyi* Warb.), this reduces locally the LAI at the end of the sampling period. Rain events during the monitoring period of 62 days had a random distribution, recording a total precipitation of 536.2 mm (Figure 3.4). After 2018-02-01, the rain events intensity experienced a diminution, while the frequency and length of dry periods increased after this date. The occurrence of precipitation affects the VPD, registering maximum values above 2.0 kPa during the hottest and driest days (Figure 3.4). The wind was predominantly from the South–East, with an average magnitude of $0.97\,\mathrm{m\,s^{-1}}$ and a maximum of $4.34\,\mathrm{m\,s^{-1}}$. The low average is a consequence of the high frequency of wind speed lower than $2\,\mathrm{m\,s^{-1}}$ and the wide presence of calms. These calms ($u < 0.25\,\mathrm{m\,s^{-1}}$) are present during 27.8 % of the monitoring period. Daily air temperature oscillates between 17.8 °C and 32.5 °C. The presence of rains reduces the vapor pressure deficit (VPD) which does not exceed 3 kPa.

Air temperature differs among canopy heights and between day and night times (Figure 3.5). At 43 m and 8 m height the air temperature has a daily range of more than 10 °C, while at 2 m height the range is smaller (< 10 °C). However, night time conditions along the canopy profile keep the same pattern without strong differences. Superficial soil temperature does not have differences between day and night time, showing the same range of temperatures. However, the differences during day and night time are driven by the median temperature as a consequence of energy dynamics at ground level.

The VPD at the forest canopy changes with respect to the height. VPD at 43 m height registered the largest values along the monitoring period during day time, droping below 1.0 kPa at night (Figure 3.5). VPD day time conditions at 8 m height are similar to those at 43 m. Beneath the canopy at 2 m height the VPD have a similar trend to night conditions at 43 m height with values not larger than 1.0 kPa. Thus reflects the saturated air conditions close to the forest floor despite the high air temperatures at the site, as it is evidenced by the larger frequency of VPD with 0 kPa. Soil moisture conditions at the MRI-plot oscillates between $0.42\,\mathrm{m^3\,m^{-3}}$ and $0.48\,\mathrm{m^3\,m^{-3}}$, without differences between day and night time conditions.

Daily variation of relative humidity along the canopy profile differs depending on the canopy height. During sunny days, the conditions at 43 m shows are the driest reaching a lower point of 45.2 % and only goes to 100 % during rainfall events. The average relative humidity at 43 m height is 80.9 $\pm$14.3 %. At 8 m height the relative humidity has an average of 90.1 $\pm$11.3 % with a driest point of 52.3 %. Close to the forest floor the relative humidity remains close to saturation even during sunny days. At 2 m height average is 97.2 $\pm$ 4.8 % with a driest point of 71.0 % during the driest day.

3.3.2. Fluxes

Between 2018-01-26 and 2018-03-25 a total amount of 492.8 mm of precipitation was recorded, with 4 days of more than 20 mm d^{-1} (Figure 3.6). Daily measurements of throughfall performed manually at the MRI-plot show that the canopy is able to intercept 11.7 % of the accumulated precipitation. This interception includes the effect of the 3 canopy layers, which remain wet 61.2 % of the time according to the leaf wetness sensor. Most of the events registered an interception fraction between 0.38 to 0.40. It is important to mention the lack of stem flow measurements at the MRI-plot due to the diversity of plant types and species, as well as the high tree density. This can result in an overestimation of the interception in no more than 2.0 % of precipitation for tropical forests (Cavelier and Vargas, 2002; Tobón Marin et al., 2000; Sá et al., 2016). Soil moisture conditions during the study period remain stable with few minor changes during the monitoring period (Figure 3.5). The larger values observed in soil moisture are the result of the large amount of throughfall during rain events.

$R_{\downarrow S}$ varies depending on the location along the canopy. At 43 m height the R_n has a homogeneous frequency during day time, reaching a maximum value close to 1130 W m^{-2}. While at 8 m and 2 m the frequency of larger $R_{\downarrow S}$ (> 500 W m^{-2}) is sporadic reaching not more than 400 W m^{-2} and 100 W m^{-2}, respectively. The sporadic presence of $R_{\downarrow S}$ is due to the presence of sunbeams filtering through the canopy openings. The reduction of $R_{\downarrow S}$ is linked to the attenuation of the $R_{\downarrow S}$ before reaching the forest floor due to the canopy layers. Forest canopy absorbs, reflects and diffuses more than 95 % of $R_{\downarrow S}$. This attenuation influences the energy availability on the understory and forest floor (Figure 3.5). The effective energy reaching the forest floor drives the G daily variations, allowing the soil to store up to 32.3 W m^{-2} (Figure 3.5). This energy is released at night with fluxes up to 39.6 W m^{-2}. This pattern makes G the most important energy flux during night periods at the MRI-plot. Net radiation along the forest canopy profile decreases its magnitude from top to bottom. R_{n43m} had a maximum of 1000.8 W m^{-2}, while the R_{n2m} is just a fraction of this flux. Net radiation at 43 m, 8 m and 2 m during clear nights had similar fluxes, however this pattern differs when rainy conditions are present (Figure 3.4). Those conditions allows R_{n2} to transfer less energy to the atmosphere than R_{n8} and R_{n43}.

At 2 m height H does not have strong changes oscillating between -50 W m^{-2}

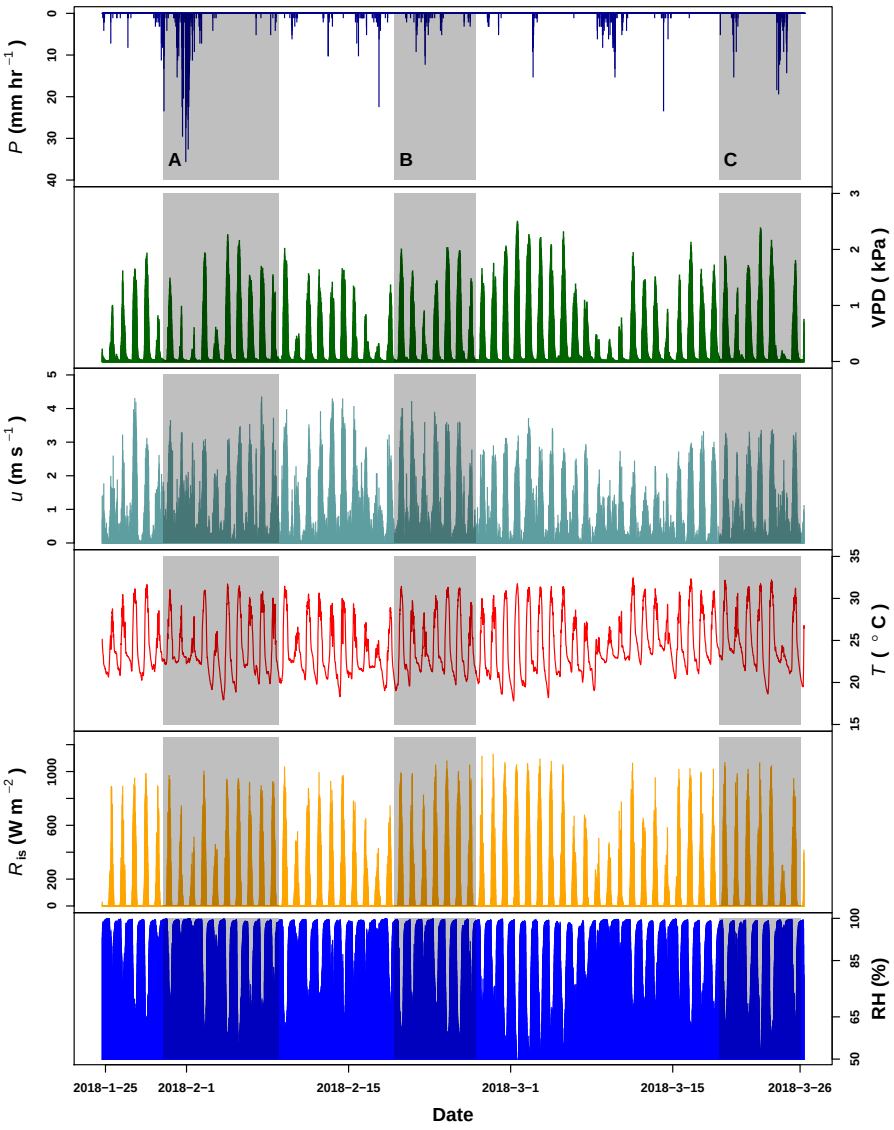

Figure 3.4: Precipitation (P), vapor pressure deficit (VPD), wind speed (u) and temperature (T) registered by the meteorological station at La Selva Biological Station (LSBS). The monitoring period cover from 2018-01-20 to 2018-03-25. Shadowed areas represent the 3 periods when water samples were collected at the MRI-plot.

and 100 W m^{-2} during day time, while night time have 0 W m^{-2} most of the time (Figure 3.5). This flux increases its magnitude on the upper forest layers on day and night time. Most important differences between 8 m and 43 m are based on the maximum H that can be reached. At 8 m and 43 m do not reach 300 W m^{-2}. The frequency peak of H observed along the three heights during day time are linked at the sporadic showers experienced during the monitoring period (Figure 3.4). The residuals from the energy balance equations applied to the three canopy layers (Equation 4.8) represents the $\rho\lambda E$. This flux has strong differences among the canopy heights (Figure 3.5) where at 43 m the $\rho\lambda E$ goes from -100 W m^{-2} to 910 W m^{-2}, while at 8 m and 2 m height the minimum $\rho\lambda E$ is almost the same (-67.5 W m^{-2} and -66.5 W m^{-2}, respectively).

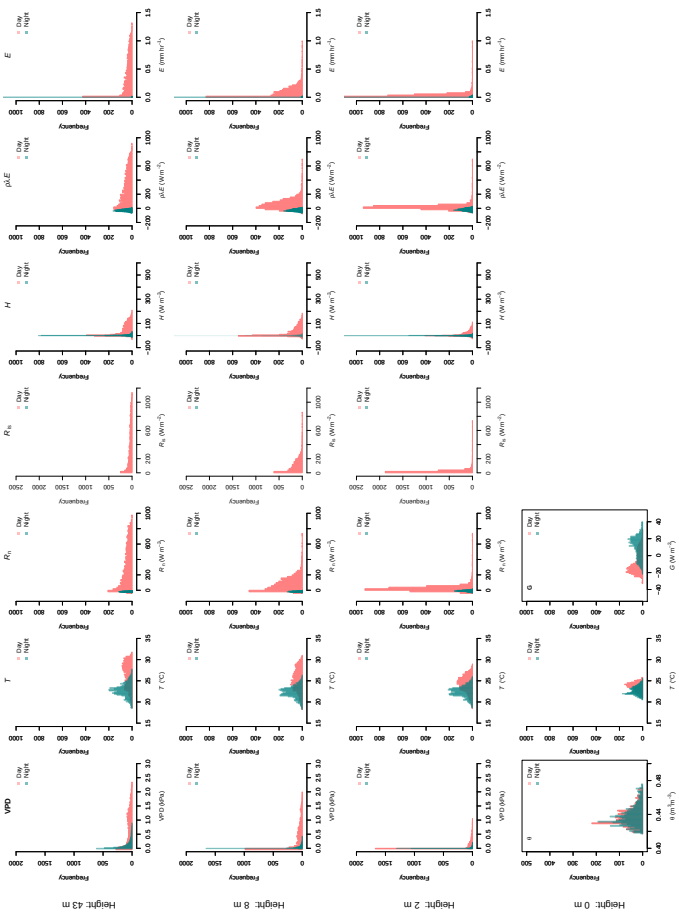

Figure 3.5: Histograms of the data collected during 62 days of monitoring along the canopy profile of the forest. The variables vapor pressure deficit (VPD), soil moisture (θ), air and soil temperature (T), as well as the energy fluxes (R_n, G, R_{ns}, H, $\lambda\rho E$) and evaporation (E) at 43 m, 8 m, 2 m and 0 m height are compared during day and night time. Day time is defined as the period between 06:00 and 18:00 hours and night time between 18:00 and 06:00 hours. Negative values of $\lambda\rho E$ were considered as 0 mm hr^{-1} of E.

Along this period, we estimated an evaporation of 275.5 mm accounting for 55.9 % of the precipitation registered at the MRI-plot. A portion of 24.3 mm is originated from 2 m height and 40.7 mm from between 2 m and 8 m height (Figure 3.6). The contribution of individual canopy layers to evaporation varies among days. The presence of large precipitation events reduces the evaporation (e.g., from 2018-01-31 to 2018-02-01), meanwhile periods with continuous wet conditions but small rain events allows the evaporation to increase (e.g., from 2018-02-17 to 2018-03-03). The overstory layer contributes with an average of 66 ± 8 %, while the upper understory and the lower understory layers contribute with 15 ± 2 % and 9 ± 4 %, respectively.

3.3.3. Isotope Signatures

Figure 3.7 and 3.8 show the variability of all the water samples collected at the MRI-plot. Precipitation samples are located on the LMWL defined for La Selva Biological Station by Sánchez-Murillo et al. (2013), with a slight fractionated signature with respect to the LMWL (Figure 3.7). These differences in isotope signature is linked to the presence of more convective rain events during the dry season. Isotope signatures of precipitation and throughfall samples overlap, however the precipitation samples have a wider variability than throughfall samples for both isotopes. Throughfall samples have a more homogeneous isotope signature with fewer outliers than precipitation. Soil water signature at 5 cm and 10 cm depth has exactly the same pattern as the LMWL, with only 1 sample with a fractionated signature at 10 cm depth. The lack of fractionation in soil water and the high values of soil moisture depict a low proportion of soil evaporation during the sampling period. The samples of stream water collected in the stream nearby the plot have an isotope signature that matches with the LMWL. However, the isotope signature differs widely from the precipitation, throughfall and soil water samples collected on the same period.

Transpired water samples have a more fractionated signature with respect to the xylem water (Figure 3.8). Despite the presence of fractionated xylem water, it does not match with the soil water signature (χ^2: 324.04, p-value < 0.001). Samples of transpired water have a wide variation on their isotopic signatures (Figure 3.7). Transpired water samples of trees, bushes and palms show a similar pattern among them. This pattern has a lumped group of samples with an isotope signature slightly fractionated with respect to the LMWL and some fractionated samples linked to the dryer days. The samples of transpired water collected in the lianas have a different pattern than the other plant types with a clear fractionation linked with the dryer days.

Xylem water samples show clear differences among plant types. The xylem water from palms has an isotope signature close to the LMWL, depicting a quick access to rain water that can be stored in the palm trunks. The lianas have access to different water sources differing in their isotope signatures (Figure 3.7). These

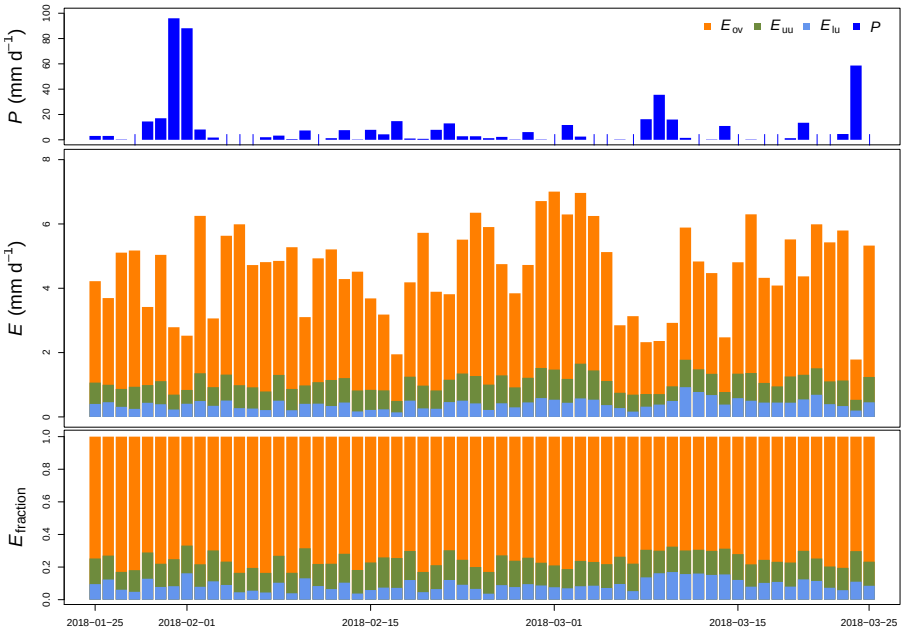

Figure 3.6: Measured precipitation (P), estimated evaporation (E) and its fraction (E_{fraction}) per canopy layer at La Selva Biological Station (LSBS) during the monitoring period from 2018-01-25 to 2018-03-25.

sources include water from precipitation, stream water and soil water affected by evaporation not present in the collected samples at the MRI–plot (Figure 3.8)). The isotope signature of the xylem water in trees and bushes depict the use of rain water as well as fractionated water. The bushes show a more fractionated signature than trees. This signature can indicate the access to more superficial soil water (<5 cm) that can be affected by fractionation.

Temporal differences in lc-excess values were not significant ($p = 0.05$) for most of the sample types excepting the soil water at 5 cm depth ($\chi^2 = 25.297$, $p = 0.000$), throughfall ($\chi^2 = 9.614$, $p = 0.008$) and tree transpiration ($\chi^2 = 9.884$, $p = 0.007$). Figure 3.9 shows the tendency lc-excess for each sampling period per sample type. Main differences in throughfall samples are depicted between the beginning (A) and the end of the monitoring period (C). Samples from the sampling period C showed a more fractionated signature meanwhile the sampling period B has an intermediate value between periods. Soil water at 5 cm shows a clear decreasing trend in lc-excess with the pass of time, increasing considerably the fractionation of soil water signature. Finally, trees transpiration differed between the mid sampling period (B) and the end of sampling period (C).

Isotope signature of water vapor samples from the 3 sampling heights overlap with each other. These samples have a wide range for both isotopes (δ^2H and

δ^{18}O), but only some outliers matches with the xylem water samples. However, few vapor samples overlap with other sample types and only 4 samples at 43 m height and 5 samples from 22 m height overlap with the LMWL. Figure 3.10 shows the keeling plots applied to lc-excess and $\delta^{18}O$ of the air samples collected at 43 m and 22 m height. In both cases, the regression lines are not significant ($p_{value} > 0.05$ and $R^2 \approx 0$). The closeness of water samples exemplifying the source of water vapor (e.g., soil water, transpired water, xylem water) and high absolute humidity during the sampling period affected the goodness of fit.

3.4. Discussion

Evaporation in wet forests is governed by the transpiration process, following a direct link between leaf area index and transpiration (Zhang et al., 2017). However, the role played by the forest canopy during evaporation is more complex and involves processes such as canopy interception (Carlyle-Moses and Gash, 2011; Gerrits et al., 2010) or splash droplet evaporation (Bassette and Bussière, 2008; Murakami, 2006). Broadleaf evergreen forests are able to intercept 13.0 % of the precipitation for subsequent evaporation (Miralles et al., 2010), this matches the observed interception on the MRI-plot with 11.7 % of interception. This proportion accounts for one third of the measured evaporation, leaving the remaining 44.2 % of the evaporated precipitation to canopy transpiration. The distribution of interception along the forest canopy will depend on the accumulated leaf biomass along the canopy, although is not possible to differentiate the proportion of the individual canopy layers. On the MRI-plot, 29.4 % of LAI is allocated between 0 and 10 m height, hence the area intercepting precipitation on the understory increases as well as the potential sources of transpiration. Loescher et al. (2005) suggested that transpiration on the lower canopy can affect the lack of ecosystem response to the vapor pressure deficit variations in the upper part in La Selva Biological Station. Thus supports the contribution of 9 % and 15 % of the evaporation by the lower and upper understory recorded during this dry season. Soil evaporation is negligible in respect to transpiration and canopy interception. However, the presence of litter on the forest floor may contribute to the evaporation at 2 m height as part of the forest floor interception. The presence of larger $\rho\lambda E$ at 2 m and 8 m heights are linked to the sunbeams and to their low frequency of occurrence. Negative $\rho\lambda E$ values are linked to the water condensation along the forest canopy. This condensation will trigger the release of latent heat similarly as it happen during the cloud formation processes (Goosse, 2015).

Allen et al. (2016) described the capacity to modify the isotope signature of precipitation when the water passes through the forest canopy. This pattern has been identified in different locations (Allen et al., 2015; Hsueh et al., 2016; Liu et al., 2008). Instead, the throughfall signature at the MRI-plot is more homogeneous than the isotope signature of precipitation. This as a consequence of two factors first, the small number of throughfall samplers used (n = 4), and second the fixed

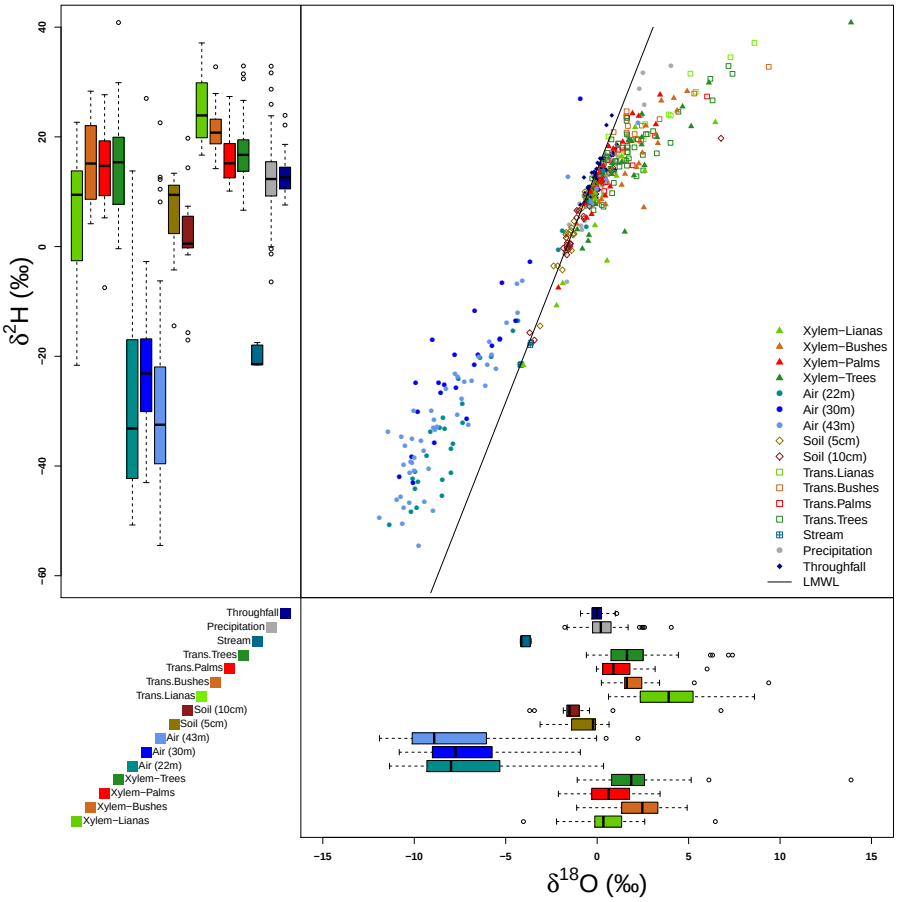

Figure 3.7: Isotopic signatures of δ^2H and δ^{18}O of all the samples collected at the MRI-plot. Dual isotope plot shows the relationship among the local meteoric water line (LMWL) and all the samples. The box plots of δ^2H (upper–left) and δ^{18}O (bottom–right) show the distribution of isotope signatures per sample type.

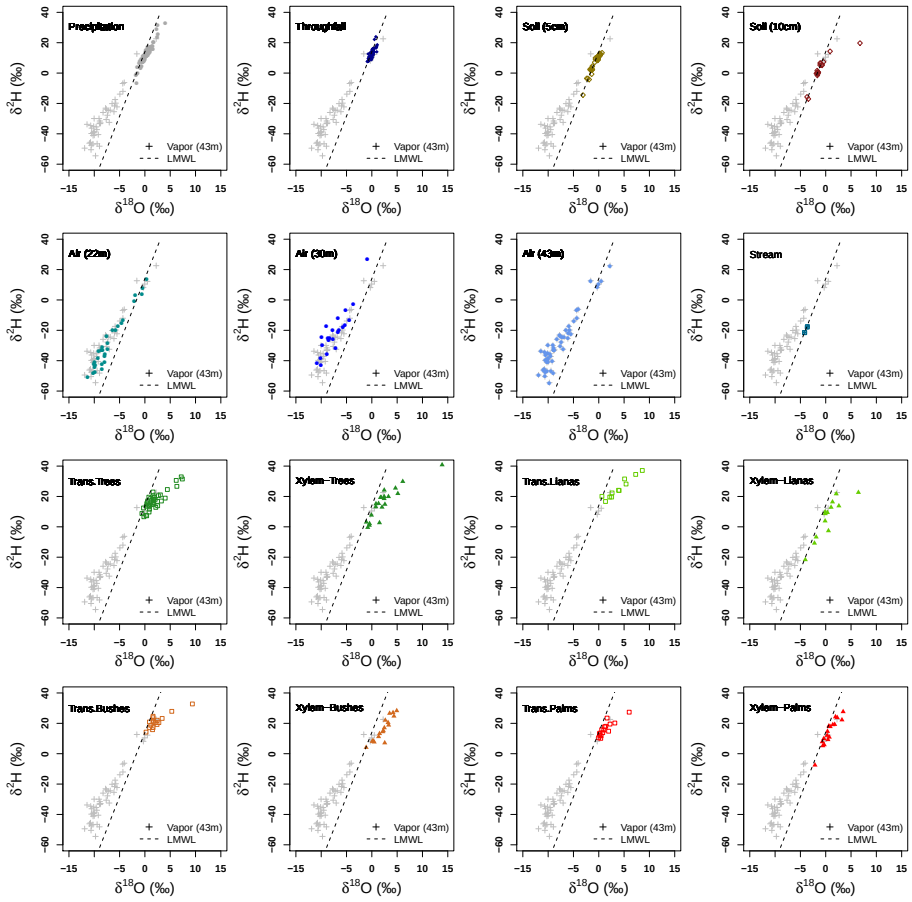

Figure 3.8: Dual isotope plots of δ^2H and δ^{18}O per sample type collected at La Selva Biological Station. Vapor samples collected at 43 m height and local meteoric water line (LMWL) are used in each plot as references.

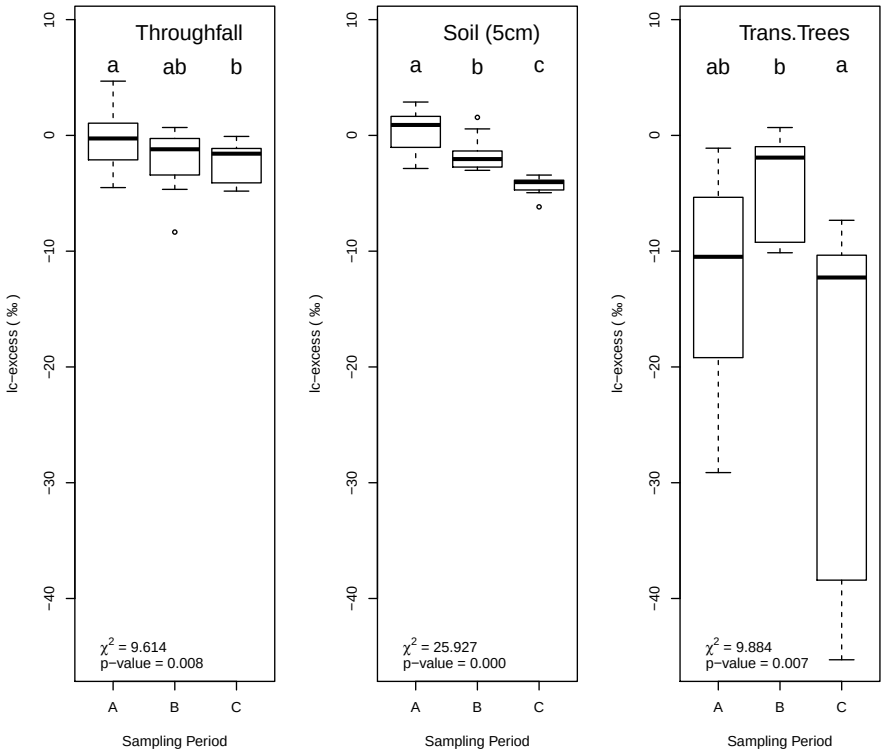

Figure 3.9: Box plots showing the temporal differences in lc-excess for throughfall, soil water at 5 cm depth, and trees transpiration. The other sample types did not showed significant differences ($p = 0.05$). Sampling periods with the same lower case character per sample type do not differ ($p = 0.05$).

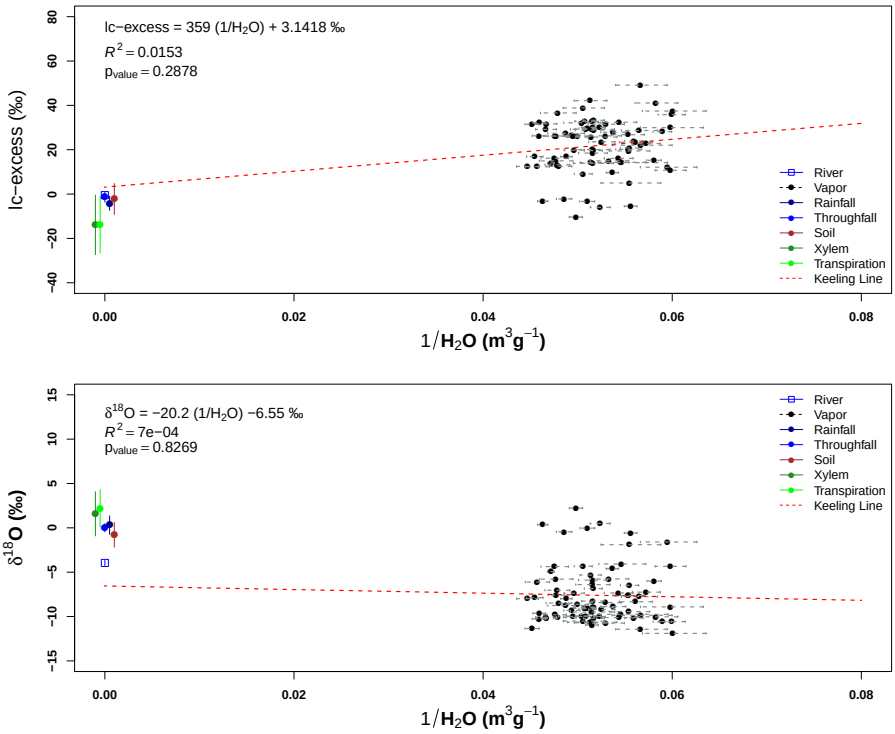

Figure 3.10: Line-conditioned excess (lc-excess) and oxygen-18 (δ^{18}O) mixing relationships ("Keeling plots") for the monitoring period. Air samples collected at 43 m and 22 m height. The standard deviation of each air sample shows the variation of the absolute humidity of the air (ρ_v) for each sampling.

location of each of them. These two factors reduces the possibility to depict the spatial variability of the sampled forest despite the differences on sampling dates. However, the temporal differences among sampling periods show a clear effect of the evaporation process at end of the dry season. The intercepted water is affected by evaporation during the rain events, modifying the isotope signature of the water that drips from the canopy. This water has a more fractionated signature than the precipitation. The higher temperatures experienced during day time and larger VPD conditions at 43 m and 8 m height drive this change the fractionation of stable water isotopes. Soil water signatures have a larger variability than throughfall signatures, showing lighter signatures than precipitation and throughfall. Soil water does not show the expected fractionation of soil under evaporation processes, where the isotope signature is characterized by heavier fractionated soil water signatures respect to throughfall or precipitation (Allison et al., 1984; Sprenger et al., 2017a). This reflects the small contribution to evaporation from the mineral soil, which is supported by the high soil moisture recorded during the monitoring period. However, this does not include the effect of evaporation from litter interception on the forest floor. This effect modifies the soil water isotope signature at 5 cm depth with the development of the dry season. The decreasing trend of lc-excess values shows the effect of evaporation process that is able to modify the water signature that reaches this depth. This process is cumulative since the evaporation process started modifying the isotope signature at canopy level, before reaching the litter layer before reaching the mineral soil. This evaporation is linked to the available energy at the lower understory that drives the evaporation process.

Water use by riparian forests in La Selva Biological Station has been linked to groundwater withdrawal (Cadol et al., 2012). Isotope signature of stream water during low flows reflects the isotope signature of groundwater (Blumstock et al., 2015), allowing its use as a proxy of to describe the groundwater isotope signature. The collected stream water has a lighter isotope signature than precipitation, throughfall and soil water however, its lc-excess depict its meteoric origin supporting it use as a reference to describe the groundwater. The stream water signature is lighter than the fractionated water used by trees and bushes, meanwhile some lianas have similar signature to stream water. This can lead to link a deep water use by the lianas, which has been reported in some karstic and seasonal environments (Chen et al., 2015b) however, it differs from the findings of (De Deurwaerder et al., 2018) in a similar tropical forest. However, as xylem water and transpired water of lianas have fractionated signatures with respect to the LMWL, but do not match completely with soil neither throughfall samples. Temporal differences showed by transpired water by trees are linked to a variation on the strategies to access different water sources. During the second period of sampling the rain events were smaller but more frequent than during the first and last sampling periods. This allowed the trees to make used more recently precipitated than the other two periods. Palm and bushes samples are the ones that cover the isotopic range of precipitation and throughfall samples, depicting the use of rain water. Canopy architecture of palm trees allows the concentration of water as stemflow (Germer et al., 2010; Ger-

mer, 2013) allowing the quick soil saturation near the root zone with precipitation water. Additionally, palm species have the capacity to store large amounts of water in their stem for their later use (Renninger and Phillips, 2016). This enables these species to have a stable isotope signature close to precipitation water.

Tropical bushes and treelets have most of their root system in the upper 20 cm of the soil (Becker and Castillo, 1990), allowing their access to superficial soil water and nutrients. However, it is important to underline that root allocation strategy depends on the species (Jackson et al., 1995). The water signature of xylem water and transpired water of trees and lianas showed a large variability. Differently to palms, tree species are able to develop extensive root systems depending on the nutrient availability more than water access in wet environments (Kerfoot, 1963). Whilst the growth strategies of lianas allow them to have an extensive shallow root system due to their sprout capacity all over the forest floor (Campanello et al., 2016). This root system allow the lianas to have access to superficial soil water (De Deurwaerder et al., 2018), making use of the dripping water after convective fog during dry season (Liu et al., 2010) and the dry season rains.

The overlapping isotope signatures of transpiration and xylem samples with the precipitation water, do not allow to identify proportion of individual sources of water vapor. The highly variable water vapor concentrations during the gas sampling and signature closeness of possible water vapor sources did not allow neither to identify individual sources such as transpiration or evaporation. Determining the source of water vapor with techniques such as the keeling method did not work for this monitoring as a consequence of two factors. First, the similar isotope signatures of the possible sources of water vapor. Secondly, the high concentration of water molecules even in the dryer days. The keeling method has been applied in conditions with clear differences between the sources of water vapor such as in semiarid environments (Yepez et al., 2003, 2005), homogeneous plantations (Sun et al., 2014) or comparing between inland and lake evaporation (Yamanaka and Shimizu, 2007). The presence of few plant species in those cases allowed a more homogeneous signature of transpiration, which is not the case at the MRI-plot which has 88 plant species. Secondly, the similar signature of sources of water vapor (transpired water, soil water of rain water) do not allow a clear differentiation. Finally, the high variability of the water vapor concentration during the different sampling methods did not allow to produce a significant linear regression.

The structural complexity of a tropical wet forest requires the inclusion of different parameters to better understand the water fluxes such as evaporation. Tackling the structure in terms of canopy layers is possible to homogenized important differences like plant types or number of species. This as a consequence of the larger variability of water sources to which the plants have access or to specific characteristics of the plants that defines how much water can be transpired (Chen et al., 2015b; Silvertown, 2004; Silvertown et al., 2015). Traditional evaporation partitioning defines the fluxes in terms of soil evaporation, plant transpiration and evaporation of

intercepted water (Roberts, 1999; Savenije, 2004; Shuttleworth, 1993). However, in complex environments partitioning the evaporation in terms of canopy structure can trigger new insights of the hydrological processes involved within them.

Additionally, it is necessary to understand how individual plant species in tropical environments use the different water sources. Water uptake by tropical trees is linked to leaf phenology and transpiration rates (Schwendenmann et al., 2015) however, the use of stable isotopes in xylem water could by affected due to evaporative fractionation during the transport within the plant tissues (Barbeta et al., 2019; Martín-Gómez et al., 2016; Zhao et al., 2016) or selective acquisition (Vargas et al., 2017). This evidence depicts the need to better understand the effect on stable water isotope signatures during the water transport within the plant. Despite the xylem is considered as a close transport system within the plants, the presence of lenticels along the tree stem, twigs and branches allows the gas exchange by the plant growing tissues (Crang et al., 2018; Hopkins and Hüner, 2008). These organs are present in most of the sampled tree species of this study (e.g., *P. macroloba*, *Sacoglottis trichogyna* Cuatrec., *V. koshnyi*, *Virola sebifera* Aubl.). This can trigger additional fractionation processes along the water transport in the xylem that can affect the isotope signatures of xylem water, making difficult to point out the water sources for those plants. Also, providing different water vapor signatures to the tree surroundings. This sampling is representative of the riparian forests located within the life zone Troipcal Wet Forest according to Holdridge (1967). This because the location in a middle terrace of the Puerto Viejo river allows the formation of riparian forest structures with a high dominance of palm species such as *W. regia* and trees like *P. macroloba*. Also, the ample distribution of these two species in Mesoamerica (Borchsenius et al., 1998; Orwa et al., 2009) allows the application of this outcome to other latitudes within the tropics.

3.5. Conclusions

Forest evaporation during the monitoring period accounted for 55.9 % of the recorded precipitation. The evaporation did not experience an increment or diminution during the dry season, showing no water limitations for the evaporation process at stand level. The evaporation includes 11.7 % originated from the intercepted water by plant surfaces, which modifies the isotope signature of the water before reaching the ground. The lower evaporation rates recorded (up to 2 mm d^{-1}) were linked to rainy conditions and despite this variability, the contribution of the upper and lower understory layers remains constant along the monitoring period (23.6 %). The main differences between lower and upper understory layers rely on the average contribution. The lower understory provides on average a 9.0 % and the upper understory 15.0 % of the evaporation. The ample water availability did not affect the contribution of individual layers. The low variability of soil moisture during this dry season depicts a small contribution to evaporation from forest soil, a pattern that is supported by the lack of fractionated signature of stable water isotopes. The use of keeling plots to differentiate between transpiration and other sources of

water vapor was affected by the highly similar signature of sources of water vapor, by the larger number of plant species and the high water concentration and variability. Evaporation processes during the dry season in Tropical wet forests are not restricted by water availability. However, understory plants and palm species can be affected during drought periods due to the reduction of superficial water availability triggered by a diminution of rains and/or changes in water dripping after fog events.

4

Drop, drop, drop, and the vapor goes

Spotting the invisible water vapor

Like a ghost in an old house
the water vapor moves around,
no one has seen it close enough
until the rain falls on the canopy top.

This chapter are based on:

Jiménez–Rodríguez, C.D., Coenders–Gerrits, M., Schilperoort, B., Gonzalez-Angarita, A.P. and Savenije, H. (2020). *Vapor plumes in a tropical wet forest: spotting the invisible evaporation.*Hydrol. Earth Syst. Sci. Discuss. in review.

4.1. Introduction

Forest cover in tropical regions is endangered by deforestation (Curtis et al., 2018; Rosa et al., 2016), compromising the evaporation flux from land. Forest evaporation is a mixture of water vapor originated from water intercepted on plant surfaces, soil water and plant transpiration (Roberts, 1999; Savenije, 2004; Shuttleworth, 1993). Forest evaporation is considered of major importance as a regional and local cooling system (Ellison et al., 2017) as a result of their capacity to recycle the atmospheric moisture at different time scales (van der Ent and Savenije, 2011). The water vapor originated from evaporation at the surface is horizontally transported in the atmosphere by advection (Lavers et al., 2015; Strong et al., 2007), whilst vertical transport is linked to wind shear (Chen et al., 2015a) and convection (Trzeciak et al., 2017). Large ecosystems influence the formation of convective clouds at the top of the atmospheric boundary layer (Fuentes et al., 2016; Manoli et al., 2016). This process plays an important role in the formation of precipitation in tropical basins (Adams et al., 2011; van der Ent and Savenije, 2011), because of the contribution of water vapor originated from local evaporation (Brubaker et al., 1993).

Evaporation is usually neglected or considered of minor importance during rain events in dense forest ecosystems (Klaassen et al., 1998). This because during rainfall the vapor pressure deficit is close to zero (Bosveld and Bouten, 2003; Loescher et al., 2005; Mallick et al., 2016), reducing the atmospheric water demand and stopping the transpiration process (Gotsch et al., 2014). However, the increment of evaporation with the size of rain events suggest that evaporation also occurs during the events and not only afterwards (Allen et al., 2020). This has been evidenced by discrepancies found between modelled and measured evaporation rates in tropical forests (Schellekens et al., 2000). When it rains part of the precipitation is intercepted and evaporated directly to the atmosphere (David et al., 2006), even when vapor pressure deficit and available radiation are low (Lankreijer et al., 1999). Under high humidity conditions a portion of the precipitation can evaporate after a raindrop splashes on the canopy or the forest floor. This process is known as ”splash droplet evaporation” (Dunin et al., 1988; Dunkerley, 2009; Murakami, 2006) and is based on the principle that raindrop size increases with rain intensity. Consequently, when larger drops hit the surface (e.g., ground, leaves, branches) allow the formation of smaller rain droplets that can be easily evaporated after the splash. This process has been pointed out as the main source of evaporation to explain the difference between intercepted water and measured evaporation in studies carried out in banana plants (Bassette and Bussière, 2008) and Eucalyptus plantations (Dunin et al., 1988).

Forest evaporation produce coherent structures of water vapor called plumes, cells or rolls (Couvreux et al., 2010). Plumes of water vapor have been identified above forest ecosystems during day time with high resolution scanning Raman LIDAR technique (Cooper et al., 2006; Kao et al., 2000). These plumes reached heights above the canopy up to 100 m, depicting their importance as water vapor providers at local scale. This phenomenon has been studied in astrophysics (Berg

et al., 2016; Sparks et al., 2019), vulcanology (Kern et al., 2017; Sioris et al., 2016), regional and global meteorology (Herman et al., 2017; Knoche and Kunstmann, 2013; Wang, 2003; Wright et al., 2017). However, to the authors best knowledge little attention has been drawn to small events observed during rain events. Additionally, Couvreux et al. (2010) highlighted the lack of sampling techniques able to characterize the occurrence of these plumes close to the surface. This chapter aims to identify the presence of visible vapor plumes in a Tropical Wet Forest. It also tries to explain when and why these plumes occur using meteorological data vertically distributed along the forest canopy layer.

4.2. Methods

4.2.1. Experimental Design

The monitoring was carried out on the Major Research Infrastructure (MRI) plot at La Selva Biological station (LSBS) on the Caribbean lowlands of Costa Rica (Figure 3.1). A detailed description of the study site is available in Chapter 3. Air temperature (°C) and relative humidity (%) were measured along the vertical axis of the tower with HOBO® smart sensors (part code: S-THB-M008). The sensors were located at 2 m, 8 m and 43 m height, placed at a distance of 1.5 m from the tower and protected with a radiation shield (HOBO® part code: RS-3) of 10 cm diameter. At the highest point of the tower, the precipitation (mm min^{-1}) was recorded with a Davis® rain gauge. Soil temperature (°C) was measured in two different locations at 5 cm and 15 cm depth with a soil temperature sensor (HOBO® part code: TMC20-HD). Soil moisture (Θ, m^3 m^{-3}) was measured at the same locations as soil temperature at 5 cm depth with an ECH_2O® EC sensor. Soil temperature was recorded with a 4-channel data logger (HOBO® part code: U12-008) and the other sensors with a USB Micro Station (HOBO® part code: H21-USB) every 5 min. A Bushnell® Natureview® Essential HD camera (12 megapixels) was installed at the top of the tower facing North–West.

All environmental variables were monitored between 2018-01-24 and 2018-03-26. The camera was installed to collect photographs above the canopy between 2018-03-21 and 2018-03-25 at different time windows. The photographs were collected continuously from 5:00 to 18:30 hours local time (UTC-6). These pictures were used to determine the timing when the vapor plumes were visible at the MRI–plot. The photographs were classified into three conditions (Figure 4.1):

- Clear View: includes all the pictures with clear and cloudy sky where the canopy is clearly visible and there is neither mist nor plumes present (Figure 4.1 A and B).
- Mist and Fog: includes the presence of a homogeneous blurry view of the canopy. The blurriness of each picture varies depending on the humidity conditions. Special care was taken to prevent the erroneous classification of photographs affected by a fogged–up lens. This category is called ”mist” from

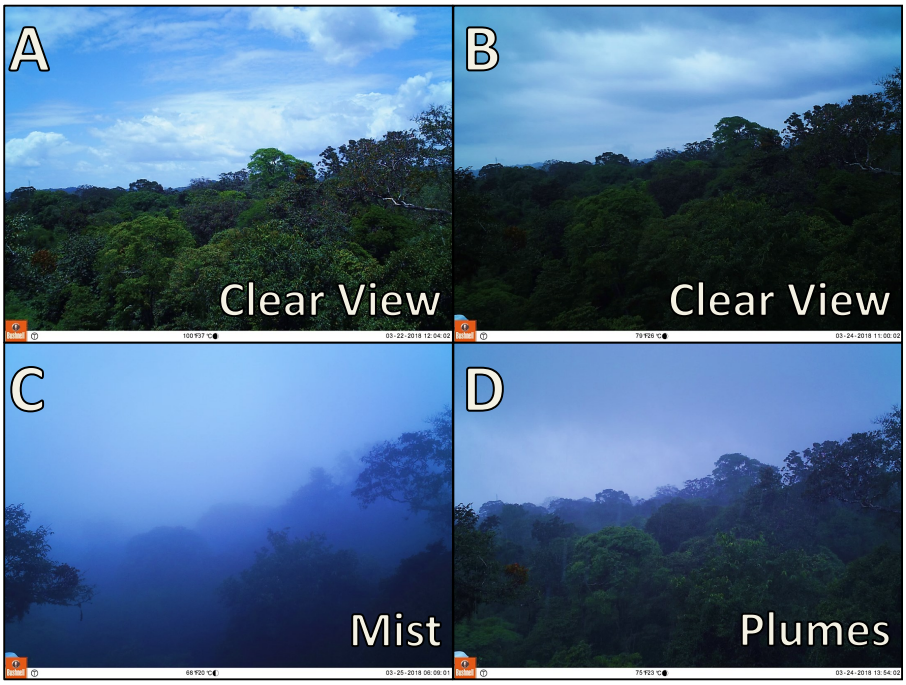

Figure 4.1: Visual monitoring showing the 3 conditions used to classify the canopy photographs on the time-lapse videos. The pictures A and B show the "Clear View" classification, picture A on a sunny day and picture B during rain. Picture C describes the Mist and picture D shows the plumes rising from the forest canopy.

now onwards (Figure 4.1 C).

- Plumes: includes the presence of buoyant vapor clouds risen from the forest canopy (Figure 4.1 D). These cloud bodies change their vertical position in consecutive frames. Rising vapor plumes can be observed in the online video of 2018-03-24 available at https://doi.org/10.4121/uuid:997cc9d8-2281-453e-b631-5f93cfebe00e (Jiménez-Rodríguez et al., 2019b).

4.2.2. Data Analysis

Data processing and analysis was performed with the open source software R (R Core Team, 2017). All temperatures were converted from K to °C. Superficial soil temperature ($T_{s.0}$, °C) was estimated with equation 4.1 (Holmes et al., 2008). This equation describes the diurnal variations of soil temperature as sine waves depending on the 24 h moving averages of soil temperature at 5 cm depth ($T_{s.5}$, °C). The daily amplitude of air temperature (T_A, °C) is defined as the difference between $T_{s.5}$ and the air temperature at 2 m (T_{2m}). The oscillations are determined by the damping depth (ν, m) which is calculated with equation 4.2. Depth differ-

ence between the T_{ss} and $T_{s.5}$ is defined as z_b (m). The sine pattern depends on the angular frequency (ω, s^{-1}), time (t) in s and ϕ (-) as a constant for phase change. Equation 4.3 is used to determine ω with τ (s) as the wave period. Equation 4.2 calculates ν with the soil thermal diffusivity (η, $m^2\,s^{-1}$) and ω. Equation 4.4 (Nakshabandi and Kohnke, 1965) is used to determine η, where ρ_s is the soil bulk density of 0.76 g cm^{-3} (Sollins et al., 1994) for the experimental plot, c_s is the specific heat for clay soils (837.36 W kg^{-1} °C^{-1}) and k is the soil thermal conductivity of 1.58 W m^{-1} °C^{-1} (Pielke, 2013). These last two parameters were chosen according to the soil water conditions during the monitoring period, which was close to soil field capacity.

$$T_{s.0} = T_{s.5} + T_A\, e^{\left(\frac{-z_s}{\nu}\right)} \sin\left(\omega t - \frac{z_b}{\nu} + \phi\right) \tag{4.1}$$

$$\nu = \sqrt{\frac{2\eta}{\omega}} \tag{4.2}$$

$$\omega = \frac{2\pi}{\tau} \tag{4.3}$$

$$\eta = \frac{k}{\rho_s c_s} \tag{4.4}$$

Virtual potential temperature (θ_v, °) of the air was calculated to take into account the variation in the adiabatic lapse rate due to changes in pressure (Barr et al., 1994; Stull, 1988, 2016). For saturated (cloudy) air conditions equation 4.5 calculates the θ_v based on the water-vapor mixing ratio (ψ_s) of the moist air, the liquid water mixing ratio (ψ_L) and the virtual temperature (θ). The parameters ψ_s and ψ_L were determined using the vapor pressure deficit of the air on each height (Stull, 2016). The virtual temperature was estimated with equation 4.6 where Γ_d is the dry adiabatic lapse rate near the surface (0.0098 °C m^{-1}), z is the height above the ground in m and T_z is the air temperature at the same heights.

$$\theta_{v.z} = \theta_z(1 + 0.608\,\psi_s - \psi_L) \tag{4.5}$$

$$\theta_z = T_z + \Gamma_d\, z \tag{4.6}$$

Convection can be identified by evaluating the temperature gradient ($\frac{\Delta\theta_v}{\Delta z}$). Values of $\frac{\Delta\theta_v}{\Delta z} > 0$ are linked to stable stratification, meanwhile $\frac{\Delta\theta_v}{\Delta z} < 0$ show an unstable stratification, which will drive convection.

The condensation of vapor close to the forest canopy can be identified by calculating the lifting condensation level (z_{lcl}) in m with equation 4.7. This equation determines the elevation at which a parcel of air condensates allowing the formation of clouds. This equation uses the difference between air temperature (T_z) and

dew point temperature ($T_{\mathrm{dew.z}}$) at one specific height (z), divided by the difference between Γ_{d} and the moist adiabatic lapse rate (Γ_{dew}) at T_z and $T_{\mathrm{dew.z}}$ (Stull, 2016).

$$z_{\mathrm{lcl}} = \frac{T_z - T_{\mathrm{dew.z}}}{\Gamma_{\mathrm{d}} - \Gamma_{\mathrm{dew}}} \tag{4.7}$$

The energy balance equation (Equation 4.8) was used to estimate the evaporation (E_z) in $\mathrm{m\,s^{-1}}$ at 2 m, 8 m and 43 m height. In this equation, G is the ground heat flux ($\mathrm{W\,m^{-2}}$), $R_{\mathrm{n.z}}$ is the net radiation ($\mathrm{W\,m^{-2}}$), H_z the sensible heat flux ($\mathrm{W\,m^{-2}}$), ρ_{w} is the water density ($1000\,\mathrm{kg\,m^{-3}}$) and λ the latent heat of vaporization ($2.405 \times 10^6\,\mathrm{J\,kg^{-1}}$). $R_{\mathrm{n.z}}$ and H_z are estimated at 2 m, 8 m and 43 m. The estimation of all the fluxes is described in detail by Jiménez-Rodríguez et al. (2019a). Equation 4.8 is based on the vertical transport of heat and neglects the advected energy on the forest canopy as a consequence of the lack of more detailed measurements (e.g., eddy covariance system).

$$E_z = \frac{R_{\mathrm{n.z}} - H_z - G}{\rho_{\mathrm{w}}\lambda} \tag{4.8}$$

4.3. Results and Discussion

The monitoring period experienced a diurnal variation in air temperature along the vertical profile of the canopy, with a temperature difference of more than 10 °C at 43 m and less than 7 °C at 2 m height (Figure 4.2). The highest temperatures were registered at 43 m height reaching more than 30 °C, decreasing in magnitude towards the forest floor. These peak temperatures were recorded around noon with differences up to 5 °C between the air temperature at 43 m and 2 m height. The $T_{\mathrm{s.0}}$ oscillates between 20.7 °C and 25.4 °C. The amplitude of the oscillation increased with the sunniest days but the daily difference does not exceed the 4 °C. The maximum Θ value was $0.47\,\mathrm{m^3\,m^{-3}}$ during the heavy rains, almost reaching the saturation point for clay soils of $0.50\,\mathrm{m^3\,m^{-3}}$ (Saxton and Rawls, 2006). The minimum Θ was recorded after the driest period just before the rains on 2018-03-24 ($0.42\,\mathrm{m^3\,m^{-3}}$) getting close to soil field capacity for clay soils (Saxton and Rawls, 2006). Evaporation always occurs during daytime on all sampling days (Figure 4.2). During the four sunny days the evaporation was larger than $5\,\mathrm{mm\,d^{-1}}$, with a contribution of more than $1.0\,\mathrm{mm\,d^{-1}}$ from 8 m height and no more than $0.7\,\mathrm{mm\,d^{-1}}$ from 2 m height. In contrast, during 2018-03-24 the continuous rains sum up $58.7\,\mathrm{mm\,d^{-1}}$ and the evaporation was estimated as $1.8\,\mathrm{mm\,d^{-1}}$ at 43 m and only $0.2\,\mathrm{d^{-1}}$ at 2 m height (Table 4.1).

During the visual monitoring with the field camera, clear view conditions were predominant along four days (Figure 4.2). These days were characterized by sunny conditions with temperatures above the 25 °C, no large rain events and a decreasing trend in soil moisture. Also, on 2018-03-24 it was possible to identify three short periods with clear view conditions in between the rains. Mist formation was identify on 2018-03-23 and 2018-03-25 before 7:00 a.m. Meanwhile the photographs of the other sampling days did not show mist formation because of its timing. These

Table 4.1: Summary of daily precipitation and evaporation at 43 m, 8 m and 2 m height estimated based on the meteorological data collected on site.

Date	Precipitation ($mm\,d^{-1}$)	Evaporation ($mm\,d^{-1}$)		
		0–43 m	0–8 m	0–2 m
2018-03-21	0.0	6.0	1.5	0.7
2018-03-22	0.0	5.4	1.1	0.4
2018-03-23	4.6	5.8	1.1	0.3
2018-03-24	58.7	1.8	0.5	0.2
2018-03-25	0.0	5.3	1.2	0.5

Note: all evaporation values corresponds to the water vapor produced from the forest floor up to the specified height.

mist events were linked with superficial soil temperatures higher than 2 °C with respect to air temperature. Finally, the vapor plumes were visible only during rainy conditions on 2018-03-24 (videos available at Jiménez-Rodríguez et al. (2019b)). Soil temperatures during this day were warmer than the air column along the forest canopy (Figure 4.2).

Evaporation during sunny days provided the conditions to form vapor plumes as those ones described by Cooper et al. (2006) and Kao et al. (2000). The evaporation peaks during these days occurred around noon, registering a z_{lcl} higher than 500 m (Figure 4.2) which is the height required to form clouds and be visible. This is the reason why it is not possible to see the vapor rising from the surface. The vapor plumes were visible on the day with continuous precipitation (2018-03-24). On this day, the Z_{lcl} dropped beneath 100 m because during rain events the θ_{v} of all the air column dropped quickly. This drop kept the θ_{v} beneath the superficial soil temperature, allowing a localized convection event. This convection process forced the evaporated water to move upwards forming buoyant clouds close to the forest surface. The evaporation during rain events is the result of the splash droplet evaporation process (Murakami, 2006; Dunkerley, 2009), which can provide water vapor as a consequence of the fragmentation of raindrops when hitting the surface.

Energy convection plays an important role in forest ecosystems during night time (Bosveld et al., 1999). This is a consequence of the mass transport capacity of the intermittent nocturnal convective fluxes (Cooper et al., 2006). The convection process is forced by the ground heat flux (Jacobs et al., 1994), which is enhanced by the larger soil moisture in the clay soil which increases the soil heat capacity (Abu-Hamdeh, 2003). A coupled canopy system enables sensible heat and water vapor transport from the soil to the atmosphere just above the canopy layer (Göckede et al., 2007). This facilitates the generation of the convection process, allowing the ascending warm air to cool down at the canopy top and condensate forming the visible water vapor plumes. The condensation releases heat (Goosse, 2015), driving the convection. Vapor plumes are always present as a consequence of the moisture

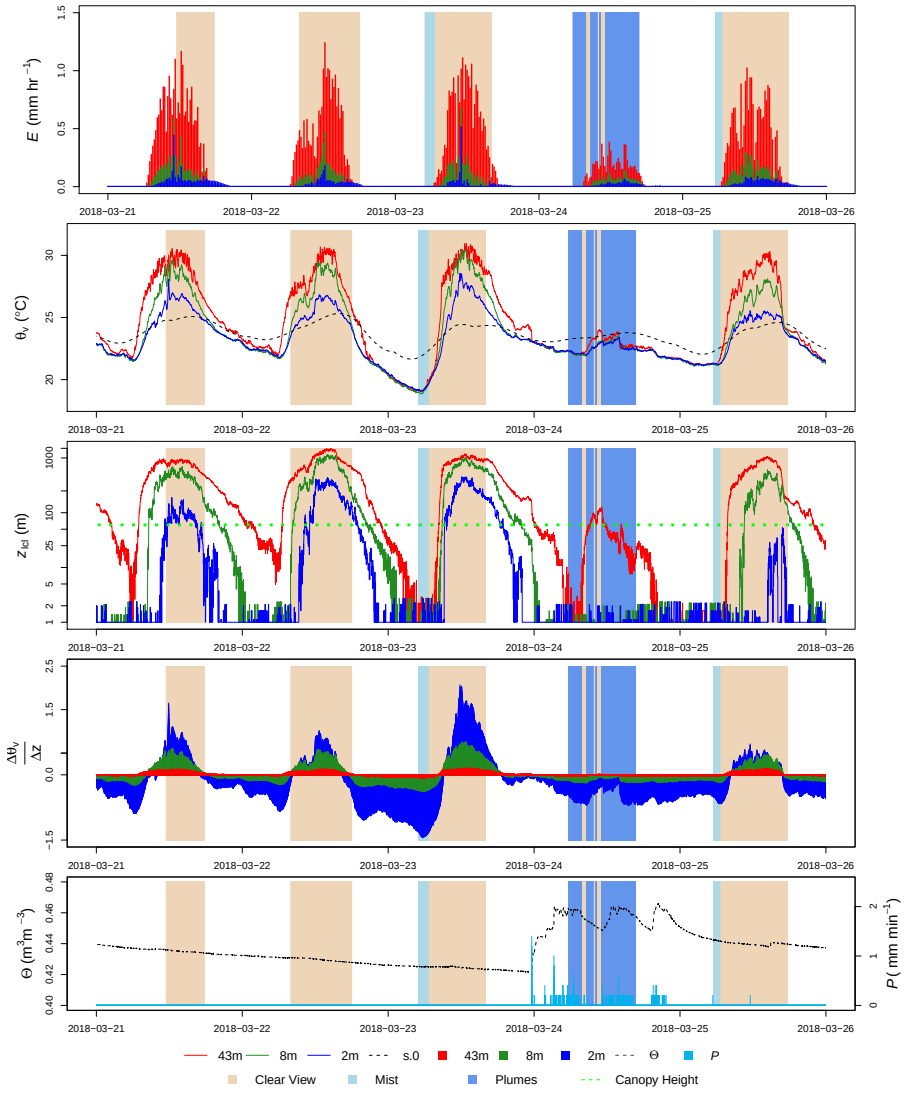

Figure 4.2: Evaporation (E), Virtual potential temperature (θ_v), lifting condensation level (z_{lcl}) in an untransformed semi–logarithmic scale and temperature gradient ($\frac{\Delta\theta_v}{\Delta z}$) at 43 m, 8 m and 2 m height. Additionally, precipitation (P) and soil moisture (Θ) are also shown during the visual monitoring between 2018-03-21 and 2018-03-25. Background colored areas denoted the three categories in which the photographs were classified: Clear View, Mist and Plumes.

exchange between the surface and the atmosphere (Lawford, 1996), where evaporation from land covers with enough water supply provides the required air moisture (Kao et al., 2000). However, the conditions needed to form a visible buoyant cloud close to the surface require a big difference in air temperature over height. Temperature gradient at 43 m, 8 m and 2 m is negative during plumes and mist conditions, meanwhile clear view conditions has a larger range with more positive values (Figure 4.3).

Visible vapor plumes are the result of the condensation of water vapor rising from a warmer surface. When a column of warm humid air reaches a lower density than air above, the water vapor condensates around aerosols in the air allowing the formation of clouds (Stull, 2016). In this regard, there are two sources of aerosols at LSBS. One source is linked to windy carrying aerosols from nearby agricultural land uses (Loescher et al., 2004). The second source is linked to convective rains that characterize the dry season at LSBS. These rains transport from the free troposphere into the boundary layer the required aerosols for the condensation process and later formation of clouds (Wang et al., 2016). Meanwhile the "splash droplet evaporation" process (Murakami, 2006) provides the main source of water vapor after rain drops hit the canopy and soil surfaces.

Cloud formation usually happens high above the surface boundary layer where the forest canopy is located, but available information of cloud formation close to the forest canopy is scarce. The temperature gradient ($\frac{\Delta\theta_v}{\Delta z}$) at 43 m, 8 m and 2 m is negative during plumes and mist conditions, meanwhile clear view conditions have a larger range with more positive gradients. Lifting condensation level is a key element that allowed to differentiate between plumes and mist conditions (Figure 4.3). The combination of variables such as Z_{lcl}, $\frac{\Delta\theta_v}{\Delta z}$, and P allows to identify the formation of vapor plumes in Tropical Wet Forests (Figure 4.4). The z_{lcl} is the height in the atmosphere at which a parcel of moist air becomes saturated if experience a forced ascent (Stull, 2016). It provides an estimate of the height at which the clouds can be formed. The temperature gradient is an indicator of how easily a parcel of air can be lifted (Spellman, 2012) and can be used as a proxy of the atmospheric stability. During unstable atmospheric conditions ($\frac{\Delta\theta_v}{\Delta z} < 0$) is more easy to move upwards the parcels of air than under stable conditions ($\frac{\Delta\theta_v}{\Delta z} > 0$). Finally, precipitation saturates the air column and provides the water vapor after the splash droplet evaporation process on the canopy and forest floor surfaces.

During the full monitoring period at La Selva Biological Station, only 1.4 % of our study period accomplished the conditions required for the formation of visible vapor plumes (precipitation, $Z_{\mathrm{lcl}} < 100$ m and $0 > \frac{\Delta\theta_v}{\Delta z} > -1$). These conditions differ from those needed to form mist. In a tropical wet forest in Costa Rica, fog and mist formation happens before sunrise (Allen et al., 1972). However, fog does not involve the upward convective flux needed for vapor plumes, while mist is affected by this upward convective flux but without rain (Stull, 2016). Vapor plumes are buoyant cloud formations with an identifiable shape (Spellman, 2012), main char-

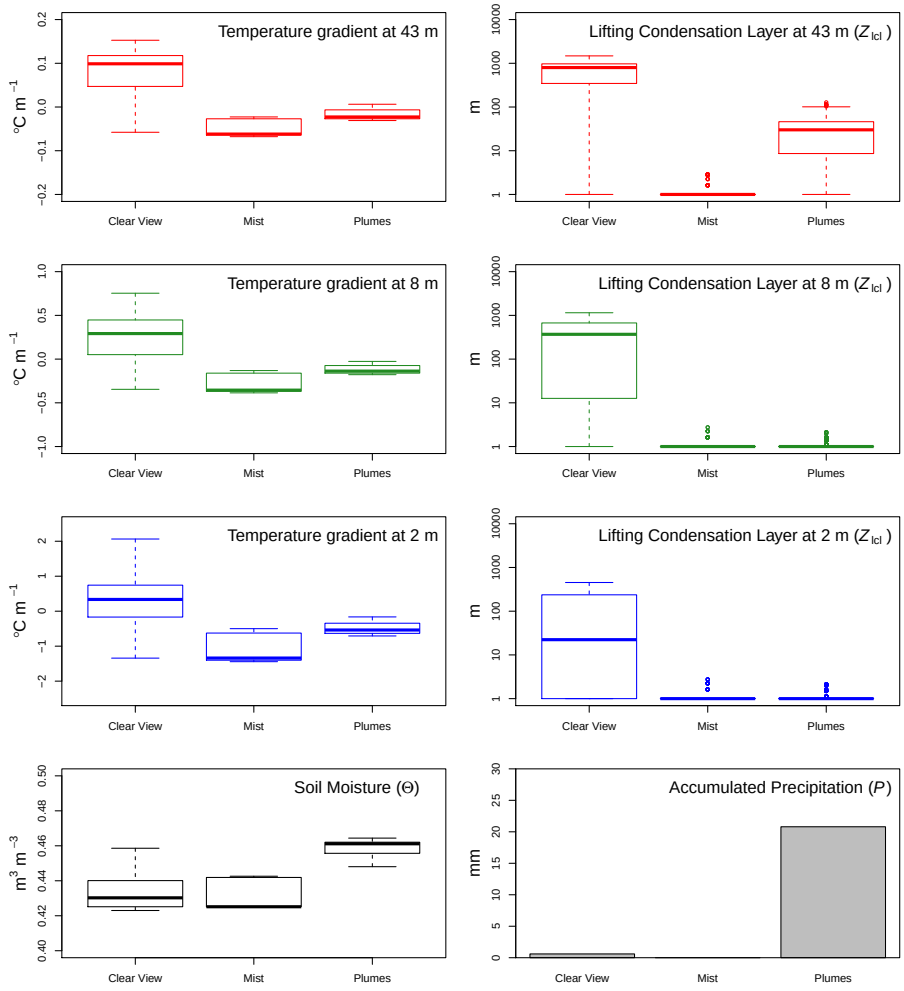

Figure 4.3: Boxplots describing the temperature gradients ($\frac{\Delta\theta_v}{\Delta z}$) and lifting condensation level (Z_{lcl}) at 43 m, 8 m and 2 m, as well as soil moisture (Θ) and total precipitation (P) of the three visual categories evaluated.

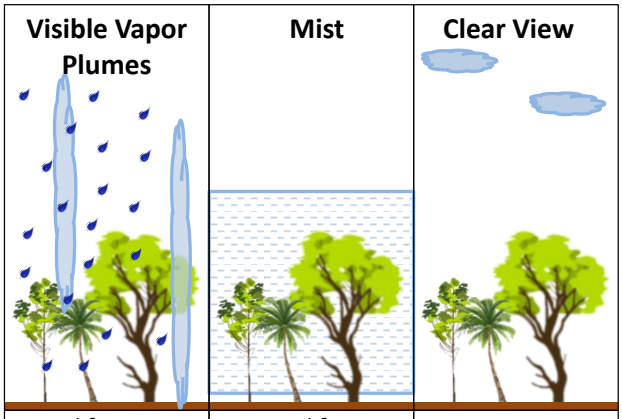

$0 > \frac{\Delta\theta_{v.2m}}{\Delta z} > -1$	$-1 > \frac{\Delta\theta_{v.2m}}{\Delta z}$	- -
$Z_{lcl.43m} < 100$ m	$Z_{lcl.43m} < 10$ m	- -
$P > 0$	$P = 0$	- -

Figure 4.4: Simplification diagram describing the required conditions to form visible vapor plumes in a Tropical Wet Forest and the differences between mist and clear view conditions.

acteristics that allow the differentiation from fog and mist events. While mist and fog are formed by microscopic water droplets floating in the air which can reduce the visibility to less than one kilometer in the case of fog or a lesser extent with the mist (Spellman, 2012).

4.4. Conclusions

The visual monitoring captured the formation of visible vapor plumes close to the surface boundary layer of a Tropical Wet Forest (TWF) during rainy conditions. These visible plumes are the visual evidence of evaporation processes happening during rain events, where the splash droplet evaporation process provides the required water vapor to form visible vapor plumes. This water vapor is part of the intercepted water evaporated from the forest floor and plant surfaces since transpiration is reduced by the low vapor pressure deficit. It is raised up by air convection driven by warm soil temperatures. Finally, condensing close to the forest canopy due to the drop in the virtual potential air temperature along the forest air column. Consequently, this phenomenon can be identified in TWF when precipitation occurs, the lifting condensation level at 43 m height (Z_{lcl}) is lower than 100 m, and the temperature gradient ($\frac{\Delta\theta_{\mathrm{v}}}{\Delta z}$) at 2 m height is between 0 and -1 °C m^{-1}. Contrary to the vapor plumes, mist appear when no precipitation occurs ($P = 0$), Z_{lcl} at 43 m is less than 10 m and $\frac{\Delta\theta_{\mathrm{v}}}{\Delta z}$ is less than -0.5 °C m^{-1}. This work also brings the

attention to the forest evaporation role during rain events, where little information is still available.

5

The tale of a tree and a shrub

The effect of two plant covers on the soil water conditions in arid environments

Sandy soils all around
with random spots and rows of green,
sucking water from below
wetting their roots for the Autumn to come.

This chapter is based on:

Jiménez–Rodríguez, C.D., Coenders–Gerrits, M., Uhlenbrook, S. and Wenninger, J. (2019). *What Do Plants Leave after Summer on the Ground?-The Effect of Afforested Plants in Arid Environments.* Water. 11(12), 2559.

5.1. Introduction

Continental arid environments are characterized by excessive heat and variable precipitation distributed all over the year, with a tendency to a peak during summer months (Abd El-Ghani et al., 2017; Salem, 1989; Bonan, 2002). These conditions favoured the presence of a discontinuous vegetation cover characterized by banded and spotted shapes, large size variability, and specialized plant species (Aguiar and Sala, 1999; Bonan, 2002; Wainwright et al., 1999). The northern arid lands in China are an example of this type of environment, where the landscape is shaped by eolic erosion due to the high erodability of this soil type and the scarce ground cover protection (FAO, 2006; Huggett, 2007; Summerfield, 1991; Yang et al., 2005; Young, 1989). Consequently, desertification in this region registered a strong growth of barren areas before 1999 (Han et al., 2015). However, after 2005 the plant cover experienced a positive change reducing the areas affected by desertification thanks to the rehabilitation and afforestation programs established in the region (Han et al., 2015; Song et al., 2015). The current implementation of afforestation and agricultural programs modified the landscape cover with additional crop areas. These afforestation practices trigger a series of impacts to the environment due to the inadequate selection of plant species (Cao et al., 2010, 2011). This increment in vegetation cover reduces the local surface temperature (Peng et al., 2014) and affects the local evaporation flux due to the increment of plant transpiration which depends mostly on groundwater (Yang et al., 2012; Yin et al., 2014; Zhou et al., 2013).

The evaporation (E) of arid environments is mainly composed of soil evaporation (E_s) and a small proportion of intercepted water by plant surfaces (E_i) and transpiration (E_t) (Roberts, 1999; Savenije, 2004; Yaseef et al., 2009). The low precipitation rates underline the importance of soil water and groundwater availability for the plants. Rainfall interception decreases the water infiltration rates of vegetated areas in respect to bare soil conditions in arid and semi-arid regions (Scanlon et al., 2006; feng Zhang et al., 2015). This is the result of the quick evaporation of the intercepted water on the leaves, branches, and stem of the plants (Roberts, 1999; Yaseef et al., 2009). The relevance of interception increases considering the precipitation characteristics of the arid and semi–arid regions where the low volume, high intensity, lower and irregular frequency hinder the plant water acquisition (Wainwright et al., 1999). Due to the scarce water resources in these regions the plants are adapted to quickly respond to environmental triggers such as the irregular rains (Noy-Meir, 1973). Thus increases the soil water acquisition by the plants and consequently its transpiration momentarily (Chesson et al., 2004; Ivans et al., 2006).

The plant root system provides anchorage for the plant and an effective water extraction system (Ogle et al., 2004) which is powered by the plant transpiration (Hopkins and Hüner, 2008). This system absorbs the water close to the meristematic region of the root, transporting it through the xylem towards the leaves, and using it during photosynthesis (Cardon and Whitbeck, 2007; Curl and Truelove,

1986; Hopkins and Hüner, 2008). However, the presence of young roots in soil layers does not mean effective absorption of water from those zones (Dawson et al., 2002). Instead, some species are able to absorb water through suberized roots under soft drought or winter conditions (Curl and Truelove, 1986; Hopkins and Hüner, 2008). As a consequence, the identification of plant water sources is a difficult task that requires the use of tracers.

Determination of water sources for the plants has been successfully done with the stable water isotopes oxygen (δ^{18}O) and hydrogen (δ^{2}H) (Evaristo et al., 2017; Jia et al., 2012; Ogle et al., 2004; Nie et al., 2011; Palacio et al., 2017; Rossatto et al., 2012; Swaffer et al., 2013; Voltas et al., 2015; Wang et al., 2010; Wei et al., 2013; Zhou et al., 2013). The specific isotopic signatures of soil water is the result of a fractionation process that modifies the isotope composition (Barbeta et al., 2018; Geyh, 2000), allowing to trace the water paths within the ecosystem (Leibundgut and Seibert, 2011). The isotope signature of the absorbed water is not modified by plant uptake until the water reaches the photosynthetic tissues (Dawson et al., 2002; Ogle et al., 2004). Here, the leaf tissues will become enriched by the escape of lighter isotopes (Butt et al., 2010). Althought the roots do not modify the soil water during uptake, the isotope signature of xylem water is affected by mixing processes when different water sources are used by the same plant. Barbeta et al. (2018) briefly describe a series of analysis tools used for the determination of water sources used by plants. Some of these methods are the bayesian isotope mixing models such as SIAR (Parnell et al., 2010, 2013) and MixSIAR (Moore and Semmens, 2008), or standard linear mixing models such as IsoSource (Phillips et al., 2005; Phillips and Gregg, 2003). IsoSource model provides all the feasible combination of water source contributions keeping the mass balance principle. It uses only the isotope signature of the water sources and the xylem water as the final mixture. SIAR and MixSIR models require more complex data sets. These models require the isotope signatures of the sources and mixtures as well as their standard deviations and an enrichment factor. As a result, the models provide the statistical uncertainties and the optimal solution for the analyzed mixture. The IsoSource tool has been used to study sand dunes bushes, corn and cotton plantations, woody species, and estuarine vegetation to determine the water sources of those covers (Jia et al., 2012; Nie et al., 2011; Rossatto et al., 2012; Swaffer et al., 2013; Wang et al., 2010; Wei et al., 2013). Thus can provide information of the origin of water within the plant and if this water can be redistributed on the soil profile.

The implementation of afforestation programs in arid environments modify the distribution patterns of local vegetation, influencing the ratio between transpiration and evaporation ($\frac{E_t}{E}$)(Zhu et al., 2015). These changes together with the usual omission of interception of precipitation (Roberts, 1999; Walker and Langridge, 1996; Yaseef et al., 2009), the irregular rains (Wainwright et al., 1999) and the large capacity to transpire soil water by arid plants (Schlesinger et al., 1987); exert a lot of pressure on the scarce water resources of arid environments. This has been the case with the introduction of Willow trees (*Salix matsudana*) and Willow

bushes (*Salix psammophila*) in afforestation programs in the Hailiutu catchment (Yang et al., 2012; Yin et al., 2014; Zhou et al., 2013). The transpiration of these species increased the demand on the groundwater resource, however its influence on the soil water conditions are poorly understood.

This chapter describe the effect of two land covers on the soil water conditions after summer in arid environments. The monitoring included the soil moisture, fine root distribution and transpiration fluxes that provided information about water availability, access and use by the plants. Meanwhile the monitoring of stable water isotopes collected from precipitation, soil water, groundwater and xylem water linked the water fluxes. This information provided an indication of the vegetation influence on the soil water conditions beneath the covers.

5.2. Methods: Assessing plant cover in arid environments

5.2.1. Study Site: Temperate Shrubland

The study site is located within the Hailiutu catchment (area: 2645 km^2) in Yulin County; Shaanxi province; Northwest China (Figure 5.1). This catchment is part of the Maowusu semi-desert, which is characterized by undulating sand dunes over and dominated by a xeric scrubland. The nearest meteorological stations (Dong Shen: N 39.833° – E: 109.983°; Yanchi: N 37.800° – E 107.383°; and Yulin: N 38.233° – E: 109.700°) described a semi-arid continental climate with a mean annual precipitation of 386.1 mm yr^{-1} and a mean annual temperature of 8.6 °C (seasonal range: -17.4 °C to 27.1 °C) based on 12 years of meteorological records (period: 2000-2011). The soil type is classified as Calcaric Arenosols (ARc) with a high concentration of basic cations (Ca^{2+}, Mg^{2+}, K^+ and Na^+) and a pH value over 8.0; with an excessive drainage due to its sandy texture (IIASA/FAO, 2012). The study site is composed of two experimental plots located at 300 m from each other. The first plot is dominated by Willow bushes (*Salix psammophila* C. Wang & Chang Y. Yang) and has an area of 625 m^2 (25m x 25m). The second plot covers 81 m^2 (9 m x 9 m) and contains mainly individuals of Willow trees (*Salix matsudana* Koidz.) and Poplar trees (*Populus simonii* Carr.). In both plots soil water, groundwater, plant parameters, and soil variables were measured between September and October, 2010.

5.2.2. Hydrologic Data

Meteorological data was retrieved from the stations Dong Shen (1459 m a.s.l.), Yanchi (1356 m a.s.l.), and Yulin (1058 m a.s.l.). The climatic data was downloaded from the National Oceanic and Atmospheric Administration (NOAA) (NCDC, 2012). This data set contains daily values of total precipitation (mm d^{-1}) and daily means for temperature (°C), dewpoint (°C), wind speed (m s^{-1}), and atmospheric pressure (mbar). Due the lack of solar radiation measurements in the selected study period,

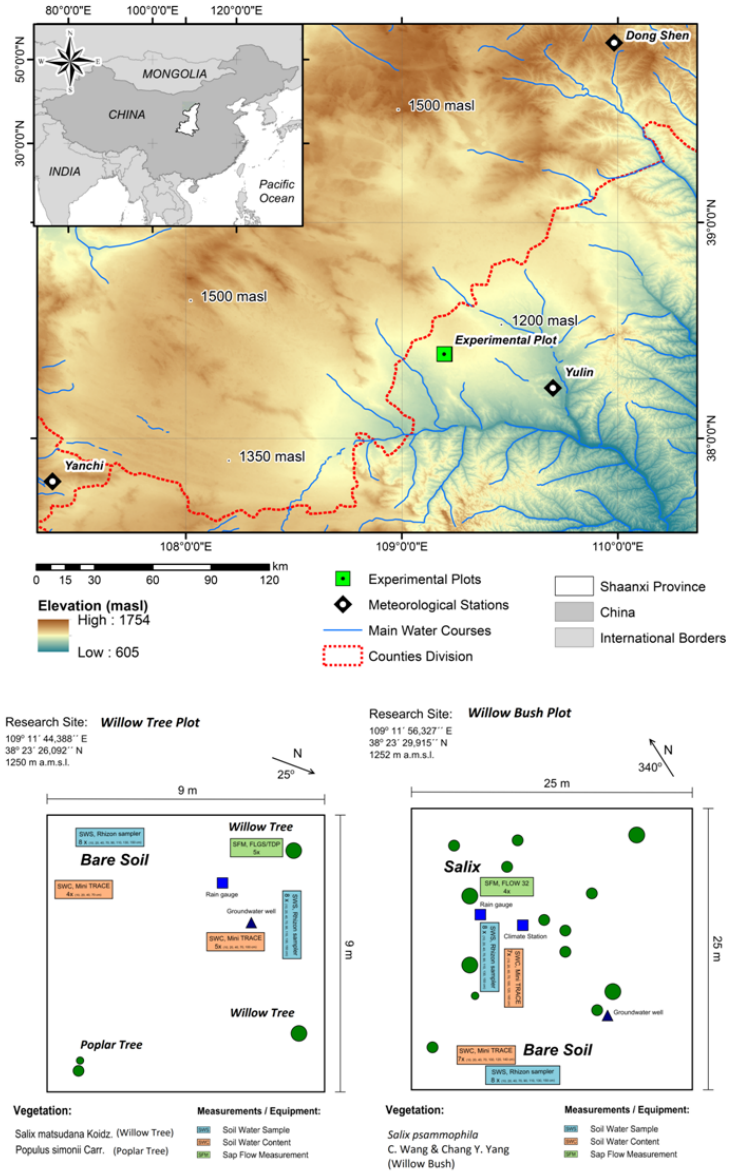

Figure 5.1: Geographical location of the experimental site and the meteorological stations Dong Shen, Yanchi and Yulin used during the study period in the Shaanxi province, China. The experimental design of both plots is shown on the bottom of the map.

this variable was estimated according to Allen et al. (1998) for missing data. Once all data were determined, the reference evaporation (E_o) in mm d^{-1} was calculated with the FAO Penman–Monteith equation (Allen et al., 1998). Soil moisture (Θ, $m^3\,m^{-3}$) and groundwater level (h, m) measurements were carried out to describe the soil water dynamics in both sites. Soil moisture measurements were carried out sporadically along the study period. The reference values of soil moisture in sandy soils for permanent wilting point (Θ_{WP}), field capacity (Θ_{FC}) and saturation point (Θ_{SP}) were 0.05 $m^3\,m^{-3}$, 0.1 $m^3\,m^{-3}$ and 0.46 $m^3\,m^{-3}$, respectively (Saxton and Rawls, 2006). Soil moisture probes were located at 10 cm, 20 cm, 40 cm, 70 cm, and 100 cm depth beneath each species. On the Willow bush plot two more depths were monitored: 120 cm and 140 cm. Considering the presence of bare soil areas within the plots, the soil moisture was also monitored at the same depths as Willow bush. The groundwater level was measured on a daily basis from the ground surface as the reference point in each plot. Groundwater depth from the surface in both plots oscillates between 136 cm to 164 cm beneath the Willow bush plot and between 150 cm to 172 cm beneath Willow tree plot (period between 21-08-2010 to 20-04-2011).

5.2.3. Water Sampling

Water samples were collected after each rainy day to determine the isotopic signature of the precipitation, groundwater, soil water, and xylem water throughout the monitoring period. Soil water samples were taken with a soil moisture sampler in both plots. The samples were collected at nine depths (10 cm, 20 cm, 40 cm, 70 cm, 90 cm, 110 cm, 140 cm, 150 cm and 160 cm), while the groundwater sampling depended on the water head elevation during the samplings. Xylem water was collected from an incision done at the twig of each tree; removing the bark, phloem, and cambium to prevent the collection of fractionated sap water. The incision location was far from the meristematic region, avoiding the fractionation linked to photosynthesis. Rain water was collected during the events to prevent fractionation by evaporation on an event basis. Each sample was sealed hermetically in 1.5 mL vials and transported to The Netherlands for their analysis. Stable water isotope signatures of the liquid samples were expressed in δ values (‰), representing the relative deviation from Vienna Standard Mean Ocean Water (VSMOW) (Craig, 1961).

5.2.4. Plant Parameters

For each plot the plant densities (plants ha^{-1}), canopy heights (m), and leaf area index (LAI, $m^2\,m^{-2}$) were measured to describe the stand conditions. Transpired water (E_t) was monitored in the Willow shrubs establishing four ring gauges in an individual of Willow bush at 35 cm height. Five probes were installed in an individual of Willow at 1.3 m height. Each probe recorded the data at 10 minute intervals and those were summarized in an hourly and daily time step. Total mobilized water as transpiration was calculated with the product between the sapwood area

and flow velocity. Considering the physiognomic differences between both plant species, the sapwood area was estimated accordingly with the plant type. Willow bush is a bush up to 4 m tall with numerous branchlets per plant (Wang and Chang, 1980), where most of the xylem within the branchlets is able to transport water. As a consequence, the sapwood area was measured through the average diameter of the measured branchlets. Willow tree is able to grow up to 10 m height with a symmetrical crown with a sole stem (Gilman and Watson, 1994). It has a clear differentiation between sapwood and hardwood, allowing to measure directly the sapwood from a tree wood ring obtained from the measured tree. The wood ring area was measured from inked water transported by capillary rise within the active sapwood sections. Sapwood area (A) for the Willow tree was 274.6 cm^2 and the average area for Willow bush was 5.1 cm^2. Transpiration flow for each plant was obtained though the empirical equation developed by Granier (1985).

The fine root system was described through the total root biomass (TRB, $kg\,m^{-3}$) and the root length density (RLD, $cm\,cm^{-3}$). The survey involved the collection of 80 samples of soil per species with an auger of 300 cm^3 within a radius of 4.0 m. The sampling procedure was based on eight equidistant points from the stem towards the canopy edge, extracting 10 samples per point until a depth of 150 cm was reached. The samples were sieved to separate the soil from the roots, photographed on a scaled paper, and dried up following the procedure proposed by Cornelissen et al. (2003) to determine the root length density (RLD, $cm\,cm^{-3}$). The total root biomass was determined by weighing the dry cleaned roots with a digital balance. The total root length (cm) was determined by processing the root images with the use of the GIS free source software (www.gvsig.org). The total root length density was obtained dividing the total root length (cm) by the core volumes (cm^3) (Huang et al., 2015).

5.2.5. Data Analysis

Plant differences were determined using an Analysis of Covariance (ANCOVA) with a p_{value} of 0.05. Statistical differences were determined with a Tukey HSD analysis. A Pearson correlation analysis was applied to evaluate the influence of meteorological conditions on plant transpiration. All the statistical analyses are based on normal distributions, so the normality, variance homogeneity and presence of outliers were tested. The plant water source of transpiration was determined using the software IsoSource (Phillips et al., 2005). This model provides the relative contributions of soil water sources to sap flow in both species, based on the isotopic mass balance principle. Consequently, the isotopic soil water contribution analysis followed the "a posteriori aggregation" method proposed by Phillips et al. (2005). This method allows the aggregation of sources with similar isotopic signatures based on specific characteristics showed by the sources, reducing the number of contributing factors.

5.3. Results

Total precipitation in 2010 was 401.0 mm yr^{-1} at the experimental site, registering a slightly wet condition in respect to the regional average of 386.1 mm yr^{-1}. However, this amount of precipitation does not supply the reference evaporation (E_o) of 1339.1 mm yr^{-1} at this site as a consequence of the irregular rain events (Figure 5.2). The 938.1 mm yr^{-1} difference between precipitation and reference evaporation support the Arid Steppe classification due to its annual water deficit (Bonan, 2002; Kottek et al., 2006; Peel et al., 2007; Wainwright et al., 1999). September and October 2010 registered 48.2 mm $month^{-1}$ and 40.5 mm $month^{-1}$ of precipitation accounting for 12.0% and 10.1% of the annual amount, respectively. The water availability experienced during the study period allowed the presence of soil moisture above the permanent wilting point (Θ_{WP}) for sandy soils (0.05 $m^3\ m^{-3}$) while the field capacity (Θ_{FC}) was exceeded only in the deepest layers in both plots (Figure 5.3). Additionally, soil moisture increases with depth in Willow bush and Willow tree stands, keeping higher values than under bare soil conditions. Soil moisture under both plant species has larger values in respect to bare soil condition until a depth of 100 cm (ANCOVA, F= 37.91, p= 0.0000). Average soil moisture shows the following order: Willow bush (Θ: 0.11 $m^3\ m^{-3}$) > Willow tree (Θ: 0.10 $m^3\ m^{-3}$) > Bare Soil (Θ: 0.08 $m^3\ m^{-3}$).

Hourly transpiration differs in amount and timing between species. Figure 5.4 shows the differences along five days where the sap flux for Willow tree is remarkably higher than Willow bush. Willow tree shows a larger capacity to transpire water with peak fluxes averaging 1549.1 g hr^{-1}; whereas Willow bush peaks do not exceed 500 g hr^{-1} on average. Daily transpiration rates in both species depict a significant decreasing trend (ANCOVA, F= 36.09; n= 87, p= 0.0000) and a statistical difference between total daily rates (ANCOVA, F= 63.05, n=87, p= 0.0000), where Willow bush transport an average of 4.57 kg d^{-1} being three times smaller than Willow tree fluxes (12.82 kg d^{-1}). In addition, as transpiration is a physiological response to environmental climatic parameters the Pearson correlation analysis (p< 0.001) shows a significant positive correlation with temperature (r= 0.47) and net radiation (r= 0.35); while wind speed (r= 0.05) and relative humidity (r= -0.27) are not significant.

Rain during the study period has a wide range of isotope signatures. The evaporation front is identifiable at 40 cm depth for Willow and at 20 cm for Willow bush in both isotopes (Figure 5.5). The isotope signature of groundwater samples (Willow Bush: $\delta^{18}O$: -9.2 ‰, $\delta^{2}H$: -66.1 ‰ and Willow Tree: $\delta^{18}O$: -8.59 ‰, $\delta^{2}H$: -60.66 ‰) lie close to the rain water signature, depicting the effect of local groundwater recharge having a similar signature to local rains. Sap water signature in both species seems to contain fractionated and non-fractionated water. However, both stable isotopes do not show statistical differences between species ($p > 0.05$) as a consequence of the wide variation in isotope signatures. After a preliminary run of the IsoSource the soil water contribution to xylem water from deeper soil layers show a similar proportion in both species. It showed that only the 40 cm and 10 cm

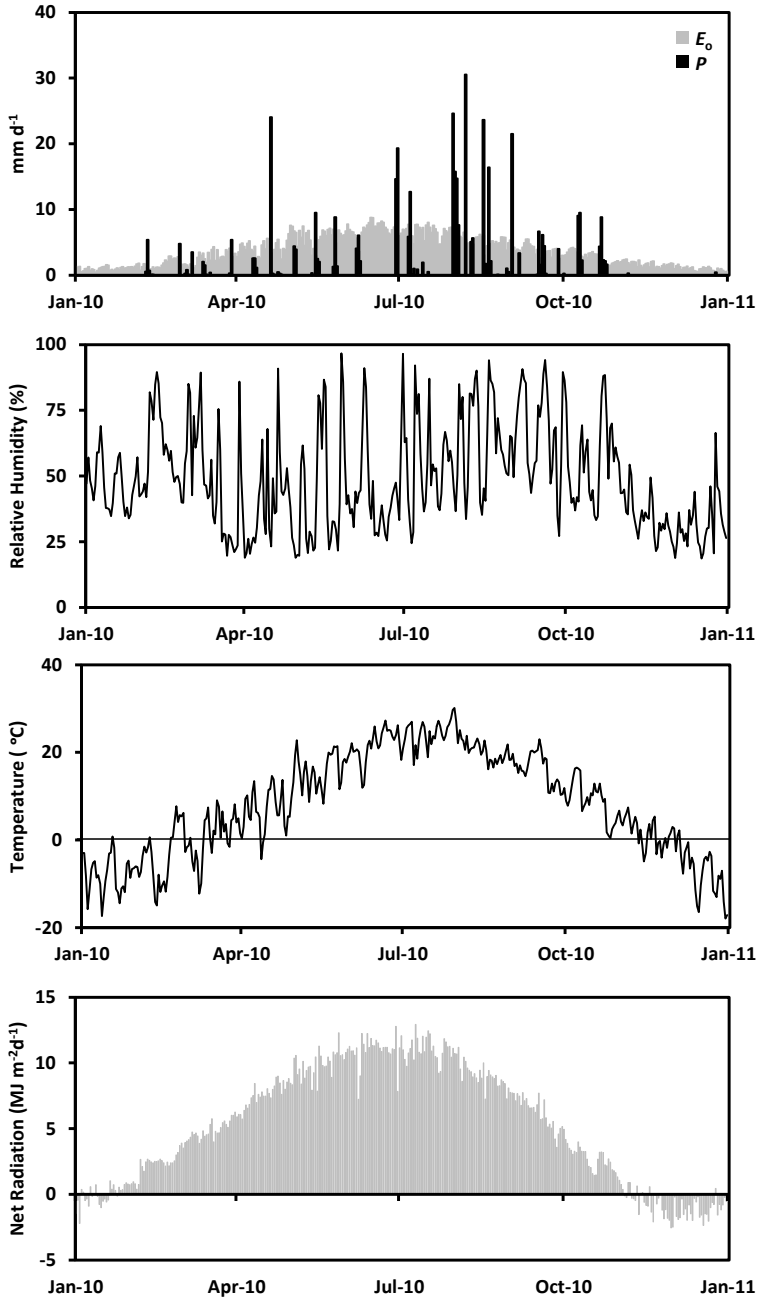

Figure 5.2: Meteorological conditions registered during 2010 at the research site based on the data of Dong Shen, Yanchi and Yulin meteorological stations

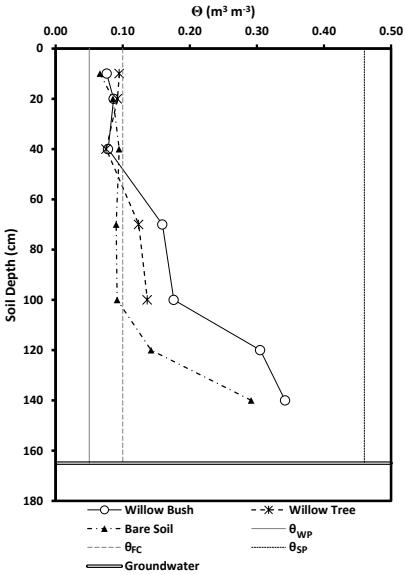

Figure 5.3: Soil moisture ($m^3\ m^{-3}$) measured in both plots for Willow bush, Willow tree and bare soil conditions during the study period.

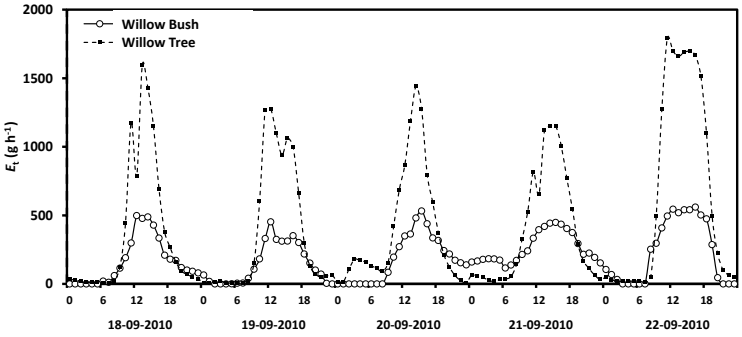

Figure 5.4: Hourly transpiration flow measured in Willow tree and Willow bush plants during the study period

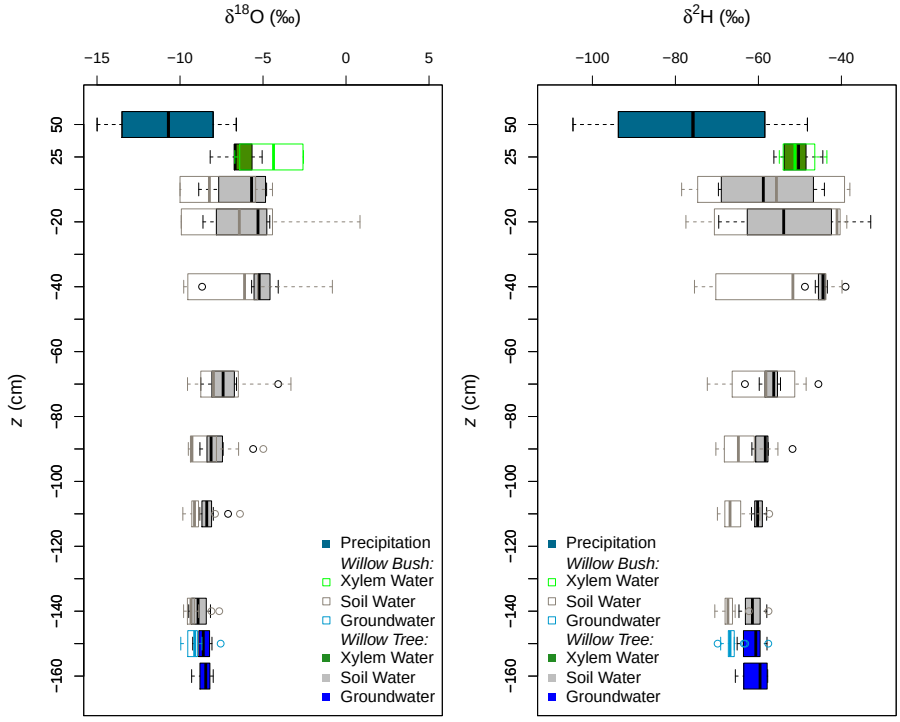

Figure 5.5: Isotopic profile of the stable water isotopes sampled in both stands during autumn 2010. Each boxplot describes the data set with the median (thick vertical line within the box), the first and third quartiles (edges of the box), and the minimum and maximum values (whiskers).

soil layers provide a strong contribution in Willow and Willow bush, respectively. Therefore "a posteriori aggregation" (Phillips et al., 2005) was performed, grouping the soil layers according to their similarities between isotopic signatures, evaporation front presence, and proximity within the soil profile. The grouping was settled as: 0-30 cm, 30-60 cm, >60 cm; including in the last soil layer the groundwater due its isotopic similarity with the deeper soil waters. The IsoSource output shows all the possible solutions to match the sap water mixture of δ^2H and δ^{18}O (Figure 5.6). The Willow tree stand shows a well-defined proportion of soil water contributions among the three water sources. The deep water source (>60 cm) contributes with a proportion lower than 0.08 to the sap water mixture, while the upper soil layers (<30 cm) provides between 0.28 and 0.48 of the mixed water, and the intermediate soil layers (30-60 cm) own the higher contribution values from 0.50 to 0.64. The clear differentiation between soil water sources in Willow is not visible for Willow bush. This species shows overlapping contributions of the water sources mainly for the superficial soil layers (0-60 cm), showing the deepest water source a contribution ranging from 0.21 to 0.54 (Figure 5.6).

Plant densities differ between stands, where the Willow bush stand has the

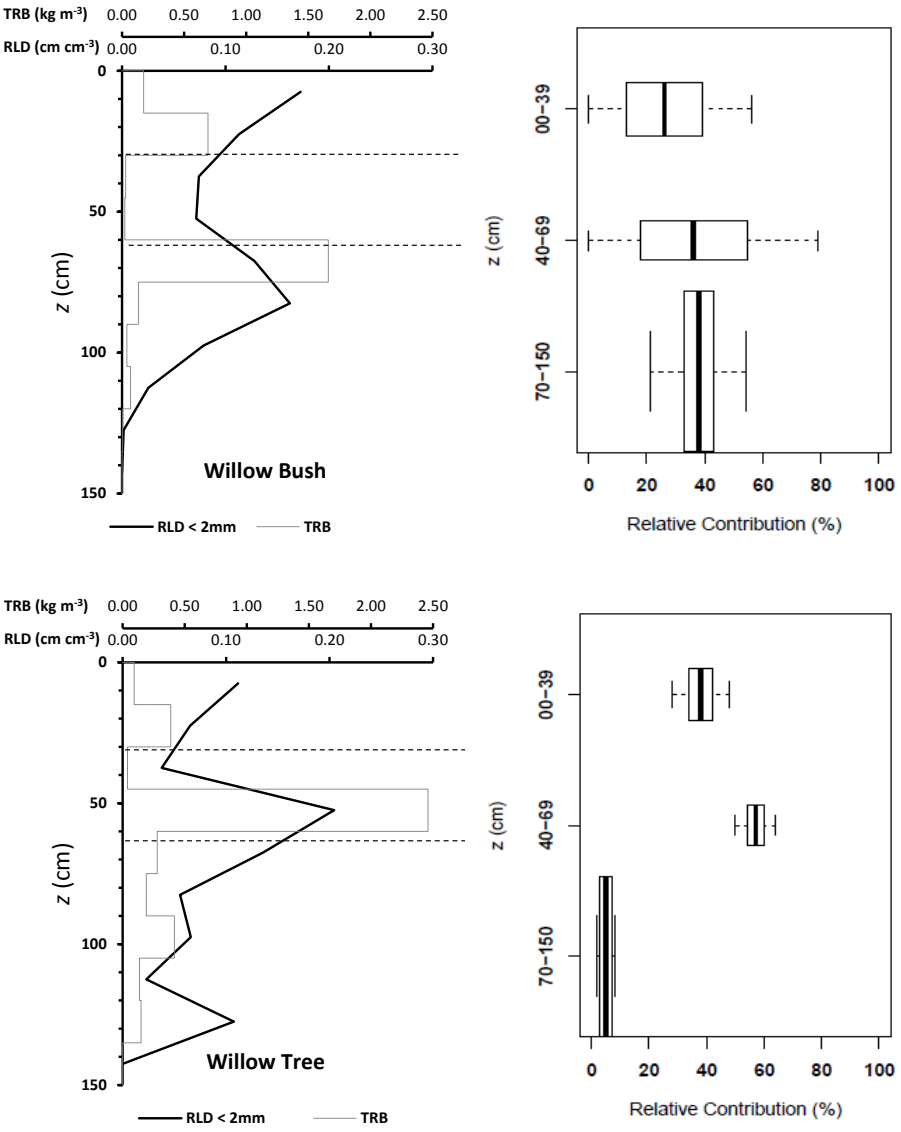

Figure 5.6: Root length density (RLD) and total root biomass (TRB) distribution along the soil profile, and its relation with the relative contribution to sap water mixture of Willow tree and Willow bush based on δ^2H and δ^{18}O isotope signatures per group of soil depth. Each boxplot describes the the median (thick vertical line within the box), the first and third quartiles (edges of the box), and the minimum and maximum values (whiskers). The boxplot height is proportional to the soil depth range.

higher plant density (900 trees ha^{-1}) with an average height of 2.6 ± 0.6 m. In contrast, the Willow tree stand has a plant density three times smaller (300 trees ha^{-1}) but with higher trees (3.5 ± 0.5 m). However, the LAI is affected by the leaf size and canopy diameter of the individual plants, where Willow bush register a leaf area index of 0.39 $m^2\ m^{-2}$ which is twice smaller than Willow tree (0.68 $m^2\ m^{-2}$). Underground stand characteristics also differ between species. Willow trees fix a larger root biomass beneath the 45 cm depth than Willow bush shrubs. Moreover, the root length density distribution shows a bimodal accumulation in Willow bush: at the soil surface (0-30 cm) and at mid depth (55-70 cm). Oppositely, Willow tree has three sections with high RLD values. The first two sections follow the Willow bush pattern, with an additional accumulation bellow 105 cm. The fine root distribution in both species expressed as RLD, provide them a good system for soil water acquisition for the superficial soil layers (Figure 5.6).

5.4. Discussion

The main differences in plant size, fine root distribution, and water uptake capacity between Willow tree and Willow bush underline the importance of selecting plant species with low water requirements in respect to their biomass for afforestation programs. Willow tree is capable to withdraw up to 12.8 kg d^{-1} of water, extracting more than 90% from soil layers above 60 cm depth. This species is capable to make use of the superficial soil water during the autumn period, even if the groundwater level is shallow. Conversely, Willow bush show lower transpiration rates not higher than 5.0 kg d^{-1} extracted uniformly from the whole soil profile including the groundwater. This extraction pattern shown by Willow bush depicts a more efficient root system acquiring water from different soil water sources due their fine root distribution. During this period, both species extract more than 50% of the water from the upper soil layers, taking advantage of the sporadic autumn rains and residual soil moisture. These results are congruent with the behavior of Willow bush during the growing season (May-July), where Willow bush uses water from both sources: soil and groundwater (Zhou et al., 2013). On the other hand, the soil water dependency during autumn of Willow trees differ in their summer behavior as documented by Yin et al. (2014). During summer, Willow trees have access to soil and groundwater to maintain their water consumption.

Shallow groundwater levels prevent desiccation processes in scarce rainfall environments, providing a vast water source for adapted plants that use the water economically (Jiang and He, 1999). Even if both species do not differ in the root amount, their vertical distribution shows different root spots. Willow bush root distribution displays two zones, supporting the hierarchy theory proposed by Schwinning and Sala (2004). The Willow bush can withdraw water from rains as stemflow, while the deeper roots can obtained from a constant source (groundwater in this case). The fine root distribution beneath the Willow tree exemplifies woody patches capacity to use rain water in a short time response (Midwood et al., 1998), as well as the hierarchy theory of Schwinning and Sala (2004). The fine root distribution of

Willow tree with three dense regions with RLD higher than 0.1 cm cm^{-3} allow them to use different soil water source depending on soil water availability.

The isotopic values of groundwater are similar to local rain water, depicting a local groundwater recharge documented for the Hailiutu catchment (Zhou et al., 2013). This is the consequence of the high capacity to infiltrate water by the sandy soils (Yaseef et al., 2009). Consequently, infiltrated water will be available for longer periods because soil water evaporation at soil depths between 10–30 cm can take several weeks in arid environments (Noy-Meir, 1973). The shallow groundwater recharge occurred during the previous growing season due to the high rainfall intensities (>5 mm d^{-1}) between July and September. This phenomena has also been documented by Li et al. (2007) in Taihang (China), reporting a daily groundwater recharge with rains ranging from 3.2 mm d^{-1} to 3.8 mm d^{-1}. This recharge capacity has been registered in the provinces of Shangxi and Inner Mongolia, gattering from 9% to 12% of the long term annual precipitation (Scanlon et al., 2006).

Conversely to groundwater, the isotopic composition of the soil water in the unsaturated zone is affected by the interaction between vegetation cover and soil evaporation. Soil evaporation affects the isotopic signature of soil water in the unsaturated zone providing particular signatures at different soil layers (Barnes, 1988; Brunel et al., 1995; Rothfuss et al., 2010; Schwinning and Ehleringer, 2001). Meanwhile the plant cover type reduces the soil evaporation, where lower Θ in the top soil layer (0-10 cm) were registered for Willow bushes in comparison to Willow trees. Conversely, the high Θ under Willow bush in respect to Willow tree reflects capacity to fix more root biomass below 40 cm depth. This enhanced the infiltration capacity by the presence of a low plant cover with a large alive root system (Basche and DeLonge, 2019; Fischer et al., 2015).

However, the stable isotope signatures of soil water beneath the plant cover differs considerably. Beneath Willow trees, both isotopes depict the theoretical evaporation front. This as a consequence of the evaporation process in the superficial soil layers, enabling the generation of heavy isotope enrichment (Barnes, 1988; Li et al., 2007; Midwood et al., 1998; Sutanto et al., 2012; Wenninger et al., 2010) (see Figure 5.5). On the other hand, beneath Willow bush only the δ^{18}O profile shows the theoretical evaporation front. The homogeneity of δ^{2}H beneath Willow bush indicates a recent redistribution of groundwater along the soil profile, which can be linked to hydraulic lift processes carried out by this bush.

Lower evaporation rates during the study period depict a lower water need for both species, that is visible in the diminution of sap flow rates. Solar radiation and air temperature are the limiting factors for transpiration as it was showed by the p_{values}. The diminution of solar radiation and air temperature in the region are the clear indication of the arrival of autumn (Bonan, 2002), which reduces the available energy for the plants to carry out the photosynthesis. Also, the access to the groundwater reservoir allowed the plants to prevent dehydration, reducing the ef-

fect of wind speed and relative humidity as triggers of the transpiration process as it happens during summer with both species (Huang et al., 2015; Yin et al., 2014). This reduction in water needs affects the water uptake of Willow tree, which registered a lower contribution of deep soil water sources while the water uptake by superficial roots is more constant. On the other hand, Willow bush shows a high dynamic root system which extracts water from all the available sources indifferently from the upper soil layers and a strong contribution of the deep sources. This contribution is linked to the root distribution, keeping a high root length density in comparison to the Willow tree. The groundwater dependency of Willow bush (Zhou et al., 2013) implies a permanent deep water extraction during summer and autumn, extracting more deep water than Willow trees during the autumn season.

Despite the few rains, water used of both plant species does not reduce the soil water storage on the soil layers above 100 cm. This can be linked to the presence of hydraulic lift, where the root system prevents the soil water depletion on upper soil layers thanks to the redistribution of deeper soil water (in this case, groundwater). The hydraulic lift allows the formation of water pools along the soil profile in water scarce environments (Horton and Hart, 1998; Liste and White, 2008). This process requires the movement of soil water by the potential difference between roots and the soil (Brooksbank et al., 2011; Horton and Hart, 1998; Liste and White, 2008; Niinemets, 2010), allowing the diffusion of water through the roots cell membranes. The hydraulic lift had been identified in different plant species such as *Prosopis tamarugo*, *Artemisia tridentata*, *Acer saccharum* and *Madicago sativa* (Horton and Hart, 1998).

The hydraulic lifted water has an isotope signature close to the groundwater. It is relocated during night periods (Caldwell et al., 1998) and once it is on the superficial soil layers evaporation will happen affecting the isotope signature of soil water (Dawson and Pate, 1996). This water relocation is maintained by Willow trees, which despite the larger transpiration rates the soil water is not shortened. Liste and White (2008) mention a Willow as a tree with the water redistribution capacity, providing evidence related to the potential of Willow to use groundwater through this process. Other tree species such as *Eucalyptus kochii* has the capacity to redistribute groundwater (Brooksbank et al., 2011), or use it as an strategy of competition in saline conditions like *Juniperus phoenicea* and *Pistacia lentiscus* (Armas et al., 2010).

The replacement of bare soil areas with different plant covers none adapted to arid environments, speed up the water use in those regions. Water needs of plants such as the Willow tree are high and require a constant water supply (Gilman and Watson, 1994; Yin et al., 2014). On the other hand, the use of plants adapted to arid environments such as the Willow bush (Wang and Chang, 1980) ensure the success of the afforestation programs without risking the scarce water resources. The plant water use during summer months is the largest of the year, as a consequence of the long light hours in temperate regions (Bonan, 2002). During this

time of the year the newly afforested zones extract more water from the soil and groundwater reservoirs. However, the diminution of solar radiation and temperature during autumn reduces the water demand by all the plants. These plants can redistribute part of the groundwater to the upper soil layers, making it available for the periods with no rains. Also, these plants have the capacity to reduce soil evaporation thanks to the shadow effect of their canopy.

5.5. Conclusions

The presence of Willow trees (*Salix matsudana*) and Willow bushes (*Salix psammophila*) reduced the effect of soil evaporation after summer, allowing a larger soil moisture beneath both species than bare soil conditions. Also, the plant cover allowed the soil moisture below 60 cm depth to be larger than the field capacity for sandy soils. This augment in soil water can be linked to water redistribution thanks to the presence of fine roots along the soil profile and the hydraulic lift carried out by the plants. This process redistributes groundwater on the spots with larger fine root allocation, enabling the plants to allocate water at night and using it later during day time. Willow trees use more water for transpiration than willow bushes, this difference in water consumption allows the Willow bushes to keep a higher soil moisture after summer (Θ: 0.11 $m^3\ m^{-3}$) followed by Willow trees (Θ: 0.10 $m^3\ m^{-3}$) and bare soil (Θ: 0.08 $m^3\ m^{-3}$). The larger transpiration rates of Willow trees with respect to Willow bushes do not match with the water source of the xylem water as it is shown by the IsoSource model. This is linked with the hydraulic lift capacity of Willow tree, redistributing groundwater that is quickly affected by evaporation processes. Fine root distribution along the soil profile allowed the water redistribution and later absorption by both plants. This is supported by both species' preferences to withdraw water from the upper soil layers. The water use by Willow bush does not show a strong differentiation among water sources. This species is capable of extracting soil and ground water with different proportions according to water availability. On the other hand, Willow tree is able to extract soil water and groundwater with specific proportions.

6

The thin barrier

The influence of a temperate forest floor cover on a water vapor flux

Like a carpet covering the ground
a silky porosity the mosses have,
tricking the water as it moves down
stopping the vapor that moves up.

6.1. Introduction

Evaporation plays an important role in the hydrological cycle (Yan and Qiu, 2016). It is directly linked to the global energy balance (Coenders-Gerrits et al., 2020) and represents the second largest flux after precipitation (Coenders-Gerrits et al., 2014; Miralles et al., 2011a; Wallace, 1995; Wang et al., 2014). A large fraction of the evaporation in forest ecosystems is product of transpiration processes (Coenders-Gerrits et al., 2014; Schlesinger and Jasechko, 2014). Evaporation processes are affected by the vegetation distribution along the canopy, which affects the within–canopy microclimate (Kumagai, 2011). Parker (1995) defines the forest canopies as all the branches, leaves and twigs located between the forest floor and the canopy interface with the atmosphere. The forest floor is made up of the uppermost layer of soil that includes organic debris (litter) and various vegetation growing attached to it as mosses (Parker, 1995; Nadkarni et al., 2004). Forest floor evaporation plays an important hydrological role as it contributes to the water and energy exchange of forest ecosystems (Heijmans et al., 2004; Sato et al., 2004). It includes the E_{i} from litter and E_{t} from small plants such as mosses, seedlings and ferns, growing on the forest floor. This process is further influenced by the available energy, wind, soil moisture, humidity, temperature and hydraulic soil properties (Baldocchi and Meyers, 1991; Raz-Yaseef et al., 2010).

Stable water isotopes are useful tools to trace the water paths along the hydrological cycle and have been applied to examine water fluxes in forest floors (Sutanto et al., 2012; Dawson and Simonin, 2011; Sprenger et al., 2017b; Magliano et al., 2017). Isotope enrichment and kinetic fractionation processes are the main factors that determine the isotope signatures in the water (Kendall and McDonell, 1998; Sprenger et al., 2016). Throughfall reaching the forest floor is characterized by isotope enrichment in respect to rain water (Allen et al., 2016), as well as soil water which has been affected by evaporation (Sprenger et al., 2016). Hence by sampling the soil water we can gather information about different water fluxes within a forest ecosystem (Hsueh et al., 2016; Sprenger et al., 2016), where soil water uptake by vascular plants does not affect isotopic water content (Ehleringer and Dawson, 1992; Guo et al., 2016). However, how non–vascular plants affect the soil water isotope signatures is poorly understood.

Forest floor evaporation depends on its cover and the above lying ground layer, understory vegetation and canopy structure; as they define the air movement rates between the soil water and the air above the forest floor (Kumagai, 2011; Magliano et al., 2017; Raz-Yaseef et al., 2010). Several studies have shown the effect of bigger plants (crops, shrubs and tree species) on evaporation and fractionation of water stable isotopes in the unsaturated zone of the soil (Allison et al., 1984; Sprenger et al., 2017b). However, the influence of smaller plant species covering the forest floor has not been studied yet. It is necessary to determine the area of influence of any individual or group of plants, because it can modify specific soil characteristics such as pH, electric conductivity or nutrient concentration (Casper et al., 2003). Consequently, any change in soil conditions will affect the vegeta-

tion growth and its response to climate patterns; where any change in the isotope signatures of soil water will help us to understand physiological processes at local scale. This chapter provides insights about the role played by specific forest floor covers during the evaporation process. Also, define if there is any influence on the isotopic signature of the soil water underneath the forest floor covers.

6.2. Methods

6.2.1. Sampling of forest floor covers

Different forest floor covers were selected beneath the canopy of a Douglas-Fir (*Pseudotsuga menziesii* (Mirb.) Franco) stand in Speulderbos, The Netherlands (see Figure 8.1 in Chapter 8). The forest understory is absent in this stand and the forest floor is covered by three types of mosses, one species of fern and patches of tree litter. The soil fermentation layer has different thicknesses ranging between 4 cm to 7 cm (Bosveld and Bouten, 2001; Tietema et al., 2002), with a predominance of fragmented and well decomposed plant residues with presence of fungal hyphae; classifying this humus form as Mormoder (Green et al., 1993; Klinka et al., 1997). The forest soil type has been described as Haplic or Cambic Podzol under the FAO/UNESCO classification system due to the low soil differentiation among layers (Koopmans et al., 1996; Tietema et al., 2002; Tiktak and Bouten, 1994).

The first sampled cover represents the litter layer made up of Douglas-Fir needles, twigs, small branches and cones (Fig. 6.1. A). This cover has different depths depending on the adjacent trees. Therefore two depths were selected for the experiment: 1 cm (Lit-1cm) and 3 cm (Lit-3cm); as these were representative for the area. The third cover is Rough Stalked Feathermoss (Bra-rut; *Brachythecium rutabulum* (Hedw.) Schimp.) which grows associated with stems and debris on the ground (Furness and Grime, 1982; Edwards et al., 2010b; Fletcher, 1991) (Fig. 6.1. B). Thamariskmoss (Thu-tam; *Thuidium tamariscinum* (Hedw.) Schimp.) is the fourth cover (Fig. 6.1. C). This species is commonly found on bare soils in woodlands and amongst grass in damp places as it prefers neutral pH conditions (Motley et al., 2010). The fifth cover is Haircapmoss (Pol-com; *Polytrichum commune* Hedw.) (Fig. 6.1. D), which is characterized by wiry shoots, strong rhizoids and thick leaves, allowing this species to draw water by capillarity from the fermentation layer (Edwards et al., 2010a; Fletcher, 1991). The last cover represents the bare soil condition composed of only the exposed fermentation layer (Bare-soil). Each forest floor cover was harvested from the field by pushing an aluminum ring of 25 cm in diameter into the ground, until the fermentation layer was reached. The core was sealed within a plastic bag for transport to the laboratory and placing it immediately in the lysimeter (see Section 6.2.2) once we arrived at the laboratory.

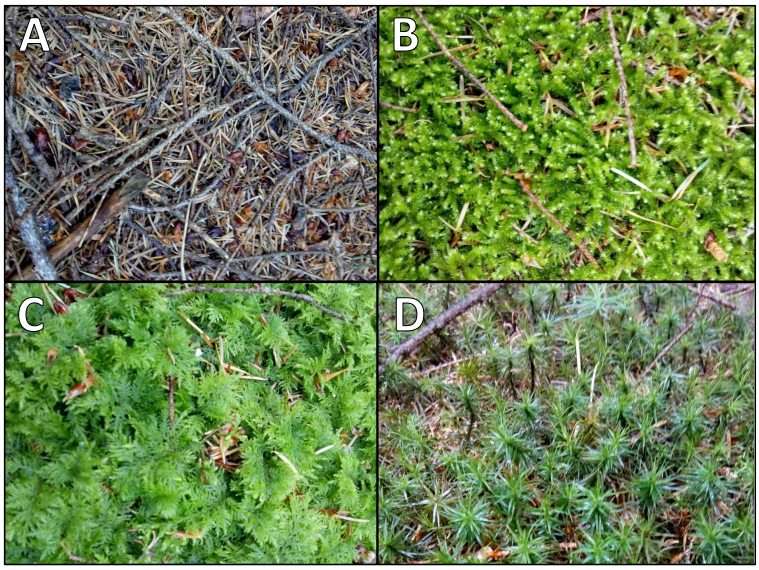

Figure 6.1: Forest floor covers used in the experiment and collected in Speulderbos, The Netherlands. Notes: Litter cover (A), *Brachythecium rutabulum* (B), *Thuidium tamariscinum* (C), and *Polytrichum commune* (D).

6.2.2. Experimental Design

A lysimeter was built from a 25 cm diameter PVC (Polyvinyl chloride) cylinder with a height of 18 cm and thickness of 5 mm (Fig. 6.2). The device consisted of five layers: below the forest floor cover was a fermentation layer of 1 cm depth, followed by 10 cm of mineral soil, then 5 cm of fine sand (grain size $\leq$ 0.25 mm diameter) and the last 2 cm were made up of coarse sand (grain size $\approx$ 2 mm diameter) at the bottom of the lysimeter to enhance the percolation process towards the lower water reservoir. The soil material used to fill the lysimeter was collected from the Speulderbos site. The device was filled two months in advance of the experiment, adding water randomly and leaving it to dry out in order to stabilize the soil core structure.

The device has two digital scales, allowing the continuous monitoring of the soil column and percolated water weights. The system stored the data automatically on a CR10X data logger every 5 min. This setup was kept in a room with a controlled temperature of 21 $\pm$0.5 °C and a relative humidity of 50 %. These settings provided stable conditions during the experiment. A light-emitting diode (LED) for indoor plant growing was installed at 1 m above the lysimeter providing a photosynthetic photon flux density of 100 μmol m^{-2}s^{-1} in a 12 hr cycle. In our experiment, the soil depth reference ($z = 0$) corresponds to the boundary between the forest floor cover and the fermentation layer. Soil water content (θ) in m^3 m^{-3} was monitored at 5 cm depth with a ECH$_2$O® EC sensor and recorded on a USB Micro Station

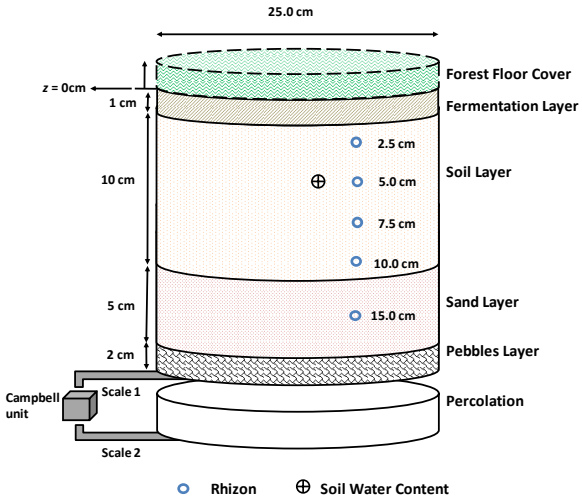

Figure 6.2: Lysimeter design used during the evaporation tests under laboratory conditions for each forest floor cover. Blue circles represent the location of the water extraction with the rhizons at 2.5 cm, 5.0 cm, 7.5 cm, 10.0 cm, and 15.0 cm depth. Each ring represents the different layers present in the lysimeter. The dashed lines in the upper lysimeter layer shows the only layer that was replaced during the experiment.

(HOBO® part code: H21-USB) every 5 min.

Each forest floor cover was placed on the same soil column after the complete set of measurements of each cover. This help to reduce the bias induced by different preferential flows. Additional PVC rings of 1 cm height were added at the top of the device according to cover floor height. to keep the forest floor surface at the edge of the lysimeter. Each ring added were attached with hot glue, adding a maximum of three rings for Lit-3cm and Pol-com. Forest floor cover testing was carried out in the following order: Bare-soil, Lit-1cm, Lit-3cm, Thu-tam, Bra-rut, and Pol-com. Each cover was evaluated three times for six days on the lysimeter. Unexpected data loss was experienced during some days due to logging issues with the device.

The initial water conditions for each forest floor cover depicts the water holding capacity of the soil column. This was achieved by sprinkling water above the soil column until percolation started and all the water was drained out, which took approximately 2 hr until the percolation stopped completely. Evaporation was evaluated after percolation ceased. Water was added by sprinkling the soil surface until the core started to percolate, thus ensuring complete soil core saturation. Three water additions were done per forest floor cover and the samples were collected along 6 days.

6.2.3. Water Sampling

Sets of the sprinkled water and soil water were collected to determine the isotope signature of the stable isotopes deuterium (δ^2H ‰) and oxygen–18 (δ^{18}O ‰). Water extraction from the different soil layers was done with soil moisture samplers of 10 cm length composed by porous plastic material with a standard porous size of 0.15 μm (Eijkelkamp part number: 19.21.SA). The suction was applied daily during two minutes. During sample collection a small amount of water ($\approx$ 0.5 ml) was discarded at the beginning to ensure no contamination from previous sampling extractions. Rhizons were located at 2.5 cm, 5 cm, 7.5 cm, 10 cm and 15 cm from the boundary between the forest floor cover and fermentation layer (Fig. 6.2). All water samples collected were stored in 1.5 mL vials sealed with silicone caps to prevent evaporation until their laboratory analysis. Stable isotope signatures were determined with a LGR-Liquid Water Isotope Analyzer (LGR). The LIMS software (version 10.083) for Light Stable Isotopes (Coplen, 2000) was used to perform the correction and calibration of the isotope signatures data. Stable water isotope signatures were expressed in δ values (‰), representing the relative deviation from Vienna Standard Mean Ocean Water (VSMOW) (Craig, 1961).

6.2.4. Data Analysis

Water fluxes (mm hr^{-1}) were determined through direct measurements and the application of the mass balance method (Eq. 6.1) to estimate total evaporation (E). Daily sprinkled water (P) was weighed before its application to the lysimeter, percolation water (Q) and water storage change ($\frac{dS}{dt}$) were measured with the lysimeter. As the evaluation of each forest floor cover started after P and Q ceased we can reduce equation 6.1 and link $\frac{dS}{dt}$ directly to E (Eq. 6.2).

$$E = P - Q - \frac{dS}{dt} \tag{6.1}$$

$$E = \frac{dS}{dt} \tag{6.2}$$

Isotope fractionation of the soil water was evaluated using the Line-conditioned excess (lc-excess) (Landwehr and Coplen, 2004) as a reference for the evaporation process within the soil profile. lc-excess is based on the relationship between δ^2H and δ^{18}O and their distribution along the Global Meteoric Water Line (GMWL) and determined through equation 6.3 (Rozanski et al., 1993). Where δ^{18}O and δ^2H represent the relative concentration (‰) of both stable isotopes.

$$\text{lc} - \text{excess} = \delta^2 H - 8.2 \times \delta^{18} O \tag{6.3}$$

6.2.5. Statistical Analysis

Parametric and non-parametric statistical analyses were used to compare the data sets. All data fulfilling with the normality assumptions were tested with an Analysis

of Variance (ANOVA) and a Z-test to compare the slopes of the linear regressions. lc-excess differences among soil depths and forest floor covers were determined with the ANOVA ($p = 0.05$). The sampling depth (z) was used to determine the evaporation front, comparing afterwards the differences among floor covers on the evaporation front. When significant differences were present ($p<0.05$) a Tukey-HSD test ($p=0.05$) was performed (Tukey, 1949). The similarities among soil evaporation lines were evaluated comparing the differences among linear regression slopes (B) with the Z-test (Eq. 6.4), where the Z_{value} is compared to the student distribution (t_{value}, $p = 0.05$). This test makes paired comparisons using the slopes of two equations under analysis (B_1 and B_2) and the standard error of each slope (SE_{B_1} and SE_{B_2}) is determined through the linear regression (Clogg et al., 1995; Paternoster et al., 1998). The evaporation among forest floor covers was evaluated with a Kruskal-Wallis test ($p=0.05$) and a pairwise Wilcoxon rank test to identify the differences among covers ($p=0.05$). The entire statistical analysis for water fluxes and isotope data was performed using R (R Core Team, 2017).

$$Z = \frac{B_1 - B_2}{\sqrt{{\text{SE}_{\text{B}_1}}^2 + {\text{SE}_{\text{B}_2}}^2}} \tag{6.4}$$

6.3. Results

6.3.1. Evaporation rates

Total evaporation over the entire period varied a lot among the tests. Bare-soil evaporated on average 1.49 mm d^{-1} and was the only forest floor cover with outliers (Fig. 6.3). Despite the two outliers, Bare-soil keeps a small standard deviation as well as Bra-rut. Evaporation from Bare-soil is exceeded only by Thu-tam with 1.61 mm d^{-1}, with the highest standard deviation among all covers. The remaining covers show evaporation values below 1.0 mm d^{-1}, with Bra-rut and Lit-3 cm showing lower evaporation values of 0.70 mm d^{-1} and 0.71 mm d^{-1}, respectively. Finally, Lit-1 cm and Pol-com evaporated 0.88 mm d^{-1} and 0.95 mm d^{-1}. The forest floor covers with the highest standard deviations (Thu-tam, Lit-3cm and Pol-com) depict differences between the median and mean evaporation values, denoting differences on the data distribution (Table.6.1).

Evaporation values are not normally distributed according to the Shapiro-Wilk normality test ($W=0.8672$, $p<0.0001$). The Kruskal-Wallis test reveals significant differences among forest floor covers ($\chi^2=26.54$, $p<0.0001$). A Wilcoxon rank test was applied to evaporation values to evaluate differences among the covers, finding two homogeneous groups. Bare-soil and Thu-tam are the covers with the highest evaporation while the remaining four covers showed considerably lower evaporation values (Fig.6.3). Bare-soil is depicted as the highest evaporative forest floor cover, with a median of 1.54 mm d^{-1} followed by Thu-tam with 1.36 mm d^{-1}. The lowest evaporation was registered by Lit-3cm with a median of 0.55 mm d^{-1}, followed by

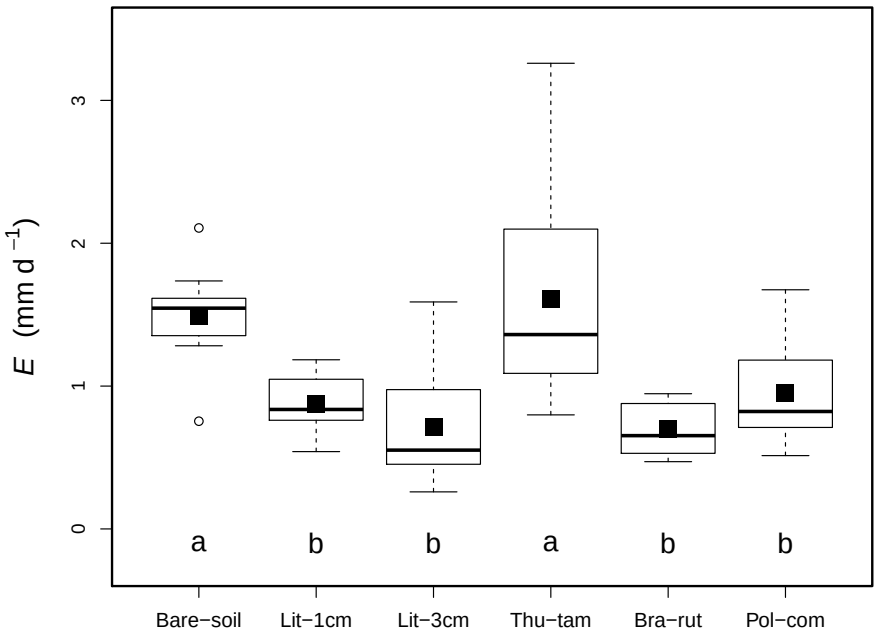

Figure 6.3: Evaporation rate differences among forest floor covers. Solid black squares are the average values, the horizontal line is the median, the boxes cover from the first to the third quartiles of data, the circles represent data outliers, while the upper and lower whiskers are the maximum and minimum values respectively. Equal lowercase letters do not have significant differences with a Wilcoxon rank test (p = 0.05).

Bra-rut, Pol-com and Lit-1cm with 0.65 mm d^{-1}, 0.82 mm d^{-1} and 0.84 mm d^{-1}, respectively (Table.6.1). Differences of evaporation rates affect the θ at 5 cm depth (Fig. 6.4). These changes show Bare-soil with the lowest θ during the experiment after percolation ceases. Litter covers have a wide variation of θ, however the higher θ of Lit-3cm depict the barrier effect of a deep litter cover. The presence of Pol-com and Bra-rut diminishes the losses of soil water by evaporation, while Thu-tam increases the evaporation process from the soil.

6.3.2. Isotope signatures

Sprinkled water showed a homogeneous isotope signature along the study period (δ^2H: -45.52±1.16 ‰, δ^{18}O: -6.6±0.33‰), lying on the GMWL. Isotope signatures of all the soil water is plotted below the GMWL (Fig.6.5). Isotope signatures from all the soil depths beneath Pol-com and Bra-rut show no strong differentiation among soil depths. However, signatures of the superficial layers of the remaining forest floor covers (Bare-soil, Lit-1cm, Lit-3cm and Thu-tam) are located on the more fractionated end of the evaporation line of each forest floor. Soil water from Lit-3cm

Table 6.1: Summary of the linear regression coefficients of the evaporation lines and line conditioned excess analysis for each forest floor cover used in the experiment. Equal lower case letters on the same column do not show statistical differences (p=0.05).

Forest Floor Cover		Evaporation		Linear	lc-excess	
Type	Depth (cm)	Mean (mm d^{-1})	Median (mm d^{-1})	regression slope	Evaporation front (‰)	Sprinkled water (‰)
Bare-soil	0	1.49	1.54^{b}	3.44^{a}	-12.80^{b}	6.84
Lit-1cm	1	0.88	0.84^{a}	3.47^{ab}	-16.28^{c}	8.11
Lit-3cm	3	0.71	0.55^{a}	3.20^{c}	-22.85^{d}	9.73
Thu-tam	3	1.61	1.36^{b}	3.17^{bc}	-18.51^{c}	9.57
Bra-rut	3	0.70	0.65^{a}	3.01^{c}	-15.85^{c}	9.57
Pol-com	4	0.95	0.82^{a}	3.18^{c}	-9.06^{a}	8.59

shows the most fractionated isotope signatures from all the covers (Fig. 6.5).

Soil water evaporation modifies the isotope signature along the soil column, creating a straight line pattern similar to the evaporation line of water bodies (Gibson et al., 1993). All evaporation lines from the forest floor covers are statistically significant ($p < 0.05$), with slopes ranging from 3.0 to 3.5 and intercepts ranging from -22.0 ‰ to -25 ‰ (Fig. 6.5). Soil water from all covers is distributed along a similar evaporation line, however the Z-test shows statistical differences among the slopes of the evaporation lines per forest floor cover. Lit-1cm and Bare-soil similarly affect the isotope concentration of the soil layers beneath, while the other forest floor covers show similar isotope signatures (Table. 6.1).

lc-excess shows statistical differences among soil depths ($F_{value} = 120.6$, $p_{value} < 0.001$, $n = 323$) showing two groups: the upper layers (2.5 cm and 5 cm) and the lower soil layers beneath (7.5 cm, 10 cm, 15 cm). This allows us to define the evaporation front of all the forest floor covers along the first 5 cm of the soil column (Fig. 6.6). Additional differences among forest floor covers on the evaporation front were found ($F_{value} = 44.2$, $p_{value} < 0.001$, $n = 128$). The Tukey-HSD test grouped the lc-excess on the evaporation front as follows: Pol-com had the lowest lc-excess, followed by Bare-soil and the group formed by Bra-rut, Lit-1cm and Thu-tam. Lit-3cm is the forest floor cover with the highest lc-excess value on the evaporation front (Table 6.1).

The evaporation front is clearly present in the covers Bare-soil, Lit-1cm, Lit-3cm, and Thu-tam, where the first 5 cm show a lc-excess below -20 ‰. All the other depths maintain a lc-excess value between -15 ‰ and -5 ‰. From all the covers, Pol-com tends to maintain a more homogeneous lc-excess signature below the forest floor cover, with the clear absence of a fractionation front (Fig. 6.6).

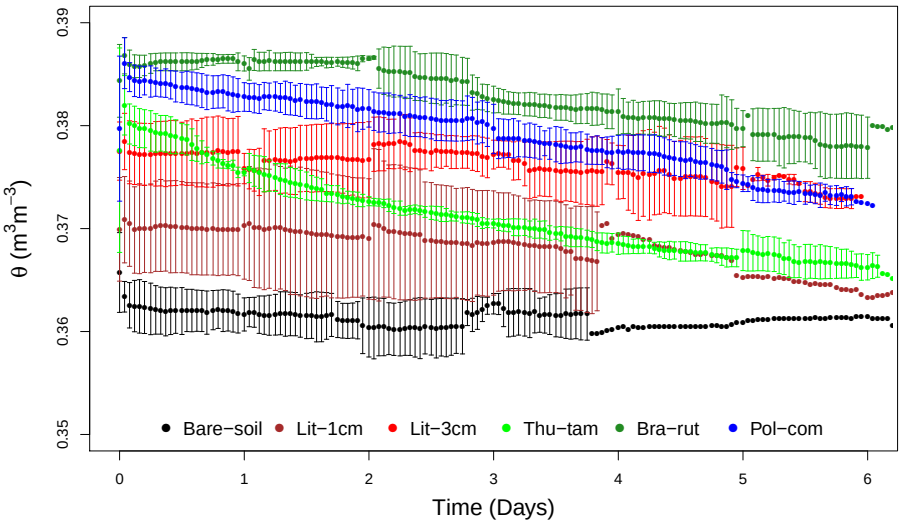

Figure 6.4: Hourly variation of the mean soil water content (θ) of each forest floor cover. Vertical whiskers represent the standard deviation of each average.

6.4. Discussion

Evaporation from the forest floor covers is in the same range as those reported under natural conditions ($\approx$ 1.0 mm d^{-1}) for different moss species (Betts et al., 1999; Price, 1991; Bond-Lamberty et al., 2011; Blok et al., 2011). Thu-tam evaporation is not unusual under natural conditions, whereas some moss species such as *Sphagnum rubellum* can evaporate up to 4.5 mm d^{-1}. This high evaporation is possible due to a water table close to the surface, which gives the mosses access to a constant water supply due to capillary rise (Price et al., 2009). Despite the sandy soil type in the lysimeter and quick percolation, there was enough available water to enable the evaporation process by the mosses. As a consequence there is a lower regression coefficient of the evaporation line than the reported ones for other bryophytes as *Sphagnum* sp. with an evaporative line slope of 3.8 (Price et al., 2009). Soil water availability in a sandy soil can be linked to the organic matter content of the soil (Leuschner and Ellenberg, 2017), however this variable was not analyzed in this study.

The stable isotope concentrations of the soil water are affected by the forest floor cover type, where both stable isotopes signatures (δ^2H and δ^{18}O) show fractionation in the upper soil layers, while the lower ones are affected by the mixing of percolating water with the previous soil water. These concentrations indicate the vapor transport zone within the soil and forest floor cover and suggest that the evaporation zone is ranging from the ground cover surface until 2.5 cm depth. Despite the similarities between the total amount of evaporation, Pol-com and Bra-rut

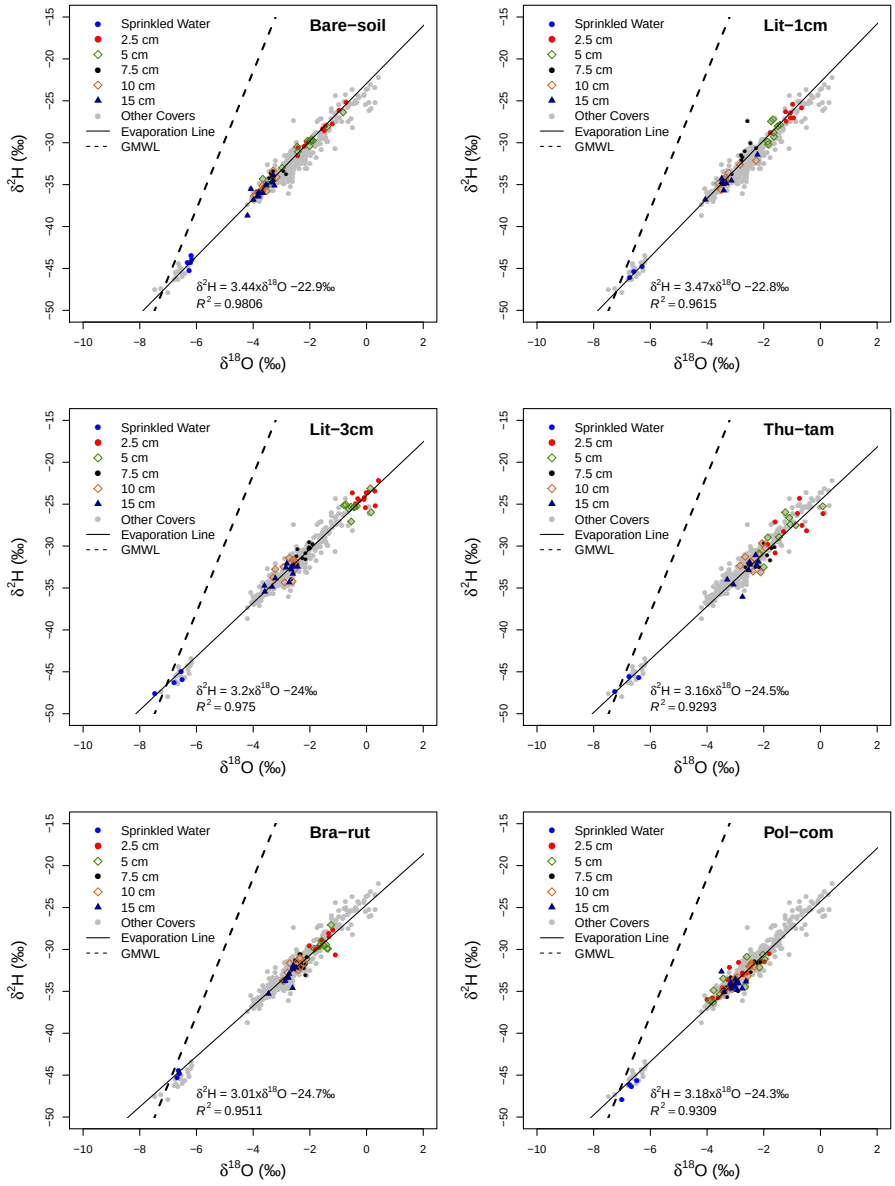

Figure 6.5: Dual isotope plot (δ^{18}O and δ^{2}H) of sprinkled and soil water per forest floor cover. Both global meteoric water line (Rozanski et al., 1993) and evaporation lines were added as references.

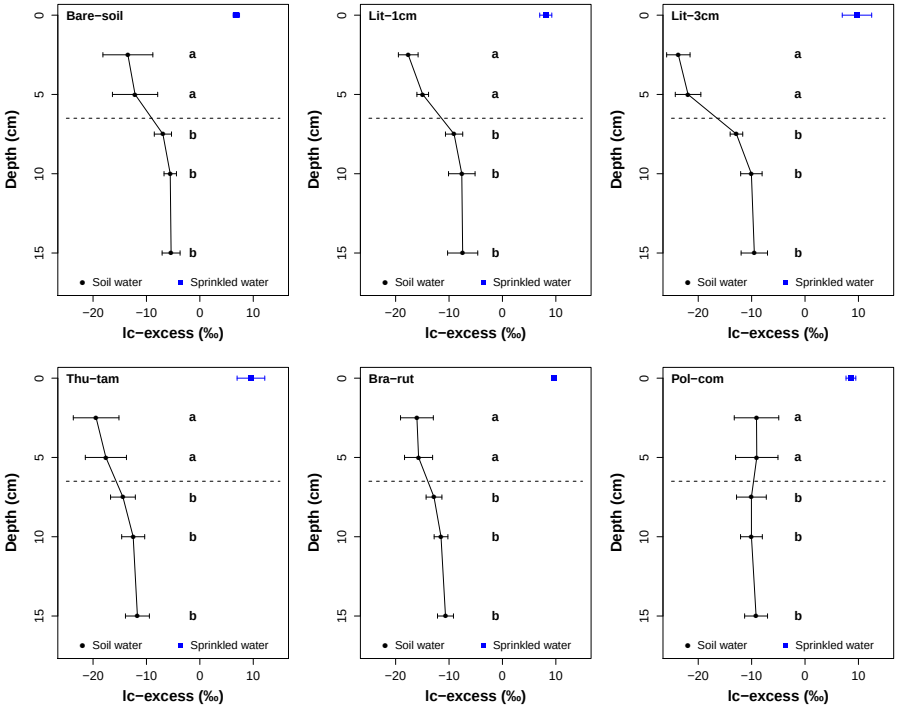

Figure 6.6: Vertical distribution of lc-excess along the soil column per forest floor cover. Different letters per soil depth in each forest floor cover indicates statistical differences in the lc-excess (p=0.05). Dashed line represents the lower limit of the evaporation front for each forest floor cover. The blue mark is the lc-excess of the sprinkled water used for each forest floor cover.

show reduced isotope fractionation within the first 5 cm of soil. The residual effect of the previous forest floor cover in the lysimeter defines the isotope signatures below the 7.5 cm depth, meanwhile evaporation and isotope diffusion are the main drivers modifying the isotope signatures on the upper layers.

Evaporation is affected by the forest floor cover. Bare-soil conditions allow high evaporation rates reaching a maximum of 2.0 mm d^{-1}. It is a result of the water stored in the fermentation layer and within the first 5 cm of soil, as evident in the changes of the isotopic signature. Changes in relative concentrations below the 7.5 cm are linked to water mixing processes and downwards leaching, modifying the signature along the lower soil layers. Both litter covers (Lit-1cm and Lit-3cm) show a high fractionation on the first 5 cm despite the low evaporation rates. This implies additional processes than evaporation affecting the soil isotope signature as isotopic diffusion. On the other hand, the presence of an alive cover allows a reduction on the fractionation on the first 5 cm. These covers allowed a homogenization of the soil water signatures from the end of the Thu-tam test time and leading to see almost equal signatures along the Pol-com test (Fig. 6.6).

The high Bare-soil evaporation highlights the importance of the buffer capacity of litter and some mosses preventing higher evaporation rates from the exposed fermentation layer (Blok et al., 2011; Deguchi et al., 2008; Magliano et al., 2017). However, overlying forest floor covers on top of the fermentation layer have a dual effect (Spieksma et al., 1997): reducing vertical vapor movement from the mineral soil towards the surface (1); and increasing interception during the rain events (2). The first dual effect in our experiment was found underneath Pol-com and Bra-rut, as both moss species showed low evaporation and a homogeneous fractionation effect below the forest floor covers. The second effect was seen in Thu-tam, as this moss species had the highest evaporation compared to the other forest floor covers.

Both litter layers (Lit-1cm and Lit-3cm) exhibited characteristics of a typical evaporation front, with the most fractionated isotope signatures close to the surface (Giuditta et al., 2018; Sutanto et al., 2012; Sprenger et al., 2016). Despite this strong signal, the evaporation of both forest floor covers remains among the lowest. This is likely related to the porosity of the litter layer, which enables more water to be temporarily stored as interception (second dual effect), allowing the isotope signature to change through gas diffusion, whereas the litter layer shows reduced evaporation but no isotope diffusion. This implies the need to reconsider field sampling techniques for soil water and stable isotopes in cases where understory conditions are characterized by low vegetation patches, which may create areas with unique isotope signatures different from the surroundings.

The capacity of bryophytes to absorb water is well known due to its preference of moist environments (Leuschner and Ellenberg, 2017; Lawley, 2010; Glime, 2017), such as bogs, tundra forests and peat lands. They have the capacity to store condensed water during early morning (before sunrise) and evaporate only after

sunrise (Deguchi et al., 2008; Pypker et al., 2017). This process is naturally enhanced by the presence of a forest overstory layer as it helps to reduce dessication (Nichols and Brown, 1980). In addition, the litter water interception had a closer correlation with the non-decomposed litter mass which provides a major area to store water (Jiamei et al., 2018). Needles and litter further intercept water and allow the mosses to allocate and retain water on their surface. The moss species *Polytrichum commune* (Pol-com) has the ability to store water between the leaves and stem and has shown special water conducting abilities (Bowen, 1931; Heijmans et al., 2004). This feature allows the absorption of water by the moss as well as the quick evaporation from the surface under low humidity conditions. The evaporation from all the mosses in our experiment represents the non reproductive phase, because the bryophytes evaporation is triggered by low air humidity, which force the water to move through the wax free cell walls towards the atmosphere. Contrary to the reproductive phase, where the sporophytes have stomata which allow a fast water and nutrient movement towards the reproductive organs controlling it evaporation flux (Glime, 2017).

6.5. Conclusions

Bare-soil and Thu-tam have the highest evaporation with 1.54 mm d^{-1} and 1.36 mm d^{-1} respectively, while all the other forest floor covers evaporate less than 1.0 mm d^{-1}. Litter and moss forest floor covers reduce evaporation of water stored in the fermentation layer. Despite the similar soil evaporation lines, Bare-soil and Lit-1cm have a different evaporation pattern than the other forest floor covers. All these influence the lc-excess from the evaporation front, where Lit-3cm have the highest fractionation with a lc-excess of -22.85 ‰. The presence of an alive cover allows a reduction on the fractionation on the first 5 cm. These results suggest a not proportional relationship between evaporation and fractionation processes beneath litter layers (Lit-1cm and Lit-3cm) and Bare-soil. Also, the lack of isotope fractionation through the soil column under Pol-com reflects the evaporation dependency on the water stored by the moss and not on the water available in the soil column.

7

Choosing paths

Comparing water vapor sampling techniques for stable isotope analysis

The water vapor comes from all around,
its footprint is quite strong,
it could be lost or found,
the only clue is its pale tone.

7.1. Introduction

The use of stable water isotopes as tracers is a well known practice in environmental sciences (Fry, 2006; Silvertown et al., 2015; Nielsen et al., 2018). Stable water isotopes (^{18}O and ^{2}H) have been widely used to track different processes such as precipitation (Allen et al., 2016; Ingraham, 1998), percolation (Kendall and McDonell, 1998), runoff (Gou et al., 2018; Song et al., 2017), plant water use (Dawson and Ehleringer, 1998; West et al., 2006a; Rothfuss and Javaux, 2017; Schwendenmann et al., 2015; Wang et al., 2017) and soil evaporation (Kendall and McDonell, 1998; Xiao et al., 2018). Sampling techniques for precipitation, soil water or river runoff require the direct collection of liquid samples. However, sampling procedures to determine plant water use or evaporated water often involve vapor samples. Water vapor samples such as transpired water or atmospheric water are good descriptors of the evaporation process, which is considered the second largest flux in the hydrological cycle (Coenders-Gerrits et al., 2014; Miralles et al., 2011a; Wang et al., 2014). It is formed by water vapor originated from open water evaporation, plant transpiration, soil evaporation and the evaporation of intercepted water on wet surfaces (Abtew and Melesse, 2013; Savenije, 2004). Many studies aim to determine the source of the water vapor (Wen et al., 2016; Xiao et al., 2018). Evaporation partitioning has been carried out with hydrometric data supported with water stable isotopes (Blyth and Harding, 2011; Dubbert et al., 2017; Lawrence et al., 2007a; Silvertown et al., 2015; Wang and Yakir, 2000). However, the sampling of water vapor is a difficult task since some methods (e.g., cryogenic extraction, cryogenic bath) involve a physical change (Fischer et al., 2019; IAEA, 2016; Orlowski et al., 2016).

Currently, the estimation of the isotope signatures of water vapor can be performed with three different methods. Firstly, the Craig-Gordon model (CG–model) (Craig and Gordon, 1965) determine the water vapor signature of evaporation originated from open waters (Horita et al., 2008) and has also been applied in transpiration and soil evaporation studies (Dubbert et al., 2013; Ferrio et al., 2009; Williams et al., 2004). The high sensitivity of ^{18}O to temperature makes some assumptions of this model unreliable for the application in soil evaporation or plant transpiration processes (Dubbert et al., 2013). The second method consists in a cryogenic bath that allow the collection of atmospheric water vapor within a canister immerse in a cooling agent (e.g.,liquid nitrogen) (IAEA, 2016; Kool et al., 2014), freezing the water vapor conveyed at a constant air flow into the collection canister (He and Smith, 1999; Sheppard, 1958; Wen et al., 2016). This sampling method for isotopic analysis is only a reliable technique when recovery rate tends towards 1 (Griffis, 2013). An incomplete recovery of water vapor fractionates the water stable isotopes following the Rayleigh distillation model (Kendall and Caldwell, 1998). The consequences of incomplete sample recoveries are similar to the effects as studied by Orlowski et al. (2018) for soil water extraction.

The most recent method involves direct measurements of the isotopic composition of water vapor using mass spectrometers or laser-based spectroscopy. This

method has been carried out in Arctic conditions (Steen-Larsen et al., 2013, 2015), oceanic climates (Steen-Larsen et al., 2014) and croplands (Wen et al., 2016). The deployment of these devices in the field has a high demand of infrastructure such as a cabin with controlled room temperature and a constant power supply. These conditions exerts pressure on projects with reduced budgets or with remote access. For these cases a way of sampling and storing water vapor in the field to later analyze them in the laboratory is needed. However, to the authors best knowledge, no sampling bag has been tested for their applicability to quickly store water vapor in the field and analyze the sampling bags with a mass or a laser-based spectroscopy device in the laboratory.

While this sampling bag does not exist for air vapor, some authors have been able to analyze the stable isotopes of water vapor from small volumes (< 1.0 L) to determine the isotope signature of soil water samples under equilibrium (Gralher et al., 2018; Hendry et al., 2015; Herbstritt et al., 2014; Wassenaar et al., 2008). They underline the risk of water vapor diffusion through the wall container when using equilibrium bags of different materials to determine the soil water isotope signature. If their findings for equilibrium bags used in soil water measurements hold for air water vapor samples as well, is still unknown. The aim of this chapter is to evaluate different sampling procedures to collect atmospheric water vapor and analyze the stable water isotopes. This experiment tested whether the stored mass of water vapor sampled in the laboratory remained unchanged as well as whether the isotope signature of the stored water vapor remains consistent in time. The experiment includes three types of sampling bags to determine their suitability for sampling, storing and analyzing water vapor isotopes. Also, the test includes the sampling with a cryogenic bath. The results were compared against direct measurements performed with laser-based spectroscopy.

7.2. Methodology

7.2.1. Instrumentation and Measurements

A dual phase Water Isotope Analyzer (WIA; model 912) from Los Gatos Research (LGR) was used to determine the isotope signature of the water vapor and liquid samples. The Water Vapor Isotope Analyzer (WVIA) setup connects the WIA to the LGR Water Vapor Isotope Standard Source (WVISS; model 908-0004-9002). This was used to provide a controllable flow of water vapor with a known liquid standard measurement for an absolute calibration of the raw measurements of the signatures of both stable isotopes: δ^2H and δ^{18}O. The WVISS was set to run the automatic pump with the following voltages 3.0 V, 2.0 V, 1.5 V and 1.0 V to provide a controlled water vapor mixing ratio (ppm) during the calibration of each set of samples, running each voltage for a period of 2 min. The dry air needed for the WVISS was provided by the Dry Air Source (DAS) device from LGR. The device pumping rate for all the samples was fixed at ~ 90 mL min^{-1}. The WIA and the WVISS were attached to a Multiport Inlet Unit (MIU; model: LGR 908-0003-9002) for the au-

tomatic control of eight inlets to measure multiple samples for specific periods of time (Figure 7.1). The MIU has eight inlets for 6 mm diameter tubing which allows the development and attachment of different sampling devices. In all the measurements, the first MIU inlet was attached to an altered air source. This altered air source had a distinctive isotope signature compared to the samples. It was used to identify the measurements of each individual sample with the order of the MIU inlets during the post-processing of the data. The data obtained from this inlet was not used during the analysis as it was used only as a distinction mark between samples. The altered air source was achieved by conveying laboratory air through a 2 L borosilicate bottle that was filled with 1.5 kg of silica gel to modify the laboratory air signature to a water vapor mixing ratio lower than 4000 ppm. All vapor samples were measured for 5 min with the WVIA, with sampling intervals of 5 s. The first 3 minutes were discarded by the memory effect, obtaining the average and standard deviation of each measurement based on the last 2 minutes of measurements.

Liquid samples (see Section 7.2.3) were measured with the Liquid Water Isotope Analyzer (LWIA, see "Liquid Mode" in Figure 7.1). This setup connects the WIA with a liquid autosampler, injecting 900 μL into a heating chamber for complete vaporization of the water and transferred into the WIA for its measurement. The correction and calibration of the isotope signatures of the liquid samples were performed with the software Laboratory Information Management System (LIMS, version 10.083) for Light Stable Isotopes, version 10.083 for Microsoft Access 2007–2013 (Coplen, 2000). Stable water isotope signatures of air vapor and liquid samples were expressed in δ values (‰), representing the relative deviation from Vienna Standard Mean Ocean Water (VSMOW) (Craig, 1961).

7.2.2. Water Vapor Isotopic Calibraton

Measurements of water vapor isotope signatures depend on the water vapor mixing ratio (ppm) and the specific drift of the laser spectrometer of the WIA unit, which makes it essential to correct each individual measurement (Aemisegger et al., 2012; Rambo et al., 2011; Kurita et al., 2012; Steen-Larsen et al., 2013, 2014). The drift of the used laser spectrometer was negligible, because the measurement period was not longer than 6 hours every day. In addition, the thermal control within the laser chamber provides stable measurements with a negligible drift as it is stated by the manufacturer (LGR, 2019). The calibration was performed with a standard water ($\delta^{18}O_{standard}$: -14.4 ‰, $\delta^{2}H_{standard}$:-104.9 ‰) injected into the WIA at different pumping rates depending on the pump voltage (see Section 7.2.1). The injection is controlled by a built–in software package that managed the WVISS pump and the DAS. This system allows the use of only one standard water to calibrate the isotope signatures carried out with the WVIA. The calibration procedure was performed every time the MIU start a new round of measurements. The measured isotope signatures ($\delta^{2}H_{raw}$ and $\delta^{18}O_{raw}$) were calibrated using the correction factors (ϕ_O and ϕ_H) determined based on the dependency of the isotope signatures of standard water ($\delta^{2}H_{standard}$ and $\delta^{18}O_{standard}$) to their water vapor mixing ratio (w) in ppm.

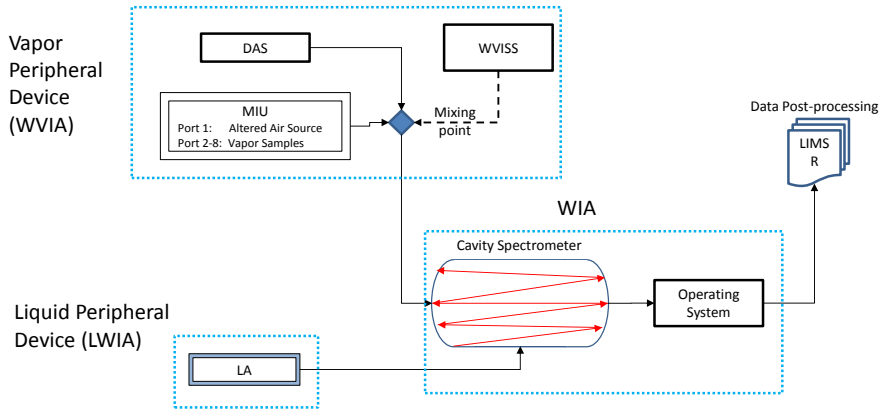

LA: Liquid Autosampler
WIA : Water Isotope Analyser
MIU : Multiport Inlet Unit
DAS : Dry Air Source
WVISS : Water Vapor Isotope Standard Source
LIMS: Laboratory Information Management System
R: Software for data processing and statistics

Note: Vapor and liquid samples are not analysed simultaneously by the WIA. The air samples were processed after the sampling. Then, the WIA was set into liquid mode to process the liquid samples collected with the cryogenic bath.

Figure 7.1: Setup of the Water Isotope Analyzer (WIA) used in this experiment. The selection between liquid and vapor mode depends on the type of samples to be analyzed.

The polynomial coefficients a, b and c in equations 7.1 and 7.2 were determined for every set of measurements per experiment (Rambo et al., 2011; Kurita et al., 2012; Steen-Larsen et al., 2013, 2014). Each data point used in equations 2 and 3 corresponds to the last minute of measurements for each voltage, obtaining an average based on 12 individual measurements for both stable isotopes and water vapor mixing ratios. The calibrated values of each stable isotope ($\delta^{18}\mathrm{O}$ and $\delta^{2}\mathrm{H}$) were determined with equations 7.3 and 7.4 (Rambo et al., 2011; Steen-Larsen et al., 2013).

$$\phi_{\mathrm{O}} = \frac{\delta^{18}\mathrm{O}_{\mathrm{raw}}}{\delta^{18}\mathrm{O}_{\mathrm{standard}}} = a_{\mathrm{O}}w^2 + b_{\mathrm{O}}w + c_{\mathrm{O}} \tag{7.1}$$

$$\phi_{\mathrm{H}} = \frac{\delta^{2}\mathrm{H}_{\mathrm{raw}}}{\delta^{2}\mathrm{H}_{\mathrm{standard}}} = a_{\mathrm{H}}w^2 + b_{\mathrm{H}}w + c_{\mathrm{H}} \tag{7.2}$$

$$\delta^{18}\mathrm{O} = \frac{1}{\phi_{\mathrm{O}}}\delta^{18}\mathrm{O}_{\mathrm{raw}} \tag{7.3}$$

$$\delta^{2}\mathrm{H} = \frac{1}{\phi_{\mathrm{H}}}\delta^{2}\mathrm{H}_{\mathrm{raw}} \tag{7.4}$$

7.2.3. Experimental Design

The 3 types of sampling bags selected to store air samples were:

1. MPE: bags of 1 L made of methalized polyethylene and manufactured with a five layer structure, with an aluminium layer in between (Commercial name: Foil Bag). According to the supplier, the sample stability is 5 days for low molecular compounds such as CH_4, CO_2, CO, and other non specified gases.
2. PVF: bags of 1 L made of polyvinyl fluoride (Commercial name: Tedlar Bag).
3. LDPE: bags of 1.1 L made of low density polyethylene used for filling packaging spaces.

Both, MPE and PVF have been designed to be filled to 90 % of its volume capacity and every bag has a 2-in-1 polytretrafluorethylene (PTFE) fitting for the injection and extraction of the air sample. Whilst the LDPE are fabricated with a simple valve made from polyethylene as well, a special inlet was built to connect the LDPE to the individual inlets of the MIU.

During a period of 3 hours, 18 air samples were collected per bag type (6 samples per hour) in the laboratory. Only 15 samples per bag type were used for the analysis, leaving 3 samples as a backup for replacements if needed. Air samples were collected manually with a medical cardiopulmonary resuscitation (CPR) balloon with a conical plastic inlet that allows to push the air into the sample bags. This device has a balloon with a volume of 1 L. It is made with sturdy Polyvinyl Chloride

(PVC) with a Positive End-Expiratory Pressure (PEEP) valve to release the air when excess of pressure is present. The isotope signature of water vapor was measured from the stored air samples during a period of 16 days. The air was analyzed on the sampling day (T_0) and after 1, 2, 9, and 16 days after collection (T_1, T_2, T_9, T_{16}, respectively).

The additional set of water vapor samples collected with a cryogenic bath were gathered in a second sampling day during four hours. These samples were collected in duplicate with a cryogenic bath with a pumping rate of $3\,\mathrm{L\,min^{-1}}$ within the same laboratory. The cryogenic bath was built with a test tube of 50 mL capacity immerse in a container filled with ethanol (100 %) inside a cooler filled with dry ice (-70 °C). The water collected in the test tubes was thaw and transferred to a 1.5 mL vial for its measurement after the experiment with the LWIA. During both samplings, the WVIA was analyzing the laboratory air during the sample collection. The isotope signature of the direct measurements performed with the WVIA was used as Benchmark for the analysis.

7.2.4. Analysis

All data processing and analysis were performed with the software R (R Core Team, 2017). The consistency analysis of the isotopic signatures was performed comparing the isotope signatures of the samples against the Benchmark. The cross comparison was performed with the Z_{score} analysis (Equation 7.5) (Orlowski et al., 2016; Wassenaar et al., 2012), where S is the isotope signature (δ^2H or δ^{18}O) of the bags air water vapor and cryogenic water samples, B is the benchmark isotope signature (WVIA) and μ is the target variability. Differing from Orlowski et al. (2016) and Wassenaar et al. (2012), μ was established as the isotope range measured with the WVIA during the sample collection (δ^2H: 2.0 ‰ and δ^{18}: 0.4 ‰) considering the transient condition in the laboratory. Thus, we adopted the limits proposed by Orlowski et al. (2016) for classifying the samples as accurate ($Z_{\mathrm{score}} < 2.0$), questionable (Z_{score}: 2.0–5.0) or unacceptable ($Z_{\mathrm{score}} > 5.0$).

$$Z_{\mathrm{score}} = \frac{S - B}{\mu} \tag{7.5}$$

7.3. Results and Discussion

Atmospheric water vapor mixing ratio during the collection of samples had a mean value of 17930 ± 369 ppm. This mixing ratio changes with time during the different days of measurement (Figure 7.2). Between the measuring days 2 and 9 the mixing ratio drops from 18000 ppm to less than 14000 ppm, while towards the measuring day 19 it increased with 1000 ppm more. This trend is tightly followed by the PVF sampling bags, followed by the LDPE sampling bags with a larger difference and the MPE with small variations respect to the atmospheric water vapor mixing ratio of the samples collection. This data shows that all the sampling bags exchange water

vapor from and towards the atmosphere with a different degree of magnitude.

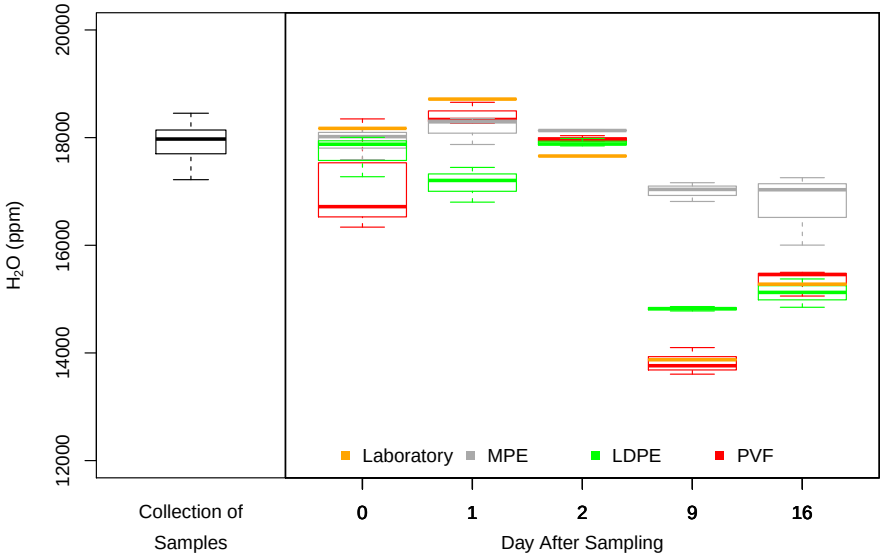

Figure 7.2: Boxplots describing the mixing ratio of atmospheric water vapor in ppm during the collection of samples and the posterior measurement of samples.

7

The stable isotope signatures of the benchmark during the three hours of the experiment were -15.61±0.14 ‰ and -115.12 ± 0.47 ‰ for δ^{18}O and δ^{2}H, respectively. The benchmark represents the center point of both graph in Figure 7.3, where the results of the consistency analysis are depicted. All the vapor samples collected with the bags that were measured on the same sampling day are classified as accurate samples based on the Z_{score} (Figure 7.3 [A]). The isotope signature of the laboratory air water vapor was not constant on the different days when the measurements were performed. The orange samples marked as "Laboratory" in Figure 7.3 [A] depict isotopic signatures of the air of the laboratory during analysis. These differences in laboratory air signatures influences the measurement results from all the air samples collected with the three types of bags but not all to the same degree. The MPE samples are the only bags used in this experiment with almost all measurements located within the accurate region of the Z_{score} plot ($Z_{\text{score}} < 2$). Despite the accuracy provided with the MPE, the measurements are influenced by the isotope signature of the air within the laboratory. All the measurements after the sampling date with the LDPE and PVF bags are located within the questionable region of the Z_{score} plot (Z_{score}: 2-5), while the PVF samples from T_9 are in the unacceptable region ($Z_{\text{score}} > 5$). These sampling bags are influenced by the isotopic signature of the laboratory air considering its location close to the laboratory signature during the measurements.

The cryogenic samples (Figure 7.3 [B]) showed a better proficiency for the description of the isotope signature of the atmospheric water vapor of the laboratory. During this sampling, only 3 samples were tagged as questionable samples while their duplicates were tagged as accurate samples. These inconsistencies among the quality of liquid samples collected with cryogenic baths depends on the capacity to collect all the water vapor from the conveyed air. These differences are likely linked to a not perfect collection efficiency during the cryogenic sampling with the cold traps (Griffis, 2013). However, as this is an open system that requires a constant flow of air and cannot be closed as the batch distillation (Koeniger et al., 2011; Vendramini and Sternberg, 2007), it requires to monitor the atmospheric water vapor mixing ratio before and after the sample collection. This can be achieved measuring the air temperature and relative humidity in both, the inlet and outlet of the cryogenic bath. This information can be used to estimate the specific humidity of the air and evaluate the efficiency of the cryogenic bath.

The Water Vapor Transmission Rate (WVTR) of each material provides insights about the reason behind the variation in the stable isotope measurements and water vapor mixing ratios, including the MPE bags. Thus, the WVTR defines the ability of a film to transfer water molecules depending on the relative humidity gradient (Kumaran, 1998; Keller and Kouzes, 2017). Note that the diffusion characteristics of foil layered materials are directly influenced by temperature and air vapor concentration (Pons et al., 2014). Among the 3 types of sampling bags in this experiment, the MPE bags have the lowest WVTR reported ($0.09\,g\,m^{-2}d^{-1}$), followed by the LDPE bags between 0.39–$0.59\,g\,m^{-2}d^{-1}$ and PVF with the highest value of $0.83\,g\,m^{-2}d^{-1}$ (Keller and Kouzes, 2017; Tock, 1983).

The tendency of drift towards the signature of the laboratory air could be linked to other factors such as welding quality between bag material and the valve (for MPE and PVF bags), fitting issues between the tubing connecting the sample bags to the MIU unit (all sample bags) or the inlet connection for the LDPE bags. In the case of MPE and PVF bags, the manufacturer states that the bags should not be filled more than 90 % of their capacity like we did in the experiment. This practice could lead to the development of fissures between the air valve and the bag material that in the case of PVF bags due to their brittle properties respect to MPE of LDPE bags. An increment on the air pressure within the MPE bags can lead to the detachment of the air valve from the layers in which it is welded. LDPE bags are susceptible to leaking as a consequence of the inlet built with in-house materials that the presence of different joints can induce the filtering of the laboratory air.

The suitability of every sampling method to collect atmospheric water vapor in the field will depend in their accuracy to keep unmodified the mass and isotope signature of every sample (Peters and Yakir, 2010). However, the logistics (e.g., the location, the travel time from and towards the laboratory, basic research infrastructure on the field) and the project budgets play an important role on the selection of the sampling methods. Assuming in this experiment the laboratory

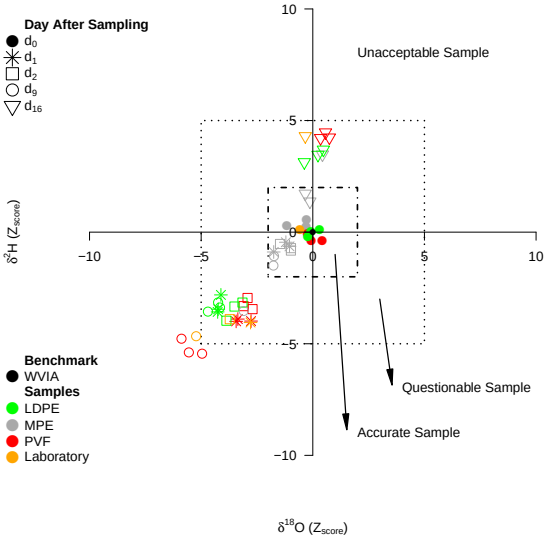

[A]

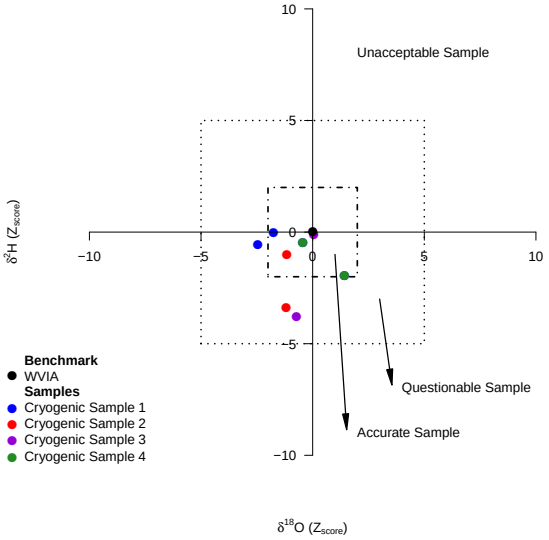

[B]

Figure 7.3: Dual plot for the Z_{score} of δ^2H and δ^{18}O of vapor samples. [A] is the main analysis of the sampling bags and [B] is the cryogenic bath sampling.

equipment (e.g., glassware, laser-based spectroscopy, air temperature and relative humidity sensors) and logistics (e.g., all the expenses related to the travel costs to the sampling) as fixed costs, the main difference will rely on the selected sampling method.

7.4. Conclusions

This chapter investigates the consistency of different sampling techniques to collect atmospheric water vapor for stable isotope analysis. The Low Density Polyethylene (LDPE) and Polyvinyl Fluoride (PVF) bags are influenced by the Water Vapor Transmission Rate (WVTR) of their material. The tested water vapor sampling techniques differ in their ability to keep reliable measurements after sampling and are highly susceptible to procedural errors. All the sampling bags perform well if the measurements are carried out on the same day of the sampling, keeping Z_{score} values within the accurate zone ($Z_{\text{score}} < 2.0$). However, if the samples are required to be stored for longer periods the Methalized Polyethylene (MPE) bags are the best option to obtain reliable signatures after the first day of storage up to two weeks after sample collection. Atmospheric water vapor sampling with cryogenic baths provides suitable accuracy when the collection efficiency is high. However, this requires a suitable system to monitor the specific humidity of the air at the inlet and outlet of the cryogenic bath. However, there is a high risk of incomplete condensation leading to the collection of fractionated water samples. MPE sampling bags are the more accurate and more expensive sampling method. The LDPE sampling bag is the cheapest sampling method with the limitation that the samples should be analyzed on the same day of collection. This method gives an additional restriction considering the transport time and susceptibility to exchange water vapor with the surrounding air. Finally, the cryogenic bath has an affordable price per sample if the project collects samples continuously, maximizes the use of the supplies such as the dry ice that tends, and monitor the collection efficiency with the estimation of the specific humidity of the sampled air.

8

A tall garden full of grownups

The influence of a temperate canopy cover in water vapor flux

Like pillars in an ancient building
the tall trees hold the roof,
the forest canopy shelters from the weather
changing the flux while the vapor moves.

8.1. Introduction

The introduction of Douglas-Fir (*Pseudotsuga menziesii* (Mirb.) Franco) trees in European forest plantations started more than 150 years ago (Schmid et al., 2014). This is the most abundant non-native tree species use in reforestation in Europe (Da Ronch et al., 2016) and has been widely used in France, Germany and The Netherlands (Bastien et al., 2013). The planted area in The Netherlands sums up 18 933 ha with most of the forest stands with ages between 61 to 80 years old (van Loo and Dobrowolska, 2019). These stands are managed as monocultures and mainly used for wood production (Derks, 2019). Douglas-Fir trees growing as a monoculture allows the creation of different microhabitats (Winter et al., 2015) that can affect local hydrological processes such as understory evaporation or soil water storage. Unthinned stands of Douglas-Fir have lower critical values of soil water storage than the thinned ones (Black, 1979). This influences the stand evaporation of this species because its dependency to soil moisture during the summer months (Bosveld and Bouten, 2001; Jassal et al., 2009; Littell et al., 2008).

Most of the evaporation studies in forests are focused on the quantification of the whole ecosystem (Paul-Limoges et al., 2020; Silva et al., 2017; Soubie et al., 2016; Sun et al., 2016). However, the available studies addressing the influence of different canopy layers is scarce. Based on the canopy classification given by Nadkarni et al. (2004) and Parker (1995), dense stands of Douglas-Fir trees have a canopy with three layers: overstory, understory, and forest floor. Overstory evaporation of Douglas-Fir stands has been assessed by means of eddy-covariance, energy balance and water balance approaches (Bosveld and Bouten, 2001; Guerrieri et al., 2016; Jassal et al., 2009; McNaughton and Black, 1973; Price and Black, 1990; Soubie et al., 2016; Spittlehouse and Black, 1981; Unsworth et al., 2004). However, evaporation from the understory and forest floor layers has been measured in rare occasions (Schaap and Bouten, 1997; Unsworth et al., 2004) and need further research.

Evaporation partitioning in forest stands has often been carried out with the combination of eddy-covariance and stable isotope techniques (Anderson et al., 2017; Kool et al., 2014; Xiao et al., 2018). The eddy-covariance provided detailed information about the fluxes (Kang et al., 2018), meanwhile the stable water isotope signatures link the flux with the different sources of vapor (Zhang et al., 2018). These links are related to isotopic processes such as fractionation, diffusion, and mixing that change the proportion of heavier and lighter stable water isotopes (Dawson et al., 2002; Gat, 2010; Gourcy et al., 2005; Lee et al., 2011). Thus allows the differentiation of hydrological processes (Gibson et al., 2005; Gupta and Deshpande, 2005; Huneau et al., 2011; Jouzel et al., 2013; West et al., 2006a). This tracing capacity is an useful tool to identify and quantify the evaporation process in forest ecosystems, where the quantification of stable water isotopes in the air will provide a better understanding of the evaporation along the forest canopy (Gemery et al., 1996; Lee et al., 2006; Yakir and Sternberg, 2000).

Sprenger et al. (2019) underline the importance of increasing the measurement frequency in time and space of stable water isotopes to understand the dynamics of hydrological systems. Here, the experimental design should include a larger sample count to reduce the effect of atmospheric variability (Good et al., 2012). High frequency measurements of stable water isotopes in the air can be done with mass spectrometers and laser-based spectroscopy. This type of monitoring had been carried out in artic environments (Steen-Larsen et al., 2013), coastal locations (Steen-Larsen et al., 2014, 2015), agricultural lands (Wei et al., 2015), grasslands (Wang et al., 2013), semi-arid environments (Gaj et al., 2016), and forest ecosystems (Berkelhammer et al., 2013; Braden-Behrens et al., 2019; Sun et al., 2014; Volkmann et al., 2016). Technologies such as laser based spectroscopy are a precise tool that allow the partitioning of evaporation (Zhang et al., 2010). However, partitioning of forest evaporation with this methodology is still an ongoing topic with few published examples (Sun et al., 2014). The application of new technologies need to be nurtured to understand the methodological uncertainties linked to the monitoring processes (Sprenger et al., 2019).

Despite the available knowledge about evaporation in Douglas-Fir forest stands, there is a gap about the role played by the understory and forest floor layers. Investigating how the evaporation process in an old growth forest takes place will allow to determine the contribution of these layers. Also, the application of continuous measurements of stable water isotopes will provide the tracing information aiming to link the water vapor fluxes at forest stand. Thus, testing the performance of laser based spectrometer in field conditions. The aim of this chapter is to measure the evaporation of an old growth Douglas-Fir forest stand, partitioning its evaporation according to forest structure. Also, to test the capacity of a commercial laser based spectrometer to carry out continuous measurements of stable water isotopes in the air at different heights along the forest canopy. The quantification of evaporation was carried out with hydrometric data, whilst the stable water isotope signatures (δ^{18}O and δ^{2}H) were used as the water vapor tracers.

8.2. Methods

8.2.1. Study Site: Temperate Evergreen Needleleaf Forest

Speulderbos forest is located at De Veluwe region in the heart of The Netherlands (N: 52°15′4″–E: 5°41′24″). This area was covered by an old Oak (*Quercus* sp.) coppice planted in 1906 and harvested in 1960, enabling the establishment in 1962 of the actual land cover with a forest stand of 2.5 ha planted with Douglas-fir (*Pseudotsuga menziesii* (Mirb.) Franco) trees. The forest canopy has a height of 34 m, with a leaf area index of 4.55 $m^2\ m^{-2}$, and a tree density of 571 trees ha^{-1} (Cisneros Vaca et al., 2018a,b; Schilperoort et al., 2018). A flux tower of 48 m is located in the center of Douglas-fir stand. Figure 8.1 shows the Douglas-fir stand surrounded by broadleaved and coniferous tree species distributed in blocks around the selected forest patch (Bosveld and Bouten, 2001; Schilperoort et al.,

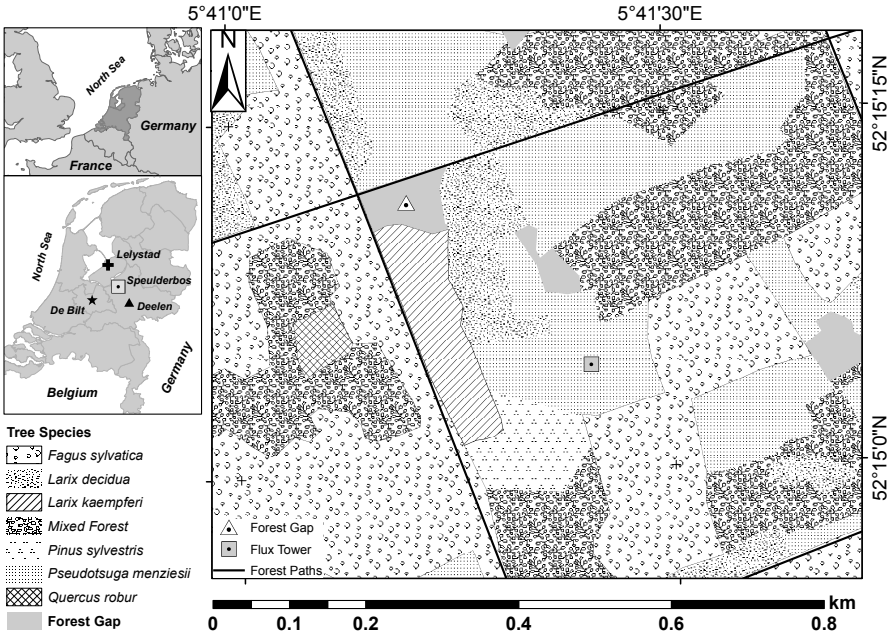

Figure 8.1: Location of the experimental site and forest tree species distribution in Speulderbos, The Netherlands.

2018). These blocks are composed by native tree species such as Beech (*Fagus sylvatica* L.), Pedunculate oak (*Quercus robur* L.) and Scots Pine (*Pinus sylvestris* L.); as well as the introduced species Hemlock (*Tsuga heterophylla* (Raf.) Sarg.) and Larch (*Larix kaempferi* (Lamb.) Carr.). The open areas located close to the flux tower within the Douglas-Fir stand are forest clearings covered by litter, mosses and sparse tree seedlings with less than 50 cm height. This area has an oceanic climate (Cfb), with a yearly average temperature of 9.8 $^{\circ}C^{-1}$ and an average precipitation of 910 mm yr^{-1} (Sluijter et al., 2011). The experimental site is located on the top of ice-pushed fluviatile deposits, enabling the aquifer recharge at De Veluwe due the geological formation of the region (Bosveld and Bouten, 2001; de Vries, 2007; Van Wijk et al., 2001). The topography is slightly undulating with smooth height differences (Raj et al., 2014) with a well-drained soil and a groundwater table beneath at 40 m depth (Tiktak and Bouten, 1994). The soil has been classified as Haplic Podzol or Cambic Podzol in the FAO/UNESCO classification system with a soil texture range from fine sand to sandy loam (Van Wijk et al., 2001; Tietema et al., 2002; Koopmans et al., 1996; Tiktak and Bouten, 1994).

The monitoring period of micro-meteorological conditions and sampling of precipitation for stable water isotope analysis had been performed since 2016. However, in situ water vapor sampling was carried out between 2019-08-14 and 2019-09-25 on the flux tower located on the Douglas-Fir stand (Figure 8.1).

8.2.2. Micro-Meterorological Data

Two micro-meteorological stations were placed in the experimental site. One within a 30 m diameter plot established on the Douglas-Fir stand (Flux Tower) and in an open area (Forest Gap) of 0.68 ha located at 300 m from the forest plot (Figure 8.1). Both meteorological stations measured at 2 m height the air temperature (°C) and relative humidity (%) with a 12-bit Temperature/Relative Humidity, model: S-THB-M008; soil moisture ($m^3\ m^{-3}$) at 5 cm depth with a ECH2O™ EC-5, wind speed ($m\ s^{-1}$) with an anemometer, model: S-WSB-M003; short wave radiation (R_{is}) with a silicon pyranometer (model: S-LIB-M003) and precipitation (P) with two different rain gauges. Precipitation under the forest canopy represented the throughfall and was collected with a half open PVC pipe of 210 cm length and 10 cm width that conveyed the collected water into a rain gauge (S-RGA-M002); while on the forest gap the precipitation was measured with a Davis rain gauge (model: S-RGD-M002). All variables were sampled every second and averaged every 5 min in a HOBO Micro Station (model: H21-USB). The data sets from both micro-meteorological stations were used to determine the understory and forest gap latent heat flux ($\rho\lambda E_u$ and $\rho\lambda E_{fg}$, respectively) according to Equation 8.1 (Mallick et al., 2013):

$$\rho\lambda E = \frac{\rho_a c_p (e_s - e_a)}{\gamma r_s} \tag{8.1}$$

where $\rho\lambda E$ is the latent heat ($W\ m^{-2}$) in both locations, ρ_a is the air density ($kg\ m^{-3}$), C_p is the heat capacity of air ($1.013x10^{-3} MJ\ kg^{-1}\ °C^{-1}$), e_a and e_s are the actual and saturation vapor pressure respectively, γ is the psychometric constant ($Pa\ °C^{-1}$) and r_s is the surface resistance ($s\ m^{-1}$). Equation 8.2 (Schaap and Bouten, 1997; Schaap et al., 1997) estimates r_s based on soil moisture (θ). This equation was developed for the same experimental plot, where the forest floor conditions hasn't changed.

$$r_s = -1.29 \times 10^4 (\theta - 0.199) \tag{8.2}$$

Latent heat ($\lambda\rho E$) above the canopy was estimated through the eddy-covariance method with a sonic anemometer (CSAT3, Campbell Sci. Inc.) and an open path gas analyser (LI7500, LI-COR Biosciences) installed at 47 m height in the tower (Cisneros Vaca et al., 2018b; Schilperoort et al., 2018). These instruments provided additional information such as air temperature, relative humidity and wind speed at 47 m. The eddy-covariance data was processed with LI-COR's EddyPro® software (LiCOR, 2016). The eddy-covariance data used in this chapter has quality flags of 0 and 1 according to Mauder and Foken (2006).

Regional meteorological data was gathered from The Royal Netherlands Meteorological Institute (KNMI) for the period between 2017-01-01 until 2019-12-31 (KNMI, 2020a). The meteorological stations Lelystad (N: 52.458° – E: 5.520°, elevation: -3.70 m asl), Deelen (N: 52.056° – E: 5.873°, elevation: 48.20 m asl) and De

Bilt (N: 52.100° – E: 5.180°, elevation: 1.90 m asl) were selected due to their proximity to the research site (Lelystad: 31.7 km, Deelen: 24.7 km, and De Bilt: 38.1 km).

8.2.3. Sampling Design

Precipitation samples were collected on a monthly basis from 2016 until 2019. It includes precipitation (P) collected at the forest gap and throughfall samples (P_{tf}) collected beneath the Douglas-Fir forest stand (Figure 8.1). Each sample was collected with a rain gauge device designed following the recommendations from Gröning et al. (2012). A 15 cm diameter funnel collected the precipitation into a 1.5 L bottle, conveying the water towards the bottom of the bottle through a 15 cm tube of 9 mm outer diameter. A 5 m tubing of 6 mm outer diameter connected the air within the bottle and the environment to reduce vapour exchange.

Water vapor samples were collected at five heights along the flux tower (Fig. 8.2), with sampling points located on the forest floor (0 m), below the canopy (17 m), on the canopy (27 m), above the canopy layer (34 m) and at the top of the tower (47 m). Air moves through a 3D printed radiation shield of 6 cm diameter and 7 cm height (Ham, 2015) adapted to support a small fan at the bottom to allow the air movement and a new top to hold a 6 mm diameter sampling tube. This device was placed on an pole extending 2.5 m East from the tower. The sampling tube at each height conveys the air along 50 m towards an air pump at the bottom of the tower, sucking the air at a rate of 3 L min^{-1} for a travel time of less than 2 min from the sampling point to the collection point. Before sampling starts the pumps were running for 15 min to ensure a continuous mixed air flow along the entire tube length.

8.2.4. Analysis of Stable Water Isotopes

Stable water isotope signatures of ^{18}O and ^{2}H of liquid and water vapor samples were obtained with a Water Isotope Analyzer (WIA; model 912) from Los Gatos Research (LGR). Liquid samples were measured with the Liquid Water Isotope Analyzer (LWIA) and the vapor samples were continuously measured with the Water Vapor Isotope Analyzer (WVIA) setup. A full description of both systems is available in Chapter 7, section 7.2.1. Stable water isotope signatures were expressed in δ values (‰), representing the relative deviation from Vienna Standard Mean Ocean Water (VSMOW) (Craig, 1961). Correction and calibration of the isotope signatures of liquid samples were performed with the software Laboratory Information Management System (LIMS, version 10.083) for Light Stable Isotopes, version 10.083 for Microsoft Access 2007-2013 (Coplen, 2000). Correction and calibration of the isotope signatures of water vapor samples collected in the field followed the procedure described in Chapter 7, section 7.2.2. The standard water used for the correction and calibration of the water vapor gas analyzer had a ^{18}O and ^{2}H signature of -14.5 $\pm$ 0.1 ‰ and -104.6 $\pm$ 0.4 ‰, respectively. Local meteoric water line (LMWL)

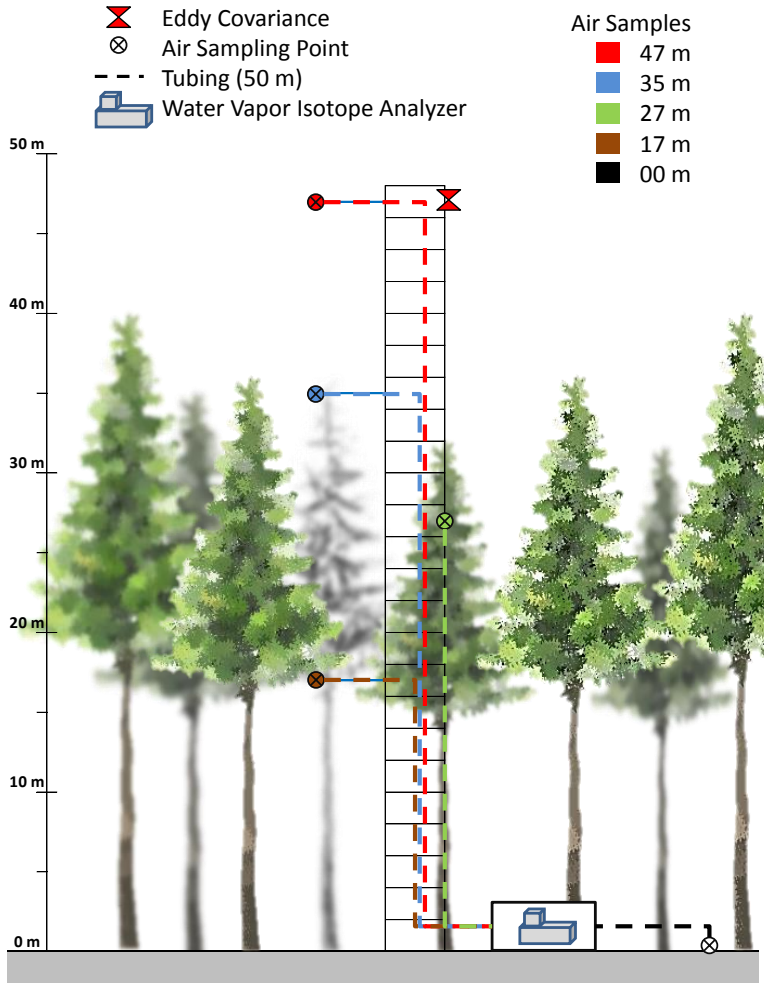

Figure 8.2: Field sampling setup established along the flux tower in Speulderbos, The Netherlands. Air sampling points are located at 2.5 m away from the tower structure to reduce the tower influence on the air flow. The air pumping system and collection points are located at the based of the tower in a non acclimatized cabin.

was determined from precipitation samples collected at the forest gap (Equation 8.3). This equation was used to determine the Line-conditioned excess (lc-excess) of the water vapor samples collected along the tower according to Equation 8.4 (Landwehr and Coplen, 2004). All data analyzes were performed with the open source software R (R Core Team, 2017).

$$\delta^2\mathrm{H} = a + b \times \delta^{18}\mathrm{O} \tag{8.3}$$

$$\mathrm{lc-excess} = \delta^2\mathrm{H} - b \times \delta^{18}\mathrm{O} - a \tag{8.4}$$

8.3. Results

The water vapor monitoring period includes the heat wave of 2019 experienced between 2019-08-23 and 2019-08-28 (KNMI, 2020b). Sporadic rain events occurred during this period registering 73.8 mm of precipitation and 39.9 mm of throughfall beneath the canopy (Figure 8.3). These values indicates that close to 40.0 % of the precipitation is intercepted by the canopy for its subsequent evaporation. This estimate of precipitation interception does not include the contribution of stemflow for the experimental plot which has been estimated in 1.1 % of the precipitation in 2015 and 2016 for this experimental site (Cisneros Vaca et al., 2018b). Including this stemflow, the precipitation intercepted by the canopy is ~ 38.9 %.

During the 42 sampling days the evaporation at 47 m was estimated to be 154.1 mm, with an average of 3.7 mm d^{-1} (Figure 8.3). Meanwhile at 2 m height on the understory evaporation was 8.4 mm (0.2 mm d^{-1}) representing the 5.5 % of the evaporation at 47 m. Wind conditions also differ strongly above and below the canopy in the Douglas-Fir forest stand. Wind speed at 47 m has an average of 3.0 m s^{-1} with a maximum speed of 6.3 m s^{-1}. At 2 m height in the understory the wind do not reach more than 1.5 m s^{-1} with an average of 0.08 m s^{-1}. Eddy-covariance footprint shows that most of the water vapor measured at the tower (~ 95 %) comes from more than 100 m from the tower, with a dominant wind direction during this period of South and South-West. This implies that most of the water vapor did not originated at the Douglas-Fir stand, instead it could be the product of evaporation at the nearest Beech, Scots Pine or Mixed forest stands (see tree species distribution in Figure 8.1).

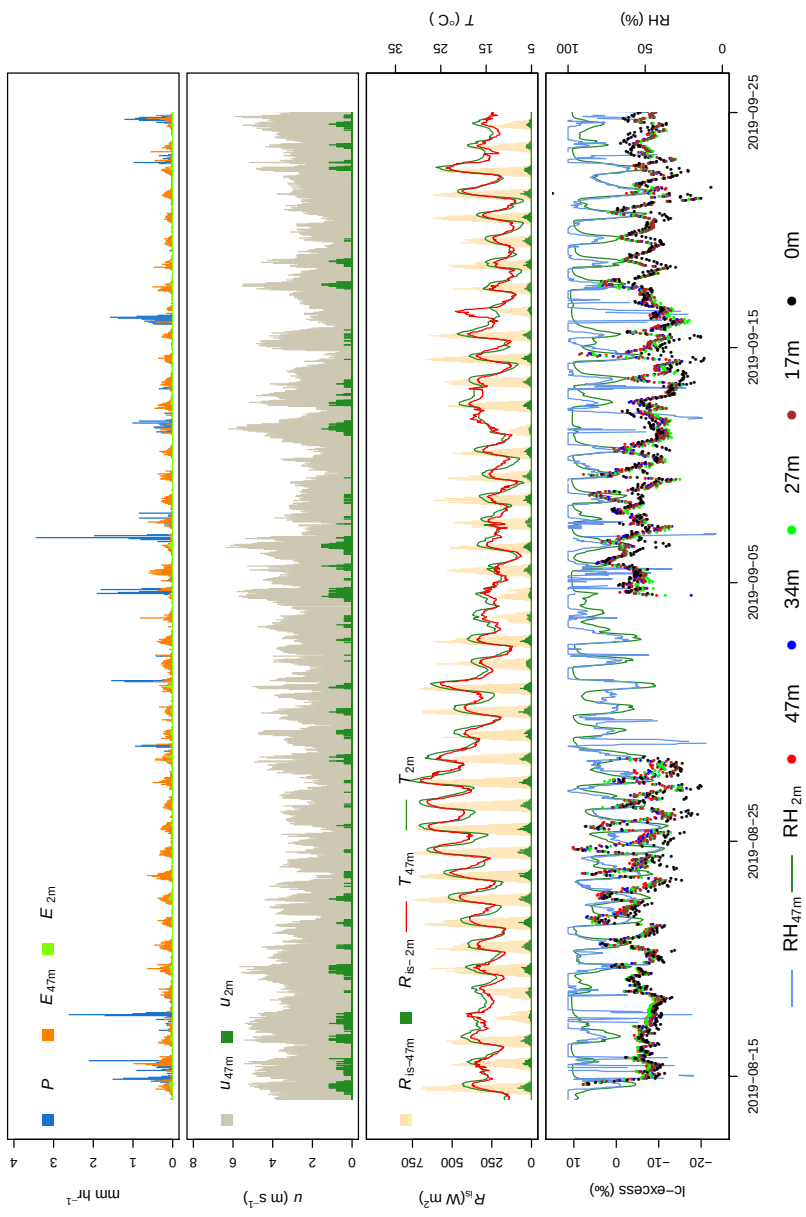

Figure 8.3: Meteorological conditions and line-conditioned excess (lc-excess) of the water vapor samples during the monitoring period (2019-08-14 to 2019-09-25). The meteorological conditions include wind speed at 47 m and 2 m height (u_{47m} and u_{2m}, respectively), incoming solar radiation (R_{is}), air temperature at 47 m and 2 m height (T_{47m} and T_{2m}, respectively), precipitation (P), evaporation at 47 m (E_{47m}), relative humidity at 47 m (RH_{47m}). Water vapor samples were collected at 47 m, 34 m, 27 m, 17 m, and 0 m.

Solar radiation varies widely among the sampling days, with daily maximum values oscillating from ~ 250 W m^{-2} during the cloudy and rainy days up to 746.3 W m^{-2} during the sunniest day (Figure 8.3). The forest canopy blocks a large amount of solar radiation, considering that the maximum solar radiation in the understory was 85.8 W m^{-2}. This translates into a direct blockage of ~ 88.5 % of the solar radiation received at the top of the canopy on a daily basis. Air temperature oscillates similarly to solar radiation, however the differences between above and below canopy are not that big. Maximum air temperature at 47 m was 29.6 °C and a minimum of 7.2 °C. The air temperature difference at the understory is larger than at 47 m, with a maximum of 31.6 °C and a minimum of 6.7 °C.

Figure 8.4 shows the distribution of δ^2H and δ^{18}O in water vapor and precipitation samples through boxplots and dual isotope plots. The boxplots of δ^2H and δ^{18}O show the similarities among water vapor samples. The dual isotope plot shows the relationship of the air vapor samples respect to the LMWL of Speulderbos, and the inserted plot depict the canopy effect on the throughfall samples.

Precipitation samples collected since 2016 defined a local meteoric water line (LMWL) for Speulderbos as $\delta^2\mathrm{H} = 7.12\delta^{18}\mathrm{O} + 3.65$ (Table 8.1), while the throughfall samples defined the following equation $\delta^2\mathrm{H} = 7.31\delta^{18}\mathrm{O} + 5.85$. The equation slopes of both, LMWL and LMWL$_u$ do not differ. Despite this lack of differences on the long term, the dense canopy does affect the stable water signature of water on its passage towards the forest floor. The inserted dual isotope plot in Figure 8.4 shows that throughfall samples have heavier isotope signatures than precipitation samples. The precipitation samples collected during the water vapor sampling have heavier isotope signatures than water vapor samples. These precipitation samples have stable isotope signatures with differences of more than 5 ‰ and 40 ‰ for δ^{18}O and δ^2H, respectively (Figure 8.4).

Table 8.1: Summary of the linear regression analyses to determine the Local Meteoric Water Line (LMWL) for gross precipitation and throughfall samples (LMWL$_u$).

Water Flux	n	R^2	SE	Regression Coefficients		Normality Test
			ϵ	a	b	W
LMWL	63	0.944	4.108	3.65 *	7.12 **	0.989
LMWL$_u$	65	0.958	3.72	5.85 **	7.31 **	0.993

Note: $\delta^2\mathrm{H} = a + b\delta^{18}\mathrm{O} + \epsilon$, n = sample size, * is statistically significant ($p < 0.01$), ** is statistically significant ($p < 0.001$), SE= standard error.

Stable isotope signatures of water vapor overlap among sampling heights during the study period (Figure 8.4). All the samples are located along the LMWL with few samples collected at 0 m with lighter isotope signatures. These samples are depicted as outliers for both stable isotopes, ^{18}O and ^{2}H. The overlap of water vapor samples around the LMWL happen continuously on a daily basis but with a differ-

ent magnitude affecting the estimates of lc-excess. The bottom plot in Figure 8.3 shows the hourly variation of lc-excess for all the sampled heights. All the samples show a sinusoidal daily pattern, with most negative values during night (1), cloudy (2) or rainy days (3). Positive values in all the heights are present during the sunny hours after midday (Figure 8.3).

The 10 days showed in Figure 8.5 aim to exemplified different meteorological conditions experienced during the monitoring period. These conditions included sunny days (e.g., 2019-08-24, 2019-09-13) and rainy days (e.g., 2019-08-15, 2019-09-05). The plots in this figure show the hourly averages of precipitation, evaporation at 47 m, relative humidity and wind speed both at 47 m and 2 m height. Also, each plot shows the lc-excess calculated for the samples collected hourly at different heights along the canopy.

Lc-excess of all heights followed a similar daily trend most of the time during sunny (e.g., 2019-08-24) or rainy days (e.g., 2019-08-15, 2019-08-17). During sunny days (e.g., 2019-08-24, 2019-09-13) the peaks of evaporation happen around 12:00, but the lc-excess changes abruptly towards more positive values than the morning pattern ($\sim 10\,‰$) after the peak of evaporation. On rainy days, the wind speed at 47 m has speeds larger than $3\,m\,s^{-1}$ whilst below the canopy at 2 m height the air speed do not surpasses $1\,m\,s^{-1}$ but is notoriously continuous. Few spikes of evaporation can be identified in the rainy days, which are being triggered by the drop in relative humidity at 2 m and 47 m (Figure 8.5, day: 2019-08-15, 2019-09-07).

Despite the daily tendency of lc-excess in all the heights, the lc-excess at 0 m remained more negative than the other heights despite the sunny conditions (e.g., 2019-09-13). During some rainy days (e.g., 2019-0-05, 2019-09-07, 2019-09-23) the air at 0 m has lighter isotope signatures than other heights. Under conditions of low wind speed at 47 m (e.g., 2019-08-27, 2019-09-05), the lc-excess at 27 m has more positive values during certain parts of the days differing from the lc-excess at 47 m.

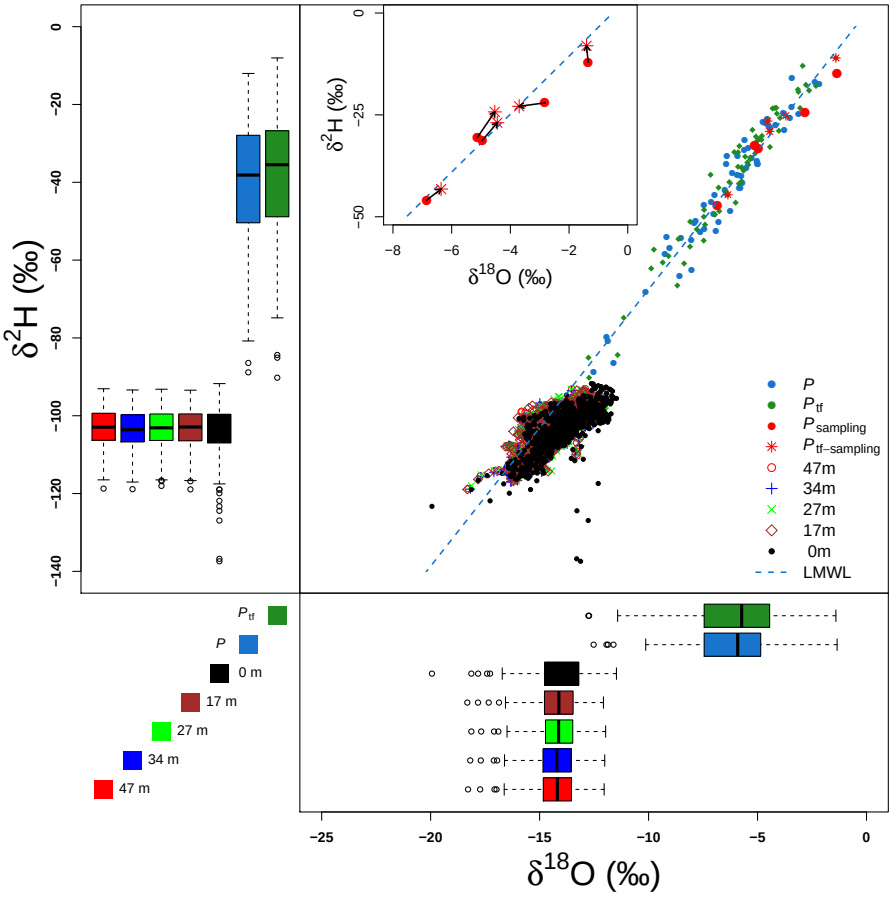

Figure 8.4: Stable water isotope signatures (δ^2H and δ^{18}O) of water vapor (47 m, 34 m, 27 m, 17 m, and 0 m), precipitation (P) and throughfall (P_{tf}) samples collected in Speulderbos. The dual isotope plot shows the relationship between local meteoric water line (LMWL) and the samples. The red dots and stars on the dual isotope plot represent the precipitation samples collected during the water vapor sampling. The inserted dual isotope plot depict the relationship between precipitation and throughfall samples during the monitoring period. The box plots of δ^2H (upper–left) and δ^{18}O (bottom–right) show the distribution of isotope signatures per sample type. Precipitation and throughfall samples were collected between 2016 and 2019 and water vapor samples between 2019-08-14 and 2019-09-25.

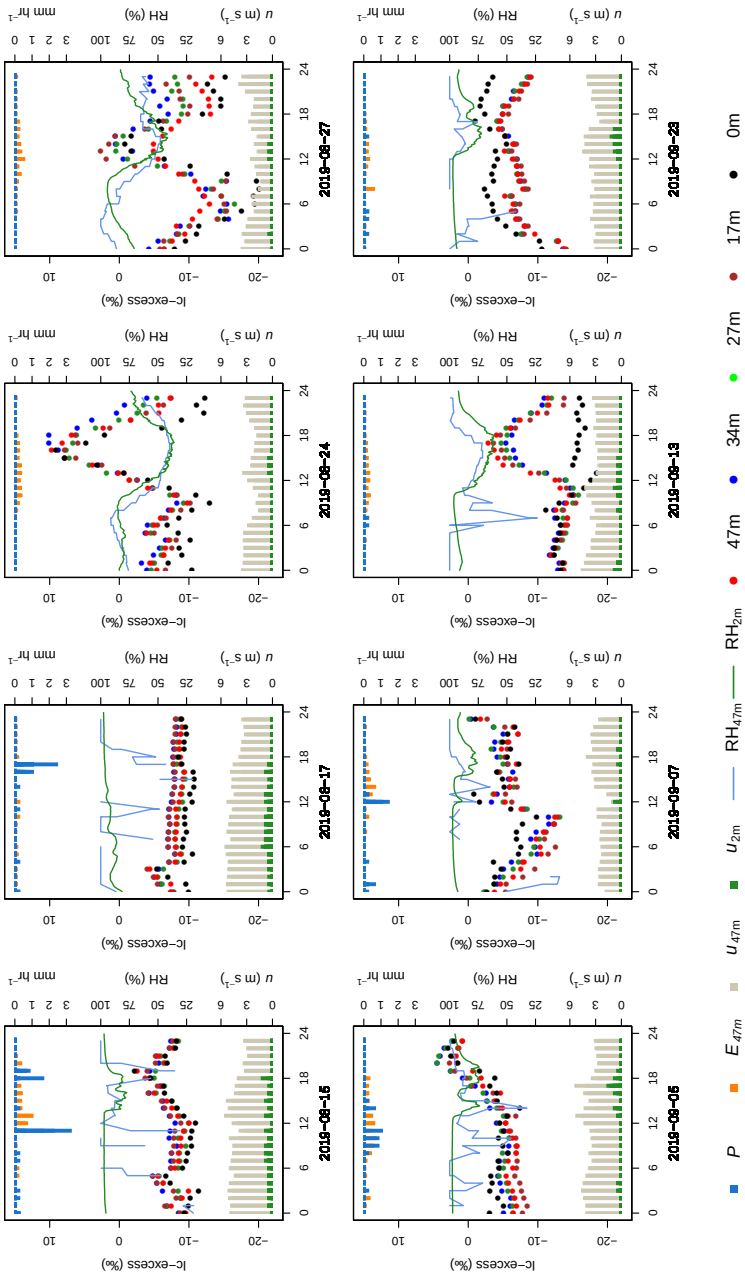

Figure 8.5: Hourly variation of the line-conditioned excess (lc-excess) of water vapor samples collected at 47 m, 34 m, 27 m, 17 m, and 0 m along the vertical canopy profile of a Douglas-fir forest stand. Secondary plots include hourly values of precipitation (P), evaporation at 47 m ($E_{47\mathrm{m}}$), relative humidity (RH) and wind speed (u) both measured at 47 m and 2 m.

8.4. Discussion

The differences between precipitation and throughfall isotope signatures during the monitoring period depict the effect of evaporative fractionation as described by Allen et al. (2017). The evaporation happened during each precipitation event, modifying the isotope signature when water passes through the canopy. Also, isotope mixing processes are not discarded at canopy level but with minor effects. This evaporation is not detectable by eddy-covariance due to measurement consistency issues during precipitation events (van Dijk et al., 2015). Evaporation during precipitation can be linked to the "splash droplet evaporation" process (Murakami, 2006). This process is favored by the surface canopy area, which in Speulderbos is fully closed. The water vapor signature during precipitation shows differences between 47 m and 27 m (e.g., 2019-08-15, 2019-08-17). This shows the effect of the tower footprint, which most of the time (> 95 %) was calculated in more than 100 m. This distance implies that most of the water vapor collected at 47 m comes from other forest stands on the surroundings such as the Beech, Scots Pine or Mixed Forest blocks located South and South-West of the tower (Figure 8.1).

Douglas-Fir trees planted at high densities are able to close the canopies when growing up, reducing the capacity of other plants to colonize the understory (North et al., 2004). Consequently, the accumulation of litter reduces the soil water availability for seedling emergence and growth (Caccia and Ballaré, 1998). This condition was found in Speulderbos where the trees closed their canopies, creating a micro-habitat where few plants are able to growth under low radiation conditions (e.g., mosses, ferns). The presence of only herbaceous vegetation reduced the evaporation contribution of understory and forest floor. The absence of bushes and shrubs reduces the local contribution to evaporation by transpiration. This leaves the forest floor as the main contributor of evaporation from beneath the canopy, explaining that less than 5.5 % of evaporation comes from beneath the canopy. This represents 0.2 mm d^{-1} which does not differ with the 0.23 mm d^{-1} reported by Schaap and Bouten (1997). Despite the stand age difference between both evaluations, the forest stand managed to keep unchanged some features such as interception of precipitation as an example (Cisneros Vaca et al., 2018b).

Understory evaporation in Douglas-Fir stands ranges from 2 % to 10 % (Schaap and Bouten, 1997; Unsworth et al., 2004) depending on the forest structure beneath the canopy. In Speulderbos, evaporation from beneath the canopy will rely on mosses and litter as the main sources because the lack of a well defined understory. Evaporation from mosses depends on their capillary capacity to suck soil water and soil wetness condition (Goetz and Price, 2015). However, the sandy soil conditions in Speulderbos restricted the available soil water for the mosses, leaving for evaporation only the throughfall they intercept. The forest floor patches covered with litter will contribute to evaporation by their interception capacity, which depends on the layer thickness (Li et al., 2017; Prijono and Sukma, 2015). Water vapor signatures at 0 m during low wind speed beneath the canopy (e.g., 2019-09-07, 2019-09-13, 2019-09-23) break apart from the isotope signature of the other

heights. This allows to detect a different source of water vapor than along the canopy. High wind speed conditions at 47 m and 2 m increases the water vapor mixing at different heights (e.g., 2019-08-15, 2019-08-17).

Unthinned mature stands of Douglas-Fir transpire between 60 % and 70 % of the evaporation (Unsworth et al., 2004; Van Wijk et al., 2001) and are able to intercept up to 40 % of the precipitation for its subsequent evaporation (Cisneros Vaca et al., 2018a). The main source of evaporation in Speulderbos is linked to transpiration (78 %), considering that only 22 % of evaporation comes from intercepted water by plant surfaces during the monitoring period. Tree transpiration of this species is strongly linked to vapor pressure deficit and solar radiation (Dekker et al., 2000). Despite the occurrence of the heat wave during the monitoring period, there was no diminution on local transpiration. This as a consequence of physiological adaptations on Douglas-fir trees that help them to photosynthesize even during periods of water stress (Woodruff et al., 2007), while the cooler climate conditions in the long term help them to create a greater drought resistance (Bansal et al., 2015). Also, residence time of sap water in old growth Douglas-Fir trees reaches up to 79 days (Meinzer et al., 2006). This residence time is enhanced by the large amounts of free water contained within the trees (Cermak et al., 2007), allowing the water supply for transpiration processes.

The daily spikes of evaporation triggers the posterior peaks in lc-excess during the sunny days (e.g., 2019-08-24, 2019-08-27, 2019-09-13). These peaks are noticeable almost at all the heights, reaching differences of lc-excess close to 15 ‰ respect to the morning values. This is linked to the transpiration process, which tends to increase the flux of lighter stable water isotopes to the atmosphere (Farquhar et al., 2007; Sprenger et al., 2016). Isotope signatures of water vapor at 27 m were expected to show the contribution of local evaporation in comparison to the water vapor at 47 m. Evaporation from Douglar-Fir trees is perceptible during low wind speed conditions (e.g., 2019-08-27). Lower wind speed conditions at 47 m reduces the mixing effect on the canopy layer, allowing to differentiate the local source of evaporation from the surroundings.

The influence of nearby forest stands is not discarded considering the mixed condition around the Douglas-Fir forest stand. This effect has been identified during the evaporation partitioning of *Quercus variabilis* Blume forests in North China (Sun et al., 2014), affecting the quantification of local transpiration based on stable water isotopes. The immediate presence of tree species such as *Fagus sylvatica*, *Larix decidua* or *Pinus sylvestris* could provide different water vapor isotope signatures which mixed with the local isotope signature of evaporation. Stable water isotope signatures of evaporation from *Fagus sylvatica* had shown important differences between periods dominated and not by transpiration processes (Braden-Behrens et al., 2019). This can contribute to the main isotope signature of water vapor registered at 47 m, considering the tree cover surrounding the Douglas-Fir stand.

Braden-Behrens et al. (2019) mention the tubing effect when measuring the air water vapor in a 44 m meteorological tower in a Beech forest (*Fagus sylvatica* L.). This can be minimized by using high pumping rates (Steen-Larsen et al., 2014), allowing to remove the smoothing effect of mixing and interaction with the tube walls (Massman and Ibrom, 2008). However, it is important to understand how this technology performs when multiple tubing lines are being monitored in a forest stand at different heights. The effectiveness of the water vapor sampling method sacrifices short term measurements (2 measurements per hour) per height for long term measurements on the experimental site (42 days). This increases the variability of atmospheric conditions during the collection of each sample but allowed to describe the daily variability in the middle term. Under these conditions, the smoothing effect of mixing along the tubing has a minor effect in our measurements because of the pumping rate used and that each measurement is an average of 2 measurements. The setting used allowed to show under specific meteorological conditions (e.g., low wind speed at 47 m, high relative humidity at 2 m) differences in isotope signatures of water vapor at different heights.

8.5. Conclusions

The closed canopy conditions of Douglas-Fir trees affect the presence of understory plants, reducing the contribution of evaporation from beneath the canopy. Only 5.5 % of the evaporation comes from the forest floor layer, assuming an effective vertical movement of the water vapor originated from beneath the canopy. Most of the water vapor is originated from transpiration (78 %), while the 22 % remaining is linked to interception of precipitation. However, the eddy-covariance footprint and stable water isotope signatures showed that the water vapor measured most of the time corresponds to water originated from the surroundings and not precisely from the Douglas-Fir forest stand. The setup used during this monitoring was able to depict the daily variability of isotope signatures of water vapor. Identifying also during specific meteorological conditions the local source of water vapor. Stable water isotope signatures are well mixed along the canopy profile as result of the high wind speed registered most of the time. Peaks of more than 15 ‰ in lc-excess values respect to the morning pattern are linked to tree transpiration. These peaks occur during the sunniest days, including the heatwave at the end of August. But only during the days with low wind speed it is possible to depict a different stable isotope signature of the water vapor with a local origin.

9
Conclusions

The water moves around the globe,
connecting the ground, the plants, and the atmosphere.
What does the vegetation do?
How does the vegetation play with the flux?

9.1. Conclusions

Evaporation studies of forests are not so straightforward as for other ecosystems such as croplands. The forests differ because they can not be described as a single plant. Forest systems are complex, because they consist of different layering of vegetation (Parker, 1995). Each layer has its own distinct features that affect evaporation as well as the availability of energy and water for the other layers (Kumagai, 2011). If one wants to fully understand forest evaporation one should consider two ways of evaporation partitioning:

- The classical partitioning whereby total evaporation consist of transpiration, evaporation from interception, and soil evaporation (Roberts, 1999; Savenije, 2004; Shuttleworth, 1993; Sun et al., 2016); and
- The partitioning based in forest layering structure (e.g., understory, overstory, ground layer, forest floor layer) (Coenders-Gerrits et al., 2020; Gordon et al., 2019).

Note that for each forest layer the evaporation can be partitioned into E_t, E_i and E_s to fully understand the evaporation process in forest ecosystems. In this thesis I addressed this twofold evaporation partitioning in four different forest ecosystems (Tropical Evergreen Broadleaf Forest, Tropical Deciduous Broadleaf Forest, Temperate Shrubland, and Temperate Evergreen Needleleaf Forest).

In tropical forest ecosystems the ecological succession, seasonality, and species diversity of plants create a set of conditions that complicates the usual partitioning of evaporation. The interception capacity of forest ecosystems is affected by seasonal changes (Sadeghi et al., 2018) and the growing stage of forests and it is not well known how this characterization may affect the canopy interception (Allen et al., 2020). The Tropical Deciduous Broadleaf Forest in Costa Rica showed how ecological succession affects the interception of precipitation (Chapter 2). Forest stand structure depends on the ecological succession stage, which determines the capacity of forest canopy to intercept precipitation.

The main structural differences among the stages of tropical dry forest are linked to tree height (early: 9.9 m, intermediate: 16.5 m, late:22.4 m), tree densities (early: 417 trees ha^{-1}, intermediate: 943 trees ha^{-1}, late: 620 trees ha^{-1}), and plant area index (early: 2.9 m^2 m^{-2}, intermediate: 5.6 m^2 m^{-2}, late: 6 m^2 m^{-2}) (Table 9.1). The combination of these structural differences affect forest characteristics like stemflow and throughfall. The early stage has the lower interception of precipitation (9.9 %) as a consequence of the sparse distribution of trees and low plant area index. The intermediate has more trees than early and late stages per hectare, the interception capacity reaches 22.1 % of precipitation. The late stage has the higher trees with larger diameters, conditions that influence the interception capacity of the forest canopy (43 %). The structural changes of growing forest imply an increment on the precipitation interception capacity of the forest, allowing

to evaporate more water when the forest stands become older in the ecological succession.

Tropical wet and rain forests contain more canopy biomass than dry forests due to the effect of variables such as water availability, soil fertility and elevation (Ali et al., 2019; Álvarez-Dávila et al., 2017; Asner et al., 2015). A larger biomass requires more water to maintain the site productivity, and this translates into a larger transpiration flux. However, the high diversity of tropical lowland forests makes it difficult the species selection to monitor the transpiration flux. Measuring the transpiration flux by means of sap flow sensors allow to partition the transpiration contribution to forest evaporation (Kool et al., 2014). However, the number and diversity of tree species makes it difficult to quantify the transpiration. Additional methods such as stable water isotopes have been used to determine the transpiration contribution to evaporation by means of techniques such as keeling plots (Keeling, 1958; Yakir and Sternberg, 2000; Xiao et al., 2018; Zhang et al., 2010).

In the Tropical Evergreen Broadleaf Forest in Costa Rica (Chapter 3), we did not manage to apply the keeling plot method successfully, due to the highly variable atmospheric conditions to which this method is highly sensitive (Good et al., 2012). Instead, applying the evaporation partitioning according to forest structure in terms of overstory (E_{ov}), upper understory (E_{uu}), and lower understory (E_{lu}) allowed to define the contribution of the whole canopy mixing different fluxes (Table 9.1). The lower and upper understory layers contribute 9 % and 15 % to total evaporation, while the remaining 76 % is produced by the overstory layer. These understory layers are characterized by bushes, shrubs and trees of small size. Despite the monitoring was carried out during the dry season, the large water availability and atmospheric variability did not allow to identify the transpiration contribution using stable water isotopes and the keeling plot method.

During rainy days, the evaporation decreases in magnitude but the proportion of contribution by the different canopy layers remains stable (Chapter 3). Evaporation is reduced two thirds during rainy days in comparison with sunny days (Chapter 4). However, the atmospheric conditions during rain events allowed to spot the ascending vapor flux after evaporation occurs on the canopy. This phenomenon occurs thanks to the convection powered by the energy store in the lower understory and the water vapor produced during the ”splash droplet evaporation” process (Dunin et al., 1988; Dunkerley, 2009; Murakami, 2006).

Contrary to tropical ecosystems, plants growing in arid environments of temperate regions, experience water as a scarce resource. Under these environmental conditions, the vegetation grows forming shrublands that do not classified as forest. However, the introduction of tree species to fight desertification changed the landscape introducing a forest–like land cover. This characteristic makes it easier to evaluate the transpiration of individual species. New land covers change the evaporation flux as a consequence of the differences between transpiration rates (Chapter

5). New canopies also change the soil moisture content as a consequence of plant adaptation to cope with water scarcity. In an environment with scarce precipitation and a mono-specific canopy, transpiration becomes the main vapor flux (Nagler et al., 2007). Here, soil evaporation and interception are present only during and shortly after the precipitation leaving the transpiration as the main source of evaporation. Willow trees (*Salix matsudana*) and Willow bushes (*Salix psammophila*) transfer water from the soil and groundwater reservoirs at rates of 0.41 mm d^{-1} and 0.39 mm d^{-1}, respectively (Table 9.1). However, when water is the limiting resource the plants are able to redistribute water in the soil. This redistribution is based in the hydraulic lift capacity of Willow trees (*Salix matsudana*) and Willow bushes (*Salix psammophila*), which transfer water with the isotope signature of groundwater to the upper soil layers. Under these circumstances, transpiration is the dominant water vapor flux that allows the allocation of deeper soil water in upper soil layers. Consequently, the canopy becomes a water pump exporting water to the atmosphere while redistributing groundwater in shallower soil layers. Also, the canopy becomes a shield that reduce the direct radiation reaching the soil reducing the soil evaporation.

Mono–specific forest ecosystems in temperate regions may modify the micro–meteorological conditions beneath their canopies. This is the case of a Temperate Evergreen Needleleaf Forest in The Netherlands (Chapters 6, 7, and 8). The forest stand conditions of Douglas–Fir (*Pseudotsuga menziesii*) in Speulderbos are characterized by a dense canopy (overstory) and the forest floor layer (Table 9.1). Thanks to the water availability, the forest floor is covered with mosses and litter. These forest floor covers kept evaporation rates lower than 1.5 mm d^{-1} in laboratory conditions (Chapter 6), however, the estimations performed in the field are not larger than 0.2 mm d^{-1} (Chapter 8). Also, the presence of these covers impact the soil moisture at different degrees due two their differences in interception capacity when it rains and because their porosity presence affects the water vapor flux from the soil to the atmosphere (Spieksma et al., 1997). This was observed thanks to the effect on the isotopic fractionation of soil water after evaporation occurs. This isotopic fractionation should be reflected on the water vapor signatures and may be observable under field conditions.

Sampling water vapor in the field is a difficult task, because some methods require a physical change that may lead to isotopic fractionation (Fischer et al., 2019; IAEA, 2016; Orlowski et al., 2016). Preventing these physical changes during water vapor sampling will help to retrieve better data of evaporation processes with stable water isotopes. After testing 5 methods for sampling water vapor in the air, the best way to sample air vapor in the field without applying physical changes to the samples is using Methalized Polyethylene (MPE) bags. This method allowed to keep reliable water vapor samples up to 2 weeks of storage but the sampling efforts and processing time in the laboratory make it less suitable for continuous measurements in the field. This type of measurements can be carried out with laser-based spectroscopy methods if the field infrastructure allows its deployment.

In Speulderbos (Chapter 8), the closed canopy modifies the underneath micro–meteorological conditions. This creates specific micro–habitats (Winter et al., 2015) that restrict the growth of bushes and shrubs due to low solar radiation levels and more stable temperature. Under these conditions, the mosses thrive due to the lower desiccation capacity of the air and export only 0.2 mm d^{-1} meanwhile at 47 m the evaporation reach a flux of 3.7 mm d^{-1} (Table 9.1). However, wind conditions above and below the canopy make it difficult to link the vertical flux of water vapor. Both methodologies, the eddy–covariance and stable water isotope measurements showed how the water vapor measured along the canopy has a different origin than the forest stand where the measurements were performed. The use of laser-based spectrometry to understand the evaporation process along the canopy. This thanks to the increment of number of samples in longer periods of time (Sprenger et al., 2019) help to increase the number of samples in time, but sacrifice the short time sampling capacity.

Finally, partitioning the evaporation based on canopy structure is suitable for complex ecosystems with a large number of species and a multilayered canopy (e.g., Mixed temperate forests, tropical forests). This will reduce the bias given by direct measurements of transpiration of trees that may not be suitable to describe the wide variation of a complex forest. This leaves the classical partitioning for more homogeneous ecosystems (e.g., forest plantations, forest covers with canopies dominated by few tree species) where the differentiation between transpiration, soil evaporation and evaporation from intercepted water is feasible with a smaller monitoring investment.

Table 9.1: Summary table describing the main features and results obtained from the experimental sites in Costa Rica, China, and The Netherlands.

Features	**Experimental Sites**											
Country:	Costa Rica			Costa Rica			China		The Netherlands			
Latitude:	Tropical			Tropical			Temperate		Temperate			
Seasonality:	Deciduos			Evergreen					Evergreen			
Vegetation:	Broadleaf Forest			Broadleaf Forest			Shrubland		Needleleaf Forest			
Precipitation:	1678 mm yr^{-1}			4351 mm yr^{-1}			386.1 mm yr^{-1}		910 mm yr^{-1}			
Potential Evaporation:	1551.4 mm yr^{-1}			1585 mm yr^{-1}			1339.1 mm yr^{-1}					
Temperature:	26.6 °C			26.3 °C			8.6 °C		9.8 °C			
Seasons:	2			2			4		4			
Sampled season:	Wet			Dry			Autumn		Summer			
Elevation:	301 m a.s.l.			35 m a.s.l.			1250 m a.s.l.		50 m a.s.l.			
Forest Type:	Early	Inter.	Late	Old Growth			Bush	Tree	Old Growth			
Canopy Height (m):	9.9	16.5	22.4	45			2.6	3.5	34			
Canopy Layers:	ov	ov, u	ov, u	ov, uu, lu			ov	ov	ov		ff	
Tree species:	10	18	19	88			1	1	1			
Tree density (trees ha^{-1}):	417	943	620	371			900	300	571			
Leaf Area index (m^2 m^{-2}):		- -		3.56			0.39	0.68	4.55			
Plant Area index (m^2 m^{-2}):	2.9	5.6	6.0	- -			- -		- -			
Total Evaporation:	4.2 mm d^{-1}			4.4 mm d^{-1}			3.67 mm d^{-1}		3.7 mm d^{-1}			
Transpiration (mm d^{-1})		- -		- -			0.41	0.39	2.9		0.2	
Interception (% of P)	9.8	22.1	43.0	11.7					38.9			
Interception (% of E)		- -		19.6					22			
Evapo. Contrib. per Layer:		- -		9 %	15 %	76 %	100 %	100 %	94.5 %		5.5 %	

9.2. Recommendations

Sprenger et al. (2019) underlined the importance to increase the frequency of measurements in space and time to better understand the water in the critical zone. As vegetation works as a set of valves that redistribute the water fluxes in the critical zone (Brantley et al., 2017), partitioning the evaporation in terms of canopy structure will help to better understand the role of vegetation in the critical zone. Partitioning the evaporation of complex ecosystems according to the canopy structure, will also provide better estimates for the evaluation of hydrological processes under climate change scenarios. This considering that it is expected to have a vegetation redistribution in land ecosystems (Pecl et al., 2017), modifying the forest canopy structure. This will translate into further changes of evaporation at landscape level (Dai et al., 2018).

This partitioning is feasible at different scales thanks to the Light Detection and Ranging (LiDAR) technology that allows to describe the forest canopy structure at local (Pardini et al., 2019; Tan et al., 2013), regional (Hansen et al., 2014), and global scales (Tang et al., 2019). This technology will help to define the canopy structure, meanwhile local measurements of evaporation will allow to determine the relative contribution of the different layers (e.g., overstory -E_{ov}, understory -E_{u}, ground -E_{g}, and forest floor -E_{ff}).

Evaporation partitioning based on forest structure can be carried out with the current data available worldwide. Scientific networks such as AmeriFlux (Ameriflux, 2020) or FLUXNET (FLUXNET, 2020) provide the right data sets of evaporation that can be reprocessed including the canopy description of each site. Producing as the main product the historical contribution of different canopy layers already measured worldwide. The minimum requirement will be the temperature along the vertical profile of the canopy.

10

References

Abd El-Ghani, M.M., Huerta-Martínez, F.M., Hongyan, L., Qureshi, R., 2017. Arid Deserts of the World: Origin, Distribution, and Features. Springer International Publishing, Cham. pp. 1–7. doi:10.1007/978-3-319-59135-3_1.

Abtew, W., Melesse, A., 2013. Wetland Evapotranspiration. Springer Netherlands, Dordrecht. pp. 93–108. doi:10.1007/978-94-007-4737-1_7.

Abu-Hamdeh, N.H., 2003. Thermal properties of soils as affected by density and water content. Biosystems Engineering 86, 97–102. doi:10.1016/S1537-5110(03)00112-0.

Adams, D.K., Fernandes, R.M.S., Kursinski, E.R., Maia, J.M., Sapucci, L.F., Machado, L.A.T., Vitorello, I., Monico, J.F.G., Holub, K.L., Gutman, S.I., Filizola, N., Bennett, R.A., 2011. A dense gnss meteorological network for observing deep convection in the amazon. Atmospheric Science Letters 12, 207–212. doi:10.1002/asl.312.

Adelman, J.D., Ewers, B.E., MacKay, D.S., 2008. Use of temporal patterns in vapor pressure deficit to explain spatial autocorrelation dynamics in tree transpiration. Tree Physiology 28, 647–658. doi:10.1093/treephys/28.4.647.

Aemisegger, F., Sturm, P., Graf, P., Sodemann, H., Pfahl, S., Knohl, A., Wernli, H., 2012. Measuring variations of delta;^{18}o and delta;^{2}h in atmospheric water vapour using two commercial laser-based spectrometers: an instrument characterisation study. Atmospheric Measurement Techniques 5, 1491–1511. doi:10.5194/amt-5-1491-2012.

Aguiar, M.R., Sala, O.E., 1999. Patch structure, dynamics and implications for the functioning of arid ecosystems. Trends in Ecology Evolution 14, 273 – 277. doi:10.1016/S0169-5347(99)01612-2.

Ah-Peng, C., Cardoso, A.W., Flores, O., West, A., Wilding, N., Strasberg, D., Hedderson, T.A., 2017. The role of epiphytic bryophytes in interception, storage, and the regulated release of atmospheric moisture in a tropical montane cloud forest. Journal of Hydrology 548, 665–673. URL: http://www.sciencedirect.com/science/article/pii/S0022169417301853, doi:10.1016/j.jhydrol.2017.03.043.

Ahlstrom, A., Canadell, J.G., Schurgers, G., Wu, M., Berry, J.A., Guan, K., Jackson, R.B., 2017. Hydrologic resilience and amazon productivity. Nature Communications 8. doi:10.1038/s41467-017-00306-z.

Ali, A., Lin, S.L., He, J.K., Kong, F.M., Yu, J.H., Jiang, H.S., 2019. Climate and soils determine aboveground biomass indirectly via species diversity and stand structural complexity in tropical forests. Forest Ecology and Management 432, 823–831. doi:10.1016/j.foreco.2018.10.024.

Allen, L.H., Lemon, E., Muller, L., 1972. Environment of a costa rican forest. Ecology 53, 102–111. doi:10.2307/1935714.

Allen, R.G., Pereira, L.S., Raes, D., Smith, M., et al., 1998. Crop evapotranspiration-guidelines for computing crop water requirements-fao irrigation and drainage paper 56. Fao, Rome 300, D05109. URL: http://www.fao.org/3/X0490E/X0490E00.htm.

Allen, S.T., Aubrey, D.P., Bader, M.Y., Coenders-Gerrits, M., Friesen, J., Gutmann, E.D., Guillemette, F., Jiménez-Rodríguez, C., Keim, R.F., Klamerus-Iwan, A., Mendieta-Leiva, G., Porada, P., Qualls, R.G., Schilperoort, B., Stubbins, A., Van Stan II, J.T., 2020. Key Questions on the Evaporation and Transport of Intercepted Precipitation. Springer International Publishing, Cham. pp. 269–280. doi:10.1007/978-3-030-29702-2_16.

Allen, S.T., Keim, R.F., Barnard, H.R., McDonnell, J.J., Renée, B.J., 2016. The role of stable isotopes in understanding rainfall interception processes: a review. Wiley Interdisciplinary Reviews: Water 4, e1187. doi:10.1002/wat2.1187.

Allen, S.T., Keim, R.F., McDonnell, J.J., 2015. Spatial patterns of throughfall isotopic composition at the event and seasonal timescales. Journal of Hydrology 522, 58–66. doi:10.1016/j.jhydrol.2014.12.029.

Allen, S.T., Reba, M.L., Edwards, B.L., Keim, R.F., 2017. Evaporation and the subcanopy energy environment in a flooded forest. Hydrological Processes 31, 2860–2871. doi:10.1002/hyp.11227.

Allison, G., Barnes, C., Hughes, M., Leaney, F., 1984. Effect of climate and vegetation on oxygen-18 and deuterium profiles in soils. Isotopes Hydrology, IAEA, Vienna , 105–122.

Álvarez-Dávila, E., Cayuela, L., González-Caro, S., Aldana, A.M., Stevenson, P.R., Phillips, O., Cogollo, A., Peñuela, M.C., von Hildebrand, P., Jiménez, E., Melo, O., Londoño Vega, A.C., Mendoza, I., Velásquez, O., Fernández, F., Serna, M., Velázquez-Rua, C., Benítez, D., Rey-Benayas, J.M., 2017. Forest biomass density across large climate gradients in northern south america is related to water availability but not with temperature. PLOS ONE 12, 1–16. doi:10.1371/journal.pone.0171072.

Ameriflux, 2020. About data. URL: https://ameriflux.lbl.gov/. accessed: 2020-04-05.

Anderson, R.G., Zhang, X., Skaggs, T.H., 2017. Measurement and partitioning of evapotranspiration for application to vadose zone studies. Vadose Zone Journal 16. doi:10.2136/vzj2017.08.0155.

Aparecido, L.M.T., Miller, G.R., Cahill, A.T., Moore, G.W., 2016. Comparison of tree transpiration under wet and dry canopy conditions in a costa rican premontane tropical forest. Hydrological Processes 30, 5000–5011. doi:10.1002/hyp.10960.

Armas, C., Padilla, F.M., Pugnaire, F.I., Jackson, R.B., 2010. Hydraulic lift and tolerance to salinity of semiarid species: consequences for species interactions. Oecologia 162, 11–21. URL: 10.1007/s00442-009-1447-1, doi:10.1007/s00442-009-1447-1.

Asner, G.P., Martin, R.E., Anderson, C.B., Knapp, D.E., 2015. Quantifying forest canopy traits: Imaging spectroscopy versus field survey. Remote Sensing of Environment 158, 15–27. doi:10.1016/j.rse.2014.11.011.

Aubinet, M., Vesala, T., Papale, D., 2012. Eddy covariance: a practical guide to measurement and data analysis. Springer, Dordrecht. doi:10.1007/978-94-007-2351-1.

Baldocchi, D.D., Meyers, T.P., 1991. Trace gas exchange above the floor of a deciduous forest: 1. evaporation and co2 efflux. Journal of Geophysical Research: Atmospheres 96, 7271–7285. doi:10.1029/91JD00269.

Baldocchi, D.D., Ryu, Y., 2011. A Synthesis of Forest Evaporation Fluxes – from Days to Years – as Measured with Eddy Covariance. Springer Netherlands, Dordrecht. pp. 101–116. doi:10.1007/978-94-007-1363-5_5.

Bansal, S., Harrington, C.A., Gould, P.J., St.Clair, J.B., 2015. Climate-related genetic variation in drought-resistance of douglas-fir (pseudotsuga menziesii). Global Change Biology 21, 947–958. doi:10.1111/gcb.12719.

Barbeta, A., Jones, S.P., Clavé, L., Wingate, L., Gimeno, T.E., Fréjaville, B., Wohl, S., Ogée, J., 2019. Unexplained hydrogen isotope offsets complicate the identification and quantification of tree water sources in a riparian forest. Hydrology and Earth System Sciences 23, 2129–2146. doi:10.5194/hess-23-2129-2019.

Barbeta, A., Ogée, J., Peñuelas, J., 2018. Stable-Isotope Techniques to Investigate Sources of Plant Water. Springer International Publishing, Cham. pp. 439–456. doi:10.1007/978-3-319-93233-0_26.

Barnes, C.J., Turner, J.V., 1998. Chapter 5 - Isotopic Exchange in Soil Water. Elsevier, Amsterdam. pp. 137 – 163. doi:10.1016/B978-0-444-81546-0.50012-4.

Barnes, C.J.and Allison, G., 1988. Tracing of water movement in the unsaturated zone using stable isotopes of hydrogen and oxygen. Journal of Hydrology 100, 143–176. doi:10.1016/0022-1694(88)90184-9.

Barr, A.G., King, K.M., Gillespie, T.J., Den Hartog, G., Neumann, H.H., 1994. A comparison of bowen ratio and eddy correlation sensible and latent heat flux measurements above deciduous forest. Boundary-Layer Meteorology 71, 21–41. doi:10.1007/BF00709218.

Basche, A.D., DeLonge, M.S., 2019. Comparing infiltration rates in soils managed with conventional and alternative farming methods: A meta-analysis. PLOS ONE 14, 1–22. doi:10.1371/journal.pone.0215702.

Bassette, C., Bussière, F., 2008. Partitioning of splash and storage during raindrop impacts on banana leaves. Agricultural and Forest Meteorology 148, 991 – 1004. doi:10.1016/j.agrformet.2008.01.016.

Bastien, J.C., Sanchez, L., Michaud, D., 2013. Douglas-Fir (Pseudotsuga menziesii (Mirb.) Franco). Springer Netherlands, Dordrecht. pp. 325–369. doi:10.1007/978-94-007-6146-9_7.

Becker, P., Castillo, A., 1990. Root architecture of shrubs and saplings in the understory of a tropical moist forest in lowland panama. Biotropica 22, 242–249. doi:10.2307/2388534.

Berg, J., Goldstein, D., Varghese, P., Trafton, L., 2016. Dsmc simulation of europa water vapor plumes. Icarus 277, 370–380. doi:10.1016/j.icarus.2016.05.030.

Berkelhammer, M., Hu, J., Bailey, A., Noone, D.C., Still, C.J., Barnard, H., Gochis, D., Hsiao, G.S., Rahn, T., Turnipseed, A., 2013. The nocturnal water cycle in an open-canopy forest. Journal of Geophysical Research: Atmospheres 118, 10,225–10,242. doi:10.1002/jgrd.50701.

Betts, A.K., Goulden, M., Wofsy, S., 1999. Controls on evaporation in a boreal spruce forest. Journal of Climate 12, 1601–1618. doi:10.1175/1520-0442(1999)012<1601:COEIAB>2.0.CO;2.

Bialkowski, R., Buttle, J.M., 2015. Stemflow and throughfall contributions to soil water recharge under trees with differing branch architectures. Hydrological Processes 29, 4068–4082. doi:10.1002/hyp.10463.

Black, T.A., 1979. Evapotranspiration from douglas fir stands exposed to soil water deficits. Water Resources Research 15, 164–170. doi:10.1029/WR015i001p00164.

Blanken, P.D., Black, T.A., Yang, P.C., Neumann, H.H., Nesic, Z., Staebler, R., den Hartog, G., Novak, M.D., Lee, X., 1997. Energy balance and canopy conductance of a boreal aspen forest: Partitioning overstory and understory components. Journal of Geophysical Research: Atmospheres 102, 28915–28927. doi:10.1029/97JD00193.

Blok, D., Heijmans, M.M.P.D., Schaepman-Strub, G., van Ruijven, J., Parmentier, F.J.W., Maximov, T.C., Berendse, F., 2011. The cooling capacity of mosses: Controls on water and energy fluxes in a siberian tundra site. Ecosystems 14, 1055–1065. doi:10.1007/s10021-011-9463-5.

Blumstock, M., Tetzlaff, D., Malcolm, I., Nuetzmann, G., Soulsby, C., 2015. Baseflow dynamics: Multi-tracer surveys to assess variable groundwater contributions to montane streams under low flows. Journal of Hydrology 527, 1021–1033. doi:10.1016/j.jhydrol.2015.05.019.

Blyth, E., Harding, R.J., 2011. Methods to separate observed global evapotranspiration into the interception, transpiration and soil surface evaporation components. Hydrological Processes 25, 4063–4068. doi:10.1002/hyp.8409.

Bonan, G., 2002. Ecological climatology: concepts and applications. Cambridge University Press.

Bond-Lamberty, B., Gower, S.T., Amiro, B., Ewers, B.E., 2011. Measurement and modelling of bryophyte evaporation in a boreal forest chronosequence. Ecohydrology 4, 26–35. doi:10.1002/eco.118.

Borchsenius, F., Borgtoft-Pedersen, H., Baslev, H., 1998. Manual to the palms of ecuador. aau reports 37. department of systematic botany, university of aarhus, denmark in collaboration with pontificia universidad catolica del ecuador world checklist of arecaceae .

Bosveld, F., Bouten, W., 2001. Evaluation of transpiration models with observations over a douglas-fir forest. Agricultural and Forest Meteorology 108, 247 – 264. doi:10.1016/S0168-1923(01)00251-9.

Bosveld, F.C., Bouten, W., 2003. Evaluating a model of evaporation and transpiration with observations in a partially wet douglas-fir forest. Boundary-Layer Meteorology 108, 365–396. doi:10.1023/A:1024148707239.

Bosveld, F.C., Holtslag, A.M., Van Den Hurk, B.J., 1999. Nighttime convection in the interior of a dense douglas fir forest. Boundary-Layer Meteorology 93, 171–195. doi:10.1023/A:1002039610790.

Bowen, E.J., 1931. Water conduction in *Polytrichum commune*. Annals of Botany 45, 175–200.

Bowen, I.S., 1926. The ratio of heat losses by conduction and by evaporation from any water surface. Phys. Rev. 27, 779–787. doi:10.1103/PhysRev.27.779.

Braden-Behrens, J., Markwitz, C., Knohl, A., 2019. Eddy covariance measurements of the dual-isotope composition of evapotranspiration. Agricultural and Forest Meteorology 269-270, 203 – 219. doi:10.1016/j.agrformet.2019.01.035.

Brantley, S.L., Eissenstat, D.M., Marshall, J.A., Godsey, S.E., Balogh-Brunstad, Z., Karwan, D.L., Papuga, S.A., Roering, J., Dawson, T.E., Evaristo, J., Chadwick, O., McDonnell, J.J., Weathers, K.C., 2017. Reviews and syntheses: on the roles trees play in building and plumbing the critical zone. Biogeosciences 14, 5115–5142. doi:10.5194/bg-14-5115-2017.

Brenes-Arguedas, T., Roddy, A.B., Coley, P.D., Kursar, T.A., 2011. Do differences in understory light contribute to species distributions along a tropical rainfall gradient? Oecologia 166, 443–456. doi:10.1007/s00442-010-1832-9.

Brooksbank, K., White, D.A., Veneklaas, E.J., Carter, J.L., 2011. Hydraulic redistribution in eucalyptus kochii subsp. borealis with variable access to fresh groundwater. Trees 25, 735–744. doi:10.1007/s00468-011-0551-0.

Brubaker, K.L., Entekhabi, D., Eagleson, P.S., 1993. Estimation of continental precipitation recycling. Journal of Climate 6, 1077–1089. doi:10.1175/1520-0442(1993)006<1077:EOCPR>2.0.CO;2.

Bruijnzeel, L., 2004. Hydrological functions of tropical forests: not seeing the soil for the trees? Agriculture, Ecosystems Environment 104, 185 – 228. doi:10.1016/j.agee.2004.01.015. environmental Services and Land Use Change: Bridging the Gap between Policy and Research in Southeast Asia.

Brunel, J.P., Walker, G.R., Kennett-Smith, A.K., 1995. Field validation of isotopic procedures for determining sources of water used by plants in a semi-arid environment. Journal of Hydrology 167, 351–368. doi:10.1016/0022-1694(94)02575-V.

Bulcock, H.H., Jewitt, G.P.W., 2012. Field data collection and analysis of canopy and litter interception in commercial forest plantations in the kwazulu-natal midlands, south africa. Hydrology and Earth System Sciences 16, 3717–3728. URL: https://www.hydrol-earth-syst-sci.net/16/3717/2012/, doi:10.5194/hess-16-3717-2012.

Butt, S., Ali, M., Fazil, M., Latif, Z., 2010. Seasonal variations in the isotopic composition of leaf and stem water from an arid region of southeast asia. Hydrological Sciences Journal 55, 844–848. doi:10.1080/02626667.2010.487975.

Caccia, F.D., Ballaré, C.L., 1998. Effects of tree cover, understory vegetation, and litter on regeneration of douglas-fir (pseudotsuga menziesii) in southwestern argentina. Canadian Journal of Forest Research 28, 683–692. doi:10.1139/x98-036.

Cadol, D., Kampf, S., Wohl, E., 2012. Effects of evapotranspiration on baseflow in a tropical headwater catchment. Journal of Hydrology 462-463, 4–14. doi:10.1016/j.jhydrol.2012.04.060.

Calder, I., Wright, I., Murdiyarso, D., 1986. A study of evaporation from tropical rain forest — west java. Journal of Hydrology 89, 13 – 31. doi:10.1016/0022-1694(86)90139-3.

Calder, I.R., 1998. Water use by forests, limits and controls. Tree Physiology 18, 625–631. doi:10.1093/treephys/18.8-9.625.

Caldwell, M.M., Dawson, T.E., Richards, J.H., 1998. Hydraulic lift: consequences of water efflux from the roots of plants. Oecologia 113, 151–161. doi:10.1007/s004420050363.

Calvo-Alvarado, J., Sánchez-Azofeifa, A., Portillo-Quintero, C., 2013. Neotropical Seasonally Dry Forests. Academic Press. URL: https://www.elsevier.com/books/encyclopedia-of-biodiversity/levin/978-0-12-384719-5.

Campanello, P.I., Manzané, E., Villagra, M., Zhang, Y.J., Panizza, A.M., di Francescantonio, D., Rodriguez, S.A., Chen, Y.J., Santiago, L.S., Goldstein, G., 2016. Carbon Allocation and Water Relations of Lianas Versus Trees. Springer International Publishing, Cham. pp. 103–124. doi:10.1007/978-3-319-27422-5_5.

Cao, S., Chen, L., Shankman, D., Wang, C., Wang, X., Zhang, H., 2011. Excessive reliance on afforestation in china's arid and semi-arid regions: Lessons in ecological restoration. Earth-Science Reviews 104, 240–245. doi:10.1016/j.earscirev.2010.11.002.

Cao, S., Tian, T., Chen, L., Dong, X., Yu, X., Wang, G., 2010. Damage caused to the environment by reforestation policies in arid and semi-arid areas of china. AMBIO 39, 279–283. doi:10.1007/s13280-010-0038-z.

Capell, R., Tetzlaff, D., Malcolm, I., Hartley, A., Soulsby, C., 2011. Using hydrochemical tracers to conceptualise hydrological function in a larger scale catchment draining contrasting geologic provinces. Journal of Hydrology 408, 164–177. doi:10.1016/j.jhydrol.2011.07.034.

Cardon, Z.G., Whitbeck, J.L., 2007. The rhizosphere. An Ecological Perspective. Elsevier Academic Press, Amsterdam.

Carlyle-Moses, D., 2004. Throughfall, stemflow, and canopy interception loss fluxes in a semi-arid sierra madre oriental matorral community. Journal of Arid Environments 58, 181 – 202. doi:10.1016/S0140-1963(03)00125-3.

Carlyle-Moses, D.E., Gash, J.H.C., 2011. Rainfall Interception Loss by Forest Canopies. Springer Netherlands, Dordrecht. pp. 407–423. doi:10.1007/978-94-007-1363-5_20.

Carminati, A., Moradi, A.B., Vetterlein, D., Vontobel, P., Lehmann, E., Weller, U., Vogel, H.J., Oswald, S.E., 2010. Dynamics of soil water content in the rhizosphere. Plant and Soil 332, 163–176. doi:10.1007/s11104-010-0283-8.

Carvajal-Vanegas, D., Calvo-Alvarado, J., 2013. Tree Diameter Growth of Three Successional Stages of Tropical Dry Forests, Santa Rosa National Park, Costa Rica. CRC Press, UK. chapter 19. pp. 351–365. URL: https://www.crcpress.com/

Tropical-Dry-Forests-in-the-Americas-Ecology-Conservation-and-Mana
Sanchez-Azofeifa-Powers-Fernandes-Quesada/p/book/
9780367379490.

Casper, B.B., Schenk, H.J., Jackson, R.B., 2003. Defining a plant's belowground zone of influence. Ecology 84, 2313–2321. doi:10.1890/02-0287.

Cavelier, J., Vargas, G., 2002. Procesos Hidrológicos. Libro Regional Universitario (LUR). pp. 144–166.

Cermak, J., Kucera, J., Bauerle, W.L., Phillips, N., Hinckley, T.M., 2007. Tree water storage and its diurnal dynamics related to sap flow and changes in stem volume in old-growth douglas-fir trees. Tree Physiology 27, 181–198. doi:10.1093/treephys/27.2.181.

Cernusak, L.A., Barbour, M.M., Arndt, S.K., Cheesman, A.W., English, N.B., Feild, T.S., Helliker, B.R., Holloway-Phillips, M.M., Holtum, J.A., Kahmen, A., McInerney, F.A., Munksgaard, N.C., Simonin, K.A., Song, X., Stuart-Williams, H., West, J.B., Farquhar, G.D., 2016. Stable isotopes in leaf water of terrestrial plants. Plant, Cell & Environment 39, 1087–1102. doi:10.1111/pce.12703.

Chazdon, R.L., 1986. The costs of leaf support in understory palms: Economy versus safety. The American Naturalist 127, 9–30. doi:10.1086/284464.

Chazdon, R.L., 1992. Photosynthetic plasticity of two rain forest shrubs across natural gap transects. Oecologia 92, 586–595. doi:10.1007/BF00317853.

Chen, Q., Fan, J., Hagos, S., Gustafson Jr., W.I., Berg, L.K., 2015a. Roles of wind shear at different vertical levels: Cloud system organization and properties. Journal of Geophysical Research: Atmospheres 120, 6551–6574. doi:10.1002/2015JD023253.

Chen, Y.J., Cao, K.F., Schnitzer, S.A., Fan, Z.X., Zhang, J.L., Bongers, F., 2015b. Water-use advantage for lianas over trees in tropical seasonal forests. New Phytologist 205, 128–136. doi:10.1111/nph.13036.

Chesson, P., Gebauer, R.L.E., Schwinning, S., Huntly, N., Wiegand, K., Ernest, M.S.K., Sher, A., Novoplansky, A., Weltzin, J.F., 2004. Resource pulses, species interactions, and diversity maintenance in arid and semi-arid environments. Oecologia 141, 236–253. doi:10.1007/s00442-004-1551-1.

Cirpka, O.A., Fienen, M.N., Hofer, M., Hoehn, E., Tessarini, A., Kipfer, R., Kitanidis, P.K., 2007. Analyzing bank filtration by deconvoluting time series of electric conductivity. Groundwater 45, 318–328. doi:10.1111/j.1745-6584.2006.00293.x.

Cisneros Vaca, C., Ghimire, C.P., van der Tol, C., 2018a. Spatial patterns and temporal stability of throughfall in a mature douglas-fir forest. Water 10. doi:10.3390/w10030317.

Cisneros Vaca, C., van der Tol, C., Ghimire, C.P., 2018b. The influence of long-term changes in canopy structure on rainfall interception loss: a case study in speulderbos, the netherlands. Hydrology and Earth System Sciences 22, 3701–3719. doi:10.5194/hess-22-3701-2018.

Clogg, C.C., Petkova, E., Haritou, A., 1995. Statistical methods for comparing regression coefficients between models. American Journal of Sociology 100, 1261–1293. doi:10.1086/230638.

Coenders-Gerrits, A., Van der Ent, R., Bogaard, T., Wang-Erlandsson, L., Hrachowitz, M., Savenije, H., 2014. Uncertainties in transpiration estimates. Nature 506, E1. doi:10.1038/nature12925.

Coenders-Gerrits, M., Schilperoort, B., Jiménez-Rodríguez, C., 2020. Evaporative Processes on Vegetation: An Inside Look. Springer International Publishing, Cham. pp. 35–48. doi:10.1007/978-3-030-29702-2_3.

Cooper, D., Leclerc, M., Archuleta, J., Coulter, R., Eichinger, W., Kao, C., Nappo, C., 2006. Mass exchange in the stable boundary layer by coherent structures. Agricultural and Forest Meteorology 136, 114–131. doi:10.1016/j.agrformet.2004.12.012. advances in Surface-Atmosphere Exchange - A Tribute to Marv Wesely.

Coplen, T., 2000. A guide for the laboratory information management system (lims) for light stable isotopes–versions 7 and 8: U.s. geological survey open-file report 00-345, 121 p. URL: https://water.usgs.gov/software/code/geochemical/lims/doc/ofr00345.pdf.

Cornelissen, J., Lavorel, S., Garnier, E., Diaz, S., Buchmann, N., Gurvich, D., Reich, P., Ter Steege, H., Morgan, H., Van Der Heijden, M., Pausas, J., Poorter, H., 2003. A handbook of protocols for standardised and easy measurement of plant functional traits worldwide. Australian journal of Botany 51, 335–380. doi:10.1071/BT02124.

Couvreux, F., Hourdin, F., Rio, C., 2010. Resolved versus parametrized boundary-layer plumes. part i: A parametrization-oriented conditional sampling in large-eddy simulations. Boundary-Layer Meteorology 134, 441–458. doi:10.1007/s10546-009-9456-5.

Craig, H., 1961. Standard for reporting concentrations of deuterium and oxygen-18 in natural waters. Science 133, 1833–1834. doi:10.1126/science.133.3467.1833.

Craig, H., Gordon, L.I., 1965. Deuterium and oxygen 18 variations in the ocean and the marine atmosphere .

Crang, R., Lyons-Sobaski, S., Wise, R., 2018. Plant Anatomy: A Concept-Based Approach to the Structure of Seed Plants. Springer.

Crockford, R.H., Richardson, D.P., 2000. Partitioning of rainfall into throughfall, stemflow and interception: effect of forest type, ground cover and climate. Hydrological Processes 14, 2903–2920. doi:10.1002/1099-1085(200011/12)14:16/17<2903::AID-HYP126>3.0.CO;2-6.

Crowther, T.W., Glick, H.B., Covey, K.R., Bettigole, C., Maynard, D.S., Thomas, S.M., Smith, J.R., Hintler, G., Duguid, M.C., Amatulli, G., et al., 2015. Mapping tree density at a global scale. Nature 525, 201. doi:10.1038/nature14967.

Curl, E., Truelove, B., 1986. The rhizosphere. springer-verlag, new york. The rhizosphere. Springer-Verlag, New York. .

Curtis, P.G., Slay, C.M., Harris, N.L., Tyukavina, A., Hansen, M.C., 2018. Classifying drivers of global forest loss. Science 361, 1108–1111. doi:10.1126/science.aau3445.

Da Ronch, F., Caudullo, G., De Rigo, D., 2016. Pseudotsuga menziesii in Europe: distribution, habitat, usage and threats. Publication Office of the European Union, Luxembourg. pp. 146–147. URL: https://ies-ows.jrc.ec.europa.eu/efdac/download/Atlas/pdf/Pseudotsuga_menziesii.pdf.

Dai, A., Zhao, T., Chen, J., 2018. Climate change and drought: a precipitation and evaporation perspective. Current Climate Change Reports 4, 301–312. doi:10.1007/s40641-018-0101-6.

David, J.S., Valente, F., Gash, J.H., 2006. Evaporation of Intercepted Rainfall. American Cancer Society. chapter 43. doi:10.1002/0470848944.hsa046.

Dawson, T.E., Ehleringer, J.R., 1998. Chapter 6 - Plants, Isotopes and Water Use: A Catchment-Scale Perspective. Elsevier, Amsterdam. pp. 165 – 202. doi:10.1016/B978-0-444-81546-0.50013-6.

Dawson, T.E., Mambelli, S., Plamboeck, A.H., Templer, P.H., Tu, K.P., 2002. Stable isotopes in plant ecology. Annual Review of Ecology and Systematics 33, 507–559. doi:10.1146/annurev.ecolsys.33.020602.095451.

Dawson, T.E., Pate, J.S., 1996. Seasonal water uptake and movement in root systems of australian phraeatophytic plants of dimorphic root morphology: a stable isotope investigation. Oecologia 107, 13–20. doi:10.1007/BF00582230.

Dawson, T.E., Simonin, K.A., 2011. The Roles of Stable Isotopes in Forest Hydrology and Biogeochemistry. Springer Netherlands, Dordrecht. pp. 137–161.

De Deurwaerder, H., Hervé-Fernández, P., Stahl, C., Burban, B., Petronelli, P., Hoffman, B., Bonal, D., Boeckx, P., Verbeeck, H., 2018. Liana and tree below-ground water competition—evidence for water resource partitioning during the dry season. Tree Physiology 38, 1071–1083. doi:10.1093/treephys/tpy002.

De Wispelaere, L., Bodé, S., Hervé-Fernández, P., Hemp, A., Verschuren, D., Boeckx, P., 2017. Plant water resource partitioning and isotopic fractionation during transpiration in a seasonally dry tropical climate. Biogeosciences 14, 73.

Deguchi, A., Hattori, S., Daikoku, K., Park, H.T., 2008. Measurement of evaporation from the forest floor in a deciduous forest throughout the year using microlysimeter and closed-chamber systems. Hydrological Processes 22, 3712–3723. doi:10.1002/hyp.6974.

Dekker, S.C., Bouten, W., Verstraten, J.M., 2000. Modelling forest transpiration from different perspectives. Hydrological Processes 14, 251–260. doi:10.1002/(SICI)1099-1085(20000215)14:2<251::AID-HYP923>3.0.CO;2-R.

Derks, J., 2019. Chapter 5.2. An (un)welcome guest – perception of Douglas-fir in seven European countries from the perspectives of forestry and nature conservation. European Forest Institute. pp. 105–110. URL: https://www.efi.int/sites/default/files/files/publication-bank/2019/efi_wsctu9_2019.pdf.

van Dijk, A.I., Gash, J.H., van Gorsel, E., Blanken, P.D., Cescatti, A., Emmel, C., Gielen, B., Harman, I.N., Kiely, G., Merbold, L., Montagnani, L., Moors, E., Sottocornola, M., Varlagin, A., Williams, C.A., Wohlfahrt, G., 2015. Rainfall interception and the coupled surface water and energy balance. Agricultural and Forest Meteorology 214-215, 402 – 415. doi:10.1016/j.agrformet.2015.09.006.

Dubayah, R.O., Sheldon, S.L., Clark, D.B., Hofton, M.A., Blair, J.B., Hurtt, G.C., Chazdon, R.L., 2010. Estimation of tropical forest height and biomass dynamics using lidar remote sensing at la selva, costa rica. Journal of Geophysical Research: Biogeosciences 115. doi:10.1029/2009JG000933.

Dubbert, M., Cuntz, M., Piayda, A., Maguás, C., Werner, C., 2013. Partitioning evapotranspiration – testing the craig and gordon model with field measurements of oxygen isotope ratios of evaporative fluxes. Journal of Hydrology 496, 142 – 153. doi:10.1016/j.jhydrol.2013.05.033.

Dubbert, M., Cuntz, M., Piayda, A., Werner, C., 2014. Oxygen isotope signatures of transpired water vapor: the role of isotopic non-steady-state transpiration under natural conditions. New Phytologist 203, 1242–1252. doi:10.1111/nph.12878.

Dubbert, M., Kübert, A., Werner, C., 2017. Impact of leaf traits on temporal dynamics of transpired oxygen isotope signatures and its impact on atmospheric vapor. Frontiers in plant science 8. doi:10.3389/fpls.2017.00005.

Dunin, F.X., O'Loughlin, E.M., Reyenga, W., 1988. Interception loss from eucalypt forest: Lysimeter determination of hourly rates for long term evaluation. Hydrological Processes 2, 315–329. doi:10.1002/hyp.3360020403.

Dunkerley, D.L., 2009. Evaporation of impact water droplets in interception processes: Historical precedence of the hypothesis and a brief literature overview.

Journal of Hydrology 376, 599 – 604. doi:10.1016/j.jhydrol.2009.08.004.

Edwards, S., Callaghan, D., Rothero, G., Genney, D., Rumsey, F., 2010a. Polytrichum commune, Key 95. British Bryological Society Plymouth. pp. 322–323.

Edwards, S., Rumsey, F., Callaghan, D., Tom, B., 2010b. Brachythecium rutabulum, Key 364. British Bryological Society Plymouth. pp. 746–747.

Ehleringer, J., Dawson, T., 1992. Water uptake by plants: perspectives from stable isotope composition. Plant, Cell & Environment , 1073–1082doi:10.1111/j.1365-3040.1992.tb01657.x.

Eilu, G., Hafashimana, D.L.N., Kasenene, J.M., 2004. Density and species diversity of trees in four tropical forests of the albertine rift, western uganda. Diversity and Distributions 10, 303–312. doi:10.1111/j.1366-9516.2004.00089.x.

Ellison, D., Morris, C.E., Locatelli, B., Sheil, D., Cohen, J., Murdiyarso, D., Gutierrez, V., van Noordwijk, M., Creed, I.F., Pokorny, J., Gaveau, D., Spracklen, D.V., Tobella, A.B., Ilstedt, U., Teuling, A.J., Gebrehiwot, S.G., Sands, D.C., Muys, B., Verbist, B., Springgay, E., Sugandi, Y., Sullivan, C.A., 2017. Trees, forests and water: Cool insights for a hot world. Global Environmental Change 43, 51–61. doi:10.1016/j.gloenvcha.2017.01.002.

Ellsworth, P.Z., Williams, D.G., 2007. Hydrogen isotope fractionation during water uptake by woody xerophytes. Plant and Soil 291, 93–107. doi:10.1007/s11104-006-9177-1.

van der Ent, R.J., Savenije, H.H.G., 2011. Length and time scales of atmospheric moisture recycling. Atmospheric Chemistry and Physics 11, 1853–1863. URL: https://www.atmos-chem-phys.net/11/1853/2011/, doi:10.5194/acp-11-1853-2011.

van der Ent, R.J., Savenije, H.H.G., Schaefli, B., Steele-Dunne, S.C., 2010. Origin and fate of atmospheric moisture over continents. Water Resources Research 46. doi:10.1029/2010WR009127.

Euser, T., Luxemburg, W.M.J., Everson, C.S., Mengistu, M.G., Clulow, A.D., Bastiaanssen, W.G.M., 2014. A new method to measure bowen ratios using high-resolution vertical dry and wet bulb temperature profiles. Hydrology and Earth System Sciences 18, 2021–2032. doi:10.5194/hess-18-2021-2014.

Evaristo, J., McDonnell, J.J., Clemens, J., 2017. Plant source water apportionment using stable isotopes: A comparison of simple linear, two-compartment mixing model approaches. Hydrological Processes 31, 3750–3758. doi:10.1002/hyp.11233.

FAO, 2006. Guidelines for Soil Description. Food and Agriculture Organization (FAO).

Farquhar, G.D., Cernusak, L.A., Barnes, B., 2007. Heavy water fractionation during transpiration. Plant Physiology 143, 11–18. doi:10.1104/pp.106.093278.

Feng, F., Li, Z., Zhang, M., Jin, S., Dong, Z., 2013a. Deuterium and oxygen 18 in precipitation and atmospheric moisture in the upper urumqi river basin, eastern tianshan mountains. Environmental Earth Sciences 68, 1199–1209. doi:10.1007/s12665-012-1820-y.

Feng, X., Porporato, A., Rodriguez-Iturbe, I., 2013b. Changes in rainfall seasonality in the tropics. Nature Climate Change 3. doi:10.1038/nclimate1907.

Ferrio, J.P., Cuntz, M., Offermann, C., Siegwolf, R., Saurer, M., Gessler, A., 2009. Effect of water availability on leaf water isotopic enrichment in beech seedlings shows limitations of current fractionation models. Plant, Cell & Environment 32, 1285–1296. doi:10.1111/j.1365-3040.2009.01996.x.

Fetcher, N., Oberbauer, S.F., Strain, B.R., 1985. Vegetation effects on microclimate in lowland tropical forest in costa rica. International Journal of Biometeorology 29, 145–155. doi:10.1007/BF02189035.

Fischer, B.M.C., Frentress, J., Manzoni, S., Cousins, S.A.O., Hugelius, G., Greger, M., Smittenberg, R.H., Lyon, S.W., 2019. Mojito, anyone? an exploration of low-tech plant water extraction methods for isotopic analysis using locally-sourced materials. Frontiers in Earth Science 7, 150. doi:10.3389/feart.2019.00150.

Fischer, C., Tischer, J., Roscher, C., Eisenhauer, N., Ravenek, J., Gleixner, G., Attinger, S., Jensen, B., de Kroon, H., Mommer, L., Scheu, S., Hildebrandt, A., 2015. Plant species diversity affects infiltration capacity in an experimental grassland through changes in soil properties. Plant and Soil 397, 1–16. doi:10.1007/s11104-014-2373-5.

Fitzjarrald, D., Moore, K., 1995. Physical Mechanisms of heat and mass exchange between forests and the atmosphere. Academic Press. pp. 45–72.

Fletcher, M., 1991. Moss Grower's Handbook: An Illustrated Beginner's Guide to Finding, Naming and Growing Over 100 Common British Species. Seventy Press.

FLUXNET, 2020. Fluxdata. the data portal serving the fluxnet community. URL: https://fluxnet.fluxdata.org/. accessed: 2020-04-05.

Forrester, D.I., 2015. Transpiration and water-use efficiency in mixed-species forests versus monocultures: effects of tree size, stand density and season. Tree Physiology 35, 289–304. doi:10.1093/treephys/tpv011.

Franssen, H.H., Stockli, R., Lehner, I., Rotenberg, E., Seneviratne, S., 2010. Energy balance closure of eddy-covariance data: A multisite analysis for european fluxnet stations. Agricultural and Forest Meteorology 150, 1553–1567. doi:10.1016/j.agrformet.2010.08.005.

Frazer, G.W., Canham, C., Lertzman, K., 1999. Gap light analyzer (gla), version 2.0: Imaging software to extract canopy structure and gap light transmission indices from true-colour fisheye photographs, users manual and program documentation. Simon Fraser University, Burnaby, British Columbia, and the Institute of Ecosystem Studies, Millbrook, New York 36.

Frey, S.J.K., Hadley, A.S., Johnson, S.L., Schulze, M., Jones, J.A., Betts, M.G., 2016. Spatial models reveal the microclimatic buffering capacity of old-growth forests. Science Advances 2. doi:10.1126/sciadv.1501392.

Fry, B., 2006. Stable isotope ecology. volume 521. Springer. doi:10.1007/0-387-33745-8.

Fuentes, J.D., Chamecki, M., Nascimento dos Santos, R.M., Von Randow, C., Stoy, P.C., Katul, G., Fitzjarrald, D., Manzi, A., Gerken, T., Trowbridge, A., Souza Freire, L., Ruiz-Plancarte, J., Furtunato Maia, J.M., TÃ³ta, J., Dias, N., Fisch, G., Schumacher, C., Acevedo, O., Rezende Mercer, J., YaÃ±ez-Serrano, A.M., 2016. Linking meteorology, turbulence, and air chemistry in the amazon rain forest. Bulletin of the American Meteorological Society 97, 2329–2342. doi:10.1175/BAMS-D-15-00152.1.

Furness, S.B., Grime, J.P., 1982. Growth rate and temperature responses in bryophytes: I. an investigation of brachythecium rutabulum. Journal of Ecology 70, 513–523.

Gaj, M., Beyer, M., Koeniger, P., Wanke, H., Hamutoko, J., Himmelsbach, T., 2016. In situ unsaturated zone water stable isotope (^{2}h and ^{18}o) measurements in semi-arid environments: a soil water balance. Hydrology and Earth System Sciences 20, 715–731. doi:10.5194/hess-20-715-2016.

Gat, J., 2005. Some classical concepts of isotope hydrology: "Rayleigh fractionation, Meteoric Water Lines, the Daansgaard effects (altitude, latitude, distance from coast and ammount effects) and the d-excess parameter,". Springer. pp. 127–137.

Gat, J., 2010. Isotope Hydrology: A Study of the Water Cycle. Series on environmental science and management, Imperial College Press.

Gat, J., Mook, w., Meijer, H., 2000. Volume ii. atmospheric water. in: Environmental isotopes in the hydrological cycle. principles and aplications .

Gat, J.R., 2008. The isotopic composition of evaporating waters– review of the historical evolution leading up to the craig–gordon model. Isotopes in Environmental and Health Studies 44, 5–9. doi:10.1080/10256010801887067.

Gemery, P.A., Trolier, M., White, J.W.C., 1996. Oxygen isotope exchange between carbon dioxide and water following atmospheric sampling using glass flasks. Journal of Geophysical Research: Atmospheres 101, 14415–14420. doi:10.1029/96JD00053.

Germer, S., 2013. Development of near-surface perched water tables during natural and artificial stemflow generation by babassu palms. Journal of Hydrology 507, 262–272. doi:10.1016/j.jhydrol.2013.10.026.

Germer, S., Werther, L., Elsenbeer, H., 2010. Have we underestimated stemflow? lessons from an open tropical rainforest. Journal of Hydrology 395, 169–179. doi:10.1016/j.jhydrol.2010.10.022.

Gerrits, A.M.J., Pfister, L., Savenije, H.H.G., 2010. Spatial and temporal variability of canopy and forest floor interception in a beech forest. Hydrological Processes 24, 3011–3025. doi:10.1002/hyp.7712.

Gerrits, A.M.J., Savenije, H.H.G., 2011. Forest Floor Interception. Springer Netherlands, Dordrecht. pp. 445–454. doi:10.1007/978-94-007-1363-5_22.

Gerrits, A.M.J., Savenije, H.H.G., Hoffmann, L., Pfister, L., 2007. New technique to measure forest floor interception ndash; an application in a beech forest in luxembourg. Hydrology and Earth System Sciences 11, 695–701. URL: https://www.hydrol-earth-syst-sci.net/11/695/2007/, doi:10.5194/hess-11-695-2007.

Gerrits, A.M.J., Savenije, H.H.G., Veling, E.J.M., Pfister, L., 2009. Analytical derivation of the budyko curve based on rainfall characteristics and a simple evaporation model. Water Resources Research 45. doi:10.1029/2008WR007308.

Geyh, M., 2000. Volume IV. Groundwater. Saturated and unsaturated zone. UNESCO.

Ghimire, C.P., Lubczynski, M.W., Bruijnzeel, L.A., Zwartendijk, B.W., van Meerveld, H.J.I., Odongo, V.O., Ravelona, M., 2018. Transpiration and stomatal conductance in a young secondary tropical montane forest: contrasts between native trees and invasive understorey shrubs. Tree Physiology 38, 1053–1070. doi:10.1093/treephys/tpy004.

Gibson, J., Edwards, T., Bursey, G., Prowse, T., 1993. Estimating evaporation using stable isotopes: Quantitative results and sensitivity analysis for two catchments in northern canada. Hydrology Research 24, 79–94. doi:10.2166/nh.1993.0015.

Gibson, J.J., Edwards, T.W.D., Birks, S.J., St Amour, N.A., Buhay, W.M., McEachern, P., Wolfe, B.B., Peters, D.L., 2005. Progress in isotope tracer hydrology in canada. Hydrological Processes 19, 303–327. doi:10.1002/hyp.5766.

Gilman, E., Watson, G., 1994. *Salix matsudana* 'tortuosa' corkscrew willow. fact sheet st-577 environmental horticulture department, florida cooperative extension service, institute of food and agricultural sciences, university of florida. URL: https://edis.ifas.ufl.edu/st577.

Giuditta, E., Coenders-Gerrits, A., Bogaard, T., Wenninger, J., Greco, R., Rutigliano, F., 2018. Measuring changes in forest floor evaporation after prescribed burning in southern italy pine plantations. Agricultural and Forest Meteorology 256-257, 516 – 525. doi:10.1016/j.agrformet.2018.04.004.

Giuggiola, A., Zweifel, R., Feichtinger, L.M., Vollenweider, P., Bugmann, H., Haeni, M., Rigling, A., 2018. Competition for water in a xeric forest ecosystem – effects of understory removal on soil micro-climate, growth and physiology of dominant scots pine trees. Forest Ecology and Management 409, 241–249. doi:10.1016/j.foreco.2017.11.002.

Glime, J., 2017. Chapter 7 - Water Relations. Michigan Technological University and the International Association of Bryologists. URL: http://digitalcommons.mtu.edu/bryophyte-ecology/.

Göckede, M., Thomas, C., Markkanen, T., Mauder, M., Ruppert, J., Foken, T., 2007. Sensitivity of lagrangian stochastic footprints to turbulence statistics. Tellus B: Chemical and Physical Meteorology 59, 577–586. doi:10.1111/j.1600-0889.2007.00275.x.

Goetz, J.D., Price, J.S., 2015. Role of morphological structure and layering of sphagnum and tomenthypnum mosses on moss productivity and evaporation rates. Canadian Journal of Soil Science 95, 109–124. doi:10.4141/cjss-2014-092.

Gomez, L., 1986. Vegetacion de Costa Rica: Apuntes para una biogeografia Costarricense: vegetacion y clima de Costa Rica. EUNED.

Good, S.P., Soderberg, K., Wang, L., Caylor, K.K., 2012. Uncertainties in the assessment of the isotopic composition of surface fluxes: A direct comparison of techniques using laser-based water vapor isotope analyzers. Journal of Geophysical Research: Atmospheres 117. doi:10.1029/2011JD017168.

Goosse, H., 2015. The energy balance, hydrological and carbon cycles. Cambridge University Press. chapter 2.

Gordon, D.A.R., Coenders-Gerrits, M., Sellers, B.A., Sadeghi, S.M.M., Van Stan II, J.T., 2019. Rainfall interception and redistribution by a common north american understory and pasture forb, *Eupatorium capillifolium* (lam. dogfennel). Hydrology and Earth System Sciences Discussions 2019, 1–22. doi:10.5194/hess-2019-579.

Gotsch, S.G., Asbjornsen, H., Holwerda, F., Goldsmith, G.R., Weintraub, A.E., Dawson, T.E., 2014. Foggy days and dry nights determine crown-level water balance in a seasonal tropical montane cloud forest. Plant, Cell & Environment 37, 261–272. doi:10.1111/pce.12151.

Gotsch, S.G., Nadkarni, N., Amici, A., 2016. The functional roles of epiphytes and arboreal soils in tropical montane cloud forests. Journal of Tropical Ecology 32, 455—468. doi:10.1017/S026646741600033X.

Gou, J., Qu, S., Shi, P., Li, D., Chen, X., Wang, Y., Shan, S., Si, W., 2018. Application of stable isotope tracer to study runoff generation during different types of rainfall events. Water 10. doi:10.3390/w10050538.

Gourcy, L., Groening, M., Aggarwal, P., 2005. Stable oxygen and hydrogen isotopes. Springer. pp. 39–51.

Gralher, B., Herbstritt, B., Weiler, M., Wassenaar, L.I., Stumpp, C., 2018. Correcting for biogenic gas matrix effects on laser-based pore water-vapor stable isotope measurements. Vadose Zone Journal 17. doi:10.2136/vzj2017.08.0157.

Granier, A., 1985. Une nouvelle méthode pour la mesure du flux de sève brute dans le tronc des arbres. Annales des Sciences Forestières 42, 193–200. URL: https://hal.archives-ouvertes.fr/hal-00882347.

Granier, A., 1987. Evaluation of transpiration in a Douglas-fir stand by means of sap flow measurements. Tree Physiology 3, 309–320. doi:10.1093/treephys/3.4.309.

Green, R., Trowbridge, R., Klinka, K., 1993. Towards a taxonomic classification of humus forms. Forest Science 39, a0001–z0002.

Griffis, T.J., 2013. Tracing the flow of carbon dioxide and water vapor between the biosphere and atmosphere: A review of optical isotope techniques and their application. Agricultural and Forest Meteorology 174-175, 85 – 109. doi:10.1016/j.agrformet.2013.02.009.

Groff, P.A., Kaplan, D.R., 1988. The relation of root systems to shoot systems in vascular plants. The Botanical Review 54, 387–422. doi:10.1007/BF02858417.

Gröning, M., Lutz, H., Roller-Lutz, Z., Kralik, M., Gourcy, L., Pöltenstein, L., 2012. A simple rain collector preventing water re-evaporation dedicated for δ18o and δ2h analysis of cumulative precipitation samples. Journal of Hydrology 448–449, 195–200. doi:10.1016/j.jhydrol.2012.04.041.

Guariguata, M., Ostertag, R., 2002. Sucesión secundaria. Libro Regional Universitario (LUR). pp. 591–624.

Guerrieri, R., Lepine, L., Asbjornsen, H., Xiao, J., Ollinger, S.V., 2016. Evapotranspiration and water use efficiency in relation to climate and canopy nitrogen in u.s. forests. Journal of Geophysical Research: Biogeosciences 121, 2610–2629. doi:10.1002/2016JG003415.

Guo, F., juan MA, J., jian Zheng, L., huan Sun, X., hong Guo, X., lan Zhang, X., 2016. Estimating distribution of water uptake with depth of winter wheat by hydrogen and oxygen stable isotopes under different irrigation depths. Journal of Integrative Agriculture 15, 891–906. doi:10.1016/S2095-3119(15)61258-8.

Guo, X., Tian, L., Wang, L., Yu, W., Qu, D., 2017. River recharge sources and the partitioning of catchment evapotranspiration fluxes as revealed by stable isotope signals in a typical high-elevation arid catchment. Journal of Hydrology 549, 616–630. doi:10.1016/j.jhydrol.2017.04.037.

Gupta, A., Usharani, L., 2009. Rainfall partitioning in a tropical forest of manipur, north east india. Tropical Ecology 50, 355–358.

Gupta, S.K., Deshpande, R.D., 2005. Groundwater isotopic investigations in india: What has been learned? Current Science 89, 825–835. doi:10.2307/24111027.

Guswa, A.J., 2012. Canopy vs. roots: Production and destruction of variability in soil moisture and hydrologic fluxes. Vadose Zone Journal 11. doi:10.2136/vzj2011.0159.

Ham, J., 2015. Radiation shield for weather station temperature/humidity. licensed under the creative commons - attribution license. URL: https://www.thingiverse.com/thing:1067700.

Han, K.S., Park, Y.Y., Yeom, J.M., 2015. Detection of change in vegetation in the surrounding desert areas of northwest china and mongolia with multi-temporal satellite images. Asia-Pacific Journal of Atmospheric Sciences 51, 173–181. doi:10.1007/s13143-015-0068-3.

Hansen, A.J., Phillips, L.B., Dubayah, R., Goetz, S., Hofton, M., 2014. Regional-scale application of lidar: Variation in forest canopy structure across the southeastern us. Forest Ecology and Management 329, 214 – 226. doi:10.1016/j.foreco.2014.06.009.

Harper, A., Baker, I.T., Denning, A.S., Randall, D.A., Dazlich, D., Branson, M., 2014. Impact of evapotranspiration on dry season climate in the amazon forest. Journal of Climate 27, 574–591. doi:10.1175/JCLI-D-13-00074.1.

Hartshorn, G., 2002. Biogeografía de los bosques neotropicales. Libro Regional Universitario (LUR). pp. 59–82.

Haverd, V., Cuntz, M., Leuning, R., Keith, H., 2007. Air and biomass heat storage fluxes in a forest canopy: Calculation within a soil vegetation atmosphere transfer model. Agricultural and Forest Meteorology 147, 125–139. doi:10.1016/j.agrformet.2007.07.006.

He, H., Smith, R.B., 1999. Stable isotope composition of water vapor in the atmospheric boundary layer above the forests of new england. Journal of Geophysical Research: Atmospheres 104, 11657–11673. doi:10.1029/1999JD900080.

He, Z.B., Yang, J.J., Du, J., Zhao, W.Z., Liu, H., Chang, X.X., 2014. Spatial variability of canopy interception in a spruce forest of the semiarid mountain regions of china. Agricultural and Forest Meteorology 188, 58–63. doi:10.1016/j.agrformet.2013.12.008.

Heijmans, M.M.P.D., Arp, W.J., Chapin, F.S., 2004. Controls on moss evaporation in a boreal black spruce forest. Global Biogeochemical Cycles 18, 1–8. doi:10.1029/2003GB002128. gB2004.

Hendry, M.J., Schmeling, E., Wassenaar, L.I., Barbour, S.L., Pratt, D., 2015. Determining the stable isotope composition of pore water from saturated and unsaturated zone core: improvements to the direct vapour equilibration laser spectrometry method. Hydrology and Earth System Sciences 19, 4427–4440. doi:10.5194/hess-19-4427-2015.

Herbstritt, B., Limprecht, M., Gralher, B., Weiler, M., 2014. Effects of soil properties on the apparent water-vapor isotope equilibrium fractionation: Implications for the headspace equilibration method [poster presentation]. UNI Freiburg: http://www. hydro. uni-freiburg. de/publ/pubpics/post229 (last access: 7 October 2015) .

Herman, R.L., Ray, E.A., Rosenlof, K.H., Bedka, K.M., Schwartz, M.J., Read, W.G., Troy, R.F., Chin, K., Christensen, L.E., Fu, D., Stachnik, R.A., Bui, T.P., Dean-Day, J.M., 2017. Enhanced stratospheric water vapor over the summertime continental united states and the role of overshooting convection. Atmospheric Chemistry and Physics 17, 6113–6124. doi:10.5194/acp-17-6113-2017.

Hilje, B., Calvo-Alvarado, J., Jiménez-Rodríguez, C., Sánchez-Azofeifa, A., 2015. Tree species composition, breeding systems, and pollination and sispersal syndromes in three forest successional stages in a tropical dry forest in Mesoamerica. Tropical Conservation Science 8, 76 – 94. doi:10.1177/194008291500800109.

Hogan, K., Kattan, J., 2002. La luz solar: consecuencias biológicas y medición. Libro Regional Universitario (LUR). pp. 119–143.

Hogg, E.H., Hurdle, P.A., 1997. Sap flow in trembling aspen: implications for stomatal responses to vapor pressure deficit. Tree Physiology 17, 501–509. doi:10.1093/treephys/17.8-9.501.

Holdridge, L.R., 1967. Life zone ecology. Tropical Science Center, San José, Costa Rica.

Holmes, T.R.H., Owe, M., De Jeu, R.A.M., Kooi, H., 2008. Estimating the soil temperature profile from a single depth observation: A simple empirical heatflow solution. Water Resources Research 44, 1–11. doi:10.1029/2007WR005994.

Holwerda, F., Bruijnzeel, L., Scatena, F., Vugts, H., Meesters, A., 2012. Wet canopy evaporation from a puerto rican lower montane rain forest: The importance of realistically estimated aerodynamic conductance. Journal of Hydrology 414-415, 1–15. doi:10.1016/j.jhydrol.2011.07.033.

Hopkins, W.G., Hüner, N.P., 2008. Introduction to Plant Physiology. Wiley.

Horita, J., Rozanski, K., Cohen, S., 2008. Isotope effects in the evaporation of water: a status report of the craig–gordon model. Isotopes in Environmental and Health Studies 44, 23–49. doi:10.1080/10256010801887174.

Horton, J.L., Hart, S.C., 1998. Hydraulic lift: a potentially important ecosystem process. Trends in Ecology Evolution 13, 232–235. doi:10.1016/S0169-5347(98)01328-7.

Hsueh, Y.H., Allen, S.T., Keim, R.F., 2016. Fine-scale spatial variability of throughfall amount and isotopic composition under a hardwood forest canopy. Hydrological Processes 30, 1796–1803. doi:10.1002/hyp.10772.

Hu, B., long Han, C., Jia, Y., hong Zhao, Z., min Li, F., Siddique, K.H., 2013. Visualization of the three-dimensional water-flow paths in calcareous soil using iodide water tracer. Geoderma 200-201, 85 – 89. doi:10.1016/j.geoderma.2013.01.009.

Huang, J., Zhou, Y., Yin, L., Wenninger, J., Zhang, J., Hou, G., Zhang, E., Uhlenbrook, S., 2015. Climatic controls on sap flow dynamics and used water sources of salix psammophila in a semi-arid environment in northwest China. Environmental Earth Sciences 73, 289–301. doi:10.1007/s12665-014-3505-1.

Huggett, R., 2007. Fundamentals of geomorphology. Second ed., Routledge Fundamentals of Physical Geography.

Huneau, F., Dakoure, D., Celle-Jeanton, H., Vitvar, T., Ito, M., Traore, S., Compaore, N., Jirakova, H., Coustumer, P.L., 2011. Flow pattern and residence time of groundwater within the south-eastern taoudeni sedimentary basin (burkina faso, mali). Journal of Hydrology 409, 423 – 439. doi:10.1016/j.jhydrol.2011.08.043.

IAEA, 2016. Supporting sampling and sample preparation tools for isotope and nuclear analysis. IAEA–TECDOC–1783. URL: https://www.iaea.org/publications/10991/supporting-sampling-and-sample-preparation-tools-for-isotope-and-n

Iannone, R.Q., Romanini, D., Cattani, O., Meijer, H.A.J., Kerstel, E.R.T., 2010. Water isotope ratio (δ2h and δ18o) measurements in atmospheric moisture using an optical feedback cavity enhanced absorption laser spectrometer. Journal of Geophysical Research: Atmospheres 115. doi:10.1029/2009JD012895.

IIASA/FAO, 2012. Global Agro–Ecological Zones (GAEZ v3.0). IIASA, Laxenburg, Austria and FAO, Rome, Italy.

Iida, S., Ohta, T., Matsumoto, K., Nakai, T., Kuwada, T., Kononov, A.V., Maximov, T.C., van der Molen, M.K., Dolman, H., Tanaka, H., Yabuki, H., 2009. Evapotranspiration from understory vegetation in an eastern siberian boreal larch forest. Agricultural and Forest Meteorology 149, 1129–1139. doi:10.1016/j.agrformet.2009.02.003.

IMGBIN, 2020. Download transparent png images, for free. all rights reserved 0.014. URL: https://imgbin.com/. Accessed: 2020-03-10.

Ingraham, N.L., 1998. Chapter 3 - Isotopic Variations in Precipitation. Elsevier, Amsterdam. pp. 87 – 118. URL: http://www.sciencedirect.com/science/article/pii/B9780444815460500100, doi:10.1016/B978-0-444-81546-0.50010-0.

Ivans, S., Hipps, L., Leffler, A.J., Ivans, C.Y., 2006. Response of water vapor and co2 fluxes in semiarid lands to seasonal and intermittent precipitation pulses. Journal of Hydrometeorology 7, 995–1010. doi:10.1175/JHM545.1.

Jackson, P.C., Cavelier, J., Goldstein, G., Meinzer, F.C., Holbrook, N.M., 1995. Partitioning of water resources among plants of a lowland tropical forest. Oecologia 101, 197–203. doi:10.1007/BF00317284.

Jacobs, A.F.G., Van Boxel, J.H., El-Kilani, R.M.M., 1994. Nighttime free convection characteristics within a plant canopy. Boundary-Layer Meteorology 71, 375–391. doi:10.1007/BF00712176.

Janzen, D., 1988. Tropical Dry Forests: The Most Endangered Major Tropical Ecosystem. National Academy Press, Washington D.C. pp. 130–144.

Jassal, R.S., Black, T.A., Spittlehouse, D.L., Brummer, C., Nesic, Z., 2009. Evapotranspiration and water use efficiency in different-aged pacific northwest douglas-fir stands. Agricultural and Forest Meteorology 149, 1168 – 1178. doi:10.1016/j.agrformet.2009.02.004.

Jia, Z., Zhu, Y., Liu, L., 2012. Different water use strategies of juvenile and adult *Caragana intermedia* plantations in the gonghe basin, tibet plateau. PLOS ONE 7, 1–6. doi:10.1371/journal.pone.0045902.

Jiamei, S., Xinxiao, Y., Henian, W., Guodong, J., Yang, Z., Zhihua, T., Wenping, D., Jianbo, J., Jungang, C., 2018. Effects of forest structure on hydrological processes in china. Journal of Hydrology 561, 187–199. doi:10.1016/j.jhydrol.2018.04.003.

Jiang, G., He, W., 1999. Species- and habitat-variability of photosynthesis, transpiration and water use efficiency of different plant species in maowusu sand area. Acta Botanica Sinica 41, 1114—1124. URL: http://europepmc.org/abstract/CBA/329392.

Jiménez-Rodríguez, C., Calvo-Alvarado, J., 2013. An evaluation of rainfall interception in secondary tropical dry forests. CRC Press, UK. chapter 14. pp. 249–266.

Jiménez-Rodríguez, C.D., Coenders-Gerrits, M., Wenninger, J., Gonzalez-Angarita, A., Savenije, H., 2019a. Contribution of understory evaporation in a tropical wet forest. Hydrology and Earth System Sciences Discussions 2019, 1–32. doi:10.5194/hess-2019-566.

Jiménez-Rodríguez, C.D., González-Angarita, A.P., Coenders-Gerrits, A.M.J., 2019b. Vapor plumes video at la selva biological station. 4tu.centre for research data. dataset. *4TU.Centre for Research Data* https://data.4tu.nl/repository/uuid:997cc9d8-2281-453e-b631-5f93cfebe00e.

Jouzel, J., Delaygue, G., Landais, A., Masson-Delmotte, V., Risi, C., Vimeux, F., 2013. Water isotopes as tools to document oceanic sources of precipitation. Water Resources Research 49, 7469–7486. doi:10.1002/2013WR013508.

Jung, E.Y., Otieno, D., Kwon, H., Lee, B., Lim, J.H., Kim, J., Tenhunen, J., 2013. Water use by a warm-temperate deciduous forest under the influence of the asian monsoon: contributions of the overstory and understory to forest water use. Journal of Plant Research 126, 661–674. doi:10.1007/s10265-013-0563-5.

Kalacska, M., Sanchez-Azofeifa, G., Calvo-Alvarado, J., Quesada, M., Rivard, B., Janzen, D., 2004. Species composition, similarity and diversity in three successional stages of a seasonally dry tropical forest. Forest Ecology and Management 200, 227–247. doi:10.1016/j.foreco.2004.07.001.

Kang, M., Kim, J., Malla Thakuri, B., Chun, J., Cho, C., 2018. New gap-filling and partitioning technique for h_2o eddy fluxes measured over forests. Biogeosciences 15, 631–647. doi:10.5194/bg-15-631-2018.

Kao, C.Y., Hang, Y.H., Cooper, D., Eichinger, W., Smith, W., Reisner, J., 2000. High-resolution modeling of lidar data: Mechanisms governing surface water vapor variability during salsa. Agricultural and Forest Meteorology 105, 185 – 194. doi:10.1016/S0168-1923(00)00182-9.

Kasurinen, V., Alfredsen, K., Kolari, P., Mammarella, I., Alekseychik, P., Rinne, J., Vesala, T., Bernier, P., Boike, J., Langer, M., Belelli Marchesini, L., van Huissteden, K., Dolman, H., Sachs, T., Ohta, T., Varlagin, A., Rocha, A., Arain, A., Oechel, W., Lund, M., Grelle, A., Lindroth, A., Black, A., Aurela, M., Laurila, T., Lohila, A., Berninger, F., 2014. Latent heat exchange in the boreal and arctic biomes. Global Change Biology 20, 3439–3456. doi:10.1111/gcb.12640.

Keeling, C.D., 1958. The concentration and isotopic abundances of atmospheric carbon dioxide in rural areas. Geochimica et Cosmochimica Acta 13, 322–334. doi:10.1016/0016-7037(58)90033-4.

Keller, P.E., Kouzes, R., 2017. Water vapor permeation in plastics. prepared for the u.s. department of homeland security domestic nuclear detection office under u.s. department of energy contract de-ac05-76rl01830. URL: https://www.pnnl.gov/main/publications/external/technical_reports/PNNL-26070.pdf.

Kendall, C., Caldwell, E.A., 1998. Chapter 2 - Fundamentals of Isotope Geochemistry. Elsevier, Amsterdam. pp. 51 – 86. doi:10.1016/B978-0-444-81546-0.50009-4.

Kendall, C., McDonell, J.J. (Eds.), 1998. Chapter 5 - Isotopic Exchange in Soil Water. Elsevier, Amsterdam. pp. 137 – 163. doi:10.1016/B978-0-444-81546-0.50012-4.

Kerfoot, O., 1963. The root systems of tropical forest trees. The Commonwealth Forestry Review 42, 19–26. URL: http://www.jstor.org/stable/42602976.

Kern, C., Masias, P., Apaza, F., Reath, K.A., Platt, U., 2017. Remote measurement of high preeruptive water vapor emissions at sabancaya volcano by passive differential optical absorption spectroscopy. Journal of Geophysical Research: Solid Earth 122, 3540–3564. doi:10.1002/2017JB014020.

Klaassen, W., Bosveld, F., de Water, E., 1998. Water storage and evaporation as constituents of rainfall interception. Journal of Hydrology 212–213, 36–50. doi:10.1016/S0022-1694(98)00200-5.

Klamerus-Iwan, A., Link, T.E., Keim, R.F., Van Stan II, J.T., 2020. Storage and Routing of Precipitation Through Canopies. Springer International Publishing, Cham. pp. 17–34. doi:10.1007/978-3-030-29702-2_2.

Klinka, K., Krestov, P., Fons, J., Chourmouzis, C., 1997. Towards a taxonomic classification of humus forms: third approximation. Scientia Silvica , 1–4URL: https://open.library.ubc.ca/cIRcle/collections/facultyresearchandpublications/52383/items/1.0107268.

Klos, P.Z., Chain-Guadarrama, A., Link, T.E., Finegan, B., Vierling, L.A., Chazdon, R., 2014. Throughfall heterogeneity in tropical forested landscapes as a focal mechanism for deep percolation. Journal of Hydrology 519, 2180–2188. doi:10.1016/j.jhydrol.2014.10.004.

KNMI, 2020a. Koninklijk nederlands meteorologisch instituut. klimatologie. uurgegevens van het weer in nederland - download. URL: http://projects.knmi.nl/klimatologie/uurgegevens/selectie.cgi. accessed: 2020-01-10.

KNMI, 2020b. Koninklijk nederlands meteorologisch instituut. year 2019: Zeer warm, zeer zonnig en landelijk gemiddeld vrij droog. Visited on: March 02, 2020.

Knoche, H.R., Kunstmann, H., 2013. Tracking atmospheric water pathways by direct evaporation tagging: A case study for west africa. Journal of Geophysical Research: Atmospheres 118, 12,345–12,358. doi:10.1002/2013JD019976.

Koeniger, P., Marshall, J.D., Link, T., Mulch, A., 2011. An inexpensive, fast, and reliable method for vacuum extraction of soil and plant water for stable isotope analyses by mass spectrometry. Rapid Communications in Mass Spectrometry 25, 3041–3048. doi:10.1002/rcm.5198.

Kool, D., Agam, N., Lazarovitch, N., Heitman, J., Sauer, T., Ben-Gal, A., 2014. A review of approaches for evapotranspiration partitioning. Agricultural and Forest Meteorology 184, 56 – 70. doi:10.1016/j.agrformet.2013.09.003.

Koopmans, C., Tietema, A., Boxman, A., 1996. The fate of 15 n enriched throughfall in two coniferous forest stands at different nitrogen deposition levels. Biogeochemistry 34, 19–44. doi:10.1007/BF02182953.

Kottek, M., Grieser, J., Beck, C., Rudolf, B., Rubel, F., 2006. World map of the köppen-geiger climate classification updated. Meteorologische Zeitschrift 15, 259–263. doi:10.1127/0941-2948/2006/0130.

Kramer, I., Holscher, D., 2009. Rainfall partitioning along a tree diversity gradient in a deciduous old-growth forest in central germany. Ecohydrology 2, 102–114. doi:10.1002/eco.44.

Kumagai, T., 2011. Transpiration in Forest Ecosystems. Springer Netherlands, Dordrecht. pp. 389–406. doi:10.1007/978-94-007-1363-5_19.

Kumagai, T., Nagoya, H.K., Chappell, N., 2016. Tropical Forest Hydrology. CABI, UK. chapter 6. pp. 88–102.

Kumaran, M., 1998. Interlaboratory comparison of the astm standard test methods for water vapor transmission of materials (e 96-95). Journal of Testing and Evaluation 26, 83–88.

Kunert, N., Aparecido, L.M.T., Wolff, S., Higuchi, N., dos Santos, J., de Araujo, A.C., Trumbore, S., 2017. A revised hydrological model for the central amazon: The importance of emergent canopy trees in the forest water budget. Agricultural and Forest Meteorology 239, 47–57. doi:10.1016/j.agrformet.2017.03.002.

Kunert, N., Schwendenmann, L., Potvin, C., Holscher, D., 2012. Tree diversity enhances tree transpiration in a panamanian forest plantation. Journal of Applied Ecology 49, 135–144. doi:10.1093/treephys/3.4.309.

Kurita, N., Newman, B.D., Araguas-Araguas, L.J., Aggarwal, P., 2012. Evaluation of continuous water vapor δd and δ^{18}o measurements by off-axis integrated cavity output spectroscopy. Atmospheric Measurement Techniques 5, 2069–2080. doi:10.5194/amt-5-2069-2012.

Lamontagne, S., Cook, P.G., O'Grady, A., Eamus, D., 2005. Groundwater use by vegetation in a tropical savanna riparian zone (daly river, australia). Journal of Hydrology 310, 280–293. doi:10.1016/j.jhydrol.2005.01.009.

Landwehr, J., Coplen, T., 2004. Line-conditioned excess: a new method for characterizing stable hydrogen and oxygen isotope ratios in hydrologic systems. IAEA Vienna. pp. 132–135.

Lankreijer, H., Lundberg, A., Grelle, A., Lindroth, A., Seibert, J., 1999. Evaporation and storage of intercepted rain analysed by comparing two models applied to a boreal forest. Agricultural and Forest Meteorology 98-99, 595–604. URL: http://www.sciencedirect.com/science/article/pii/S0168192399001264, doi:10.1016/S0168-1923(99)00126-4.

Lauenroth, W.K., Bradford, J.B., 2006. Ecohydrology and the partitioning aet between transpiration and evaporation in a semiarid steppe. Ecosystems 9, 756–767. doi:10.1007/s10021-006-0063-8.

Lavers, D.A., Ralph, F.M., Waliser, D.E., Gershunov, A., Dettinger, M.D., 2015. Climate change intensification of horizontal water vapor transport in cmip5. Geophysical Research Letters 42, 5617–5625. doi:10.1002/2015GL064672.

Lawford, R., 1996. Some scientific questions and issues for the GEWEX Continental-scale International Project (GCIP) research community. pp. 162–167.

Lawley, M., 2010. Introduction. British Bryological Society Plymouth. pp. 1–4.

Lawrence, D.M., Thornton, P.E., Oleson, K.W., Bonan, G.B., 2007a. The partitioning of evapotranspiration into transpiration, soil evaporation, and canopy evaporation in a gcm: impacts on land–atmosphere interaction. Journal of Hydrometeorology 8, 862–880. doi:10.1175/JHM596.1.

Lawrence, D.M., Thornton, P.E., Oleson, K.W., Bonan, G.B., 2007b. The partitioning of evapotranspiration into transpiration, soil evaporation, and canopy evaporation in a gcm: Impacts on land–atmosphere interaction. Journal of Hydrometeorology 8, 862–880. doi:10.1175/JHM596.1.

Lee, J., Worden, J., Noone, D., Bowman, K., Eldering, A., LeGrande, A., Li, J.L.F., Schmidt, G., Sodemann, H., 2011. Relating tropical ocean clouds to moist processes using water vapor isotope measurements. Atmospheric Chemistry and Physics 11, 741–752. doi:10.5194/acp-11-741-2011.

Lee, X., Smith, R., Williams, J., 2006. Water vapour 18o/16o isotope ratio in surface air in new england, usa. Tellus B 58, 293–304. doi:10.1111/j.1600-0889.2006.00191.x.

Leibundgut, C., Seibert, J., 2011. 2.09. Tracer Hydrology. Elsevier. pp. 215–236.

Leiterer, R., Furrer, R., Schaepman, M.E., Morsdorf, F., 2015. Forest canopy-structure characterization: A data-driven approach. Forest Ecology and Management 358, 48–61. doi:10.1016/j.foreco.2015.09.003.

Leiva, J.A., Mata, R., Rocha, O.J., Gutiérrez Soto, M.V., 2009. Cronología de la regeneración del bosque tropical seco en santa rosa, guanacaste, costa rica. i. características edáficas. Revista de Biología Tropical 57, 801–815. doi:10.15517/RBT.V57I3.5495.

Leuschner, C., Ellenberg, H., 2017. Abiotic conditions, flora, ecosystem functions and recent human influence. Springer. pp. 119–347.

LGR, 2019. Los gatos research, inc. isotopic water analyzer (liquid+vapor) - enhanced performance. https://www.lgrinc.com/analyzers/isotope/isotopic-water-analyzer. Visited on: August 27, 2019.

Li, F., Song, X., Tang, C., Liu, C., Yu, J., Zhang, W., 2007. Tracing infiltration and recharge using stable isotope in taihang mt., north china. Environmental Geology 53, 687–696. doi:10.1007/s00254-007-0683-0.

Li, X., Xiao, Q., Niu, J., Dymond, S., McPherson, E.G., van Doorn, N., Yu, X., Xie, B., Zhang, K., Li, J., 2017. Rainfall interception by tree crown and leaf litter: An interactive process. Hydrological Processes 31, 3533–3542. doi:10.1002/hyp.11275.

Lichner, L., Eldridge, D., Schacht, K., Zhukova, N., Holko, L., Sir, M., Pecho, J., 2011. Grass cover influences hydrophysical parameters and heterogeneity of water flow in a sandy soil. Pedosphere 21, 719–729. doi:10.1016/S1002-0160(11)60175-6.

LiCOR, 2016. Li-cor inc.: Eddypro® version 6.2 [computer software].

Lieberman, D., Lieberman, M., 1987. Forest tree growth and dynamics at la selva, costa rica (1969-1982). Journal of Tropical Ecology 3, 347–358. doi:10.1017/S0266467400002327.

Lindroth, A., Mölder, M., Lagergren, F., 2010. Heat storage in forest biomass improves energy balance closure. Biogeosciences 7, 301–313. doi:10.5194/bg-7-301-2010.

Lion, M., Kosugi, Y., Takanashi, S., Noguchi, S., Itoh, M., Katsuyama, M., Matsuo, N., Shamsuddin, S.A., 2017. Evapotranspiration and water source of a tropical rainforest in peninsular malaysia. Hydrological Processes 31, 4338–4353. doi:10.1002/hyp.11360.

Liste, H.H., White, J.C., 2008. Plant hydraulic lift of soil water – implications for crop production and land restoration. Plant and Soil 313, 1–17. URL: 10.1007/s11104-008-9696-z, doi:10.1007/s11104-008-9696-z.

Littell, J.S., Peterson, D.L., Tjoelker, M., 2008. Douglas-fir growth in mountain ecosystems: Water limits tree growth from stand to region. Ecological Monographs 78, 349–368. URL: http://www.jstor.org/stable/27646139.

Liu, H., Foken, T., 2001. A modified bowen ratio method to determine sensible and latent heat fluxes. Meteorologische Zeitschrift 10, 71–80. doi:10.1127/0941-2948/2001/0010-0071.

Liu, S.M., Xu, Z.W., Wang, W.Z., Jia, Z.Z., Zhu, M.J., Bai, J., Wang, J.M., 2011. A comparison of eddy-covariance and large aperture scintillometer measurements with respect to the energy balance closure problem. Hydrology and Earth System Sciences 15, 1291–1306. doi:10.5194/hess-15-1291-2011.

Liu, W., Liu, W., Li, P., Duan, W., Li, H., 2010. Dry season water uptake by two dominant canopy tree species in a tropical seasonal rainforest of xishuangbanna, sw china. Agricultural and Forest Meteorology 150, 380–388. doi:10.1016/j.agrformet.2009.12.006.

Liu, W.J., Liu, W.Y., Li, J.T., Wu, Z.W., Li, H.M., 2008. Isotope variations of throughfall, stemflow and soil water in a tropical rain forest and a rubber plantation in Xishuangbanna, SW China. Hydrology Research 39, 437–449. doi:10.2166/nh.2008.110.

Liu, Y., Yu, G., Wang, Q., Zhang, Y., 2014. How temperature, precipitation and stand age control the biomass carbon density of global mature forests. Global Ecology and Biogeography 23, 323–333. doi:10.1111/geb.12113.

Livesley, S., Baudinette, B., Glover, D., 2014. Rainfall interception and stem flow by eucalypt street trees – the impacts of canopy density and bark type. Urban Forestry Urban Greening 13, 192–197. doi:10.1016/j.ufug.2013.09.001.

Lloyd, C., F., A.O.M., 1988. Spatial variability of throughfall and stemflow measurements in amazonian rainforest. Agricultural and Forest Meteorology 42, 63–73. doi:10.1016/0168-1923(88)90067-6.

Loescher, H., Gholz, H., Jacobs, J., Oberbauer, S., 2005. Energy dynamics and modeled evapotranspiration from a wet tropical forest in costa rica. Journal of Hydrology 315, 274–294. doi:10.1016/j.jhydrol.2005.03.040.

Loescher, H.W., Bentz, J.A., Oberbauer, S.F., Ghosh, T.K., Tompson, R.V., Loyalka, S.K., 2004. Characterization and dry deposition of carbonaceous aerosols in a wet tropical forest canopy. Journal of Geophysical Research: Atmospheres 109. doi:10.1029/2002JD003353.

van Loo, M., Dobrowolska, D., 2019. Chapter 2.2. Current situation. European Forest Institute. pp. 21–32. URL: https://www.efi.int/sites/default/files/files/publication-bank/2019/efi_wsctu9_2019.pdf.

Lorenzon, A.S.A., Dias, H.C.T., Leite, H.A.G., 2013. Precipitação efetiva e interceptação da chuva em um fragmento florestal com diferentes estágios de regeneração . Revista Árvore 37, 619 – 627. doi:10.1590/S0100-67622013000400005.

Lu, H.Y., 2014. Hydrochemistry and boron isotopes as natural tracers in the study of groundwaters from north chianan plain, taiwan. Isotopes in Environmental and Health Studies 50, 18–32. doi:10.1080/10256016.2013.821468.

Magliano, P.N., Giménez, R., Houspanossian, J., Páez, R.A., Nosetto, M.D., Fernández, R.J., Jobbágy, E.G., 2017. Litter is more effective than forest canopy reducing soil evaporation in dry chaco rangelands. Ecohydrology 10, e1879–n/a. doi:10.1002/eco.1879.

Mallick, K., Jarvis, A., Fisher, J.B., Tu, K.P., Boegh, E., Niyogi, D., 2013. Latent heat flux and canopy conductance based on penman–monteith, priestley–taylor equation, and bouchet's complementary hypothesis. Journal of Hydrometeorology 14, 419–442.

Mallick, K., Trebs, I., Boegh, E., Giustarini, L., Schlerf, M., Drewry, D.T., Hoffmann, L., von Randow, C., Kruijt, B., Araùjo, A., Saleska, S., Ehleringer, J.R., Domingues, T.F., Ometto, J.P.H.B., Nobre, A.D., de Moraes, O.L.L., Hayek, M., Munger, J.W., Wofsy, S.C., 2016. Canopy-scale biophysical controls of transpiration and evaporation in the amazon basin. Hydrology and Earth System Sciences 20, 4237–4264. doi:10.5194/hess-20-4237-2016.

Manoli, G., Domec, J.C., Novick, K., Oishi, A.C., Noormets, A., Marani, M., Katul, G., 2016. Soilâ€"plantâ€"atmosphere conditions regulating convective cloud formation above southeastern us pine plantations. Global Change Biology 22, 2238–2254. doi:10.1111/gcb.13221.

Martín-Gómez, P., Serrano, L., Ferrio, J.P., 2016. Short-term dynamics of evaporative enrichment of xylem water in woody stems: implications for ecohydrology. Tree Physiology 37, 511–522. doi:10.1093/treephys/tpw115.

Massman, W.J., Ibrom, A., 2008. Attenuation of concentration fluctuations of water vapor and other trace gases in turbulent tube flow. Atmospheric Chemistry and Physics 8, 6245–6259. doi:10.5194/acp-8-6245-2008.

Mauder, M., Foken, T., 2006. Impact of post-field data processing on eddy covariance flux estimates and energy balance closure. Meteorologische Zeitschrift 15, 597–609. doi:10.1127/0941-2948/2006/0167.

McNaughton, K.G., Black, T.A., 1973. A study of evapotranspiration from a douglas fir forest using the energy balance approach. Water Resources Research 9, 1579–1590. doi:10.1029/WR009i006p01579.

Meinzer, F.C., Brooks, J.R., Domec, J.C., Gartner, B.L., Warren, J.M., Woodruff, D.R., Bible, K., Shaw, D.C., 2006. Dynamics of water transport and storage in conifers studied with deuterium and heat tracing techniques. Plant, Cell and Environment 29, 105–114. doi:10.1111/j.1365-3040.2005.01404.x.

Midwood, A., Boutton, T., Archer, S., Watts, S., 1998. Water use by woody plants on contrasting soils in a savanna parkland: assessment with δ^2h and δ^{18}o. Plant and Soil 205, 13–24. doi:10.1023/A:1004355423241.

Miller, G.R., Chen, X., Rubin, Y., Ma, S., Baldocchi, D.D., 2010. Groundwater uptake by woody vegetation in a semiarid oak savanna. Water Resources Research 46. doi:10.1029/2009WR008902.

Miralles, D.G., De Jeu, R.A.M., Gash, J.H., Holmes, T.R.H., Dolman, A.J., 2011a. Magnitude and variability of land evaporation and its components at the global scale. Hydrology and Earth System Sciences 15, 967–981. doi:10.5194/hess-15-967-2011.

Miralles, D.G., Gash, J.H., Holmes, T.R.H., de Jeu, R.A.M., Dolman, A.J., 2010. Global canopy interception from satellite observations. Journal of Geophysical Research: Atmospheres 115. doi:10.1029/2009JD013530.

Miralles, D.G., Holmes, T.R.H., De Jeu, R.A.M., Gash, J.H., Meesters, A.G.C.A., Dolman, A.J., 2011b. Global land-surface evaporation estimated from satellite-based observations. Hydrology and Earth System Sciences 15, 453–469. URL: https://www.hydrol-earth-syst-sci.net/15/453/2011/, doi:10.5194/hess-15-453-2011.

Moore, G.W., Orozco, G., Aparecido, L.M., Miller, G.R., 2018. Upscaling transpiration in diverse forests: Insights from a tropical premontane site. Ecohydrology 11, e1920. doi:10.1002/eco.1920.

Moore, J.W., Semmens, B.X., 2008. Incorporating uncertainty and prior information into stable isotope mixing models. Ecology Letters 11, 470–480. doi:10.1111/j.1461-0248.2008.01163.x.

Mora, F., Martínez-Ramos, M., Ibarra-Manríquez, G., Pérez-Jiménez, A., Trilleras, J., Balvanera, P., 2015. Testing chronosequences through dynamic approaches: Time and site effects on tropical dry forest succession. Biotropica 47, 38–48. doi:10.1111/btp.12187.

Motley, G., Genney, D., Lawley, M., 2010. Thuidium tamariscinum, Key 336. British Bryological Society Plymouth. p. 696.

Murakami, S., 2006. A proposal for a new forest canopy interception mechanism: Splash droplet evaporation. Journal of Hydrology 319, 72 – 82. doi:10.1016/j.jhydrol.2005.07.002.

Murphy, P., Lugo, A., 1986. Ecology of tropical dry forest. Annual Review of Ecology and Systematics 17, 67–88. doi:10.1146/annurev.es.17.110186.000435.

Nadkarni, N.M., Parker, G.G., Rinker, H.B., Jarzen, D.M., 2004. CHAPTER 1 - The Nature of Forest Canopies. second edition ed.. Academic Press, San Diego. Physiological Ecology, pp. 3–23. doi:10.1016/B978-012457553-0/50005-8.

Nagler, P., Glenn, E., Kim, H., Emmerich, W., Scott, R., Huxman, T., Huete, A., 2007. Relationship between evapotranspiration and precipitation pulses in a semiarid rangeland estimated by moisture flux towers and modis vegetation indices. Journal of Arid Environments 70, 443 – 462. doi:10.1016/j.jaridenv.2006.12.026.

Naidu, M.T., Kumar, O.A., 2016. Tree diversity, stand structure, and community composition of tropical forests in eastern ghats of andhra pradesh, india. Journal of Asia-Pacific Biodiversity 9, 328 – 334. doi:10.1016/j.japb.2016.03.019.

Nakamura, A., Kitching, R.L., Cao, M., Creedy, T.J., Fayle, T.M., Freiberg, M., Hewitt, C., Itioka, T., Koh, L.P., Ma, K., Malhi, Y., Mitchell, A., Novotny, V., Ozanne, C.M., Song, L., Wang, H., Ashton, L.A., 2017. Forests and their canopies: Achievements and horizons in canopy science. Trends in Ecology Evolution 32, 438–451. doi:10.1016/j.tree.2017.02.020.

Nakshabandi, G.A., Kohnke, H., 1965. Thermal conductivity and diffusivity of soils as related to moisture tension and other physical properties. Agricultural Meteorology 2, 271–279. doi:10.1016/0002-1571(65)90013-0.

NCDC, 2012. NNDC climate data online. http://www7.ncdc.noaa.gov/CDO/cdoselect.cmd.

Nichols, D.S., Brown, J.M., 1980. Evaporation from a sphagnum moss surface. Journal of Hydrology 48, 289 – 302. doi:10.1016/0022-1694(80)90121-3.

Nie, Y.p., Chen, H.s., Wang, K.l., Tan, W., Deng, P.y., Yang, J., 2011. Seasonal water use patterns of woody species growing on the continuous dolostone outcrops and nearby thin soils in subtropical China. Plant and Soil 341, 399–412. doi:10.1007/s11104-010-0653-2.

Nielsen, J.M., Clare, E.L., Hayden, B., Brett, M.T., Kratina, P., 2018. Diet tracing in ecology: Method comparison and selection. Methods in Ecology and Evolution 9, 278–291. doi:10.1111/2041-210X.12869.

Niinemets, U., 2010. Responses of forest trees to single and multiple environmental stresses from seedlings to mature plants: Past stress history, stress interactions, tolerance and acclimation. Forest Ecology and Management 260, 1623 – 1639. doi:10.1016/j.foreco.2010.07.054.

North, M., Chen, J., Oakley, B., Song, B., Rudnicki, M., Gray, A., Innes, J., 2004. Forest Stand Structure and Pattern of Old-Growth Western Hemlock/Douglas-Fir and Mixed-Conifer Forests. Forest Science 50, 299–311. doi:10.1093/forestscience/50.3.299.

Noy-Meir, I., 1973. Desert ecosystems: Environment and producers. Annual Review of Ecology and Systematics 4, 25–51. doi:10.1146/annurev.es.04.110173.000325.

Ogle, K., Wolpert, R.L., Reynolds, J.F., 2004. Reconstructing plant root area and water uptake profiles. Ecology 85, 1967–1978. doi:10.1890/03-0346.

Oliveira-Freitas, J., Dias, H.C.T., Silva, E., Tonello, K.C., 2016. Net precipitation in a semideciduous forest fragment in Viçosa City, MG. Revista Árvore 40, 793–801. doi:10.1590/0100-67622016000500003.

Orlowski, N., Breuer, L., Angeli, N., Boeckx, P., Brumbt, C., Cook, C.S., Dubbert, M., Dyckmans, J., Gallagher, B., Gralher, B., Herbstritt, B., Hervé-Fernández, P., Hissler, C., Koeniger, P., Legout, A., Macdonald, C.J., Oyarzún, C., Redelstein, R., Seidler, C., Siegwolf, R., Stumpp, C., Thomsen, S., Weiler, M., Werner, C., McDonnell, J.J., 2018. Inter-laboratory comparison of cryogenic water extraction systems for stable isotope analysis of soil water. Hydrology and Earth System Sciences 22, 3619–3637. doi:10.5194/hess-22-3619-2018.

Orlowski, N., Pratt, D.L., McDonnell, J.J., 2016. Intercomparison of soil pore water extraction methods for stable isotope analysis. Hydrological Processes 30, 3434–3449. doi:10.1002/hyp.10870.

Orwa, C., Mutua, A., Kindt, R., Jamnadass, R., Anthony, S., 2009. Agroforestree-database: a tree reference and selection guide version 4.0. http://old.worldagroforestry.org/treedb/index.php.

Palacio, S., Montserrat-Martí, G., Ferrio, J.P., 2017. Water use segregation among plants with contrasting root depth and distribution along gypsum hills. Journal of Vegetation Science 28, 1107–1117. doi:10.1111/jvs.12570.

Pardini, M., Armston, J., Qi, W., Lee, S.K., Tello, M., Cazcarra Bes, V., Choi, C., Papathanassiou, K.P., Dubayah, R.O., Fatoyinbo, L.E., 2019. Early lessons on combining lidar and multi-baseline sar measurements for forest structure characterization. Surveys in Geophysics 40, 803–837. doi:10.1007/s10712-019-09553-9.

Parker, G.G., 1995. CHAPTER 4 - Structure and microclimate of forest Canopies. first edition ed.. Academic Press, San Diego. pp. 73–106.

Parnell, A.C., Inger, R., Bearhop, S., Jackson, A.L., 2010. Source partitioning using stable isotopes: coping with too much variation. PloS one 5, e9672. doi:10.1371/journal.pone.0009672.

Parnell, A.C., Phillips, D.L., Bearhop, S., Semmens, B.X., Ward, E.J., Moore, J.W., Jackson, A.L., Grey, J., Kelly, D.J., Inger, R., 2013. Bayesian stable isotope mixing models. Environmetrics 24, 387–399. doi:10.1002/env.2221.

Paternoster, R., Brame, R., Mazerolle, P., Piquero, A., 1998. Using the correct statistical test for the equality of regression coefficients. Criminology 36, 859–866. doi:10.1111/j.1745-9125.1998.tb01268.x.

Paul-Limoges, E., Wolf, S., Schneider, F.D., Longo, M., Moorcroft, P., Gharun, M., Damm, A., 2020. Partitioning evapotranspiration with concurrent eddy covariance measurements in a mixed forest. Agricultural and Forest Meteorology 280, 107786. doi:10.1016/j.agrformet.2019.107786.

Pecl, G.T., Araújo, M.B., Bell, J.D., Blanchard, J., Bonebrake, T.C., Chen, I.C., Clark, T.D., Colwell, R.K., Danielsen, F., Evengård, B., Falconi, L., Ferrier, S., Frusher, S., Garcia, R.A., Griffis, R.B., Hobday, A.J., Janion-Scheepers, C., Jarzyna, M.A.,

Jennings, S., Lenoir, J., Linnetved, H.I., Martin, V.Y., McCormack, P.C., McDonald, J., Mitchell, N.J., Mustonen, T., Pandolfi, J.M., Pettorelli, N., Popova, E., Robinson, S.A., Scheffers, B.R., Shaw, J.D., Sorte, C.J.B., Strugnell, J.M., Sunday, J.M., Tuanmu, M.N., Vergés, A., Villanueva, C., Wernberg, T., Wapstra, E., Williams, S.E., 2017. Biodiversity redistribution under climate change: Impacts on ecosystems and human well-being. Science 355. doi:10.1126/science.aai9214.

Peel, M.C., Finlayson, B.L., Mcmahon, T.A., 2007. Updated world map of the Köppen-Geiger climate classification. Hydrology and Earth System Sciences Discussions 4, 439–473. URL: https://hal.archives-ouvertes.fr/hal-00298818.

Peng, S.S., Piao, S., Zeng, Z., Ciais, P., Zhou, L., Li, L.Z.X., Myneni, R.B., Yin, Y., Zeng, H., 2014. Afforestation in china cools local land surface temperature. Proceedings of the National Academy of Sciences 111, 2915–2919. doi:10.1073/pnas.1315126111.

Peters, L.I., Yakir, D., 2010. A rapid method for the sampling of atmospheric water vapour for isotopic analysis. Rapid Communications in Mass Spectrometry 24, 103–108. doi:10.1002/rcm.4359.

Peters, T., 2016. Climatic types of water balances in the tropics. Tropical Forestry Handbook , 405–412.

Phillips, D.L., Gregg, J.W., 2003. Source partitioning using stable isotopes: coping with too many sources. Oecologia 136, 261–269. doi:10.1007/s00442-003-1218-3.

Phillips, D.L., Newsome, S.D., Gregg, J.W., 2005. Combining sources in stable isotope mixing models: alternative methods. Oecologia 144, 520–527. doi:10.1007/s00442-004-1816-8.

Pielke, R., 2013. Mesoscale Meteorological Modeling. International Geophysics, Elsevier Science. URL: https://books.google.nl/books?id=ExlFulltapcC.

Pons, E., Yrieix, B., Heymans, L., Dubelley, F., Planes, E., 2014. Permeation of water vapor through high performance laminates for vips and physical characterization of sorption and diffusion phenomena. Energy and Buildings 85, 604–616. doi:10.1016/j.enbuild.2014.08.032.

Poorter, L., Bongers, F., Aide, T.M., Almeyda Zambrano, A.M., Balvanera, P., Becknell, J.M., Boukili, V., Brancalion, P.H.S., Broadbent, E.N., Chazdon, R.L., Craven, D., de Almeida-Cortez, J.S., Cabral, G.A.L., de Jong, B.H.J., Denslow, J.S., Dent, D.H., DeWalt, S.J., Dupuy, J.M., Durán, S.M., Espírito-Santo, M.M., Fandino, M.C., César, R.G., Hall, J.S., Hernandez-Stefanoni, J.L., Jakovac, C.C., Junqueira, A.B., Kennard, D., Letcher, S.G., Licona, J.C., Lohbeck, M., Marín-Spiotta, E., Martínez-Ramos, M., Massoca, P., Meave, J.A., Mesquita, R., Mora, F., Muñoz, R., Muscarella, R., Nunes, Y.R.F., Ochoa-Gaona, S., de Oliveira, A.A., Orihuela-Belmonte,

E., Peña Claros, M., Pérez-García, E.A., Piotto, D., Powers, J.S., Rodríguez-Velázquez, J., Romero-Pérez, I.E., Ruíz, J., Saldarriaga, J.G., Sanchez-Azofeifa, A., Schwartz, N.B., Steininger, M.K., Swenson, N.G., Toledo, M., Uriarte, M., van Breugel, M., van der Wal, H., Veloso, M.D.M., Vester, H.F.M., Vicentini, A., Vieira, I.C.G., Bentos, T.V., Williamson, G.B., Rozendaal, D.M.A., 2016. Biomass resilience of neotropical secondary forests. Nature doi:10.1038/nature16512.

Poorter, L., van der Sande, M.T., Arets, E.J.M.M., Ascarrunz, N., Enquist, B.J., Finegan, B., Licona, J.C., Martínez-Ramos, M., Mazzei, L., Meave, J.A., Muñoz, R., Nytch, C.J., de Oliveira, A.A., Pérez-García, E.A., Prado-Junior, J., Rodríguez-Velázques, J., Ruschel, A.R., Salgado-Negret, B., Schiavini, I., Swenson, N.G., Tenorio, E.A., Thompson, J., Toledo, M., Uriarte, M., Hout, P.v.d., Zimmerman, J.K., Peña Claros, M., 2017. Biodiversity and climate determine the functioning of neotropical forests. Global Ecology and Biogeography 26, 1423–1434. doi:10.1111/geb.12668.

Poorter, L., van der Sande, M.T., Thompson, J., Arets, E.J.M.M., Alarcón, A., Álvarez-Sánchez, J., Ascarrunz, N., Balvanera, P., Barajas-Guzmán, G., Boit, A., Bongers, F., Carvalho, F.A., Casanoves, F., Cornejo-Tenorio, G., Costa, F.R.C., de Castilho, C.V., Duivenvoorden, J.F., Dutrieux, L.P., Enquist, B.J., Fernández-Méndez, F., Finegan, B., Gormley, L.H.L., Healey, J.R., Hoosbeek, M.R., Ibarra-Manríquez, G., Junqueira, A.B., Levis, C., Licona, J.C., Lisboa, L.S., Magnusson, W.E., Martínez-Ramos, M., Martínez-Yrizar, A., Martorano, L.G., Maskell, L.C., Mazzei, L., Meave, J.A., Mora, F., Muñoz, R., Nytch, C., Pansonato, M.P., Parr, T.W., Paz, H., Pérez-García, E.A., Rentería, L.Y., Rodríguez-Velazquez, J., Rozendaal, D.M.A., Ruschel, A.R., Sakschewski, B., Salgado-Negret, B., Schietti, J., Simões, M., Sinclair, F.L., Souza, P.F., Souza, F.C., Stropp, J., ter Steege, H., Swenson, N.G., Thonicke, K., Toledo, M., Uriarte, M., van der Hout, P., Walker, P., Zamora, N., Peña Claros, M., 2015. Diversity enhances carbon storage in tropical forests. Global Ecology and Biogeography 24, 1314–1328. doi:10.1111/geb.12364.

Porada, P., Van Stan, J.T., Kleidon, A., 2018. Significant contribution of non-vascular vegetation to global rainfall interception. Nature Geoscience 11, 563. doi:10.13031/2013.19812.

Portillo-Quintero, C., Sanchez-Azofeifa, A., Calvo-Alvarado, J., Quesada, M., do Espirito Santo, M.M., 2015. The role of tropical dry forests for biodiversity, carbon and water conservation in the neotropics: lessons learned and opportunities for its sustainable management. Regional Environmental Change 15, 1039–1049. doi:10.1007/s10113-014-0689-6.

Portillo-Quintero, C., Sánchez-Azofeifa, G., 2010. Extent and conservation of tropical dry forests in the americas. Biological Conservation 143, 144–155. doi:10.1016/j.biocon.2009.09.020.

Price, D., Black, T., 1990. Effects of short-term variation in weather on diurnal canopy co2 flux and evapotranspiration of a juvenile douglas-fir stand. Agricul-

tural and Forest Meteorology 50, 139 – 158. doi:10.1016/0168-1923(90)90050-G.

Price, J.S., 1991. Evaporation from a blanket bog in a foggy coastal environment. Boundary-Layer Meteorology 57, 391–406. doi:10.1007/BF00120056.

Price, J.S., Edwards, T.W., Yi, Y., Whittington, P.N., 2009. Physical and isotopic characterization of evaporation from sphagnum moss. Journal of Hydrology 369, 175 – 182. doi:10.1016/j.jhydrol.2009.02.044.

Prijono, S., Sukma, Y., 2015. The role of litter in rainwater interception. Current Journal of Applied Science and Technology 8, 567–575. doi:10.9734/BJAST/2015/17502.

Putman, A.L., Fiorella, R.P., Bowen, G.J., Cai, Z., 2019. A global perspective on local meteoric water lines: Meta-analytic insight into fundamental controls and practical constraints. Water Resources Research 55, 6896–6910. doi:10.1029/2019WR025181.

Pypker, T.G., Levia, D.F., Staelens, J., Van Stan, J.T., 2011. Canopy Structure in Relation to Hydrological and Biogeochemical Fluxes. Springer Netherlands, Dordrecht. pp. 371–388. doi:10.1007/978-94-007-1363-5_18.

Pypker, T.G., Unsworth, M.H., Van Stan, J.T., Bond, B.J., 2017. The absorption and evaporation of water vapor by epiphytes in an old-growth douglas-fir forest during the seasonal summer dry season: Implications for the canopy energy budget. Ecohydrology 10, e1801–n/a. doi:10.1002/eco.1801. e1801 ECO-16-0085.R1.

R Core Team, 2017. R: A Language and Environment for Statistical Computing. R Foundation for Statistical Computing. Vienna, Austria. URL: https://www.R-project.org/.

Raghunath, H.M., 2006. Hydrology: principles, analysis and design. New Age International.

Raich, J.W., 2017. Temporal variability of soil respiration in experimental tree plantations in lowland costa rica. Forests 8. doi:10.3390/f8020040.

Raj, R., Hamm, N.A., van der Tol, C., Stein, A., 2014. Variance-based sensitivity analysis of biome-bgc for gross and net primary production. Ecological modelling 292, 26–36.

Rambo, J., Lai, C.T., Farlin, J., Schroeder, M., Bible, K., 2011. On-site calibration for high precision measurements of water vapor isotope ratios using off-axis cavity-enhanced absorption spectroscopy. Journal of Atmospheric and Oceanic Technology 28, 1448–1457. doi:10.1175/JTECH-D-11-00053.1.

Raz-Yaseef, N., Rotenberg, E., Yakir, D., 2010. Effects of spatial variations in soil evaporation caused by tree shading on water flux partitioning in a semi-arid pine forest. Agricultural and Forest Meteorology 150, 454–462. doi:10.1016/j.agrformet.2010.01.010.

Read, R.G., 1968. Evaporative power in the tropical forest of the panama canal zone. Journal of Applied Meteorology 7, 417–424. doi:10.1175/1520-0450(1968)007<0417:EPITTF>2.0.CO;2.

Renninger, H.J., Phillips, N.G., 2016. Palm Physiology and Distribution in Response to Global Environmental Change. Springer International Publishing, Cham. pp. 67–101. doi:10.1007/978-3-319-27422-5_4.

Rice, K.C., Hornberger, G.M., 1998. Comparison of hydrochemical tracers to estimate source contributions to peak flow in a small, forested, headwater catchment. Water Resources Research 34, 1755–1766. doi:10.1029/98WR00917.

Roberts, J., 1999. Plants and water in forests and woodlands. Routledge. pp. 181–236.

da Rocha, H.R., Manzi, A.O., Cabral, O.M., Miller, S.D., Goulden, M.L., Saleska, S.R., R.-Coupe, N., Wofsy, S.C., Borma, L.S., Artaxo, P., Vourlitis, G., Nogueira, J.S., Cardoso, F.L., Nobre, A.D., Kruijt, B., Freitas, H.C., von Randow, C., Aguiar, R.G., Maia, J.F., 2009. Patterns of water and heat flux across a biome gradient from tropical forest to savanna in brazil. Journal of Geophysical Research: Biogeosciences 114. doi:10.1029/2007JG000640.

Roden, J.S., Ehleringer, J.R., 1999. Observations of hydrogen and oxygen isotopes in leaf water confirm the craig-gordon model under wide-ranging environmental conditions. Plant Physiology 120, 1165–1174. doi:10.1104/pp.120.4.1165.

Rodríguez-Ronderos, M.E., Bohrer, G., Sanchez-Azofeifa, A., Powers, J.S., Schnitzer, S.A., 2016. Contribution of lianas to plant area index and canopy structure in a panamanian forest. Ecology 97, 3271–3277. doi:10.1002/ecy.1597.

Rosa, I.M., Smith, M.J., Wearn, O.R., Purves, D., Ewers, R.M., 2016. The environmental legacy of modern tropical deforestation. Current Biology 26, 2161–2166. URL: http://www.sciencedirect.com/science/article/pii/S096098221630625X, doi:10.1016/j.cub.2016.06.013.

Rossatto, D.R., da Silveira Lobo Sternberg, L., Franco, A.C., 2012. The partitioning of water uptake between growth forms in a neotropical savanna: do herbs exploit a third water source niche? Plant Biology 15, 84–92. doi:10.1111/j.1438-8677.2012.00618.x.

Rothfuss, Y., Biron, P., Braud, I., Canale, L., Durand, J.L., Gaudet, J.P., Richard, P., Vauclin, M., Bariac, T., 2010. Partitioning evapotranspiration fluxes into soil evaporation and plant transpiration using water stable isotopes under controlled conditions. Hydrological Processes 24, 3177–3194. doi:10.1002/hyp.7743.

Rothfuss, Y., Javaux, M., 2017. Reviews and syntheses: Isotopic approaches to quantify root water uptake: a review and comparison of methods. Biogeosciences 14, 2199–2224. doi:10.5194/bg-14-2199-2017.

Roupsard, O., Bonnefond, J.M., Irvine, M., Berbigier, P., Nouvellon, Y., Dauzat, J., Taga, S., Hamel, O., Jourdan, C., Saint-André, L., Mialet-Serra, I., Labouisse, J.P., Epron, D., Joffre, R., Braconnier, S., Rouzière, A., Navarro, M., Bouillet, J.P., 2006. Partitioning energy and evapo-transpiration above and below a tropical palm canopy. Agricultural and Forest Meteorology 139, 252–268. doi:10.1016/j.agrformet.2006.07.006.

Rozanski, K., 2005. Isotopes in atmospheric moisture. Springer. pp. 291–302.

Rozanski, K., Araguás□Araguás, L., Gonfiantini, R., 1993. Isotopic Patterns in Modern Global Precipitation. American Geophysical Union (AGU). pp. 1–36. doi:10.1029/GM078p0001.

Sá, J.a.H.M., Chaffe, P.L.B., Quillet, M.J.J., 2016. The influence of the interception process on the precipitation quality in a catchment covered by subtropical Atlantic Forest. RBRH 21, 742–751. doi:10.1590/2318-0331.011616045.

Sadeghi, S.M.M., Van Stan, J.T., Pypker, T.G., Tamjidi, J., Friesen, J., Farahnaklangroudi, M., 2018. Importance of transitional leaf states in canopy rainfall partitioning dynamics. European Journal of Forest Research 137, 121–130. doi:10.1007/s10342-017-1098-4.

Saito, T., Matsuda, H., Komatsu, M., Xiang, Y., Takahashi, A., Shinohara, Y., Otsuki, K., 2013. Forest canopy interception loss exceeds wet canopy evaporation in japanese cypress (hinoki) and japanese cedar (sugi) plantations. Journal of Hydrology 507, 287 – 299. doi:10.1016/j.jhydrol.2013.09.053.

Salem, B., 1989. Arid zone forestry: a guide for field technicians. 20, Food and Agriculture Organization (FAO).

Salvador, M.M.S., KÃ, S., KÃ, J.M., Lennartz, B., Libardi, P.L., 2011. Dye tracer and morphophysical properties to observe water flow in a Gleyic Luvisol. Scientia Agricola 68, 160 – 166. doi:10.1590/S0103-90162011000200005.

Sánchez-Murillo, R., Esquivel-Hernández, G., Welsh, K., Brooks, E.S., Boll, J., Alfaro-Solís, R., Valdés-González, J., 2013. Spatial and temporal variation of stable isotopes in precipitation across costa rica: An analysis of historic gnip records. Open Journal of Modern Hydrology doi:10.4236/ojmh.2013.34027.

Sanford Jr., R.L., Paaby, P., Luvall, J.C., Phillips, E., 1994. Climate, geomorphology, and aquatic systems.. The University of Chicago Press. chapter 3. pp. 19–33.

Sato, Y., Kumagai, T., Kume, A., Otsuki, K., Ogawa, S., 2004. Experimental analysis of moisture dynamics of litter layers—the effects of rainfall conditions and leaf shapes. Hydrological Processes 18, 3007–3018. doi:10.1002/hyp.5746.

Sauer, T.J., Singer, J.W., Prueger, J.H., DeSutter, T.M., Hatfield, J.L., 2007. Radiation balance and evaporation partitioning in a narrow-row soybean canopy. Agricultural and Forest Meteorology 145, 206–214. doi:10.1016/j.agrformet.2007.04.015.

Savenije, H.H.G., 2004. The importance of interception and why we should delete the term evapotranspiration from our vocabulary. Hydrological Processes 18, 1507–1511. doi:10.1002/hyp.5563.

Saxton, K.E., Rawls, W.J., 2006. Soil water characteristic estimates by texture and organic matter for hydrologic solutions. Soil science society of America Journal 70, 1569–1578. doi:10.2136/sssaj2005.0117.

Scanlon, B.R., Keese, K.E., Flint, A.L., Flint, L.E., Gaye, C.B., Edmunds, W.M., Simmers, I., 2006. Global synthesis of groundwater recharge in semiarid and arid regions. Hydrological Processes 20, 3335–3370. doi:10.1002/hyp.6335.

Schaap, M., Bouten, W., 1997. Forest floor evaporation in a dense douglas fir stand. Journal of Hydrology 193, 97–113. doi:10.1016/S0022-1694(96)03201-5.

Schaap, M., Bouten, W., Verstraten, J., 1997. Forest floor water content dynamics in a douglas fir stand. Journal of Hydrology 201, 367–383. doi:10.1016/S0022-1694(97)00047-4.

Schellekens, J., Bruijnzeel, L.A., Scatena, F.N., Bink, N.J., Holwerda, F., 2000. Evaporation from a tropical rain forest, luquillo experimental forest, eastern puerto rico. Water Resources Research 36, 2183–2196. doi:10.1029/2000WR900074.

Schilperoort, B., Coenders-Gerrits, M., Luxemburg, W., Jiménez Rodríguez, C., Cisneros Vaca, C., Savenije, H., 2018. Technical note: Using distributed temperature sensing for bowen ratio evaporation measurements. Hydrology and Earth System Sciences 22, 819–830. doi:10.5194/hess-22-819-2018.

Schlesinger, W.H., Fonteyn, P.J., Marion, G.M., 1987. Soil moisture content and plant transpiration in the chihuahuan desert of new mexico. Journal of Arid Environments 12, 119–126. doi:10.1016/S0140-1963(18)31182-0.

Schlesinger, W.H., Jasechko, S., 2014. Transpiration in the global water cycle. Agricultural and Forest Meteorology 189-190, 115–117. doi:10.1016/j.agrformet.2014.01.011.

Schmid, M., Pautasso, M., Holdenrieder, O., 2014. Ecological consequences of douglas fir (pseudotsuga menziesii) cultivation in europe. European Journal of Forest Research 133, 13–29. doi:10.1007/s10342-013-0745-7.

Schumacher, J., Christiansen, J.R., 2015. Forest canopy water fluxes can be estimated using canopy structure metrics derived from airborne light detection and ranging (lidar). Agricultural and Forest Meteorology 203, 131–141. doi:10.1016/j.agrformet.2014.12.007.

Schwendenmann, L., Pendall, E., Sanchez-Bragado, R., Kunert, N., Holscher, D., 2015. Tree water uptake in a tropical plantation varying in tree diversity: interspecific differences, seasonal shifts and complementarity. Ecohydrology 8, 1–12. doi:10.1002/eco.1479.

Schwinning, S., Ehleringer, J.R., 2001. Water use trade-offs and optimal adaptations to pulse-driven arid ecosystems. Journal of Ecology 89, 464–480. doi:10.1046/j.1365-2745.2001.00576.x.

Schwinning, S., Sala, O.E., 2004. Hierarchy of responses to resource pulses in arid and semi-arid ecosystems. Oecologia 141, 211–220. doi:10.1007/s00442-004-1520-8.

Scott, R.L., Watts, C., Payan, J.G., Edwards, E., Goodrich, D.C., Williams, D., Shuttleworth, W.J., 2003. The understory and overstory partitioning of energy and water fluxes in an open canopy, semiarid woodland. Agricultural and Forest Meteorology 114, 127–139. doi:10.1016/S0168-1923(02)00197-1.

Sheppard, P., 1958. Transfer across the earth's surface and through the air above. Quarterly Journal of the Royal Meteorological Society 84, 205–224. doi:10.1002/qj.49708436102.

Shuttleworth, W., 1993. Evaporation. Mc-Graw Hill, Inc., New York. chapter 4. pp. 4.1–4.53.

Silva, B., Alava-Nunez, P., Strobl, S., Beck, E., Bendix, J., 2017. Area-wide evapotranspiration monitoring at the crown level of a tropical mountain rain forest. Remote Sensing of Environment 194, 219– 229. doi:10.1016/j.rse.2017.03.023.

Silvertown, J., 2004. Plant coexistence and the niche. Trends in Ecology Evolution 19, 605 – 611. doi:10.1016/j.tree.2004.09.003.

Silvertown, J., Araya, Y., Gowing, D., 2015. Hydrological niches in terrestrial plant communities: a review. Journal of Ecology 103, 93–108. doi:10.1111/1365-2745.12332.

de Simón, B.F., Sanz, M., Cervera, M.T., Pinto, E., Aranda, I., Cadahía, E., 2017. Leaf metabolic response to water deficit in pinus pinaster ait. relies upon ontogeny and genotype. Environmental and Experimental Botany 140, 41–55. doi:10.1016/j.envexpbot.2017.05.017.

Sioris, C.E., Malo, A., McLinden, C.A., D'Amours, R., 2016. Direct injection of water vapor into the stratosphere by volcanic eruptions. Geophysical Research Letters 43, 7694–7700. doi:10.1002/2016GL069918.

Sluijter, R., Leenaers, H., Camarasa, M., 2011. De Bosatlas van het klimaat. Noordhoff uitgevers.

Sollins, P., Sancho M., F., Mata Ch., R., Sanford Jr., R.L., 1994. Soils and soil process research. The University of Chicago Press. chapter 4. pp. 34–53.

Song, C., Wang, G., Liu, G., Mao, T., Sun, X., Chen, X., 2017. Stable isotope variations of precipitation and streamflow reveal the young water fraction of a permafrost watershed. Hydrological Processes 31, 935–947. doi:10.1002/hyp.11077.

Song, X., Wang, T., Xue, X., Yan, C., Li, S., 2015. Monitoring and analysis of aeolian desertification dynamics from 1975 to 2010 in the heihe river basin, northwestern china. Environmental Earth Sciences 74, 3123–3133. doi:10.1007/s12665-015-4350-6.

Song, X.P., Hansen, M.C., Stehman, S.V., Potapov, P.V., Tyukavina, A., Vermote, Eric F.and Townshend, J.R., 2018. Global land change from 1982 to 2016. Nature 560, 639–643. doi:10.1038/s41586-018-0411-9.

Soubie, R., Heinesch, B., Granier, A., Aubinet, M., Vincke, C., 2016. Evapotranspiration assessment of a mixed temperate forest by four methods: Eddy covariance, soil water budget, analytical and model. Agricultural and Forest Meteorology 228-229, 191–204. doi:10.1016/j.agrformet.2016.07.001.

Soulsby, C., Braun, H., Sprenger, M., Weiler, M., Tetzlaff, D., 2017. Influence of forest and shrub canopies on precipitation partitioning and isotopic signatures. Hydrological Processes 31, 4282–4296. doi:10.1002/hyp.11351.

Sparks, W.B., Richter, M., deWitt, C., Montiel, E., Russo, N.D., Grunsfeld, J.M., McGrath, M.A., Weaver, H., Hand, K.P., Bergeron, E., Reach, W., 2019. A search for water vapor plumes on europa using SOFIA. The Astrophysical Journal 871, L5. doi:10.3847/2041-8213/aafb0a.

Speed, M., Tetzlaff, D., Soulsby, C., Hrachowitz, M., Waldron, S., 2010. Isotopic and geochemical tracers reveal similarities in transit times in contrasting mesoscale catchments. Hydrological Processes 24, 1211–1224. doi:10.1002/hyp.7593.

Spellman, F.R., 2012. The Handbook of Meteorology. Scarecrow Press. URL: http://ebookcentral.proquest.com/lib/delft/detail.action?docID=1077405.

Spencer, S.A., van Meerveld, H.J., 2016. Double funnelling in a mature coastal british columbia forest: spatial patterns of stemflow after infiltration. Hydrological Processes 30, 4185–4201. doi:10.1002/hyp.10936.

Spieksma, J., Moors, E., Dolman, A., Schouwenaars, J., 1997. Modelling evaporation from a drained and rewetted peatland. Journal of Hydrology 199, 252–271. doi:10.1016/S0022-1694(96)03337-9.

Spittlehouse, D.L., Black, T.A., 1981. A growing season water balance model applied to two douglas fir stands. Water Resources Research 17, 1651–1656. doi:10.1029/WR017i006p01651.

Sprenger, M., Leistert, H., Gimbel, K., Weiler, M., 2016. Illuminating hydrological processes at the soil-vegetation-atmosphere interface with water stable isotopes. Reviews of Geophysics 54, 674–704. doi:10.1002/2015RG000515.

Sprenger, M., Stumpp, C., Weiler, M., Aeschbach, W., Allen, S.T., Benettin, P., Dubbert, M., Hartmann, A., Hrachowitz, M., Kirchner, J.W., McDonnell, J.J., Orlowski, N., Penna, D., Pfahl, S., Rinderer, M., Rodriguez, N., Schmidt, M., Werner, C., 2019. The demographics of water: A review of water ages in the critical zone. Reviews of Geophysics 57, 800–834. doi:10.1029/2018RG000633.

Sprenger, M., Tetzlaff, D., Soulsby, C., 2017a. Soil water stable isotopes reveal evaporation dynamics at the soil–plant–atmosphere interface of the critical zone. Hydrology and Earth System Sciences 21, 3839–3858. doi:10.5194/hess-21-3839-2017.

Sprenger, M., Tetzlaff, D., Soulsby, C., 2017b. Soil water stable isotopes reveal evaporation dynamics at the soil–plant–atmosphere interface of the critical zone. Hydrology and Earth System Sciences 21, 3839–3858. doi:10.5194/hess-21-3839-2017.

Staelens, J., De Schrijver, A., Verheyen, K., Verhoest, N.E.C., 2008. Rainfall partitioning into throughfall, stemflow, and interception within a single beech (fagus sylvatica l.) canopy: influence of foliation, rain event characteristics, and meteorology. Hydrological Processes 22, 33–45. doi:10.1002/hyp.6610.

Staff, S.S., 2014. Keys to Soil Taxonomy. Twelfth ed., USDA - Natural Resources Conservation Service.

Steen-Larsen, H.C., Johnsen, S.J., Masson-Delmotte, V., Stenni, B., Risi, C., Sodemann, H., Balslev-Clausen, D., Blunier, T., Dahl-Jensen, D., Ellehøj, M.D., Falourd, S., Grindsted, A., Gkinis, V., Jouzel, J., Popp, T., Sheldon, S., Simonsen, S.B., Sjolte, J., Steffensen, J.P., Sperlich, P., Sveinbjörnsdottir, A.E., Vinther, B.M., White, J.W.C., 2013. Continuous monitoring of summer surface water vapor isotopic composition above the greenland ice sheet. Atmospheric Chemistry and Physics 13, 4815–4828. doi:10.5194/acp-13-4815-2013.

Steen-Larsen, H.C., Sveinbjörnsdottir, A.E., Jonsson, T., F., R., Bonne, J.L., Masson-Delmotte, V., Sodemann, H., Blunier, T., Dahl-Jensen, D., Vinther, B.M., 2015. Moisture sources and synoptic to seasonal variability of north atlantic water vapor isotopic composition. Journal of Geophysical Research: Atmospheres 120, 5757–5774. doi:10.1002/2015JD023234.

Steen-Larsen, H.C., Sveinbjörnsdottir, A.E., Peters, A.J., Masson-Delmotte, V., Guishard, M.P., Hsiao, G., Jouzel, J., Noone, D., Warren, J.K., White, J.W.C., 2014. Climatic controls on water vapor deuterium excess in the marine boundary layer of the north atlantic based on 500 days of in situ, continuous measurements. Atmospheric Chemistry and Physics 14, 7741–7756. doi:10.5194/acp-14-7741-2014.

Strong, M., Sharp, Z.D., Gutzler, D.S., 2007. Diagnosing moisture transport using d/h ratios of water vapor. Geophysical Research Letters 34. doi:10.1029/2006GL028307.

Stull, R.B., 1988. An introduction to boundary layer meteorology. volume 4. 1 ed., Springer Netherlands, Dordrecht. doi:10.1007/978-94-009-3027-8.

Stull, R.B., 2016. Practical meteorology: an algebra based survey of atmospheric science. BC Campus. URL: http://www.eos.ubc.ca/books/Practical_Meteorology/.

Sulman, B.N., Roman, D.T., Scanlon, T.M., Wang, L., Novick, K.A., 2016. Comparing methods for partitioning a decade of carbon dioxide and water vapor fluxes in a temperate forest. Agricultural and Forest Meteorology 226-227, 229–245. doi:10.1016/j.agrformet.2016.06.002.

Summerfield, M., 1991. Global Geomorphology. Longman.

Sun, G., Domec, J., Amatya, D., 2016. Forest Evapotranspiration: Measurement and Modelling at Multiple Scales. CABI, UK. chapter 3. pp. 88–102. doi:10.1079/9781780646602.0032.

Sun, S., Meng, P., Zhang, J., Wan, X., Zheng, N., He, C., 2014. Partitioning oak woodland evapotranspiration in the rocky mountainous area of north china was disturbed by foreign vapor, as estimated based on non-steady-state 18o isotopic composition. Agricultural and Forest Meteorology 184, 36–47. doi:10.1016/j.agrformet.2013.08.006.

Sutanto, S.J., Wenninger, J., Coenders-Gerrits, A.M.J., Uhlenbrook, S., 2012. Partitioning of evaporation into transpiration, soil evaporation and interception: a comparison between isotope measurements and a hydrus-1d model. Hydrology and Earth System Sciences 16, 2605–2616. doi:10.5194/hess-16-2605-2012.

Swaffer, B.A., Holland, K.L., Doody, T.M., Li, C., Hutson, J., 2013. Water use strategies of two co-occurring tree species in a semi–arid karst environment. Hydrological Processes 28, 2003–2017. doi:10.1002/hyp.9739.

Tamkevičiūtė, M., Edvardsson, J., Pukienė, R., Taminskas, J., Stoffel, M., Corona, C., Kibirkštis, G., 2018. Scots pine (pinus sylvestris l.) based reconstruction of 130 years of water table fluctuations in a peatland and its relevance for moisture variability assessments. Journal of Hydrology 558, 509–519. doi:10.1016/j.jhydrol.2018.01.067.

Tan, Z.H., Cao, M., Yu, G.R., Tang, J.W., Deng, X.B., Song, Q.H., Tang, Y., Zheng, Z., Liu, W.J., Feng, Z.L., Deng, Y., Zhang, J.L., Liang, N., Zhang, Y.P., 2013. High sensitivity of a tropical rainforest to water variability: Evidence from 10 years of inventory and eddy flux data. Journal of Geophysical Research: Atmospheres 118, 9393–9400. doi:10.1002/jgrd.50675.

Tang, H., Armston, J., Hancock, S., Marselis, S., Goetz, S., Dubayah, R., 2019. Characterizing global forest canopy cover distribution using spaceborne lidar. Remote Sensing of Environment 231, 111262. doi:10.1016/j.rse.2019.111262.

Tang, H., Dubayah, R., Swatantran, A., Hofton, M., Sheldon, S., Clark, D.B., Blair, B., 2012. Retrieval of vertical lai profiles over tropical rain forests using waveform lidar at la selva, costa rica. Remote Sensing of Environment 124, 242 – 250. doi:10.1016/j.rse.2012.05.005.

Thornthwaite, C.W., 1948. An approach toward a rational classification of climate. Geographical Review 38, 55–94. doi:10.2307/210739.

Tietema, A., Mol-Dijkstra, J., Kros, J., Vries, W., et al., 2002. Dynamic nitrogen deposition thresholds during forest stand development in a douglas fir forest analysed with two nitrogen models smart2 and merlin. Hydrology and Earth System Sciences 6, 375–382. URL: https://hal.archives-ouvertes.fr/hal-00304698/.

Tiktak, A., Bouten, W., 1994. Soil water dynamics and long-term water balances of a douglas fir stand in the netherlands. Journal of Hydrology 156, 265–283. doi:10.1016/0022-1694(94)90081-7.

Tobón Marin, C., Bouten, W., Sevink, J., 2000. Gross rainfall and its partitioning into throughfall, stemflow and evaporation of intercepted water in four forest ecosystems in western amazonia. Journal of Hydrology 237, 40–57. doi:10.1016/S0022-1694(00)00301-2.

Tock, R.W., 1983. Permeabilities and water vapor transmission rates for commercial polymer films. Advances in Polymer Technology 3, 223–231. doi:10.1002/adv.1983.060030304.

Troch, P.A., Martinez, G.F., Pauwels, V.R.N., Durcik, M., Sivapalan, M., Harman, C., Brooks, P.D., Gupta, H., Huxman, T., 2009. Climate and vegetation water use efficiency at catchment scales. Hydrological Processes 23, 2409–2414. doi:10.1002/hyp.7358.

Trzeciak, T.M., Garcia-Carreras, L., Marsham, J.H., 2017. Cross-saharan transport of water vapor via recycled cold pool outflows from moist convection. Geophysical Research Letters 44, 1554–1563. doi:10.1002/2016GL072108.

Tukey, J.W., 1949. Comparing individual means in the analysis of variance. Biometrics , 99–114.

Tymen, B., Vincent, G., Courtois, E.A., Heurtebize, J., Dauzat, J., Marechaux, I., Chave, J., 2017. Quantifying micro-environmental variation in tropical rainforest understory at landscape scale by combining airborne lidar scanning and a sensor network. Annals of Forest Science 74, 32. doi:10.1007/s13595-017-0628-z.

Tyree, M.T., 2003. Hydraulic limits on tree performance: transpiration, carbon gain and growth of trees. Trees 17, 95–100. doi:10.1007/s00468-002-0227-x.

Ukil, A., Braendle, H., Krippner, P., 2012. Distributed temperature sensing: Review of technology and applications. IEEE Sensors Journal 12, 885–892. doi:10.1109/JSEN.2011.2162060.

Ukkola, A.M., Pitman, A.J., Decker, M., De Kauwe, M.G., Abramowitz, G., Kala, J., Wang, Y.P., 2016. Modelling evapotranspiration during precipitation deficits: identifying critical processes in a land surface model. Hydrology and Earth System Sciences 20, 2403–2419. doi:10.5194/hess-20-2403-2016.

Unsworth, M.H., Phillips, N., Link, T., Bond, B.J., Falk, M., Harmon, M.E., Hinckley, T.M., Marks, D., Paw U, K.T., 2004. Components and controls of water flux in an old-growth douglas-fir–western hemlock ecosystem. Ecosystems 7, 468–481. doi:10.1007/s10021-004-0138-3.

Van Bavel, C., Hillel, D., 1976. Calculating potential and actual evaporation from a bare soil surface by simulation of concurrent flow of water and heat. Agricultural Meteorology 17, 453–476. doi:10.1016/0002-1571(76)90022-4.

Van Wijk, M., Dekker, S., Bouten, W., Kohsiek, W., Mohren, G., 2001. Simulation of carbon and water budgets of a douglas-fir forest. Forest Ecology and Management 145, 229–241. doi:10.1016/S0378-1127(00)00439-4.

Vargas, A.I., Schaffer, B., Yuhong, L., Sternberg, L.d.S.L., 2017. Testing plant use of mobile vs immobile soil water sources using stable isotope experiments. New Phytologist 215, 582–594. doi:10.1111/nph.14616.

Vendramini, P.F., Sternberg, L.d.S.L., 2007. A faster plant stem-water extraction method. Rapid Communications in Mass Spectrometry 21, 164–168. doi:10.1002/rcm.2826.

Visser, A., Broers, H.P., Purtschert, R., Sultenfuß, J., de Jonge, M., 2013. Groundwater age distributions at a public drinking water supply well field derived from multiple age tracers (85kr, 3h/3he, and 39ar). Water Resources Research 49, 7778–7796. doi:10.1002/2013WR014012.

Vogt, T., Hoehn, E., Schneider, P., Freund, A., Schirmer, M., Cirpka, O.A., 2010. Fluctuations of electrical conductivity as a natural tracer for bank filtration in a losing stream. Advances in Water Resources 33, 1296–1308. doi:10.1016/j.advwatres.2010.02.007.

Volkmann, T.H.M., Haberer, K., Gessler, A., Weiler, M., 2016. High-resolution isotope measurements resolve rapid ecohydrological dynamics at the soil–plant interface. New Phytologist 210, 839–849. doi:10.1111/nph.13868.

Volkov, I., Banavar, J.R., He, F., Hubbell, S.P., Maritan, A., 2005. Density dependence explains tree species abundance and diversity in tropical forests. Nature 438, 658.

Voltas, J., Lucabaugh, D., Chambel, M.R., Ferrio, J.P., 2015. Intraspecific variation in the use of water sources by the circum-mediterranean conifer pinus halepensis. New Phytologist 208, 1031–1041. doi:10.1111/nph.13569.

de Vries, J., 2007. Groundwater. The name of the publisher. pp. 295–315.

Wainwright, J., Mulligan, M., Thornes, J., 1999. Plants and water in drylands. Routledge. pp. 78–126.

Walker, B.H., Langridge, J.L., 1996. Modelling plant and soil water dynamics in semi-arid ecosystems with limited site data. Ecological Modelling 87, 153 – 167. doi:10.1016/0304-3800(95)00024-0.

Wallace, J., 1995. Calculating evaporation: resistance to factors. Agricultural and Forest Meteorology 73, 353–366. doi:10.1016/0168-1923(94)05084-J.

Wang, H., Tetzlaff, D., Dick, J.J., Soulsby, C., 2017. Assessing the environmental controls on scots pine transpiration and the implications for water partitioning in a boreal headwater catchment. Agricultural and Forest Meteorology 240, 58–66.

Wang, J., Krejci, R., Giangrande, S., Kuang, C., Barbosa, H.M.J., Brito, J., Carbone, S., Chi, X., Comstock, J., Ditas, F., Lavric, J., Manninen, H.E., Mei, F., Moran-Zuloaga, D., Pohlker, C., Pohlker, M.L., Saturno, J., Schmid, B., Souza, R.A.F., Springston, S.R., Tomlinson, J.M., Toto, T., Walter, D., Wimmer, D., Smith, J.N., Kulmala, M., Machado, L.A.T., Artaxo, P., Andreae, M.O., Petaja, T., Martin, S.T., 2016. Amazon boundary layer aerosol concentration sustained by vertical transport during rainfall. Nature 539. doi:10.1038/nature19819.

Wang, L., Good, S.P., Caylor, K.K., 2014. Global synthesis of vegetation control on evapotranspiration partitioning. Geophysical Research Letters 41, 6753–6757. doi:10.1002/2014GL061439. 2014GL061439.

Wang, L., Niu, S., Good, S.P., Soderberg, K., McCabe, M.F., Sherry, R.A., Luo, Y., Zhou, X., Xia, J., Caylor, K.K., 2013. The effect of warming on grassland evapotranspiration partitioning using laser-based isotope monitoring techniques. Geochimica et Cosmochimica Acta 111, 28 – 38. doi:10.1016/j.gca.2012.12.047. hydrogen Isotopes.

Wang, P., Song, X., Han, D., Zhang, Y., Liu, X., 2010. A study of root water uptake of crops indicated by hydrogen and oxygen stable isotopes: A case in shanxi province, china. Agricultural Water Management 97, 475–482. doi:10.1016/j.agwat.2009.11.008.

Wang, P.K., 2003. Moisture plumes above thunderstorm anvils and their contributions to cross-tropopause transport of water vapor in midlatitudes. Journal of Geophysical Research: Atmospheres 108. doi:10.1029/2002JD002581.

Wang, X.F., Yakir, D., 2000. Using stable isotopes of water in evapotranspiration studies. Hydrological Processes 14, 1407–1421. doi:10.1002/1099-1085(20000615)14:8<1407::AID-HYP992>3.0.CO;2-K.

Wang, Z., Chang, Y., 1980. *Salix psammophila*. Bulletin of Botanical Laboratory of North-Eastern Forestry Institute. Harbin 9. URL: http://www.efloras.org/florataxon.aspx?flora_id=2&taxon_id=200005972.

Wassenaar, L., Hendry, M., Chostner, V., Lis, G., 2008. High resolution pore water delta2h and delta18o measurements by h2o(liquid)–h2o(vapor) equilibration laser spectroscopy. Environmental Science & Technology 42, 9262–9267. doi:10.1021/es802065s.

Wassenaar, L.I., Ahmad, M., Aggarwal, P., van Duren, M., Poltenstein, L., Araguas, L., Kurttas, T., 2012. Worldwide proficiency test for routine analysis of δ2h and δ18o in water by isotope-ratio mass spectrometry and laser absorption spectroscopy. Rapid Communications in Mass Spectrometry 26, 1641–1648. doi:10.1002/rcm.6270.

Webster, P.J., 1994. The role of hydrological processes in ocean-atmosphere interactions. Reviews of Geophysics 32, 427–476. doi:10.1029/94RG01873.

Wei, L., Lockington, D.A., Poh, S.C., Gasparon, M., Lovelock, C.E., 2013. Water use patterns of estuarine vegetation in a tidal creek system. Oecologia 172, 485–494. doi:10.1007/s00442-012-2495-5.

Wei, Z., Yoshimura, K., Okazaki, A., Kim, W., Liu, Z., Yokoi, M., 2015. Partitioning of evapotranspiration using high-frequency water vapor isotopic measurement over a rice paddy field. Water Resources Research 51, 3716–3729. doi:10.1002/2014WR016737.

Wen, X., Yang, B., Sun, X., Lee, X., 2016. Evapotranspiration partitioning through in-situ oxygen isotope measurements in an oasis cropland. Agricultural and Forest Meteorology 230-231, 89 – 96. doi:10.1016/j.agrformet.2015.12.003. oasis-desert system.

Wenninger, J., Beza, D.T., Uhlenbrook, S., 2010. Experimental investigations of water fluxes within the soil–vegetation–atmosphere system: Stable isotope mass-balance approach to partition evaporation and transpiration. Physics and Chemistry of the Earth, Parts A/B/C 35, 565–570. doi:10.1016/j.pce.2010.07.016.

West, A.G., Patrickson, S.J., Ehleringer, J.R., 2006a. Water extraction times for plant and soil materials used in stable isotope analysis. Rapid Communications in Mass Spectrometry 20, 1317–1321. doi:10.1002/rcm.2456.

West, J.B., Bowen, G.J., Cerling, T.E., Ehleringer, J.R., 2006b. Stable isotopes as one of nature's ecological recorders. Trends in Ecology Evolution 21, 408–414. doi:10.1016/j.tree.2006.04.002. twenty years of TREE - part 2.

Whitehead, D., Kelliher, F.M., Lane, P.M., Pollock, D.S., 1994. Seasonal partitioning of evaporation between trees and understory in a widely spaced pinus radiata stand. Journal of Applied Ecology 31, 528–542. URL: http://www.jstor.org/stable/2404448.

Wild, M., Folini, D., Hakuba, M.Z., Schär, C., Seneviratne, S.I., Kato, S., Rutan, D., Ammann, C., Wood, E.F., König-Langlo, G., 2015. The energy balance over land

and oceans: an assessment based on direct observations and cmip5 climate models. Climate Dynamics 44, 3393–3429. doi:10.1007/s00382-014-2430-z.

Williams, D., Cable, W., Hultine, K., Hoedjes, J., Yepez, E., Simonneaux, V., Er-Raki, S., Boulet, G., de Bruin, H., Chehbouni, A., Hartogensis, O., Timouk, F., 2004. Evapotranspiration components determined by stable isotope, sap flow and eddy covariance techniques. Agricultural and Forest Meteorology 125, 241 – 258. doi:10.1016/j.agrformet.2004.04.008.

Wilson, K.B., Hanson, P.J., Baldocchi, D.D., 2000. Factors controlling evaporation and energy partitioning beneath a deciduous forest over an annual cycle. Agricultural and Forest Meteorology 102, 83–103. doi:10.1016/S0168-1923(00)00124-6.

Winter, S., Höfler, J., Michel, A.K., Böck, A., Ankerst, D.P., 2015. Association of tree and plot characteristics with microhabitat formation in european beech and douglas-fir forests. European Journal of Forest Research 134, 335–347. doi:10.1007/s10342-014-0855-x.

Woodruff, D.R., McCulloh, K.A., Warren, J.M., Meinzer, F.C., Lachenbruch, B., 2007. Impacts of tree height on leaf hydraulic architecture and stomatal control in douglas-fir. Plant, Cell & Environment 30, 559–569. doi:10.1111/j.1365-3040.2007.01652.x.

Wright, J.S., Fu, R., Worden, J.R., Chakraborty, S., Clinton, N.E., Risi, C., Sun, Y., Yin, L., 2017. Rainforest-initiated wet season onset over the southern amazon. Proceedings of the National Academy of Sciences 114, 8481–8486. doi:10.1073/pnas.1621516114.

Xiao, W., Wei, Z., Wen, X., 2018. Evapotranspiration partitioning at the ecosystem scale using the stable isotope method—a review. Agricultural and Forest Meteorology 263, 346–361. doi:10.1016/j.agrformet.2018.09.005.

Xiao, X., Sauer, T., Singer, J., Horton, R., Ren, T., Heitman, J., 2016. Partitioning evaporation and transpiration in a maize field using heat-pulse sensors for evaporation measurement 59, 591–599. doi:10.13031/trans.59.11059.

Yakir, D., Sternberg, L.d.S.L., 2000. The use of stable isotopes to study ecosystem gas exchange. Oecologia 123, 297–311. doi:10.1007/s004420051016.

Yamanaka, T., Shimizu, R., 2007. Spatial distribution of deuterium in atmospheric water vapor: Diagnosing sources and the mixing of atmospheric moisture. Geochimica et Cosmochimica Acta 71, 3162–3169. doi:10.1016/j.gca.2007.04.014.

Yan, C., Qiu, G., 2016. The three-temperature model to estimate evapotranspiration and its partitioning at multiple scales: A review. Transactions of the ASABE 59, 661–670.

Yang, X., Zhang, K., Jia, b., Ci, L., 2005. Desertification assessment in china: An overview. Journal of Arid Environments 63, 517–531. doi:10.1016/j.jaridenv.2005.03.032.

Yang, Z., Zhou, Y., Wenninger, J., Uhlenbrook, S., 2012. The causes of flow regime shifts in the semi-arid hailiutu river, northwest china. Hydrology and Earth System Sciences 16, 87–103. doi:10.5194/hess-16-87-2012.

Yaseef, N.R., Yakir, D., Rotenberg, E., Schiller, G., Cohen, S., 2009. Ecohydrology of a semi-arid forest: partitioning among water balance components and its implications for predicted precipitation changes. Ecohydrology 3, 143–154. doi:10.1002/eco.65.

Yepez, E.A., Huxman, T.E., Ignace, D.D., English, N.B., Weltzin, J.F., Castellanos, A.E., Williams, D.G., 2005. Dynamics of transpiration and evaporation following a moisture pulse in semiarid grassland: A chamber-based isotope method for partitioning flux components. Agricultural and Forest Meteorology 132, 359–376. doi:10.1016/j.agrformet.2005.09.006.

Yepez, E.A., Williams, D.G., Scott, R.L., Lin, G., 2003. Partitioning overstory and understory evapotranspiration in a semiarid savanna woodland from the isotopic composition of water vapor. Agricultural and Forest Meteorology 119, 53–68. doi:10.1016/S0168-1923(03)00116-3.

Yin, L., Zhou, Y., Huang, J., Wenninger, J., Hou, G., Zhang, E., Wang, X., Dong, J., Zhang, J., Uhlenbrook, S., 2014. Dynamics of willow tree (salix matsudana) water use and its response to environmental factors in the semi-arid hailiutu river catchment, northwest china. Environmental Earth Sciences 71, 4997–5006. doi:10.1007/s12665-013-2891-0.

Young, A., 1989. Agroforestry for soil conservation. CAB International.

Young, E.D., Galyand, A., Nagahara, H., 2002. Kinetic and equilibrium mass-dependent isotope fractionation laws in nature and their geochemical and cosmochemical significance. Geochimica et Cosmochimica Acta 66, 1095 – 1104. doi:10.1016/S0016-7037(01)00832-8.

Zhang, J., Zhang, S., Zhang, W., Liu, B., Gong, C., Jiang, M., Lv, X., Sheng, L., 2017. Partitioning daily evapotranspiration from a marsh wetland using stable isotopes in a semiarid region. Hydrology Research 49, 1005–1015. doi:10.2166/nh.2017.005.

Zhang, S., Wen, X., Wang, J., Yu, G., Sun, X., 2010. The use of stable isotopes to partition evapotranspiration fluxes into evaporation and transpiration. Acta Ecologica Sinica 30, 201–209. doi:10.1016/j.chnaes.2010.06.003.

feng Zhang, Y., ping Wang, X., Hu, R., xia Pan, Y., Paradeloc, M., 2015. Rainfall partitioning into throughfall, stemflow and interception loss by two xerophytic shrubs within a rain-fed re-vegetated desert ecosystem, northwestern china. Journal of Hydrology 527, 1084–1095. doi:10.1016/j.jhydrol.2015.05.060.

Zhang, Y., Yu, X., Chen, L., Jia, G., 2018. Comparison of the partitioning of evapotranspiration–numerical modeling with different isotopic models using various kinetic fractionation coefficients. Plant and Soil 430, 307–328. doi:10.1007/s11104-018-3737-z.

Zhao, L., Wang, L., Cernusak, L.A., Liu, X., Xiao, H., Zhou, M., Zhang, S., 2016. Significant difference in hydrogen isotope composition between xylem and tissue water in populus euphratica. Plant, Cell & Environment 39, 1848–1857. doi:10.1111/pce.12753.

Zhao, P., Li, S., Li, F., Du, T., Tong, L., Kang, S., 2015. Comparison of dual crop coefficient method and shuttleworth–wallace model in evapotranspiration partitioning in a vineyard of northwest china. Agricultural Water Management 160, 41–56. doi:10.1016/j.agwat.2015.06.026.

Zhou, Y., Wenninger, J., Yang, Z., Yin, L., Huang, J., Hou, L., Wang, X., Zhang, D., Uhlenbrook, S., 2013. Groundwater–surface water interactions, vegetation dependencies and implications for water resources management in the semi-arid hailiutu river catchment, china ndash; a synthesis. Hydrology and Earth System Sciences 17, 2435–2447. doi:10.5194/hess-17-2435-2013.

Zhu, J., Sun, D., Young, M.H., Caldwell, T.G., Pan, F., 2015. Shrub spatial organization and partitioning of evaporation and transpiration in arid environments. Ecohydrology 8, 1218–1228. doi:10.1002/eco.1576.

Zimmermann, B., Zimmermann, A., Scheckenbach, H.L., Schmid, T., Hall, J.S., van Breugel, M., 2013. Changes in rainfall interception along a secondary forest succession gradient in lowland panama. Hydrology and Earth System Sciences 17, 4659–4670. doi:10.5194/hess-17-4659-2013.

Zotz, G., 2016. The Role of Vascular Epiphytes in the Ecosystem. Springer International Publishing, Cham. pp. 229–243. doi:10.1007/978-3-319-39237-0_9.

Acknowledgements

Almost five years have passed since I arrived in Delft to start the Ph.D. This has been a long bumpy road, with a magnificent landscape forged by the experiences and lots of unforgettable memories linked to the people that joined me on the trip.

I did draw the main path on the map, however Miriam Coenders–Gerrits and Hubert Savenije (co-promotor and promotor) stir me on the right direction, preventing losing myself on the trip. Their guidance, advice, and counseling help to drive the hard bumps of the research experience. Also, this trip couldn't be possible without the financial support of the "Programa de Innovación y Capital Humano (PINN)" of the "Ministerio de Ciencia, Tecnología y Telecomunicaciones de Costa Rica (MICITT)", the "Nederlandse Organisatie voor Wetenschappelijk (NWO)", and the "Organization for Tropical Studies (OTS)".

All the trip was traveled as well by my co-pilot, my wife Adriana González–Angarita. Her support, company, counseling, and sacrifice allowed me to succeed and accomplish the main aim of the trip. This manuscript and research couldn't be possible without her, and this effort is a clear example of a teamwork. During the last part of the trip, a new member of the team had joined, our daughter Gabriela. She became an excellent support member during the last part of the trip. She provided us with fun, joy, and more tasks on the path. She is pushing us to enjoy the landscape view of the trip while cheering us on a daily basis. While both families in Costa Rica and Colombia play as long-distance partners of this voyage. They helped us, shouldered us, cheered us, and fed us here and there. Also, some friends became our extended family in The Netherlands. María Laura Sorrentino and Nahuel Huisman shared the worries and happy moments opening their house, hearts, and kitchen to us.

The trips have important implicit rules, and there is always a group of persons available for taught and guided you through those rules. Lydia de Hoog, Betty Rothfusz, Boran Ekin Aydin, Yingrong Wen, and Remko Nijzink were those persons who taught me the rules and introduce me to the environment in the Water Management Department. Every step is a learned lesson and linked to someone who teach you sometime, and lots of persons walk next to me on the trip. Some for few days, weeks, months or even years. Bart Schilperoort joined me four years, and despite the age difference I learnt a lot from him. From João Macedo and Erika Vatiero, I learned from their confidence and obtain a nice friendship. From Laura Sepulveda, motivation. From María Warter, courage. From Tara van Iersel, breaking stereotypes. From Mónica Herrero–Huerta, endurance. From Carmen Heij, perseverance. From Sylvia van Doorn, patience. From Mohammed Jaffar, support. From Víctor

García and Pamela Cerón, positivism. From Sergio Salinas, confidence and support. From David Salas, friendship. From Juan Pablo Aguilar–López, a culinary search in my surroundings. From Santiago Gaitán–Sabogal and Bas des Tombe, fellowship. Alexander Kaune–Schmidt, support and friendship.

Some travelers were sitting close to me sharing the road, the sidewalks, the paths. They were on their own trip, may be ahead or behind me in terms of time. Yingrong wen, Elisa Ragno, Anjana Ekka, Chelsea Kandoorp, Remko Nijzink, and Alban Singirankabo were those travelers. I shared a lot of personal, academic, professional discussions with them, but the most important ones: the culinary ones. We shared a lot of things sitting next to each other, and with the different talks we had the road became more colorful.

We always have some experiences travelling around. These experiences can be small or really long trips. In this case, Julio Calvo–Alvarado, Dorian Carvajal–Vanegas, and ana Julieta Calvo–Obando travelled with me for more than five years. That trip gave me experience, confidence, friendship, and triggered the growth of the research worm that was hibernating within me.

Along the road we always have to follow practical advises. These ones were coming from Jochen Wenninger, Thom Bogaard, Wim Luxemburg, Saket Pande, Markus Hrachowitz, Maurits Ertsen, Erik Mostert, Olivier Hoes, and Edo Abraham. Also, a large number of persons were there to pull out the project from the muddy roads. Petra Jorritsma, Patricia van den Bos, Armand Middeldorp, Bernal Matarrita, Orlando Vargas, Wagner López, Danilo Brenes, Diego Dierick, Enrique Castro, and Marisol Luna helped us to carry out and improve the project when needed it.

This trip has finished and a lot of memories have created a sense of joy. Now, thanks to all of you this trip has become a landmark in my life, and a new starting point. With a new trip ahead, I just hope to see you on the road again.

CÉSAR D. JIMÉNEZ RODRÍGUEZ

Born in San José, Costa Rica on 17–August–1983

PERSONAL MOTTO

"When you enjoy your work, it becomes a paid hobby".

ABOUT ME

Strengths: Collaborative | Team Worker | Practical

Skills: R | ArcGIS | Data Collection | Statistics | Experimental Design

Hobbies: Trekking | Cooking | Bouldering | Diving

EDUCATION

Ph.D. in Hydrology
Delft University of Technology
Feb 2016 – Aug 2020 | Delft, The Netherlands

Expected Defense on 27 August 2020

M.Sc. in Hydrology and Water Resources
UNESCO–IHE
Oct 2010 – Apr 2012 | Delft, The Netherlands

Lic. in Forest Engineering
Tecnológico de Costa Rica
Jul 2008 – June 2010 | Cartago, Costa Rica

Spec. in Rural Forestry
Facultad Latinoamericana de Ciencias Sociales
Jun 2007 – Nov 2007 | San José, Costa Rica

B.Sc. in Forest Engineering
Tecnológico de Costa Rica
Feb 2001 – Feb 2006 | Cartago, Costa Rica

LANGUAGES

Spanish ●●●●●

English ●●●●●

EXPERIENCE

Guest Researcher
Delft University of Technology
Feb 2016 – Aug 2020 | Delft, The Netherlands

Online Course Lecturer
Universidad de Cundinamarca
Aug 2017 – Nov 2017 | Bogotá, Colombia

Lecturer
Universidad Manuela Beltrán
Jul 2015 – Dic 2015 | Bogotá, Colombia

Forest Hydrologist
Atención Social Integral S.A.S.
Nov 2013 – Apr 2015 | Bogotá, Colombia

Lecturer and Researcher
Tecnológico de Costa Rica
Jan 2008 – Jun 2013 | Cartago, Costa Rica

Research Assistant
FUNDATEC
Aug 2007 – Jun 2013 | Cartago, Costa Rica

Independent Engineer
SIEPAC Project
Mar 2006 – Apr 2007 | San José, Costa Rica

Field Engineer
Consultoría Colombiana S.A.
Feb 2006 – Aug 2006 | San José, Costa Rica

List of Publications

In Review

15. Schilperoort, B., Coenders-Gerrits, M., **Jiménez–Rodríguez, C.**, van der Tol, C., van de Wiel, B., and Savenije, H. (2020). *Decoupling of a Douglas fir canopy: a look into the subcanopy with continuous vertical temperature profiles.* Biogeosciences Discuss., in review.

14. **Jiménez–Rodríguez, C.D.**, Coenders–Gerrits, M., Schilperoort, B., Gonzalez-Angarita, A.P. and Savenije, H. (2020). *Vapor plumes in a tropical wet forest: spotting the invisible evaporation.*Hydrol. Earth Syst. Sci. Discuss. in review.

Book Chapters

13. Coenders-Gerrits, M., Schilperoort, B., and **Jiménez–Rodríguez, C.D.** (2020). *Evaporative Processes on Vegetation: An Inside Look.* In: Precipitation Partitioning by Vegetation. Eds: Van Stan, John, Gutmann, Ethan, Friesen, Jan. Springer.

12. Allen, S.T., Aubrey, D.P., Bader, M.Y., Coenders-Gerrits, M., Friesen, J., Gutmann, E.D., Guillemette, F., **Jiménez–Rodríguez, C.**,Keim, R.F., Klamerus-Iwan, A., Mendieta-Leiva, G., Porada, P., Qualls, R.G., Schilperoort, B., Stubbins, A., and Van Stan, JT. (2020). *Key Questions on the Evaporation and Transport of Intercepted Precipitation.* In: Precipitation Partitioning by Vegetation. Eds: Van Stan, John, Gutmann, Ethan, Friesen, Jan. Springer.

11. **Jiménez-Rodríguez, C.D.**, and Calvo-Alvarado, J. (2013). *An Evaluation of Rainfall Interception.* In: Tropical Dry Forest in the Americas: Ecology, Conservation, and Management. Eds: A. Sánchez-Azofeifa, J. Powers, Fernandes, G.W., and Quesada, M. Taylor and Francis. ISBN 9781466512009.

Research Papers

10. Powers, J.S., Vargas–G, G., Brodribb, T.J., Schwartz, N.B., Perez–Aviles, D., Smith–Martin, C.M., Becknell, J.M., Aureli, F., Blanco, R., Calderón–Morales, E., Calvo–Alvarado, J.C., Calvo–Obando, A.J., Chavarría, M.M., Carvajal–Vanegas, D., **Jiménez–Rodríguez, C.D.**, Murillo Chacon, E., Schaffner, C.M., Werden, L.K., Xu, X. and Medvigy, D. (2020). *A catastrophic tropical drought kills hydraulically vulnerable tree species.* Globlal Change Biology. 26: 3122– 3133.

9. **Jiménez-Rodríguez, C.D.**, Coenders-Gerrits, M., Wenninger, J., Gonzalez-Angarita, A., and Savenije, H. (2020). *Contribution of understory evaporation in a tropical wet forest during the dry season.* Hydrol. Earth Syst. Sci., 24, 2179–2206

8. **Jiménez–Rodríguez, C.D.**, Coenders–Gerrits, M., Uhlenbrook, S. and Wenninger, J. (2019). *What Do Plants Leave after Summer on the Ground?-The Effect of Afforested Plants in Arid Environments.* Water. 11(12), 2559.

7. **Jiménez–Rodríguez, C.D.**, Esquivel–Vargas, C., Coenders–Gerrits, M. and Sasa–Marín, M. (2019). *Quantification of the evaporation rates from six types of wetland cover in Palo Verde National Park, Costa Rica.* Water, 11 (4), 674.

6. Calvo-Alvarado, J., **Jiménez-Rodríguez, C.**, Calvo-Obando, A., Marcos do Espírito-Santo, M., and Gonçalves-Silva, T. (2018). *Interception of Rainfall in Successional Tropical Dry Forests in Brazil and Costa Rica.* Geosciences, 8(12), 486.

5. Schilperoort, B., Coenders-Gerrits, M., Luxemburg, W., **Jiménez-Rodríguez, C.**, Cisneros Vaca, C., and Savenije, H. (2018). *Using distributed temperature sensing for Bowen ratio evaporation measurements.* Hydrol. Earth Syst. Sci., 22 (1), 819-830.

4. **Jiménez-Rodríguez, C.D.**, Calvo-Alvarado, J.C., and Jackson, J.K. (2015). *Performance of two hydrological models in predicting daily flow under a climate change scenario for mountainous catchments in northwestern Costa Rica.* Mountain Research and Development, 35 (3), 240-254.

3. Hilje, B., Calvo-Alvarado, J., **Jiménez-Rodríguez, C.**, and Sánchez-Azofeifa, A. (2015). *Tree species composition, breeding systems, and pollination and dispersal syndromes in three forest successional stages in a tropical dry forest in Mesoamerica.* Tropical Conservation Science, 8 (1), 76-94.

2. Calvo-Alvarado, J.C., **Jiménez-Rodríguez, C.D.**, and Jiménez-Salazar, V. (2014). *Determining rainfall erosivity in Costa Rica: A practical approach.* Mountain Research and Development, 34 (1), 48-56.

1. Kowaljow, E., Mazzarino, M. J., Satti, P., and **Jiménez-Rodríguez, C.** (2010). *Organic and inorganic fertilizer effects on a degraded Patagonian rangeland.* Plant and Soil, 332 (1-2), 135-145.